



Department of Pure and Applied Chemistry

**UV Stabilisation of Poly(Ethylene
Terephthalate)**

by

Ömer Can Erdemli

Ph.D. Thesis

2016

A PhD thesis submitted to the Department of Pure and Applied Chemistry, University of Strathclyde, in part fulfilment of the regulations for the Degree of Doctor of Philosophy in Chemistry.

This thesis is the result of the author's original research. It has been composed by the author and has not been previously submitted for examination which has led to the award of a degree.

The copyright of this thesis belongs to the author under the terms of the United Kingdom Copyright Acts as qualified by University of Strathclyde Regulation 3.50. Due acknowledgement must always be made of the use of any material contained in, or derived from, this thesis.

Signed:

Date: June 2016

Acknowledgements

I would like to begin with a big thank you to Professor Peter Cormack and Dr Stephen Sankey for giving me this opportunity to carry out this research. I wholeheartedly appreciate their invaluable knowledge and support throughout my doctoral studies. They were always available to offer support and helped to make my project a truly enjoyable experience. I am extremely grateful for the funding from DuPont Teijin Films which has made this research possible.

I would like to acknowledge everyone in the Polymer Group and DuPont Teijin Films for their guidance throughout my PhD. You all helped to make my PhD time a pleasurable and memorable experience. I wish you guys all the best in your future endeavours.

Last, but not least, I would like to give credit to Gavin Bain, Denise Gilmour, Alex Clunie, Lindsay McCulloch, Rachel Little, James Kelly, Megan Todd, Pat Keating, Tong Zhang and Craig Irving, for their help with the analytical side of my project.

Thank you all so much.

Abstract

The aim of this project was to design novel polymerisable UV absorbers which successfully protect PET from UV degradation for a longer duration of time compared to non-polymerisable UV stabilising additives.

The polymerisable UV stabilisers for PET were synthesised using cyanuric chloride as a synthetic starting point. A number of synthetic monomers were prepared based upon one of the most effective UV stabilising additives employed currently in the polymer industry, Tinuvin 1577. UV absorbing monomers (UVAMs) with chromophores different to that of Tinuvin 1577 were synthesised, and many were found to have higher molar absorptivity than Tinuvin 1577.

The novel UVAMs were copolymerised with *bis*(hydroxyethyl)isophthalate to yield copolymers of poly(ethylene isophthalate) (PEI). In certain cases, more than one UVAM was copolymerised into the same PEI chain to obtain a broader UV coverage and to distribute the UVAMs in the middle and end of the polymer chains. Copolymers were purified to remove any unreacted monomers and characterised by UV-VIS spectrophotometry, ¹H NMR spectroscopy and DSC to demonstrate and quantify successful incorporation of the UVAMs into the polymers.

PET copolymer films containing 3-[4-(4,6-diphenyl-1,3,5-triazin-2-yl)-3-hydroxyphenoxy]-1,2-propanediol (**32**), 6,6'-(6-phenyl-1,3,5-triazine-2,4-diyl)*bis*(3-(2-hydroxyethoxy)phenol) (**37**) and both **32** and **37** were weathered alongside a PET control and PET containing Tinuvin 1577 **1.10**. The films were exposed for 1082 hrs in a QUV weatherometer and analysed periodically using FT-IR spectroscopy and GPC. The results showed that the films containing UVAMs outperformed the films containing Tinuvin 1577, offering greater protection to the polymer films against crosslinking and chain scissions.

Abbreviations

ATR	Attenuated total reflectance
BHEI	<i>Bis</i> (hydroxyethyl)isophthalate
BHET	<i>Bis</i> (hydroxyethyl)terephthalate
BT	2-(Hydroxyphenyl)benzotriazole
CPA	Calico Printer's Association
COSY	Correlation spectroscopy
DCM	Dichloromethane
DIPEA	<i>N,N</i> -Diisopropylethylamine
DMF	<i>N,N</i> -Dimethylformamide
DMSO	Dimethyl sulfoxide
DMT	Dimethyl terephthalate
DTF	DuPont Teijin Films
DSC	Differential scanning calorimetry
EG	Ethylene glycol
EI	Electron impact ionisation
ESIPT	Excited state intramolecular transfer
FFM	Friction force microscopy
FT-IR	Fourier transform infrared
GSIPT	Ground state intramolecular proton transfer
GC-MS	Gas chromatography-mass spectrometry
HFIP	Hexafluoroisopropanol

HALS	Hindered amine light stabiliser
HMBC	Heteronuclear multiple-bond correlation spectroscopy
HOMO	Highest occupied molecular orbital
HR-MS	High resolution mass spectroscopy
HSQC	Heteronuclear single quantum coherence spectroscopy
IC	Internal conversion
ICI	Imperial Chemical Industries
IMHB	Intramolecular hydrogen bond
IV	Intrinsic viscosity
LC-MS	Liquid chromatography-mass spectrometry
LUMO	Lowest unoccupied molecular orbital
MALDI	Matrix assisted laser desorption ionisation
NMR	Nuclear magnetic resonance
PC	Polycondensation
PEI	Poly(ethylene isophthalate)
PET	Poly(ethylene terephthalate)
PS	Polystyrene
SIPBS	Strathclyde Institute of Pharmacy and Biomedical Sciences
TA	2-(2-Hydroxyphenyl)-1,3,5-triazine
TGA	Thermogravimetric analysis
THF	Tetrahydrofuran

TPA	Terephthalic acid
UVA	Ultraviolet absorber
UVAM	Ultraviolet absorber monomer
XPS	X-ray photoelectron spectroscopy

Contents

Acknowledgements.....	i
Abstract.....	ii
Abbreviations	iii
Chapter 1 - Introduction	1
1.1 Polyesters.....	2
1.2 Step-Growth Polymerisation.....	3
1.3 Poly(ethylene terephthalate).....	5
1.3.1 Background	5
1.3.2 Manufacture of PET	6
1.3.3 Film Manufacture.....	7
1.4 Ultraviolet Degradation of PET	8
1.4.1 Mechanism of PET Photodegradation	9
1.4.2 Morphology and Crystallisation in PET Photodegradation.....	15
1.4.3 Depth Profiling of UV Degradation	16
1.5 Ultraviolet Stabilisation.....	19
1.5.1 Ultraviolet Absorbers	19
1.5.2 ESIPT Mechanism	21
1.5.3 2-(2-Hydroxyphenyl)-1,3,5-triazines (TA)	26
1.5.4 Tinuvin 1577.....	29
1.6 Polymerisable Ultraviolet Absorbers	31
1.6.1 Chain-Growth Polymerised Ultraviolet Absorbers	31
1.6.2 Step-Growth Polymerised Ultraviolet Absorbers	35
1.7 1,3,5-Triazine Chemistry and the Synthesis of TA Derivatives	38
1.7.1 Amine Nucleophiles	39

1.7.2 Hydroxyl Nucleophiles	40
1.7.3 Carbon Nucleophiles	41
Chapter 2 - Research Aims and Objectives	51
Chapter 3 - Synthesis of Ultraviolet Absorbing Monomers	54
3.1 Experimental	55
3.1.1 Reagents.....	55
3.1.2 Equipment	56
3.1.3 Synthesis of Ultraviolet Absorber Monomers (UVAMs)	57
3.1.3.1 Grignard Reactions.....	57
3.1.3.2 Amine and Alcohol Nucleophile Reactions	65
3.1.3.3 Friedel-Crafts Reactions	67
3.1.3.4 Incorporation of Polymerisable Functional Groups.....	82
3.2 Results and Discussion	112
3.2.1 Synthesis of UVAMs	112
3.2.1.1 Grignard Reactions.....	112
3.2.1.2 Amine and Alcohol Nucleophile Reactions	115
3.2.1.3 Friedel-Crafts Reactions	116
3.2.1.4 Incorporation of Polymerisable Functional Groups.....	124
3.2.2 UV Spectra of UVAMs	134
3.2.3 Thermal Analysis of UVAMs	141
3.3 Conclusions	146
Chapter 4 - Poly(ethylene isophthalate) Copolymers.....	147
4.1 Experimental	148
4.1.1 Reagents.....	148
4.1.2 Equipment.....	148

4.1.3 Synthesis of Poly(ethylene isophthalate) (PEI) Copolymers	149
4.1.3.1 Poly(EI-co-UVAM) Copolymers	149
4.1.3.2 Poly(EI-co-UVAM-co-UVAM) Copolymers.....	168
4.2 Results and Discussion	176
4.2.1 UV analysis of PEI Copolymers.....	179
4.2.2 DSC and GPC Analysis of PEI Copolymers	188
4.3 Conclusions	191
Chapter 5 - Poly(ethylene terephthalate) Copolymers and Accelerated Weathering Study.....	193
5.1 Experimental	194
5.1.1 Reagents.....	194
5.1.2 Equipment and Methods	194
5.1.3 Synthesis of Poly(ethylene terephthalate) (PET) Films.....	196
5.2 Results and Discussion	202
5.2.1 Synthesis and Processing of PET Films.....	202
5.2.2 Solvent Extraction	206
5.2.3 Weathering of PET Films	206
5.2.3.1 ATR FT-IR Measurements.....	207
5.2.3.2 GPC Measurements	208
5.3 Conclusions	217
6.0 General Conclusions and Future Work	219
7.0 Appendix	222
8.0 References.....	224

Chapter 1 - Introduction

The use of UV stabilisers as additives to polyester films to prevent UV-induced photodegradation of the polymer chains is an important technology, particularly for those applications where the UV exposure of the film is high, e.g. in photovoltaic cells. One major drawback of UV stabilisers is the loss of additive from the polymer over time, however this problem can be overcome by covalently incorporating the UV stabilisers in the polymer chain. For this reason, there is a market for novel UV stabilisers which are polymerisable and can therefore become an essential part of the polymer structure and prolong the lifetime of UV protection.

1.1 Polyesters

Polyesters are an integral component of life in the modern world. Their rise during the 20th century has seen them establish a ubiquitous presence in everyday life. Polyesters are a category of polymer which bear ester functional groups throughout the main-chain. There are examples of polyesters in nature,¹ but polyesters can also be synthesised by step-growth polymerisation.^{2,3}

These versatile synthetic polymers can be used as fibres, bottles, films and coatings and are often synthesised by step-growth polymerisation, which includes methods such as: (a) esterification; (b) transesterification; (c) reaction of alcohols with acid chlorides; (d) reaction of alcohols with anhydrides (Figure 1.1).² The general mechanism involves nucleophilic attack on an activated carbon-oxygen double bond. Unlike esterifications and transesterifications, reactions with acid chlorides and anhydrides are typically non-reversible.

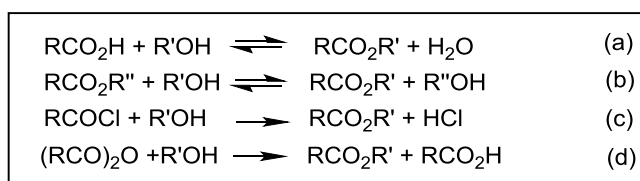


Fig. 1.1 - Different types of esterifications with: (a) esterification; (b) trans-esterification; (c) reaction between alcohols and acid chlorides; (d) reaction between alcohols and anhydrides²

1.2 Step-Growth Polymerisation

Polymers can be categorised into two different classes, condensation polymers and addition polymers.³ Condensation polymers are constructed by the elimination of a small molecule, such as water, when monomers join together, whilst addition polymers are formed in a single chain reaction with no formation of by-products.

This early classification led to a certain degree of uncertainty as a number of exceptions came to light, e.g., ring-opening polymerisation of ethylene oxide to form a polyether.⁴ To circumvent this ambiguity, Flory categorised polymerisations by their reaction mechanism.⁵

1. Step-growth polymerisations
2. Chain-growth polymerisations

Flory stated that chain-growth polymers were produced by a single chain reaction where the molecular weight increased by the successive linking of monomer molecules to the end of a growing chain. In the case of step-growth polymers, Flory stated that they were built in a stepwise manner by the joining of multifunctional monomer molecules to form dimers, trimers, tetramers, etc. These oligomeric species then reacted with each other through their functional groups. This re-classification by Flory allowed the inclusion of polymers such as polyurethanes which grow by a step-reaction without elimination of by-products.⁶

Step-growth polymerisation requires at least two functional groups on each monomer, however two different functional groups on the same monomer is also feasible. If we consider hypothetical functional groups, A and B, then they react together to form group X (Figure 1.2).⁷

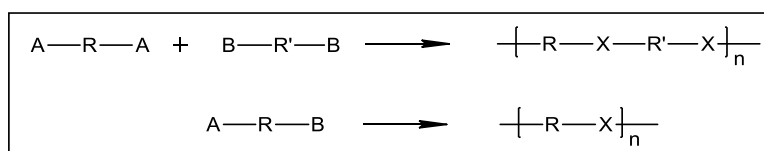


Fig. 1.2 - Step-growth polymerisation of monomers bearing two functional groups on each monomer (upper) and two different complementary functional groups on the same monomer (lower)⁷

Chain-growth polymerisation achieves higher molecular weights at a faster rate compared to step-growth polymerisation.⁷ In the latter, although the monomers quickly convert into oligomers and the concentration of growing chains is high, the polymer chains form slowly and often the reaction times stretch over several hours to days. Carothers, the founding father of step-growth polymerisation, proposed a simple equation relating the average number of monomer units in each polymer chain (\overline{DP}_n) to the extent of the reaction (p) for linear polycondensations (Equation 1.1).⁷

Eq. 1.1

$$\overline{DP}_n = \frac{1}{(1-p)}$$

This equation highlights the need for high monomer conversion, considering that $p = 1$ when there is 100 % monomer conversion. Providing the monomer conversion exceeds 99 % ($P > 0.99$), step-growth polymerisations usually yield polymers with moderate molecular weights i.e. 10,000-100,000.^{8,9} It is of the utmost importance to have a high degree of monomer purity and a tight stoichiometric balance of the reacting moieties to have any chance of achieving high molar mass products through step-growth polymerisation. Alternatively, a bifunctional monomer bearing two complementary functional groups provides an internal balance without the concern of perfect stoichiometry (Figure 1.2). The chemical reaction accountable for the polymerisation must be a very favourable one, with an absence of side reactions. Since these chemical reactions have high activation energies, elevated temperatures and a vacuum are often applied to drive such reactions to completion.

Step-growth polymerisations with bifunctional monomers yield linear polymers. The use of trifunctional or higher species results in chain branching and, potentially, the formation of polymer networks.^{3,9} Polyfunctional monomers give rise to thermoplastic or thermosetting polymers. Thermoplastic polymers are either linear or branched materials that can be melted and reformed. Thermosets are heavily crosslinked polymers which cannot be melted or reformed.^{2,3}

1.3 Poly(ethylene terephthalate)

1.3.1 Background

Poly(ethylene terephthalate) (PET) played a huge role in the rise of polyesters in the past 70 years and has applications ranging from food packaging to photovoltaics.^{10,11} PET (Figure 1.3) is a linear semi-crystalline thermoplastic polymer which has many valuable properties that make it a very useful material, some of which are listed below:¹²⁻¹⁷

- High mechanical strength
- Good gas barrier properties
- High thermal stability
- High hydrolytic resistance
- Low haze
- Electrically resistant
- Flexibility
- Low moisture absorption

Carothers synthesised the first linear polyesters in the late 1920s and this initiated the research and development of synthetic polyester materials.^{18,19} Carothers found that aliphatic polyesters possessed low melting points, poor thermomechanical strength and hydrolytic instability. He and his co-workers at DuPont therefore focused their attentions instead on polyamides, which led to the discovery of Nylon 6,6 in 1935.²⁰ Whinfield and Dickson, working for Calico Printer's Association Ltd. (CPA), cleverly concentrated on the more symmetrical and planar aromatic polyesters. Whinfield and Dickson's endeavour led to the discovery of PET, from the polycondensation of terephthalic acid (TPA, **1.1**) and ethylene glycol (**1.2**) (Figure 1.4), and the filing of a patent in 1941.²¹

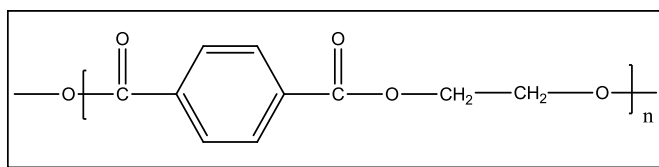


Fig. 1.3 – Chemical structure of PET

The development of PET was revolutionary and initiated vigorous negotiations between DuPont, Imperial Chemical Industries (ICI) and CPA for the rights to manufacture PET worldwide.²² DuPont licensed the Whinfield and Dickson patent in

the USA, whilst ICI owned the rights throughout the rest of the world. PET development was rife and funding was in excess of 6 million US dollars by 1950. By 1970, PET sales were in excess of 3 billion British pounds.

1.3.2 Manufacture of PET

The first step in the manufacture of PET is a pre-polymerisation process to prepare *bis*(2-hydroxyethyl)terephthalate (BHET, **1.4**) (Figure 1.4). The two different methods of pre-polymerisation are transesterification and direct esterification. The main difference between the two is that transesterification involves the reaction of dimethyl terephthalate (DMT, **1.3**) with ethylene glycol whilst direct esterification replaces DMT **1.3** with TPA **1.1**.²³ The direct esterification or transesterification is commonly catalysed by zinc or manganese acetate.²⁴

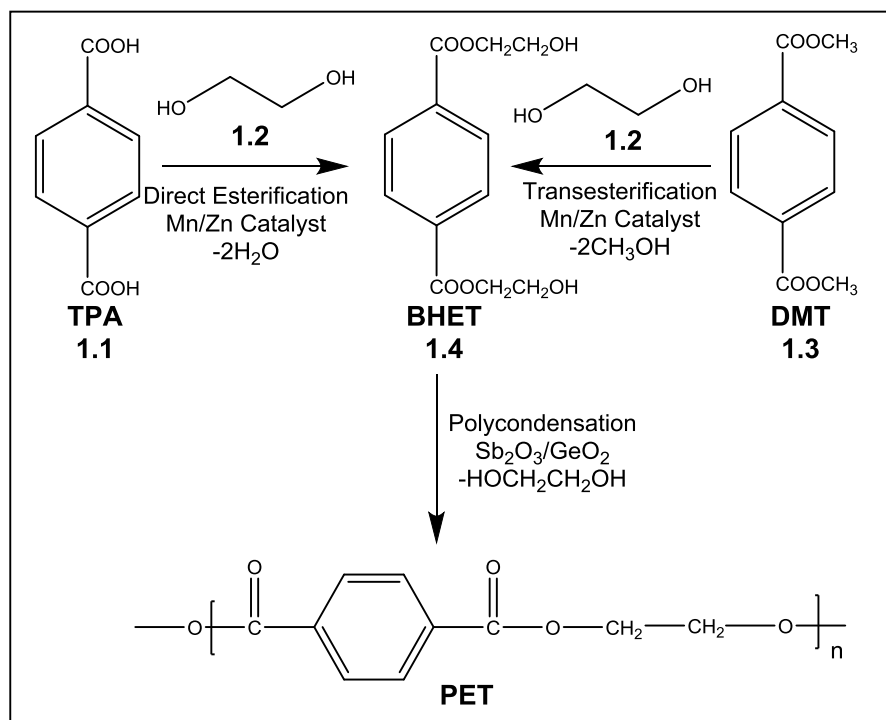


Fig. 1.4 – Route of synthesis of PET²⁴

The subsequent step is a polycondensation, which uses antimony trioxide or germanium oxide catalyst and applies temperatures of 280 °C to BHET **1.4**. The pressure of the reactor is lowered below 1 mbar and ethylene glycol **1.2** is collected

as a by-product. The duration of the entire process, including the pre-polymerisation and the polycondensation, typically takes 5-10 hours.^{24,25}

1.3.3 Film Manufacture

PET can be manipulated into orientated films by extruding molten polymer onto a casting drum and drawing the film forwards and sideways using a series of rollers and ovens (Figure 1.5). When polycondensation is complete and the target intrinsic viscosity (IV) has been reached, the vacuum is reduced to about 10 mbar and a valve is opened so that the polymer is pumped through a lace die. The laces are cut to produce chip, approximately 5 x 5 x 3 mm in size. The polymer chips have to be dried before melting to prevent moisture from the atmosphere hydrolysing the long chain molecules, which reduces the IV and in turn causes crystallisation and haze in the forward draw process. Even a minor decrease in IV would have a significant effect on the tensile strength of the polymer film.

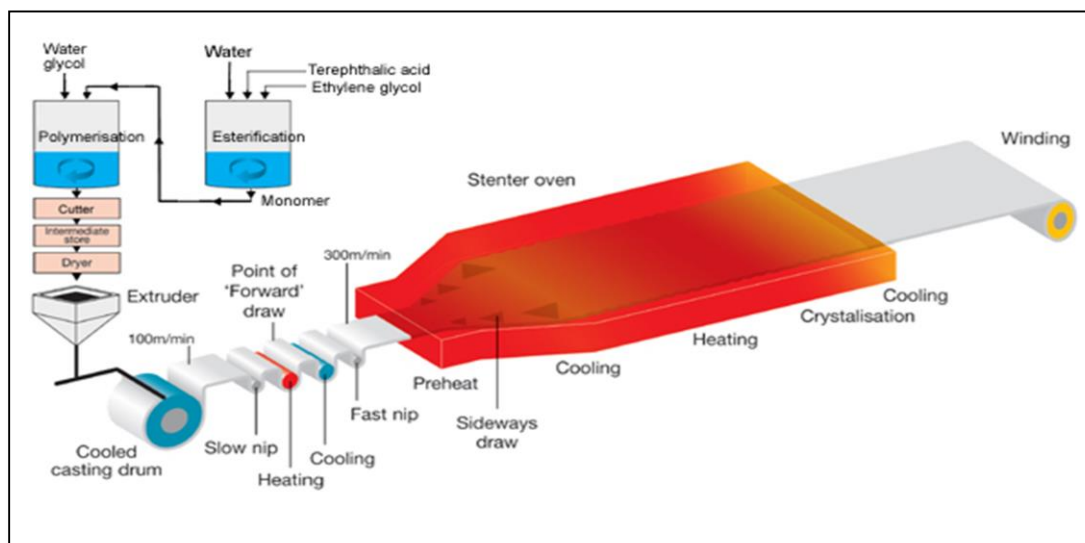


Fig. 1.5 – PET Film manufacturing process reproduced with the permission of DuPont Teijin Films

The dry polymer chips are converted into a steady stream of molten polymer in the extrusion system at a temperature of 290 °C. The molten film is extruded onto a cooled casting drum, with the aim of producing a continuous film of non-crystalline polymer with no surface blemishes. The amorphous film is oriented in the forward draw by means of stretching to produce a film of uniform thickness with high tensile

strength in both the longitudinal and transverse directions. The film is then pre-heated to 110 °C before being transferred to the stenter unit and gripped at each edge in a continuous band of clippers and passed through a series of ovens. In the stenter, the film is drawn sideways, first at 120 °C, and then passes through the crystallisation ovens where the film is heat set at temperatures up to 230 °C. After sufficient crystallisation, the film is cooled to the plant temperature by passing over water-cooled rolls at the exit of the stenter.

1.4 Ultraviolet Degradation of PET

A major problem that the PET industry faces is the degradation of the polymer chain upon exposure to UV radiation. The photochemistry of polyester degradation is a complex area which has been studied extensively over the past fifty years.

Although the UV region ranges from 10-400 nm, the ozone layer prevents wavelengths lower than 290 nm from reaching Earth's surface. The UV spectrum can be subdivided into three main regions: UV-C between 100-280 nm; UV-B between 280-315 nm; UV-A between 315-400 nm.²⁶ The UV absorbance profile of PET shows a strong absorbance at wavelengths less than 310 nm due to the highly conjugated aromatic carbonyl ester framework (Figure 1.6). The UV spectrum of poly(ethylene isophthalate) (PEI)²⁷ shows a weaker absorbance at lower wavelengths compared to PET due to a lower degree of conjugation of the PEI framework.

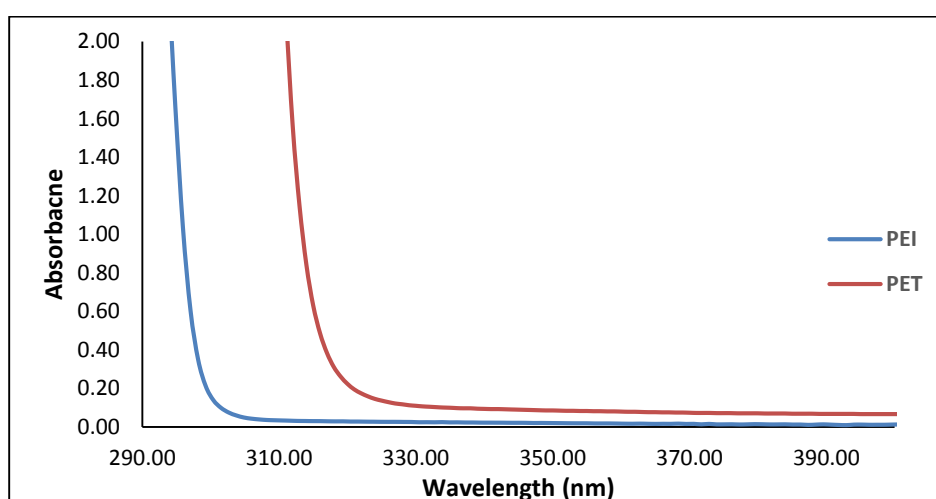


Fig. 1.6 - UV Spectra of a PEI solution (10 mg/mL in CHCl₃) and a PET film

1.4.1 Mechanism of PET Photodegradation

In the early 1970s, Day and Wiles²⁸⁻³¹ irradiated PET films with wavelengths of light between 200 – 400 nm within different environments, a series of photolysis experiments performed under vacuum and in the presence of oxygen. The PET films were sealed in quartz cells under vacuum or in an air atmosphere, whilst irradiating with different wavelengths of UV light. The volatile products of UV degradation were detected and analysed by mass spectrometry and infrared spectroscopy. The film samples were also analysed for tensile strength, molecular weight and fluorescence at regular intervals during irradiation. They discovered that the main products of PET degradation were carbon monoxide (CO), carbon dioxide (CO₂) and carboxylic acid end groups (-COOH) on the front and rear of the films, depending on the presence of oxygen.³⁰ The group found that wavelengths below 310 nm were critical for degradation; wavelengths above 315 nm led to the production of COOH end groups in the bulk, front and rear surfaces of the films.²⁹ As expected, the films showed a drastic decline in tensile strength, with the originally strong and flexible samples becoming brittle and fragile after irradiation. The commercial PET films in this study contained UV stabiliser additives and showed a slower rate of degradation compared to the unprotected samples.

Day and Wiles proposed mechanisms³⁰ for the formation of the three main products (CO, CO₂, -COOH) of degradation (Figure 1.7) by exposing PET to oxidative and non-oxidative conditions. It was apparent that the production of -COOH end groups and CO were independent of the environment.²⁹ Under non-oxidative conditions, the -COOH end groups and CO gas were generated in higher yields compared to CO₂ gas. This led Day and Wiles to conclude that the -COOH end groups and CO gas were the primary products of photolytic degradation and CO₂ was only pertinent in the later stages of decomposition. Day and Wiles believed that carboxylic acid end groups were formed by a Norrish type II photo-elimination reaction, an intramolecular rearrangement of the ester group into an olefin and carboxylic acid. There was substantial evidence for ester groups with a γ -hydrogen atom to undergo photolytic cleavage *via* an intramolecular cyclisation and since molecular motion is restricted in

the crystalline regions of PET, this reinforced the theory of chain scissions occurring in the amorphous regions of the polymer. Day and Wiles explained that the CO build up was caused by a photolytic chain scission, a Norrish type I reaction. However, one could debate that the label of “Norrish type I” is inappropriate since this involves aldehydes and ketones exclusively. The production of CO could potentially arise from photolytic cleavage of the ester or the Ar-C bond, however Day and Wiles stated that the former was more energetically favourable. The rate of CO₂ formation greatly increased for irradiations conducted in the presence of air, so it was evident that oxygen played a role in the proposed mechanism. The hydroxyl radicals produced in the process of CO₂ production could potentially substitute on an aromatic ring to yield fluorescent mono-hydroxyl terephthalate groups in the polymer backbone.

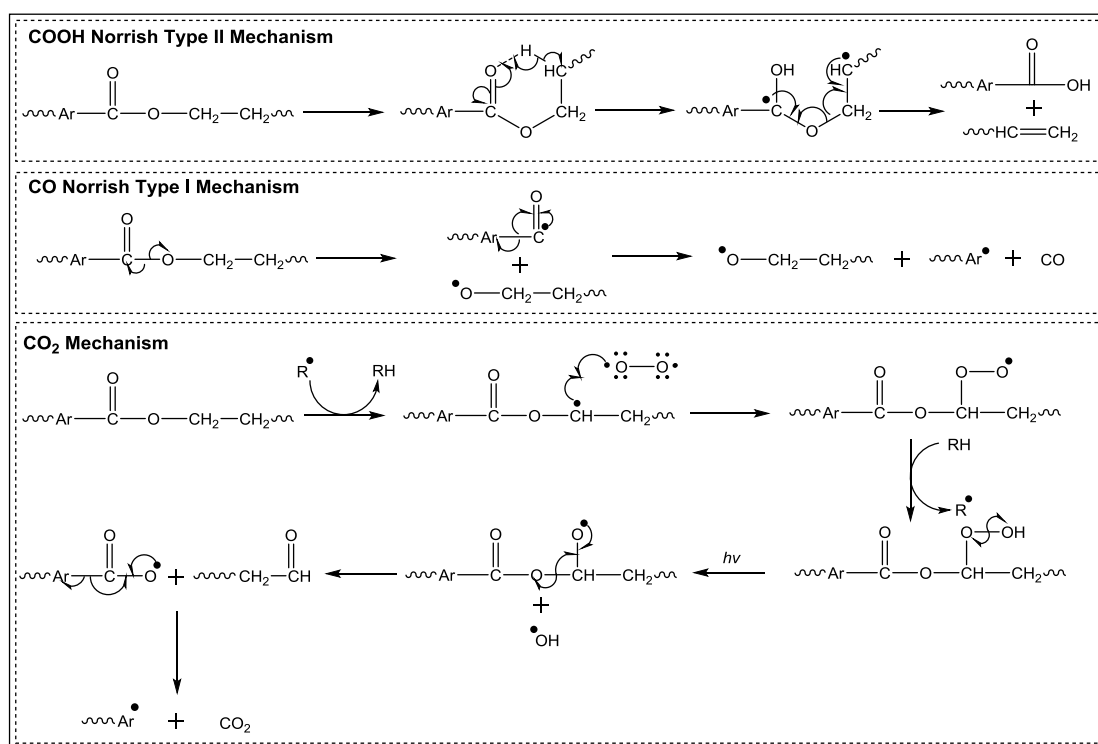


Fig. 1.7 – Mechanism proposed by Day and Wiles for the formation of –COOH, CO and CO₂ during photodegradation of PET³⁰

Day and Wiles also reported an increase in fluorescence emission for PET films which had been subjected to UV light under oxidative conditions.²⁹ Day and Wiles believed that the formation of hydroxyl radicals could give rise to fluorescent mono/di-hydroxyl terephthalate compounds **1.5** and **1.6** (Figure 1.8). The films that were

studied in vacuum showed no manifestation of fluorescent products, however the films exhibited distinct yellowing from crosslinking.

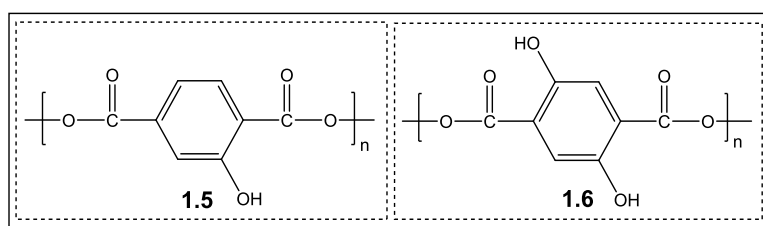


Fig. 1.8 – Structures of the fluorescent mono- and di-hydroxyl compounds formed upon PET irradiation²⁹

The production of fluorescent material required oxygen since it was absent in irradiations under vacuum. Day and Wiles proposed a photo-oxidative mechanism that produced hydroxyl radicals from peroxy radicals and hydroperoxides, which subsequently substituted on an aromatic ring to generate **1.5** and **1.6** (Figure 1.9).²⁹ The mechanism is unfeasible without oxygen, which explained the absence of fluorescent material in PET films subjected to UV under vacuum.

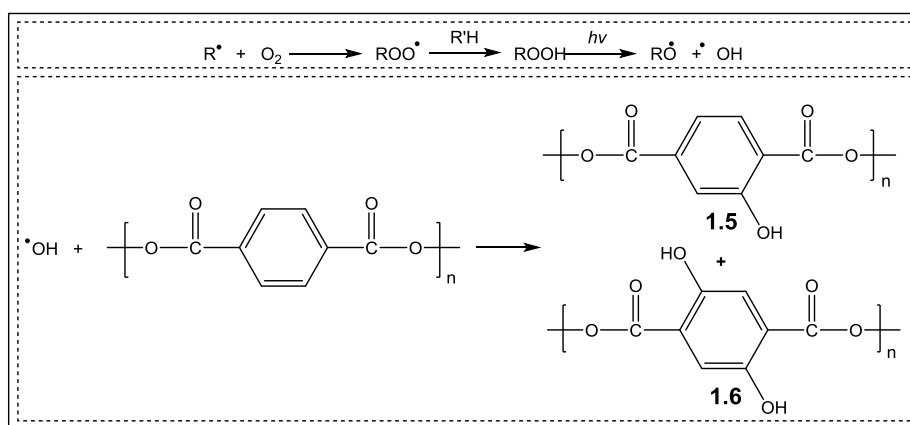


Fig. 1.9 – Photo-oxidative formation of fluorescent mono/di-hydroxyl terephthalate species in PET degradation²⁹

Under oxidative conditions, the photochemical reactions caused chain scissions and a decrease in molecular weight which, in turn, led to the deterioration of the physical properties of the PET samples. Irradiating the polymer films under non-oxidative conditions gave rise to crosslinking, an increase in molecular weight, and resulted in discoloured insoluble gels. Since oxygen seemed to inhibit crosslinking, Day and Wiles believed that crosslinking arose from the formation of an aryl radical by

hydrogen abstraction (Figure 1.10). The crosslinking biphenyl species (**1.7**) increased the degree of conjugation which accounted for the increased absorption in the visible region and the distinct yellowing of the PET films.²⁹ A clear mechanism for the formation of the biphenyl species **1.7** was not postulated and one must question the likelihood of a simple combination of two aryl radicals. The extremely reactive aryl radicals will more likely attack an aromatic ring to form, after oxidation, the biaryl linkage. A study by Gardette *et al.*³² in 2014 investigated the effects of photo-oxidation of PET on the oxygen permeability; they claimed that the oxygen transusion rate of UV degraded PET films decreased with the duration of exposure due to crosslinking from the recombination of macroradicals.

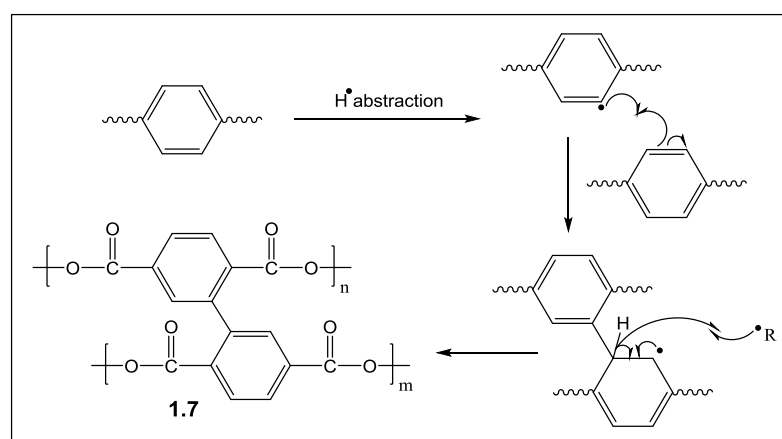


Fig. 1.10 – Mechanism for the production of conjugated biphenyl species *via* an aryl radical²⁹

The theory behind some of the work of Day and Wiles has not gone unchallenged. Fecine *et al.*^{33,34} utilised FT-IR spectroscopy to determine the difference in carboxyl index values at depths of 0.54 and 1.19 μm of irradiated film. The degree of degradation was found to decrease with distance from the surface which was explained by the lower concentration of oxygen in the bulk of the polymer film. Fecine *et al.* claimed that the Norrish Type II formation of carboxylic acid end groups failed to account for the difference between the surface and the interior of PET film. The Fecine group believed that if $-\text{COOH}$ end groups were produced by the Norrish Type II process, without the need for oxygen, the carboxylic acid end groups would be present in the bulk of the material where there are sufficient levels of UV radiation. In 2004, Fecine proposed an alternative mechanism involving a Norrish

type I reaction, which proceeded through a radical pathway in the presence of oxygen.³³ Fecine's mechanistic theory generated hydroxylated terephthalates, carboxylic acid end groups and aldehydes (Figure 1.11). A study by Grossetête *et al.*³⁵ suggested further oxidation of the aldehyde to produce additional carboxylic acid end groups. In agreement with Day and Wiles,²⁸⁻³⁰ Fecine proposed that light with a wavelength range of 310-360 nm in the presence of oxygen was responsible for the generation of fluorescent mono/di-hydroxyl terephthalates.

Hurley and Leggett³⁶ utilised friction force microscopy (FFM), contact-angle goniometry and X-ray photoelectron spectroscopy (XPS) to examine extensively the surface chemistry of PET during photodegradation. They found that the contact angle of water decreased once the PET film was exposed to UV due to an increase in oxygen concentration at the surface, hence making the material more hydrophilic. Hurley and Leggett reported that the initial decrease in contact angle levelled off, approaching zero, before falling again after further exposure which alluded to a two stage degradation process. However, they found that after immersing the film in ethanol, washing away low molecular weight hydrophilic residue, the second phase of declining contact angle was non-existent. In the FFM measurements, a polar silicon dioxide tip was used which gauges the intermolecular interactions at the surface of a material. The friction force coefficient increased with UV exposure due to increasing hydrophilicity of the material's surface. Equally to the contact angle goniometry, the friction force coefficient levelled off at approximately 200 mins of UV exposure for the washed film samples. Whilst contact angle goniometry and FFM gave an understanding of surface degradation on the micro- and macroscale, XPS was utilised to study the elemental composition upon degradation at the surface. Hurley and Leggett noted a decrease in the carbon content and a corresponding rise of the percentage composition of oxygen. They concluded by supporting Fecine's Norrish type I mechanism for the formation of carboxylic acid groups at the surface of degradation.

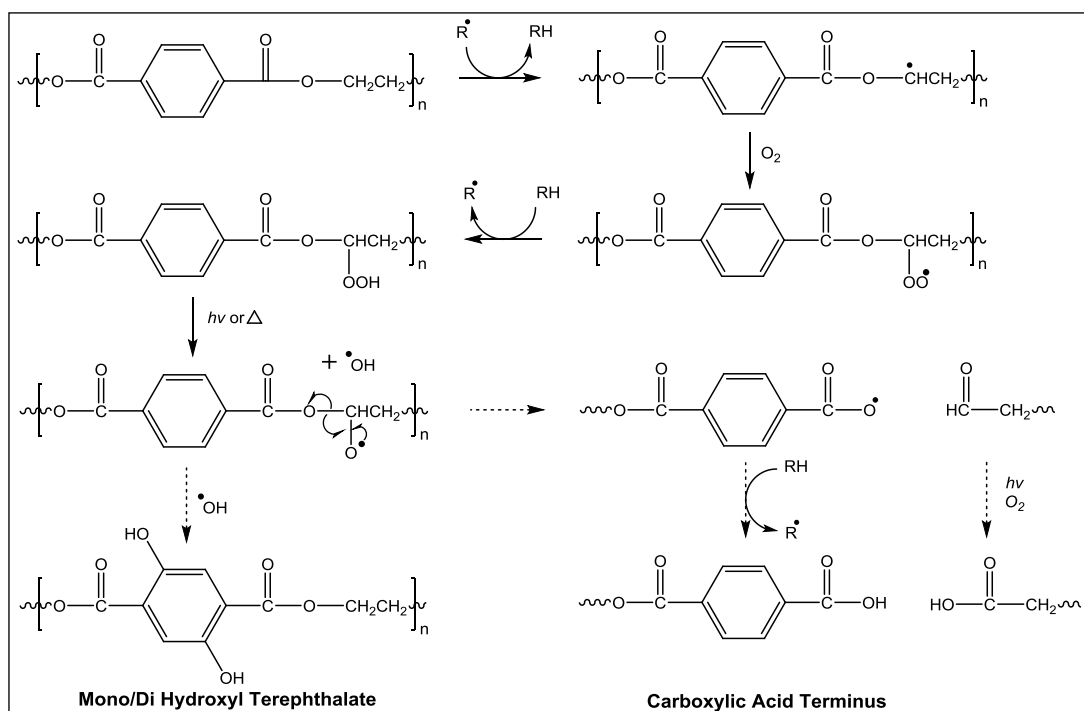


Fig. 1.11 – Mechanism of carboxylic acid end group formation proposed by Fecchine, and aldehyde oxidation proposed by Grossetête^{33–36}

A separate study by Fecchine *et al.*³⁷ monitored the evolution of CO₂ upon irradiating PET film with UV light within a specifically constructed reaction cell. Once flushed with dry nitrogen, the PET film was treated with UV under different environments and the evolved gaseous compounds trapped within the cell analysed by FT-IR spectroscopy at regular intervals. This was the first time that a technique which measured the evolution of CO₂ was applied to differentiate between UV-protected PET films and their unprotected counterparts. Fecchine also compared single layers of films to stacks of films with the aim of investigating the importance of distribution of UV absorber within the PET film. The presence of UV stabilisers reduced the rate of CO₂ formation by approximately 25 %, however the distribution and concentration of UV absorber within the PET film had no impact on the evolution of CO₂. This led Fecchine to believe that the formation of CO₂ occurred at the oxygen-rich surface, which is where UV absorber was present in all cases of protected PET. This finding was consistent with a study by Fernando *et al.*³⁸ which showed that oxidative degradation of PET occurs at the surface. The Fernando group reported that CO₂ was produced mainly in the front and rear surfaces of irradiated PET film, furthermore

thicker film samples degraded at a slower rate due to reduced exposure of the rear surface.

Fechine and co-workers found some interesting results when investigating the effect of moisture in the atmosphere during photodegradation.³⁷ Moisture in the atmosphere increased the CO₂ evolution in both nitrogen and oxygen atmospheres, whilst the presence of UV absorber retarded the formation of CO₂ in all environments. The highest level of CO₂ evolution was displayed when irradiating the films in wet oxygen, however the rate of CO₂ production was similar for irradiations carried out in dry oxygen and dry nitrogen. Initially, this contradicted the work of Day and Wiles^{28,29,31} who postulated higher levels of CO₂ evolution in the presence of oxygen. However, the experiments by Day and Wiles were conducted over a much longer time span so Fechine repeated his measurements on pre-weathered films. They noted a large difference in the CO₂ formation between films irradiated in dry oxygen compared to those irradiated in dry nitrogen with the pre-weathered films, providing better agreement with the Day and Wiles literature.

1.4.2 Morphology and Crystallisation in PET Photodegradation

Fernando *et al.*³⁸ tested different morphologies of PET, 540 µm cast, 150 µm uniaxially drawn and 85 µm biaxially drawn films with crystallinities of 11, 35 and 41 %, respectively. The films were exposed to UV in an oxygen atmosphere and the evolution of CO₂ was monitored by FT-IR spectroscopy. The CO₂ formation at the front surface of the film was similar for the three films which led Fernando to conclude that the morphology of the film had no effect on the rate of CO₂ production. They noted a decrease in the CO₂ evolution at the rear surface as the thickness of the films increased. This behaviour was attributed to the reduced exposure of UV at the rear surface.

A previously mentioned paper by Gardette³² aimed to show the effect of photodegradation on the crystallinity of PET film. The films of PET were exposed to UV light in the presence of air over 450 hours and the change in crystallinity was monitored by infrared spectroscopy at regular intervals. The height ratio of the

bands at 898 cm^{-1} (for the *gauche* conformer of amorphous PET) and 973 cm^{-1} (for the *trans* conformer of crystalline PET) remained unchanged by photo-oxidation. This was backed up by DSC analysis, integrating the normalised area of the melting peak which showed 27 % crystallinity for the degraded and non-degraded samples of PET. Fechine and Rabello³⁹ investigated the effects of photodegradation on the crystallinity of stabilised and unstabilised films. The films were exposed to UV in a weathering chamber and analysed by DSC and X-ray diffraction. DSC analysis showed that the degree of crystallinity was reduced by 0.6 % in the unstabilised film after 596 hours of exposure and 1.0 % in the stabilised film after 1020 hours of exposure. The small decrease in the melting transition temperature (T_m) after exposure was unusual since degradation can have a significant impact on the T_m of polymers such as polyethylene and polypropylene,^{40,41} so much so that it can be used to gauge the extent of degradation. It appeared that the tightly packed folds of the crystalline region in PET offered notable protection from UV degradation. Fechine also utilised X-ray diffraction in conjunction with DSC analysis, monitoring the height of the peak at $2\theta = 26.06^\circ$ (assigned to the chains in the *trans* conformation), believing this would indicate any changes to the degree of crystallinity post-exposure. They noted a decrease of 35 % in the height of the peak for the unstabilised film and a much smaller decrease for the stabilised film. Since the DSC showed no significant change in the crystalline melting temperature, it had to be questioned if the peak reduction in the X-ray diffraction for the unprotected film was accredited to a decrease in crystallinity. Fechine proposed that the decrease in peak intensity for the unstabilised film was ascribed to chain scissions in the mesophase region, a region formed by chains in the *trans* conformation that links the crystalline to the amorphous region.

1.4.3 Depth Profiling of UV Degradation

Studies which irradiated stacked films to achieve a thick PET film model proved to be an effective method for investigating the mechanism and depth of degradation. In 1961, Shultz and Leahy⁴² aimed to identify the specific wavelength of UV light which caused the chain scission in PET. A stack of 5 PET films, each with a thickness of 6.3

μm , were irradiated with filtered UV light for 18 hours in an air atmosphere. Through plotting the ratio of intrinsic viscosity against the predicted UV dosage for each film in the stack, it was possible to determine that 314 nm was the wavelength of light that was primarily responsible for random chain scissions. This value was very close to the accepted wavelength of 315 nm in the Handbook of Material Weathering.⁴³ The molar masses of the films were calculated by measuring the intrinsic viscosity and using the Mark-Houwink Equation (Equation 1.2), with $[\eta]$ being the intrinsic viscosity and M_r the relative molar mass. K and α are constants that are dependent upon the polymer, solvent and temperature. Shultz and Leahy showed that chain scissions were occurring at depths of up to 31.5 μm .

Eq. 1.2
$$[\eta] = K.M_r^\alpha$$

A study in the late 1990s, by Wang *et al.*,⁴⁴ investigated the relationship between the mechanical properties of PET and the distance from the exposed surface of film. This was in agreement with an earlier Day and Wiles study which determined a significant difference between photodegradation on the surface with respect to the interior of UV treated PET films.³¹ Wang and his colleagues irradiated a surface of a multilayer stack of 4.4 μm thick PET films for between 10 and 50 hours. They recorded the change in molecular weight and mechanical strength of each layer and with this determined that the depth of UV degradation from the exposed surface was 15 μm from the surface. The Wang group established that the decrease in molecular weight was one of the main causes for the deterioration of mechanical properties. The quantitative study determined that the rate of degradation was highest at the surface of the PET film and decreased as the distance from the exposed surface increased. In a separate study,⁴⁵ Wang compared the change in molecular weight and mechanical strength of protected and unprotected films. Interestingly, they found that the photodegradation mechanism could be divided into a two-stage process, the first being a very rapid step between 0 and 10 hours, followed by a much slower step after 10 hours. It was reported that the presence of UV absorbing stabiliser decreased the rate of both degradation stages.

A more recent study by Sankey and Raine⁴⁶ stacked 3 μm thick films in a QUV weatherometer for 108, 216 and 432 hours and measured the depth of degradation using GPC and ATR FT-IR. The ratios of the bands at 3290 and 2970 cm^{-1} showed an increase in $-\text{COOH}$ end groups in the first 0-9 μm , reaching a plateau at approximately 15 μm , which was in agreement with the study by Wang.^{44,45} There were further similarities in the GPC analysis, which showed a decrease in the Mn values down to 15 μm for the films irradiated for 432 hours. The group also measured the degree of crosslinking by monitoring the Mz values. The depth of crosslinking was much greater for films exposed for 432 hours in the first 0-9 μm compared to the films exposed for 108 and 216 hours. Although crosslinking levelled off at 18-21 μm , the 'S' type curve led the group to believe that an erosion of the top surface was thinning the surface layer and consequently leading to further degradation at greater depths.

Day and Wiles³¹ measured the fluorescence of a 100 μm thick PET film by scanning a 0.1 μm beam of electrons across a razor-sliced cross-section. An emission profile was produced after 0, 100, 500 and 1000 hours of exposure. Most of the fluorescent species were generated at the front surface, however when examining the same depths from the rear of the surface, a similar yet much slower effect was observed with respect to the front of the surface. The emission profiles showed an increase of fluorescence throughout the cross-section with exposure time. Day and Wiles stated that unexposed PET had a natural fluorescence and after 1000 hours of exposure the fluorescence was reduced. Sankey and Raine⁴⁶ exposed stacks of 50 μm films for 108, 216 and 432 hours and measured the depth of degradation using fluorescent spectroscopy. Sankey found that films exposed to a longer wavelength of 340 nm showed the formation of fluorescent material at depths of at least 450 μm in stacked PET systems and at 250 μm in thick films. The work by Sankey and co-workers supported Fachine³⁴ who hypothesised that the fluorescent material produced in photodegradation was caused by light of longer wavelength.

1.5 Ultraviolet Stabilisation

Polymer manufacturers try to reduce the rate of photodegradation of polymer materials by using UV stabiliser additives. UV additives have high absorption coefficients at the wavelengths responsible for photodegradation of polymers. Typically, 0.1-2.0 % (w/w) of any given UV additive is applied in polymer manufacture.²⁷

There are various effective UV additives which can protect a polymer matrix from UV radiation, and they can be categorised into two broad groups: ultraviolet absorbers (UVAs) and photo-antioxidants.^{47,48} Photo-antioxidants, such as hindered amine light stabilisers (HALS), produce nitroxyl radicals which deactivate harmful radical species, thus preventing oxidative degradation.⁴⁸ To remain relevant to the topic of the current PhD thesis, only the UVAs will be discussed in any detail in this review.

1.5.1 Ultraviolet Absorbers

Ultraviolet absorbers (UVAs) are commercially available additives which are commonly employed in the polymer industry due to their effectiveness in protecting polymeric materials from UV radiation. They absorb UV light and dissipate the UV energy as harmless heat energy whilst remaining chemically unchanged. UVAs can be both phenolic and non-phenolic in structure, and differ in the mechanism by which they prevent photodegradation. The UVAs which contain an intramolecular hydrogen bond (IMHB) are the most effective as this facilitates a charge transfer absorption between the donor and acceptor atoms and plays a key role in converting absorbed ultraviolet light into harmless heat energy. The most well-known phenolic UVAs with an O-H-O IMHB are the 2-hydroxybenzophenone (BP)^{49,50} family of compounds, whilst the most common phenolic UVAs with an O-H-N IMHB are the 2-(hydroxyphenyl)benzotriazole (BT)⁵¹ and 2-(2-hydroxyphenyl)-1,3,5-triazine (TA)^{52,53} derivatives (Figure 1.12).

Derivatives of BT and TA, such as **1.8** and **1.10**, respectively, usually display two absorption maxima, one in the UV-B region at approximately 300 nm and another in the UV-A region above 320 nm. The BP UV absorbers such as **1.9** display a weaker

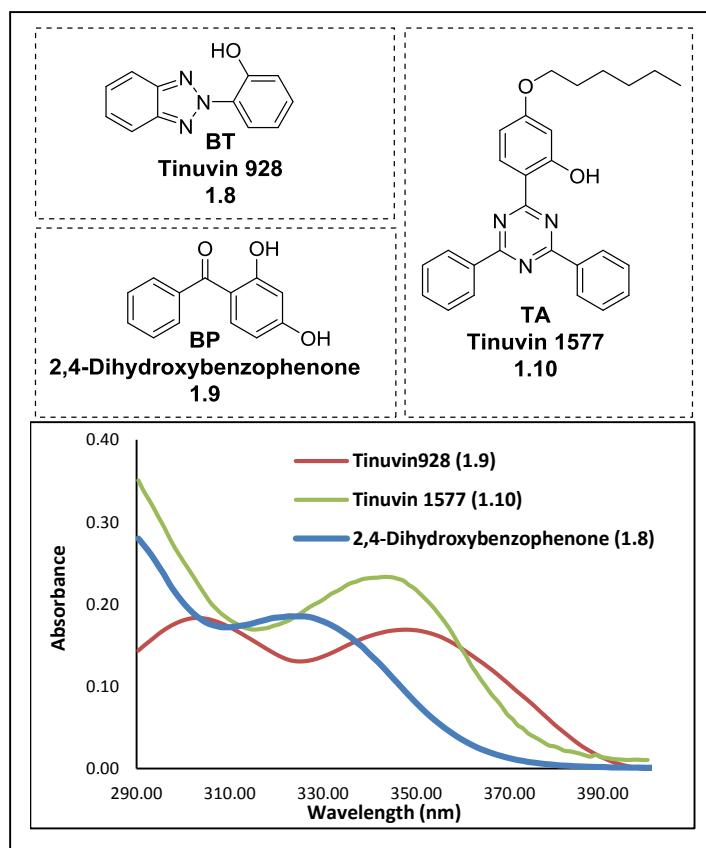


Fig. 1.12 – Chemical structures and UV spectra of 2,4-dihydroxybenzophenone, Tinuvin 928 and Tinuvin 1577 absorption in comparison to their BT and TA counterparts. The TA derivatives possess the strongest absorption in the UV-B region, and BT in the UV-A region. UVAs have high absorption coefficients at the wavelengths responsible for photodegradation of polymers. It is believed that UVAs with higher molar extinction coefficients (ϵ) at the wavelengths responsible for photodegradation are the more efficient photostabilisers. The molar extinction coefficients can be determined using the Lambert-Beer law⁵⁴ (Equation 1.3).

Eq. 1.3
$$A = \log \frac{I_0}{I} = \epsilon cl$$

Dobashi *et al.*^{55,56} disputed the relationship between the absorbance of UVAs and the photostabilisation efficiency. The group carried out photo-oxidation of a solution of styrene in chlorobenzene with UV irradiation above 210 nm, in the presence of various UVAs. Oxidation rates were obtained based on the oxidation rate in the absence of UVA. Although the study did not include TA derivatives, the findings

showed that the photostabilising effect did not depend solely on the molar extinction coefficient. Dobashi discovered a clear relationship between the photostabilising effect and the maximum wavelength of absorption (λ_{\max}) of the UVA. Dobashi demonstrated that BP and BT ultraviolet absorbers with higher λ_{\max} were the superior photostabilisers. The strength of absorbance only came into play for UVAs with the same λ_{\max} and, in this case, the UVA with the higher ϵ was the superior stabiliser. These findings support the work of Fechine,³⁴ who highlighted the importance of UVAs that absorb low energy, long wavelength light, which is deeply penetrating and causes fluorescent products in PET degradation.

1.5.2 ESIPT Mechanism

One common characteristic of phenolic UVAs is their participation in excited state intramolecular proton transfer (ESIPT) (Figure 1.13).^{57,58} This mechanism allows the conversion of UV radiation into vibrational (thermal) energy through radiationless deactivation. ESIPT is witnessed in planar 5- and 6-membered rings which have intramolecular hydrogen bonding between the phenolic hydrogen and a heteroatom. The heteroatom is either a nitrogen atom, from triazole and triazine derivatives, or an oxygen atom, from benzophenone and salicylate derivatives.

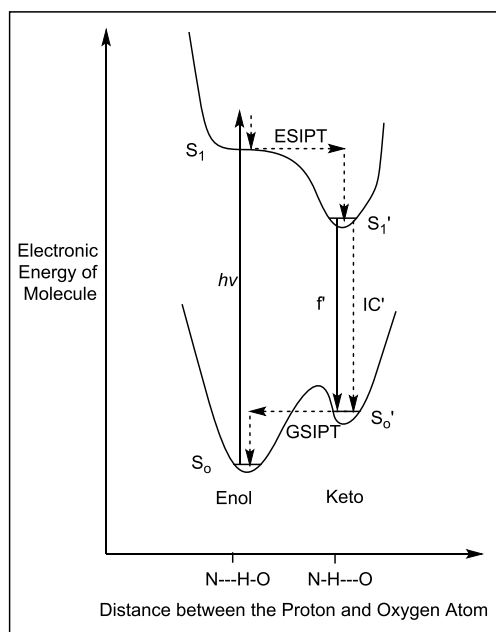


Fig. 1.13 - The radiationless deactivation scheme of a UVA⁵⁷

Once the phenolic UVA absorbs UV light, the molecule is promoted to the first excited state (S_1). The S_1 state can deactivate in a number of ways without emitting any radiation. These radiationless pathways include internal conversion (IC) followed by vibrational relaxation back to the ground state (S_0), intersystem crossing (ISC) to yield the triplet state T_1 , or excited state intramolecular proton transfer (ESIPT). ESIPT is the preferred process for an effective UVA, the reason being that the excited molecule has a much more acidic phenolic group in comparison to the ground state (S_0) species.⁵⁷ The rate of intramolecular proton transfer is greatly enhanced in molecules containing both an acidic and a basic moiety in close proximity on a single molecule. The lifetime of the S_1 excited state in an effective UVA is extremely short ($< 10^{-11}$ s) due to the rapid ESIPT process which converts S_1 enol into the keto tautomer form (S_1') (Figure 1.14).⁵⁹ This excited keto tautomer deactivates the excitation energy to form the ground state of the keto tautomer (S_0') by internal conversion (IC') and subsequently vibrational relaxation. Otterstedt⁵⁸ postulated that the rate of internal conversion was inversely proportional to the difference of energy between the excited and ground state keto tautomer. Otterstedt argued that IC' is more favourable than IC because the energy gap between the excited and ground state keto tautomer is smaller in comparison to the enol tautomer. Radiationless deactivation can occur by NH or OH stretching, out-of-plane bending and/or torsion between oxyaryl and heterocycle.⁵² The final stage is a ground state intramolecular proton transfer (GSIPT) to generate the starting phenolic form in the initial ground state (S_0), a slower process compared to ESIPT ($\sim 10^3$ s⁻¹).

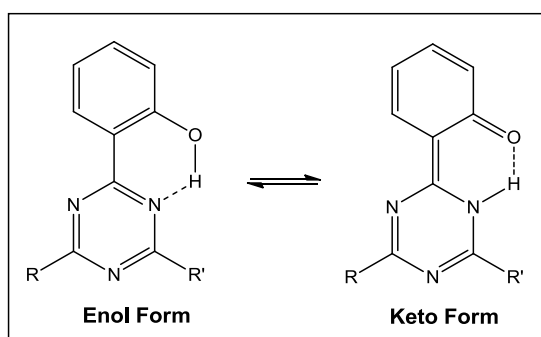


Fig. 1.14 - Intramolecular proton transfer equilibrium for keto and enol tautomers of a TA derivative⁵⁹

More recent work by Shizuka *et al.*^{60,61} studied the (1-hydroxy-2-naphthyl) triazine and pyrimidine derivatives using laser photolysis and reported that the ESIPT process was followed by a *cis-trans* isomerisation of the excited keto tautomer (Figure 1.15). Shizuka explained that the reverse intramolecular proton transfer would be more favourable in the *cis* conformation in comparison to the *trans* keto tautomer. Once the keto tautomer is in the *trans* conformation, it deactivates through vibrational relaxation, switches back to the *cis* keto conformer and GSIPT. The group ascribed a transient absorption at 450 nm to the *trans* keto tautomer. A study by Kramer⁶² compared the reorientation around the heterocycle-resorcinylyl bond in a tri-aryl triazine (**1.11**) and pyrimidine (**1.12**) compound using ¹H and ¹³C NMR spectroscopy (Figure 1.15). The group postulated that the IMHBs continually re-orientate around the triazine ring, switching between nitrogen atoms *via* rotation around the triazine-resorcinylyl bond, all within the NMR time scale. The protons *ortho* to the triazine ring display a broadening in the ¹H NMR spectrum of **1.11** due to chemical exchange broadening. The same re-orientation is not observed in **1.12** since the IMHB cannot remain intact. Broad peaks are observed for the carbons involved in the IMHB cleavage and re-closure for **1.11** in the ¹³C NMR spectrum, whilst the spectrum for **1.12** shows sharp and well defined peaks.

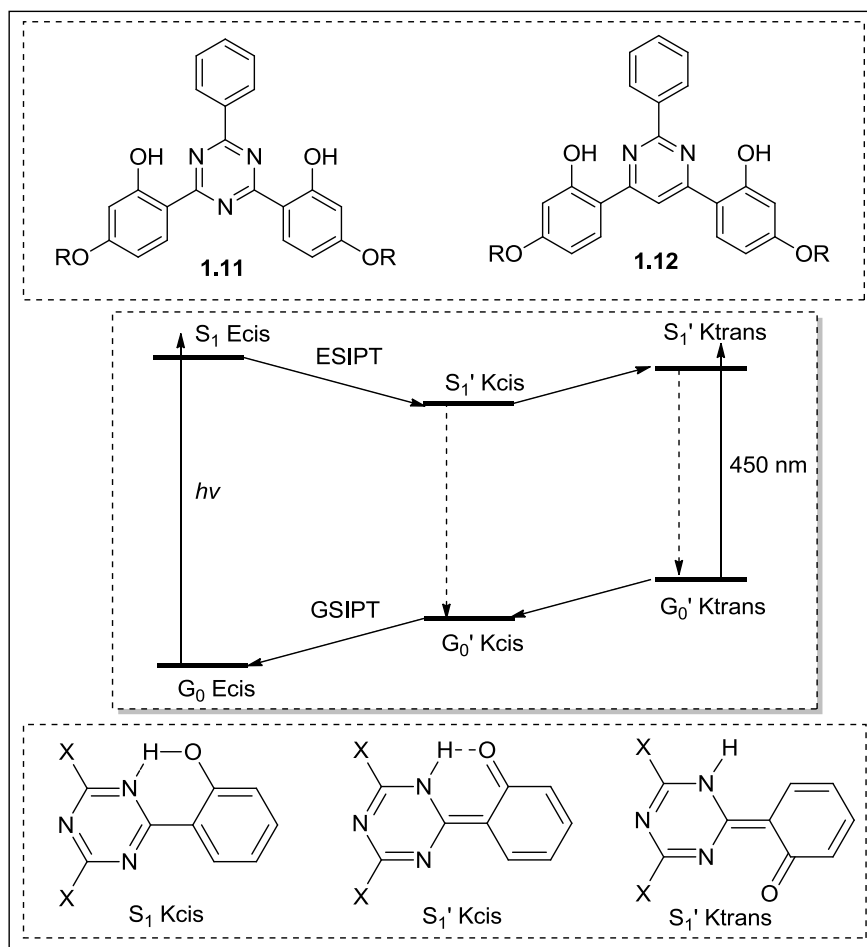


Fig. 1.15 - ES IPT process followed by *cis-trans* relaxation for a TA derivative^{52,60,61}

The ES IPT process can be repeated providing the intramolecular hydrogen bond and planarity remain in the UVA molecule. The UVA must be resistant to the breaking of the IMHB and it must maintain a planar geometry. Turro and co-workers⁶³ studied the photochemical effect of UVAs in polar solvents such as dimethyl sulfoxide (DMSO) and the effect of sterically bulky groups capable of protecting the IMHB. It is common for UVAs to fluoresce or phosphoresce upon the disruption of the IMHB. Once the intramolecular hydrogen bond is broken, ES IPT is no longer favourable and the excited state species seeks an alternative route for energy dissipation such as fluorescence, phosphorescence or IC. The group irradiated two different benzotriazoles, **1.13** and **1.14**, with a laser pulse (308 nm) in hexane and found no fluorescence emission in the non-polar environment (Figure 1.16). In DMSO solution, strong fluorescent emission was observed for **1.14**, indicating the breaking of the

IMHB. Under the same excitation condition, the fluorescence spectrum of the **1.13** was significantly lower in intensity with respect to **1.14**. The difference was attributed to the sterically bulky groups shielding the IMHB from the polar DMSO molecules.

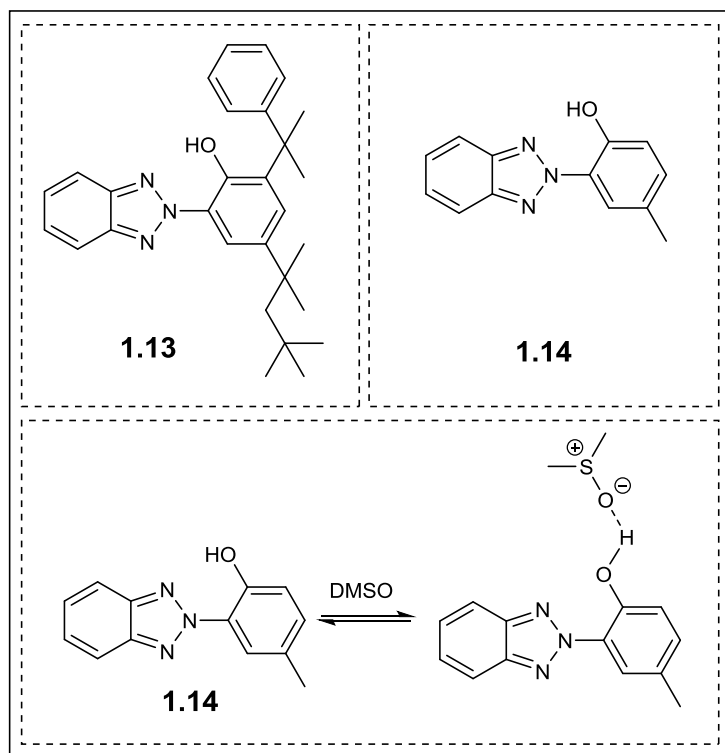


Fig. 1.16 – The disruption of an IMHB in a polar environment⁶³

Dobashi examined the relationship between the IMHB and the UVA performance⁵⁶ by comparing the photostabilising abilities of BPs, BTs and phenyl salicylates. The results determined that the strength of the IMHB does not always correlate with the performance of the UVA. The efficacy of the BPs and BTs were far superior compared to the phenyl salicylates, even although BPs and BTs have weaker IMHBs.

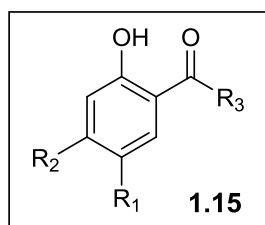


Fig. 1.17 – Chemical structure of 2'-hydroxyacetophenone template used in the Dobashi study⁵⁵

Dobashi observed the significance of various substituents on the photostabilising effect of **1.15** (Figure 1.17).⁵⁵ The group found that increasing the electron density on the hydroxyl group by having electron-donating groups in the R₁ position improved the photostabilising effect. Electron-donating groups in the R₂ position increased the electron density on the carbonyl group and this decreased the photostabilising effect. Having an electron-withdrawing group in the R₂ position showed a very slight improvement in the photostabilising ability. The most effective substituents at increasing the photostabilising effect in the R₃ position were those which enhanced the conjugation of the molecule, for example a phenyl ring.

1.5.3 2-(2-Hydroxyphenyl)-1,3,5-triazines (TA)

2-Hydroxybenzophenones were the first industrially utilised UVAs, but they were poor UV screens and were soon replaced by BT derivatives in the early 1980s. A decade later the BTs were substituted for the superior TA compounds; the latter possessing a stronger IMHB (Figure 1.18).⁶⁴ The strength of the IMHB was clear to see when comparing crystal structures of TA and BT. As a consequence of a stronger IMHB in TA, the intramolecular hydrogen bond is shorter in length. Another significant difference is the high chemical shift observed for the phenol group.⁶² In polar solvents, such as DMSO, the intensity of the absorption spectra of BPs and BTs are reduced due to the disruption of the IMHB, however this is not observed in TAs due to the more robust IMHB.⁶⁴ Additionally, TA derivatives are more resistant to heat and cause less yellowing to a polymer matrix.^{65,66} Furthermore, the spectral properties of TAs can be finely tuned, more so than BT additives, by chemical modification of the chromophoric structure. The versatile nature of triazine chemistry has played a large role in the dominance of the TA additives.

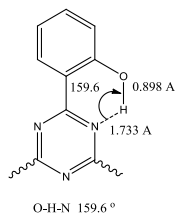
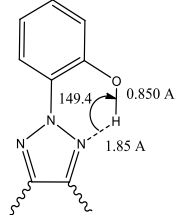
UVA	pKa	δH	$\bar{\nu}$ (O-H str.)
 <p>O-H-N 159.6°</p>	10.3	13.4 ppm	2800 cm ⁻¹
 <p>O-H-N 149.4°</p>	9.3	11.1 ppm	3080 cm ⁻¹

Fig. 1.18 - Spectral and crystallographic data of TA and BT derivatives⁶²

A paper by Shizuka⁵⁷ in 1985 studied various hydroxyphenyl-1,3,5-triazines, examining the influence of the heterocyclic ring bearing electron-donating -N(Me)₂ moieties on the fluorescence emission (Figure 1.19). All three compounds, **1.16**, **1.17** and **1.18**, showed proton transfer fluorescence emission at 500 nm, a green fluorescence with a large Stokes shift ($\sim 10,000$ cm⁻¹) ascribed to the excited keto tautomer. The study reported that increasing the electron density of the molecule increased the strength of the IMHB and increased the yield of the keto tautomer from ESIPT. Shizuka proposed that the proton transfer process from the excited enol conformer proceeds without an energy barrier, although it is in competition with the radiationless deactivation back to the ground state enol. A strong IMHB increases the activation barrier for the IC process of the excited enol and therefore the quantum yield of fluorescence for the keto tautomer increases in the order of **1.16** < **1.17** < **1.18**. Paterson *et al.*⁶⁷ reiterated that due to the minimum degree of molecular motion involved in the ESIPT pathway, a strong IMHB which maintains the planarity of the molecule is crucial. The Paterson study also agreed that the ESIPT process proceeded without an energy barrier, however it remains in competition with radiationless deactivation of the excited enol tautomer.

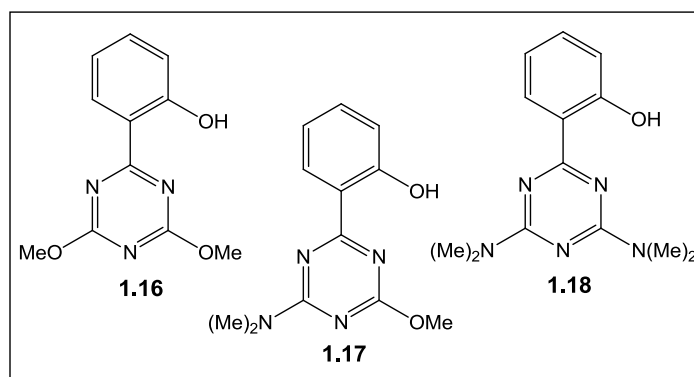


Fig. 1.19 – Structures of hydroxyphenyl-1,3,5-triazines examined in a Shizuka study⁵⁷

Kramer *et al.*⁶² measured the proton transfer fluorescence of mono-, di- and tri-aryl triazines (Figure 1.20). The mono-aryl **1.19** exhibited fluorescence from the excited keto tautomer, in high quantum yield and with a large Stokes shift ($\sim 10\,000\text{ cm}^{-1}$). The di-aryl **1.20** exhibited a decrease in the excited keto tautomer fluorescence, which was then completely quenched for the tri-aryl **1.21**. The group explained that the aryl groups offered additional vibration modes which made the vibrationless deactivation of the excited keto tautomer more favourable and lowered the quantum yield of proton transfer fluorescence.

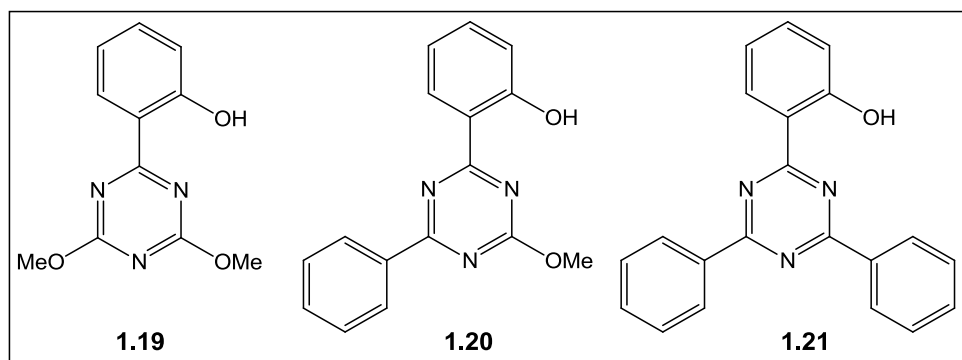


Fig. 1.20 – Structures of mono-, di- and tri-aryl triazines investigated by Kramer *et al.*⁶²

Kramer and co-workers^{52,64} showed that increasing the number of IMHBs in tri-aryl triazines (Figure 1.21) increases the yield of proton transfer fluorescence in the order **1.22** < **1.23** < **1.24** due to an increase in the electron density of the molecule. The fluorescence also increased when introducing other electron-donating groups to the phenyl rings, increasing in the order **1.25** < **1.26** < **1.27**. The electron-donating moieties increased the basicity of the heterocyclic nitrogen atoms which resulted in

stronger intramolecular hydrogen bonding. This, in turn, increased the extinction coefficient of the UVAs, however this also amplified the proton transfer fluorescence by impeding radiationless deactivation. The study went on to explain that the twisting vibration between aryl and heterocyclic moieties is more hindered as the strength of the IMHB is increased. This further supported the Shizuka theory of *cis-trans* isomerisation post intramolecular proton transfer.^{60,61} This led Kramer to conclude that the ideal UVA would be a tri-aryl triazine with an IMHB strong enough in the ground state to avoid disruption in a polar environment yet weak enough to allow radiationless deactivation. The UVA should absorb in long wavelength region with high extinction coefficients without protruding into the visible region to avoid colouring of the polymer. With these requirements in mind, a tri-aryl triazine should have no more than two electron-donating methoxy groups in the aryl moieties.

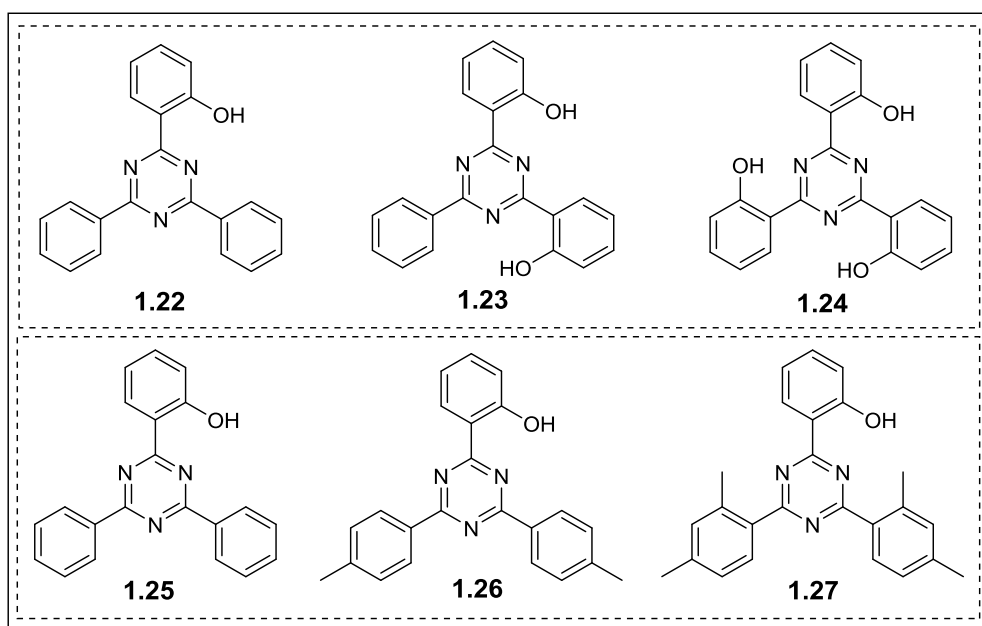


Fig. 1.21 – Structures of tri-aryl triazines investigated by Kramer^{52,64}

1.5.4 Tinuvin 1577

Tinuvin 1577 (**1.10**) is the leading UVA additive in the market today (Figure 1.22). This TA derivative is manufactured by BASF and is currently the UVA of choice for DuPont Teijin Films as an additive in PET. Tinuvin 1577 **1.10** is one of the most

effective UV stabilisers available. As well as being a powerful UV screen, Tinuvin 1577 **1.10** exhibits a robust IMHB and resilience to polar environments.^{33,34,65,66,68,69}

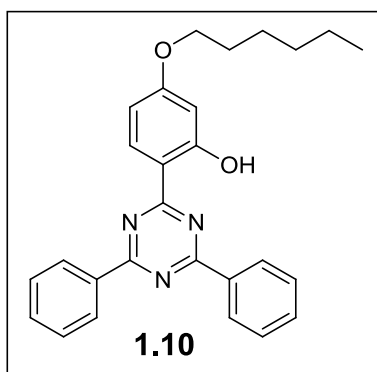


Fig. 1.22 - Tinuvin 1577 **1.10**

A study by Bottino examined the effect of various loadings of Tinuvin 1577 **1.10** in polystyrene (PS). The group studied photo-oxidation of PS films with 0, 0.1, 0.5, 1.0, 2.0 and 4.0 wt. % of Tinuvin 1577 **1.10**, using XPS analysis. The films were subjected to 22 days of UV light ($\lambda > 300$ nm) and the oxygen/carbon ratios were measured at regular intervals. The stabilising effect of the samples containing 0.1 and 0.5 wt. % of Tinuvin 1577 **1.10** showed a small stabilising effect in comparison to the control. The stabilising effect increased for PS films containing 1.0 and 2.0 wt. % of Tinuvin 1577 **1.10**, respectively, and a very small difference in stabilisation was observed between films with 2.0 and 4.0 wt. % of Tinuvin 1577 **1.10**.

Rajan *et al.*⁶⁵ compared the photostabilising effect of Tinuvin 1577 **1.10** with the BT UVA **1.28** (Figure 1.23) in polycarbonate/poly(acrylonitrile-co-butadiene-co-styrene) blends. Samples containing 0, 0.5 and 1.0 wt. % of UVA were irradiated using a xenon lamp (300-800 nm) for 672 hours in a dry atmosphere. Rajan measured the intensity of absorbance at 390 nm in the UV spectrum, and this increased with photodegradation. Tinuvin 1577 **1.10** showed a lower intensity of absorbance for 0.5 and 1.0 wt. % loadings in comparison to **1.28**. The group monitored the main products of degradation using FT-IR spectroscopy in the ATR mode, analysing the 1713 cm^{-1} band attributed to carboxylic acids. The 1713 cm^{-1} band for samples protected by **1.28** showed a larger increase in intensity than the samples containing

Tinuvin 1577 **1.10**. The polymer blends containing Tinuvin 1577 **1.10** also exhibited lower yellowing index values and lower decrease in molecular weight when compared to samples containing the BT additive.

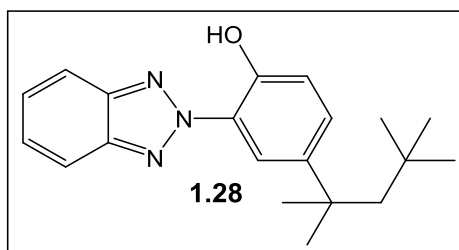


Fig. 1.23 – Structure of 1.28

1.6 Polymerisable Ultraviolet Absorbers

One major disadvantage that Tinuvin 1577 **1.10** and all other UVAs share is the potential leaching of stabiliser from the polymer matrix.^{70,71} The loss of additive with time leads to an increase in the rate of UV-induced degradation and deterioration of key mechanical properties with respect to time. This is of concern for applications where the polymers are exposed to a high level of UV radiation, e.g., PET films in photovoltaic cells. It is of the utmost importance for polymer manufacturers to increase the lifetime of UV protection, and one way in which this can potentially be achieved is by developing and exploiting polymerisable UVAs. In addition to increasing the lifetime of UV protection, polymerisable UVAs can reduce the risk of volatilisation during processing and provide a more even distribution of stabiliser across the polymer matrix.⁷¹

1.6.1 Chain-Growth Polymerised Ultraviolet Absorbers

There has been extensive work on incorporating UVAs with vinyl functionality, especially BP and BT derivatives,⁷¹⁻⁷⁶ for copolymerisation through a free radical polymerisation route. Al-Mobasher *et al.*⁷³ copolymerised BT monomers onto poly(vinyl chloride) and analysed the copolymers using GPC with UV detection. The GPC chromatogram of the copolymer showed polymerised UVA and also unreacted UVA in the oligomeric/monomeric region. The group purified the copolymers by dissolving in THF and precipitating in petroleum ether (40-60 °C). Upon purification,

the UV signal for the monomeric region in the size exclusion chromatogram disappeared. Bailey and Vogl⁷¹ reported that polymeric BPs were more resistant to solvent extraction and volatilisation during high temperature processing compared to their non-polymerisable additive counterparts. After subjecting stabilised films to one hour of trichloroethylene extraction, the films containing polymeric stabiliser were more resistant to photodegradation compared to films processed with additive BP absorbers.

Duennenberger and co-workers^{77,78} divulged the synthesis of TA monomers bearing two or three resorcinylic moieties and polymerisable vinyl groups (Figure 1.24). The inventors claimed that these monomers (**1.29-1.37**) could be incorporated into polyacrylonitrile, poly(vinyl chloride), polyethylene and polypropylene.

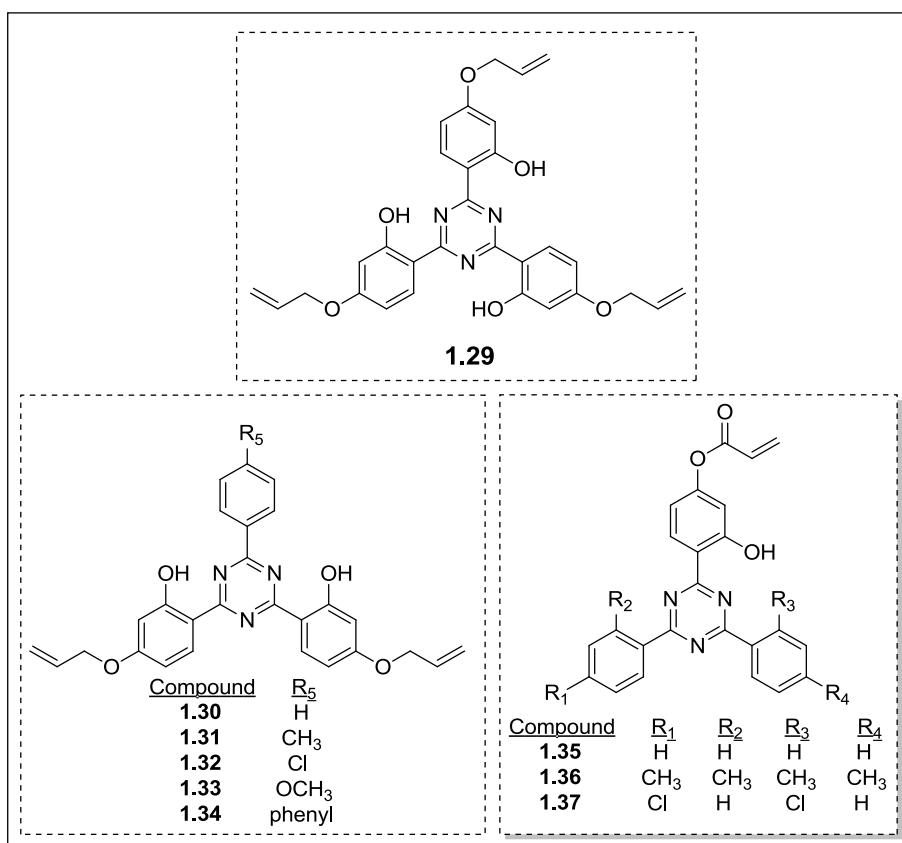


Fig. 1.24 – Polymerisable TA monomers synthesised by Duennenberger *et al.*^{77,78}

More recent studies by Kramer *et al.* described the synthesis of **1.38** and **1.39** (Figure 1.25) and their subsequent free radical copolymerisation with styrene and methyl

methacrylate.^{64,79} The absorption spectra of **1.38** and **1.39** were unchanged by copolymerisation, indicating that the IMHB was intact and that these compounds were copolymerised without detriment to the spectral properties. Kramer reported an increase in phosphorescence and a decrease in proton transfer fluorescence in the poly(methyl methacrylate) copolymer compared to the admixed polymer. The radiationless deactivation of the incorporated monomers in the poly(methyl methacrylate) matrix was less efficient due to opening of the intramolecular hydrogen bond in the polar environment. The Kramer group proposed that the increase in the triplet state population in the methyl methacrylate copolymer was due to the more crowded arrangement of the copolymer compared to the admixed polymer.

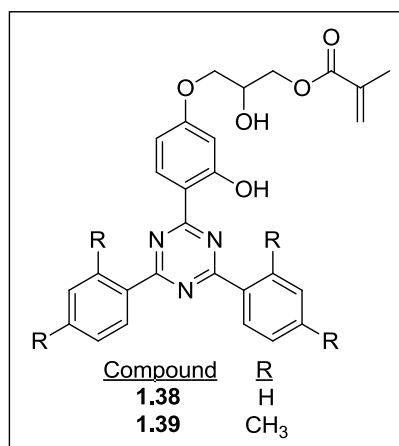


Fig. 1.25 - Polymerisable TA synthesised by Kramer *et al.*^{64,79,80}

As described in a patent, Birbaum *et al.*⁸⁰ (Figure 1.25) copolymerised **1.38** with a mixture of butyl acrylate, butyl methacrylate, hydroxyethyl acrylate and styrene. The copolymers were solvent cast on an aluminium sheet and heated in an oven to form films with a thickness of 40-45 μm . The films were weathered and the gloss retention was measured after every 400 hours of exposure. A copolymer containing 1.5 wt. % of incorporated UVA heavily outperformed the unprotected control, and the most stable samples were those containing 1.5 wt. % of **1.38** along with 0.5 wt. % of a photo-antioxidant HALS. HALS prevents photodegradation *via* different mechanisms

to UVAs and photostabilisation was enhanced when both UVA and HALS were employed together.

Recent work by Bojinov documented a “synergism” effect in molecules with both UVA and photo-antioxidant HALS fragments. Bojinov^{81–87} synthesised various polymerisable ultraviolet stabilisers with a variety of functionalities (Figure 1.26). Compounds **1.40–1.49** contained both a UVA and a photo-antioxidant fragment which gave synergistic properties and exhibited greater photostabilisation compared to compounds with only one fragment. Furthermore, the structures synthesised by Bojinov contained polymerisable vinyl groups and were incorporated in a free radical copolymerisation with acrylonitrile. The degree of incorporation of the polymerisable stabiliser into the polymer chain was higher for compounds with a second polymerisable allyl group. The compounds with two unsaturated vinyl groups were found to be superior photostabilisers compared to species with only one polymerisable allyl group.

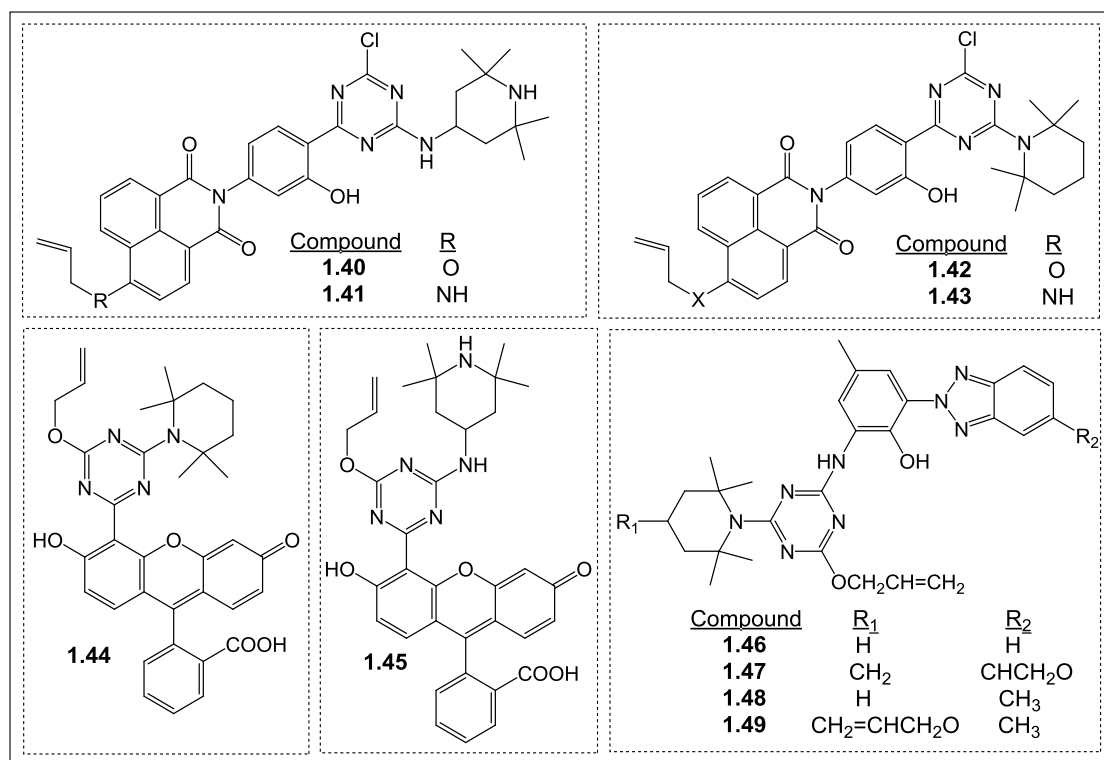


Fig. 1.26 - UVAs synthesised by Bojinov and co-workers bearing polymerisable vinyl groups^{81–87}

1.6.2 Step-Growth Polymerised Ultraviolet Absorbers

Bailey and Vogl⁷¹ reported that **1.50** and **1.51** could be copolymerised to generate polyamide and polyurethane copolymers (Figure 1.27). In addition to preventing leaching, Bailey and Vogl reported that polymeric UVAs were less prone to volatilisation and were more evenly distributed within the polymer matrix. The spectral profiles of the polymerisable UVAs remained unchanged after they were covalently incorporated into the polymer chain. A more recent study by Sankey and Jones disclosed the synthesis of benzophenone monomers **1.52** and **1.53** and a triazole monomer **1.54**. These UVA monomers were copolymerised with *bis*(hydroxyethyl)isophthalate (BHEI) to obtain copolymers of PEI.²⁷

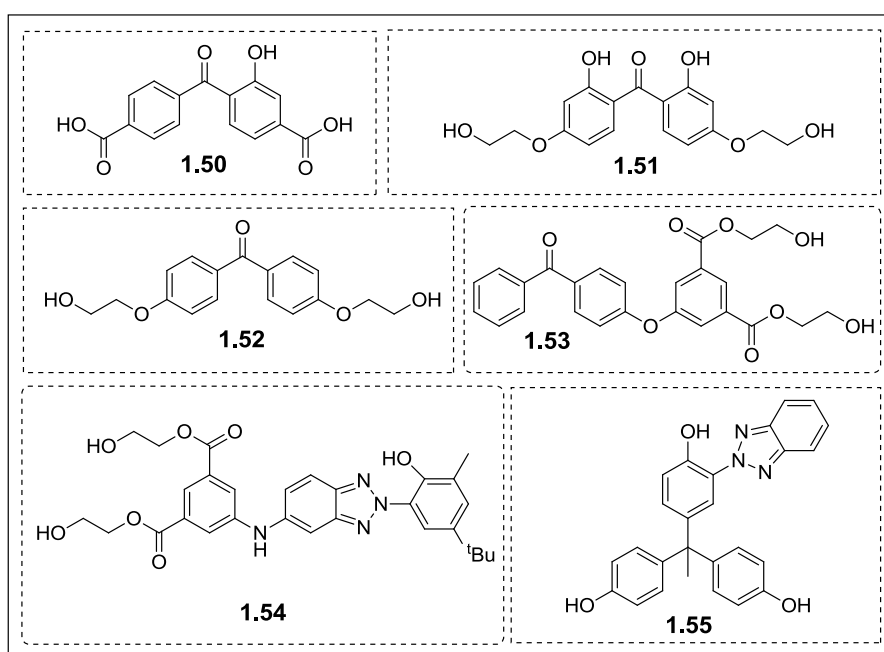


Fig. 1.27 - Polymerisable UVAs synthesised by Bailey⁷¹, Jones²⁷ and Kulia *et al.*⁸⁸

Kulia *et al.*⁸⁸ synthesised **1.55** (Figure 1.27), and incorporated it covalently into polysulfone and polycarbonate copolymer films. The UV stability of the copolymer films was compared with films with similar amounts of commercialised BT additive, **1.28** (Figure 1.23). The films were exposed to UV light of up to 340 nm in a Q-UV weatherometer and Kulia measured the yellowing index and the intensity of absorbance at 400 nm in the UV absorption spectra after regular intervals. The

copolymers exhibited superior stability against ultraviolet light compared to polycarbonate and polysulfone blends with a comparable amount of **1.28**. Furthermore, **1.55** was more thermally stable than **1.28**, which brings a significant advantage in high temperature processing.

A number of polymerisable TAs have been patented over the years. In 1966 Duenenberger *et al.*⁷⁷ synthesised a number of TA monomers (**1.56-1.62** and **1.65-1.67**) capable of undergoing step-growth polymerisation to yield polyesters (Figure 1.28). Migdal *et al.*⁸⁹ filed a patent in 1989 which included the synthesis of **1.63** and **1.64**, and their subsequent copolymerisation into PET. Migdal and co-workers reported that **1.63** and **1.64** had no adverse effects on the polymerisation kinetics and there was no evidence of volatilisation during processing.

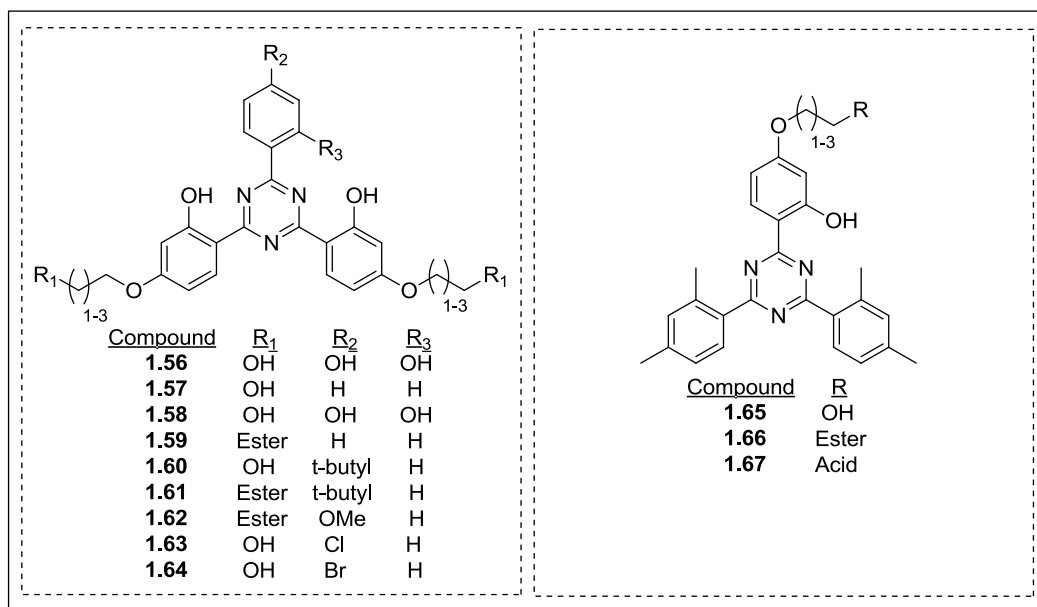


Fig. 1.28 – TA monomers synthesised and copolymerised by Duenenberger⁷⁷ and Migdal⁸⁹

Patents by Bolle *et al.*^{90,91} documented the synthesis of a number of different TA monomers (Figure 1.29). Bolle and co-workers claimed the copolymerisation of various monofunctional monomers **1.71-1.78**, where the R₁ group is a straight or branched chain alkyl of 1 to 24 carbon atoms which can bear one polymerisable moiety. Bolle also copolymerised bi- and trifunctional monomers **1.68-1.70**. The patent explains that these UV absorbing monomers were copolymerised with

polyesters, polyamides and polyisocyanates. The covalent incorporation was deemed successful by measuring the UV absorption coefficient at 332 nm before and after solvent extraction using dichloromethane.

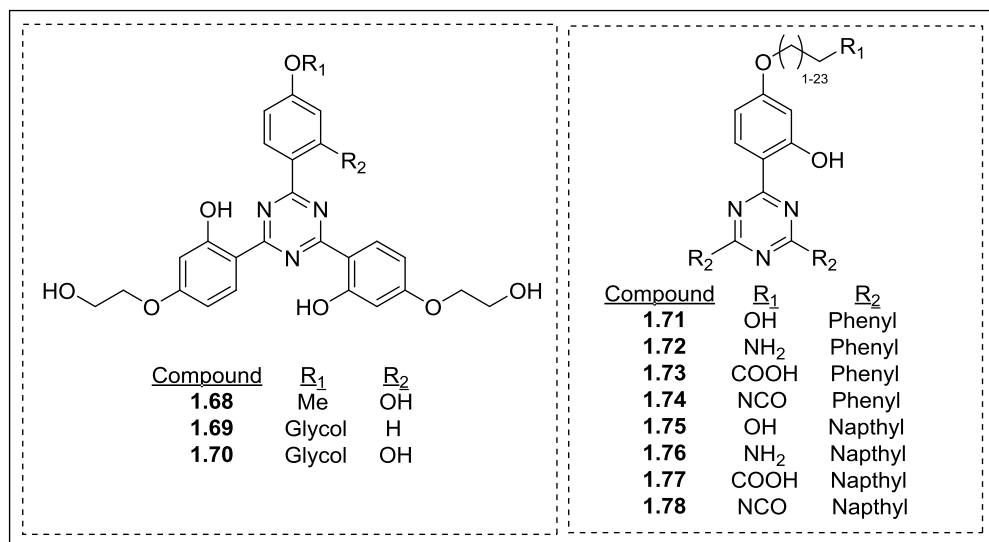


Fig. 1.29 – TA monomers synthesised and copolymerised by Bolle^{90,91}

A 1994 patent by *Valet et al.*⁹² describes the copolymerisation of a wide range of TA monomers (**1.79-1.89**) in coating compositions (Figure 1.30). The three main components of the coatings were a mixture of polyester resin binder, crosslinker, catalyst and 0.25-7.5 % of UV absorbing monomer all in a solvent in which the composition was soluble. The mixtures of polyester were cured at 50-130 °C for 30 minutes on a number of surfaces such as metal, wood and plastics. Aluminium sheets with polyurethane coatings containing 2.0 wt. % of **1.82** were exposed to UV light at 60 °C and the yellowing index was measured after 24 hours. The coatings incorporated with polymerisable **1.82** experienced less yellowing with respect to coatings containing 2.0 wt. % of UV additives which had the same chromophore.

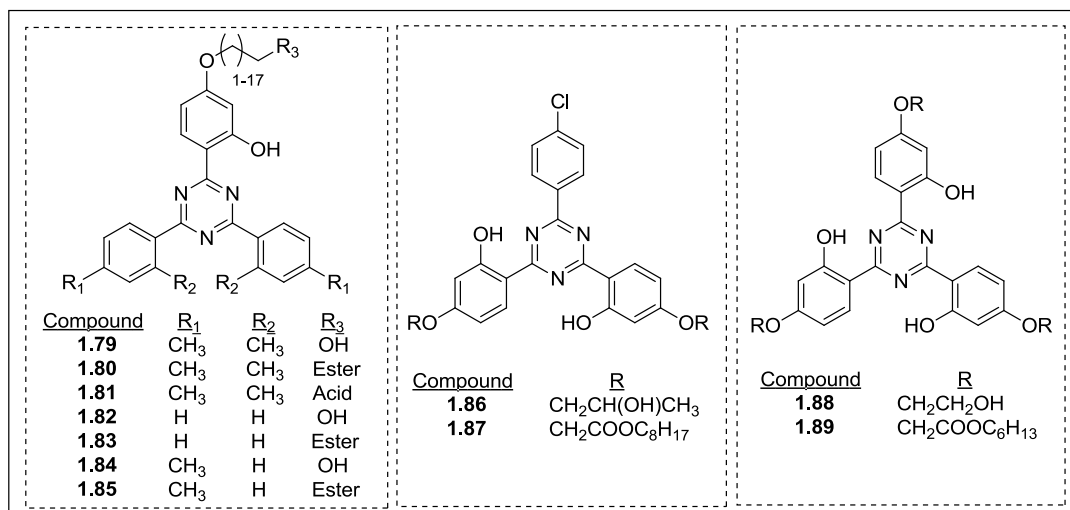


Fig. 1.30 – TA monomers copolymerised in coating compositions by Valet⁹²

1.7 1,3,5-Triazine Chemistry and the Synthesis of TA Derivatives

The core of TA derivatives is comprised of a 1,3,5-triazine ring, with one or more of the nitrogen atoms participating in an IMHB. TA-based ultraviolet absorbers can be synthesised from the readily available and inexpensive cyanuric chloride **1.90** (Figure 1.31),⁹³ which contains a 6-membered ring consisting of alternating nitrogen and carbon atoms. The carbon atoms are electrophilic, due to the presence of the more electronegative nitrogen and chlorine atoms, and are therefore susceptible to nucleophilic attack.

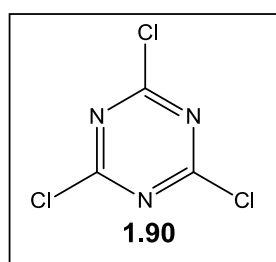


Fig. 1.31 - Cyanuric chloride **1.90**

Cyanuric chloride **1.90** is an attractive synthetic starting point as it provides a scaffold for more complex and multipurpose molecules. Each chlorine atom can be displaced independently by controlling the temperature of the reaction in the presence of nucleophilic reactants (Figure 1.32).⁹⁴ As a consequence of the first nucleophilic substitution being exothermic, the temperature must be kept at 0 °C. The second

chlorine can be displaced at room temperature, leaving the final chlorine to be substituted at the reflux temperature of the solvent used in the reaction.

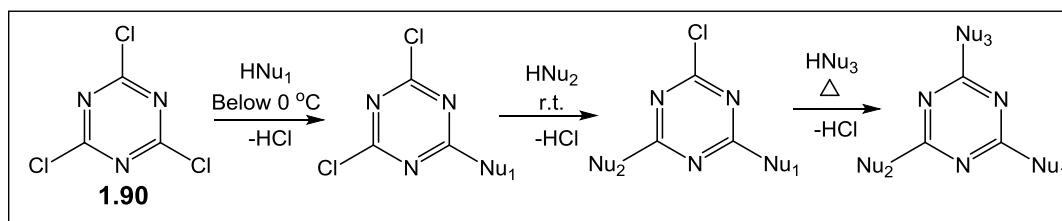


Fig. 1.32 – Temperature-controlled mono-, di- and tri- substitution of cyanuric chloride **1.90**⁹⁴

In addition to this thermally-controlled selectivity, one can potentially incorporate three different substituents. Each substitution can offer high yields and can be performed in a one-pot synthesis.⁹³ A wide range of nucleophiles have been employed in such reactions, for example amines,^{95,96} alcohols,^{97–99} phosphines^{100,101} and thiols.^{101,102} A number of the compounds in this section are relevant to UV absorbers whereas others are employed in different applications and have been included to display the synthetic potential of cyanuric chloride **1.90**.

1.7.1 Amine Nucleophiles

Amines are effective nucleophiles for displacing all the chlorines in 1,3,5-triazine systems. Usually, the substitution takes place in the presence of a base such as NaOH, NaHCO₃, K₂CO₃ or NEt₃ to neutralise the HCl produced as a by-product of the reaction (Figure 1.33). Bhat and Pandey⁹⁵ described the three-step synthesis of **1.96**, displacing the first chlorine at 0-5 °C with *p*-nitroaniline and recrystallising in ethanol to yield 83 % of **1.92**. The second chlorine was substituted with 1,2-diaminoethane at 40 °C, monitoring the reaction by TLC and recrystallising with ethanol to generate **1.94** in 75 % yield. The final stage installed piperazine by refluxing in 1,4-dioxane, using potassium carbonate as a base, to give **1.96** in 65 % yield. In another study, Pinson *et al.*⁹⁶ used morpholine to displace the first chlorine at a temperature of -20 °C in the presence of NEt₃. Pinson added water to dissolve the salts and collected the crude product by filtration and washed with methanol to yield 93 % of **1.98**. Pinson then incorporated **1.99** using potassium carbonate to displace the second chlorine at ambient reaction temperatures. The final step to incorporate a piperazine moiety

was achieved using microwave irradiation (90 W, 140 °C) for 30 minutes, recrystallising in ethyl acetate to generate **1.101** in 40 % yield.

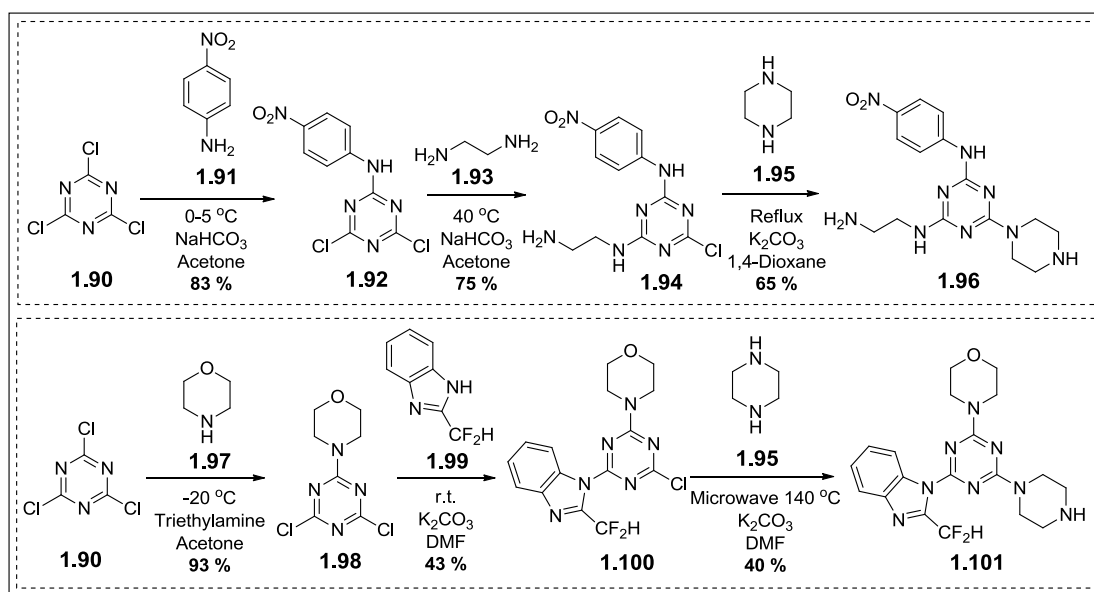


Fig. 1.33 –Amine nucleophile reactions undertaken by Bhat⁹⁵ and Pinson⁹⁶

1.7.2 Hydroxyl Nucleophiles

Aliphatic and aromatic hydroxyl groups can nucleophilically displace chlorines from cyanuric chloride **1.90**. The presence of a non-nucleophilic base is required such as *s*-collidine or *N,N*-diisopropylethylamine (DIPEA) (Figure 1.34). The Rolfe group⁹⁷ displaced the first chlorine using DIPEA and **1.103** in acetone. The reaction mixture was kept at 0 °C during the addition of **1.103** and then stirred at ambient temperature for a further 10 hours. The crude mixture was concentrated and purified by flash column chromatography to give **1.102** in an 83 % yield. A similar reaction was carried out by Bushan *et al.*⁹⁸ who employed **1.104** and *s*-collidine to generate the mono-substituted **1.105** in a yield of 79 %. Phenols can also be employed as nucleophiles and a study by Zhang⁹⁹ demonstrated this by substituting the final chlorine of **1.106** by stirring with potassium hydroxide and **1.107** at room temperature. Once the reaction was adjudged to be complete using TLC, the mixture was passed through a silica plug and washed with dichloromethane. The solvent was removed *in vacuo* to afford **1.108** in a 91 % yield without any further purification.

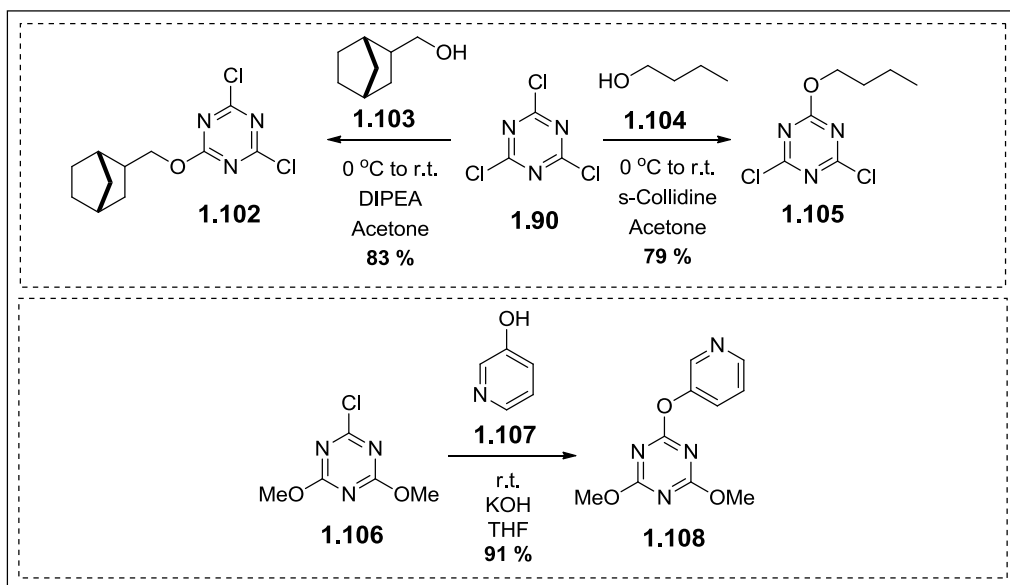


Fig. 1.34 – Alcohol nucleophile reactions demonstrated by Bushan,⁹⁸ Rolfe⁹⁷ and Zhang⁹⁹

1.7.3 Carbon Nucleophiles

In addition to amine and alcohol nucleophiles, the chlorines of cyanuric chloride **1.90** can be displaced to form carbon-carbon bonds through four different types of reactions:

- Grignard reactions
- Friedel-Crafts alkylations
- Suzuki couplings
- Halogen-lithium exchange

1.7.3.1 Grignard Reactions

Grignard reagents are most commonly employed to displace the first and second chlorine atoms in cyanuric chloride **1.90**. Grignard reactions exhibit great versatility for substituting both aliphatic and aromatic residues onto the 1,3,5-triazine framework. However, as is well known with Grignard reagents, the main disadvantage is that they cannot be employed in the presence of protic functional groups.

Mono-substituted products are commonly obtained by introducing a stoichiometric amount of the Grignard reagent at 0 °C, and once the addition is complete allowing the reaction mixture to warm to room temperature before quenching with water. (Figure 1.35).^{103–106} Pitts and colleagues synthesised **1.110** in anhydrous toluene by maintaining the reaction temperature at 0 °C.¹⁰⁴ There are examples of sp² (**1.111**), sp³ (**1.112**) and sp (**1.113**) hybridised carbon nucleophiles being employed effectively in these types of reactions.^{103,105,106}

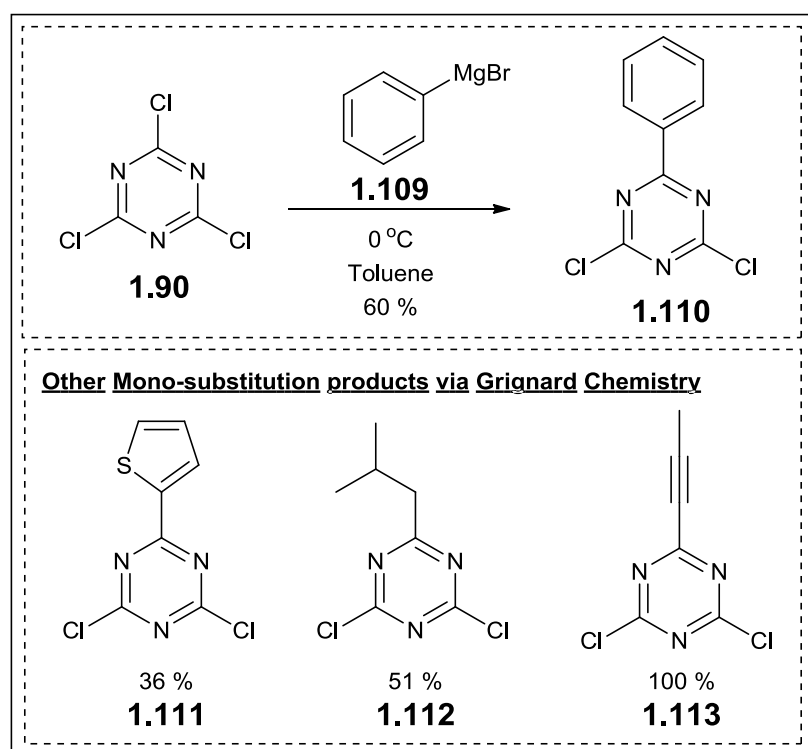


Fig. 1.35 - Mono-substituted 1,3,5-triazine products synthesised using Grignard reagents^{103–106}

The di-substituted 1,3,5-triazines are obtained by allowing the reaction to warm to room temperature (Figure 1.36).^{107–112} In a US patent by Kim *et al.*,¹⁰⁹ **1.114** (Figure 1.36) was prepared by adding a solution of phenylmagnesium bromide in dry THF to a solution of cyanuric chloride **1.90** in dry THF at 0 °C. The mixture was warmed to room temperature whilst agitating for 3 hours and purified by recrystallization from methanol. In some instances where the Grignard reagent is large or bulky, higher temperatures or catalysts are called upon to displace the second chlorine atom. For example, Kim and co-workers used two molar equivalents of 2-naphthylmagnesium

bromide in THF with respect to cyanuric chloride **1.90** and refluxed the reaction for 2 hours to generate **1.119** in 65 % yield.¹⁰⁹ Zhong *et al.*¹¹² synthesised the di-substituted **1.117** in 68 % yield by refluxing cyanuric chloride **1.90** with two equivalents of the Grignard reagent and separated the mixture by flash column chromatography. Hintermann¹⁰⁷ and co-workers carried out an extensive study involving copper catalysts in reactions between tertiary Grignard reagents and azacyclic intermediates. Hintermann prepared a solution of cyanuric chloride **1.90** in THF and added 3 mol % of CuI catalyst, two equivalents of Grignard reagent and maintained the reaction temperature at 0 °C. Employing a catalyst was an effective way of circumventing steric effects when using bulky Grignard reagents and achieving high yields in the production of **1.116** and **1.118**, respectively.

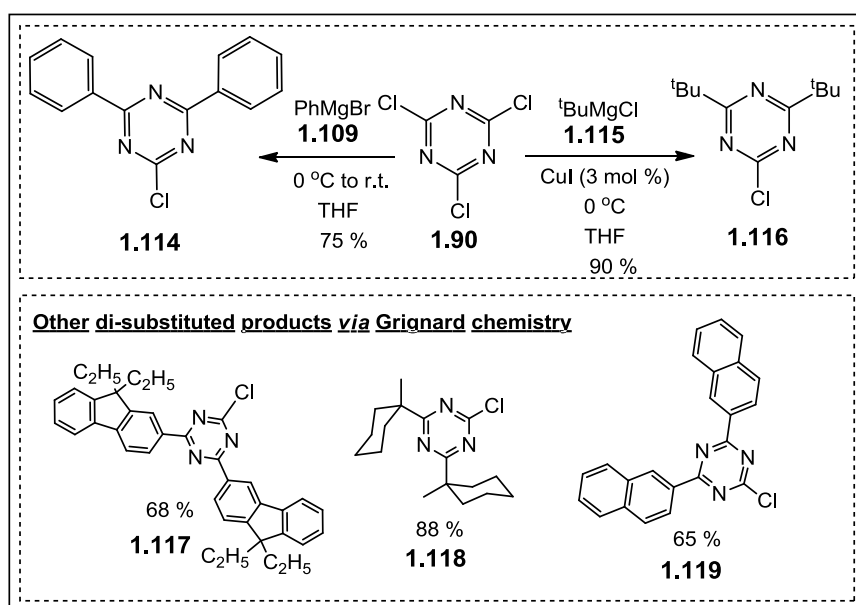


Fig. 1.36 – Di-substituted 1,3,5-triazines products synthesised *via* Grignard reagents and cyanuric chloride **1.90**^{107–112}

The Hintermann group did further work with synthesising tri-substituted 1,3,5-triazines using a copper catalyst in combination with tertiary Grignard reagents (Figure 1.37). One example had three equivalents of *tert*-butylmagnesium chloride reacting with 1 equivalent of cyanuric chloride **1.90**.¹⁰⁷ Hintermann's copper-catalysed system helped to substitute the three chlorines at room temperatures to yield 51 % of **1.120**. Naka *et al.* synthesised **1.122** in 58 % yield using 0.05 mol % of a

nickel catalyst and refluxing in THF for 12 hours.¹⁰⁹ The Naka group employed an excess of **1.121** with respect to cyanuric chloride **1.90** and purified the crude product by recrystallisation with a hexane/chloroform mixture (5/1).

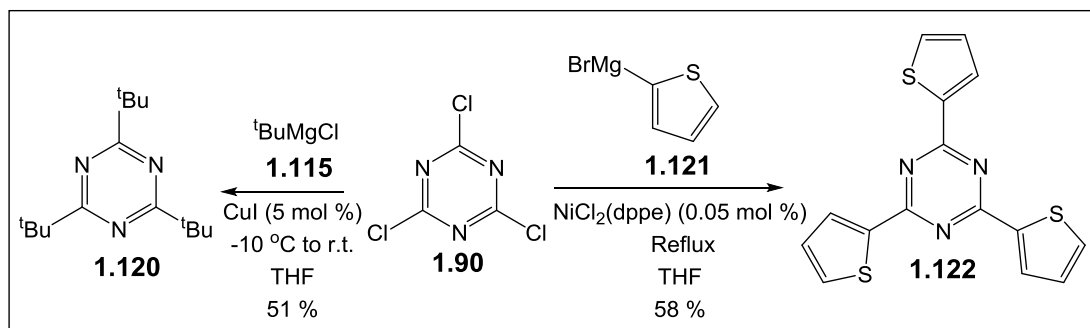


Fig. 1.37 – Tri-substituted 1,3,5-triazines synthesised *via* Grignard reagents and cyanuric chloride **1.90**^{107,113}

1.7.3.2 Friedel-Crafts Alkylations

The most common method used for incorporating aromatic residues onto a 1,3,5-triazine core is by Friedel-Crafts alkylation using aluminium trichloride catalyst (Figure 1.38). Bojinov⁸² and co-workers installed **1.125** onto cyanuric chloride **1.90** using a 1:1 stoichiometric ratio and AlCl_3 in xylene (Figure 1.38). The mixture was kept at 60 °C for 3 hours, 90 °C for 8 hours and then refluxed for 8 hours before quenching with water and hydrochloric acid. The crude material was purified *via* flash column chromatography to give 60 % of pure **1.126**. Wang¹¹⁴ and his colleagues synthesised **1.124** by stirring stoichiometric amounts of cyanuric chloride **1.90**, **1.123** and AlCl_3 at room temperature overnight. Wang removed the DCM solvent by distillation and quenched the residue with water before recrystallizing using THF. Migdal and co-workers⁸⁹ synthesised **1.127** and **1.128** by heating a mixture of cyanuric chloride **1.90** with AlCl_3 in 10 equivalents of chloro- or bromobenzene at 125 °C for 18 hours. The group quenched the reaction with water and removed the organic solvent by steam distillation. The crude products were recrystallised from acetonitrile, however the yields were unreported.

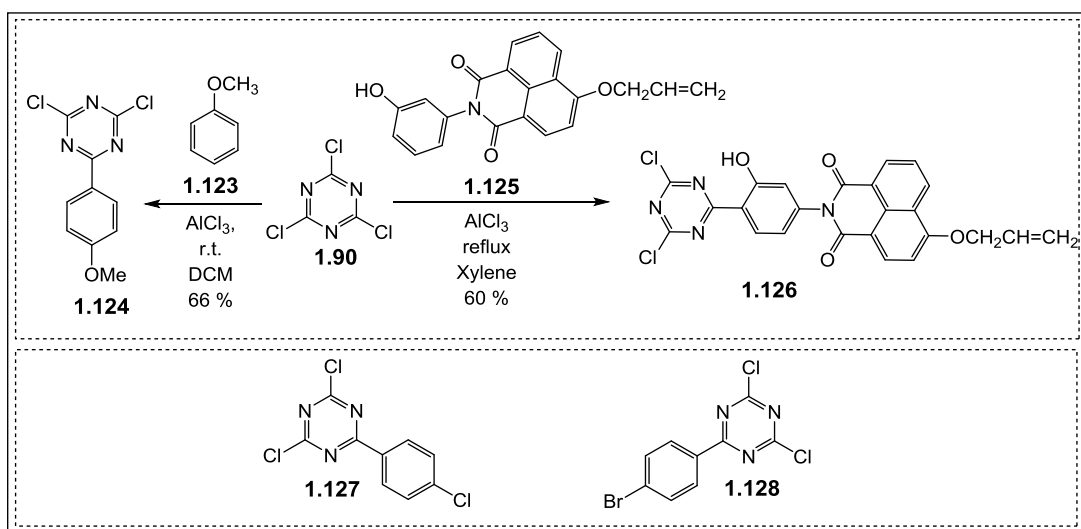


Fig. 1.38 – Examples of mono-substituted 1,3,5-triazines using Friedel-Crafts alkylation^{82,89,114}

Bojinov⁸³ employed the same method as mentioned above for displacing the second chlorine to synthesise **1.131** (Figure 1.39). A stoichiometric mixture of **1.129**, AlCl₃ catalyst and **1.130** was prepared and gradually brought to reflux over a period of 16 hours. The reaction mixture was quenched with ice water and acidified to pH 2 using 10 % aqueous HCl. The precipitate was collected by filtration, washed with water and dried to give crude **1.131** in a 51 % yield without any further purification. Gupta *et al.*¹¹⁵ replaced two chlorine atoms of cyanuric chloride **1.90** with *m*-xylene to synthesise the di-substituted **1.133**. However, and in contrast to Bojinov, Gupta and co-workers performed the reactions at ambient temperature. The reactions were monitored using HPLC analysis and it was found that, after 24 hours, 55 % of cyanuric chloride **1.90** had been converted and formed the mono-substituted by-product and the desired di-substituted product in a ratio of 95:5, respectively. However, the reaction reached 99 % conversion to **1.133** after 72 hours with a 72 % yield.

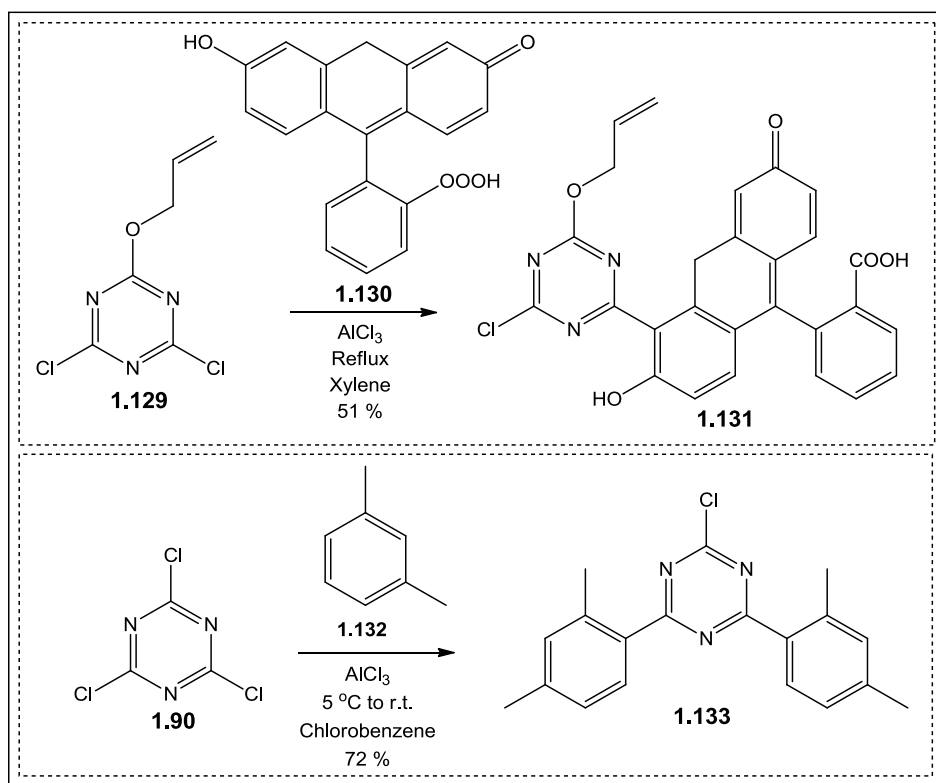


Fig. 1.39 – Examples of di-substituted 1,3,5-triazines using Friedel-Crafts alkylation^{83,115}

Eisler and Conn¹¹⁶ synthesised various 2,4,6-trisubstituted triazine derivatives by AlCl_3 catalysed Friedel-Crafts alkylations (Figure 1.40). **1.137** and **1.140** were prepared by heating resorcinol **1.136** or 1,3,5-dimethoxybenzene **1.170**, respectively, and cyanuric chloride **1.90** at 60 °C for 6 hours. Compound **1.135** was synthesised overnight by refluxing cyanuric chloride **1.90** with 3,5-dimethoxyphenol **1.134** in 1,2-dichloroethane. Eisler and Conn generated **1.142**, by heating phloroglucinol **1.159**, cyanuric chloride **1.90** and catalyst at 40 °C in a 1:4 mixture of dichloromethane and diethyl ether. Bosch and co-workers prepared **1.138** in an impressive yield of 90 % using AlCl_3 and excess mesitylene.¹¹⁷ The group recrystallised **1.138** from ethanol as white needles. Trullas *et al.*¹¹⁸ prepared **1.139** by stirring a mixture of a benzyl pyrole triazine, AlCl_3 and resorcinol in xylene at 85 °C for 3 hours. The Trullas group then added 20 % aqueous HCl, stirred at room temperature and collected the precipitate by filtration. The crude solid was washed with water and acetone to afford **1.139** in a 50 % yield. Wang and co-workers¹¹⁴ generated **1.141** by reacting **1.124** (Figure 1.38) with 2 equivalents of AlCl_3 and resorcinol **1.136** in chlorobenzene at 50 °C. The group

removed the chlorobenzene by steam distillation and collected the solid residue by filtration. The crude solid was washed with water and dried *in vacuo* at 80 °C to afford **1.141** in a 93 % yield.

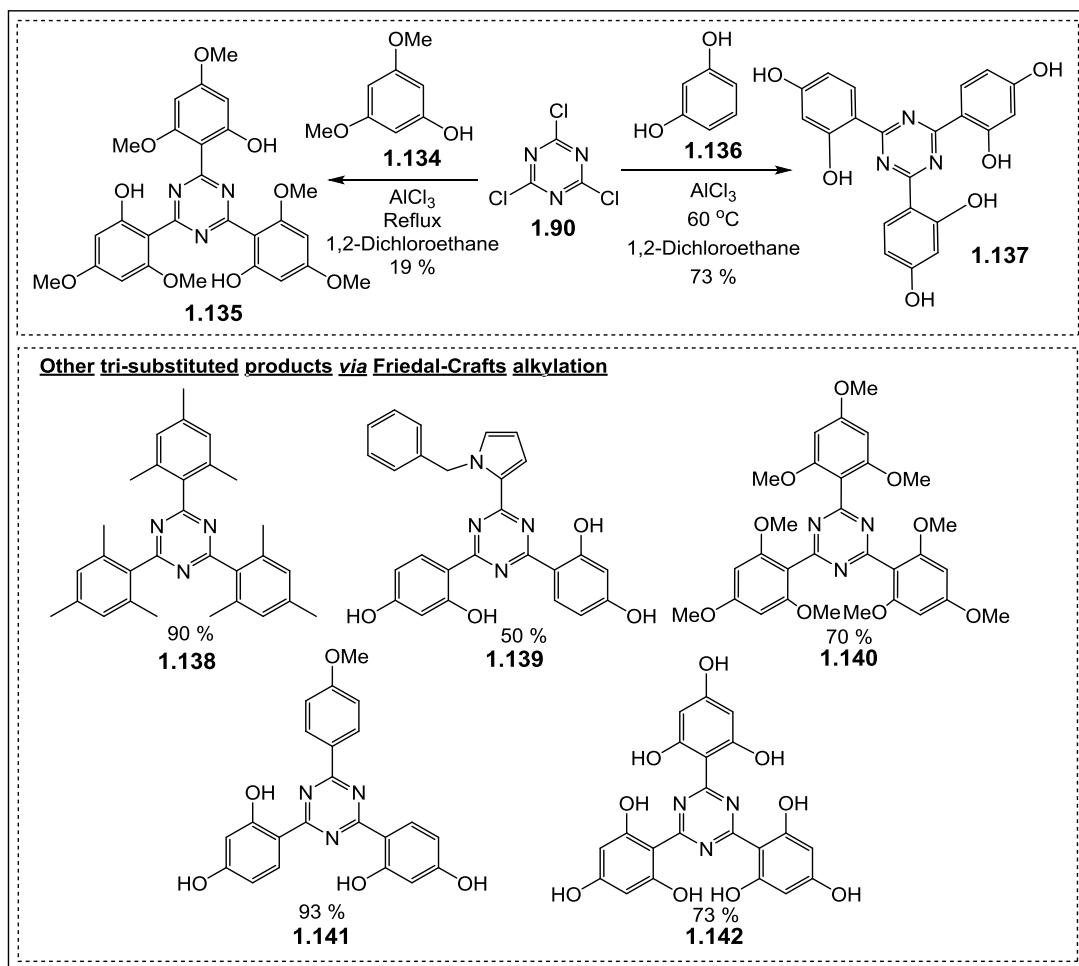


Fig. 1.40 – Examples of tri-substituted 1,3,5-triazines prepared using Friedel-Crafts alkylations^{114,116–118}

1.7.3.3 Suzuki Couplings

In addition to Friedel-Crafts alkylations and Grignard chemistry, another technique for installing aromatic residues into 1,3,5-triazines is Suzuki coupling. Suzuki coupling is a palladium-catalysed reaction between organoboronic acids and halides. Although Suzuki coupling is a more expensive route than Friedel-Crafts alkylations, the former is a regioselective process. A base, such as potassium carbonate, is required to activate the boronic acid and an organic ligand, such as triphenylphosphine, is necessary for the transmetalation step (Figure 1.41). Achelle

and co-workers¹¹⁹ refluxed cyanuric chloride **1.90** in toluene with **1.143** for 24 hours and purified the crude product by flash column chromatography to yield 42 % of **1.144** (Figure 1.41). Lahti *et al.*¹²⁰ stirred a mixture of **1.145**, cyanuric chloride **1.90**, potassium carbonate and palladium catalyst in a mixture of benzene and water at 50 °C for 7 hours. The group separated the organic layer and purified by flash column chromatography to generate **1.146** in a 30 % yield.

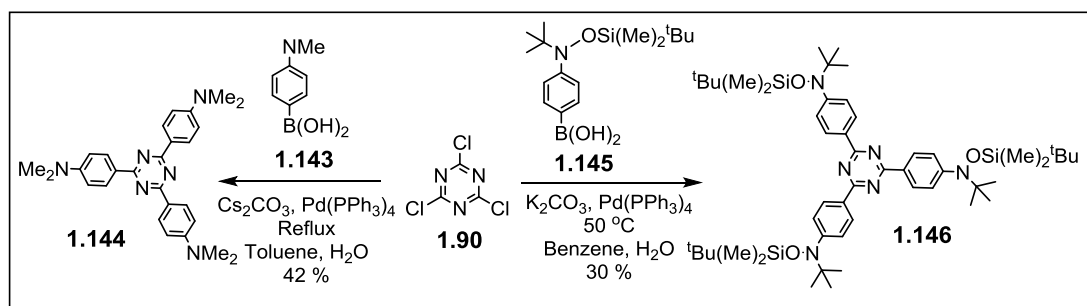


Fig. 1.41 – Examples of tri-substituted 1,3,5-triazines using Suzuki coupling with boronic acids^{119,120}

Suzuki coupling is most commonly utilised for the substitution of the third chlorine. The yields were found to be higher when the boronic acids were replaced with the boronate esters.^{109–111} The Suzuki coupling process is utilised extensively to produce organic light emitting devices with 1,3,5-triazine linkers. Abe *et al.*¹¹¹ heated a mixture of **1.147** with the boronate ester **1.148** under typical Suzuki coupling conditions to give 84 % yield of **1.149** (Figure 1.42).

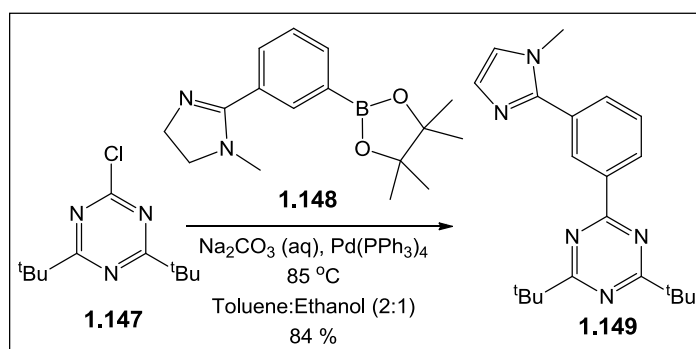


Fig. 1.42 – Example of tri-substituted 1,3,5-triazines using Suzuki coupling with boronate esters¹¹¹

1.7.3.4 Halogen-Lithium Exchange

The fourth common method of generating carbon-carbon bonds on a 1,3,5-triazine scaffold is halogen-lithium exchange between the chlorine atoms of cyanuric chloride **1.90** and an organolithium reagent. Organolithium compounds behave similarly to Grignard reagents, although they are more reactive and also more susceptible to side reactions with protic functional groups. The organolithium reagents are very reactive and are therefore introduced at low temperatures (-78 °C). There is, however, less temperature selectivity with the lithium-halogen exchange method, thus in order to obtain only the mono-substituted derivatives, such as **1.151** and **1.153**, stoichiometric ratios of the organolithium and cyanuric chloride **1.90** had to be implemented (Figure 1.43).^{121–123} Once the addition of the organolithium reagent is complete, the reaction is warmed slowly to room temperature. The organoborane derivative **1.151** was collected by filtration and not purified further. **1.153** was purified by flash column chromatography followed by recrystallisation from petroleum ether.

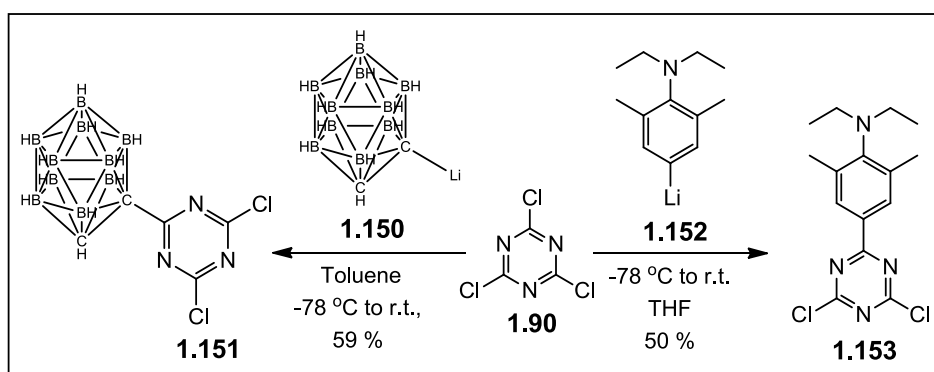


Fig. 1.43 – Examples of mono-substituted 1,3,5-triazines prepared using lithium-halogen exchange^{121–123}

The di-substituted derivatives were prepared by applying a 2:1 organolithium reagent to cyanuric chloride **1.90** ratio, as exemplified by Lim *et al.* when incorporating *o*-carboranyl polyhedra onto the triazine ring to yield 65 % of di-substituted **1.154** (Figure 1.44).¹²¹ Anemian *et al.*¹²⁴ added organolithium reagent **1.155** slowly to a stirring solution of cyanuric chloride **1.90** at -78 °C. The reaction temperature was allowed to warm to room temperature after the addition was complete, and the precipitated **1.156** was collected by filtration.

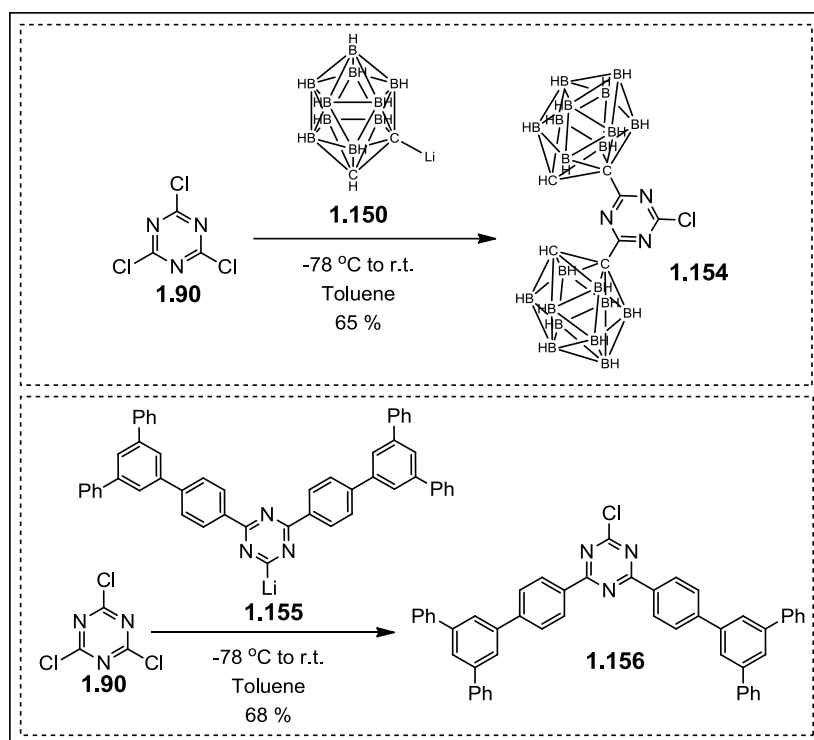


Fig. 1.44 – Examples of di-substituted 1,3,5-triazines prepared using lithium-halogen exchange^{121,124}

Di Nicola *et al.*¹²⁵ successfully incorporated three tripodal *tris*(pyrazolyl) fragments onto the 1,3,5-triazine ring using halogen-lithium exchange (Figure 1.45). **1.157** was made by adding a solution of *n*-BuLi in hexane to a solution of *tris*(1*H*-pyrazol-1-yl)methane in dry THF at -78 °C. The mixture was warmed to room temperature and added to solution of cyanuric chloride **1.90** in dry THF. The reaction was refluxed for 3 days, quenched with water and extracted using diethyl ether. Pure colourless needles of **1.158** were obtained in a yield of 60 % after recrystallisation from acetone.

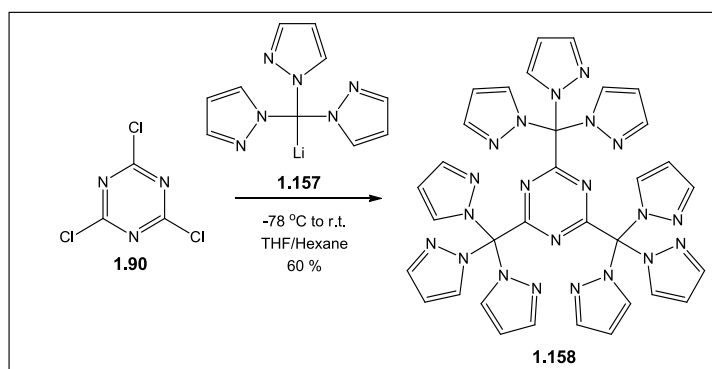


Fig. 1.45 – Example of tri-substituted 1,3,5-triazines prepared using lithium-halogen exchange¹²⁵

Chapter 2 - Research Aims and Objectives

Tinuvin 1577 **1.10** (Figure 2.1) is the leading ultraviolet absorber (UVA) additive on the market today. Tinuvin 1577 **1.10** is manufactured by BASF and is currently the UV stabiliser of choice for DuPont Teijin Films as a UV-stabilising additive for PET.

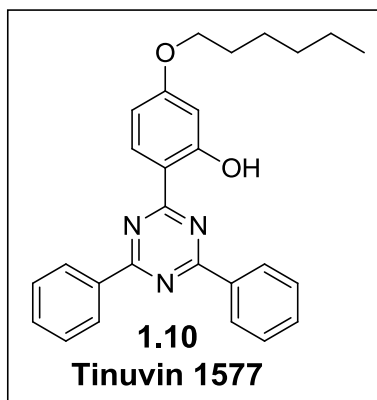


Fig. 2.1 – Structure of Tinuvin 1577 **1.10**

Although Tinuvin 1577 **1.10** performs well as a UV stabiliser, a major drawback is that it migrates out of the polymer with time. Furthermore, other imperfections include cost, uneven distribution of stabiliser in the film and thermal instability at PET processing temperatures. The volatilisation and fuming of Tinuvin 1577 **1.10** during processing can lead to increased costs and serious safety concerns.

The leaching of Tinuvin 1577 **1.10** from the polymer matrix is a problem that befalls all UV additives. One way in which to circumvent this drawback is to polymerise the UVA into the polymer chain.

The aim of this study was to design, synthesise and characterise novel polymerisable UV stabilisers based on the 2-(2-hydroxyphenyl)-1,3,5-triazine (TA) structures. Followed by demonstrating that polymerising these novel UV absorbers into the polymer matrix prevents leaching and offers superior UV protection to PET films compared to Tinuvin 1577 **1.10**.

The UV stabilising monomers must bear functional groups capable of step-growth polyesterification, e.g., aliphatic hydroxyl, carboxylic acid, acid chloride and ester groups (Figure 2.2).

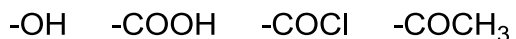


Fig. 2.2 – Functional moieties capable of participating in a step-growth polyesterification

As Tinuvin 1577 **1.10** is an effective UV stabiliser, the initial design strategy was to diverge as little as possible from the Tinuvin 1577 **1.10** structure. The aliphatic chain is a region of the molecule where structural variations can be introduced, such as polymerisable moieties, due to the minimal impact this would have on the UV profiles of the UV absorber monomers (UVAMs).

After synthesising UVAMs which are based on the structure of Tinuvin 1577 **1.10**, the next stage was to design monomers with different chromophores and UV absorption characteristics. This strategy involved increasing both the number of intramolecular hydrogen bonds (IMHBs) and the degree of conjugation in the UVAM structures. In addition to this, cheaper alternatives to the tri-aryl systems were explored in an attempt to examine the potential of more easily accessible mono-aryl and di-aryl triazine UVAMs.

The next phase was to copolymerise the UVAMs into poly(ethylene isophthalate) (PEI), an amorphous isomer of poly(ethylene terephthalate) (PET) which is soluble in organic solvents and can be characterised with greater ease. With the aim of obtaining a broader range of UV coverage, various combinations of two different UVAMs were copolymerised into the same PEI chain. The idea was to use one UVAM which absorbs strongly at short wavelengths and another which absorbs strongly at longer wavelengths to enhance the range of protection within the 290-400 nm region.

The final stage of the study was to obtain copolymers of PET films and investigate their performance in a photodegradation study. The films were weathered and analysed periodically using GPC and FT-IR spectroscopy to examine the true potential of these UVAMs by comparing their efficacy to Tinuvin 1577 **1.10**.

Chapter 3 - Synthesis of Ultraviolet Absorbing Monomers

3.1 Experimental

3.1.1 Reagents

<i>Reagent</i>	<i>Purity</i>	<i>Supplier</i>
4-Biphenylmagnesium bromide	0.5 M in THF	Acros
2-Bromoethanol	95.0 %	Aldrich
9-Bromo-1-nonanol	97.0 %	Aldrich
(±) 3-Chloropropane-1,2-diol	98.0 %	Aldrich
1,2-Dichlorobenzene	99.0 %	Aldrich
1,6-Dibromohexane	96.0 %	Aldrich
1,3-Dihydroxynaphthalene	99.0 %	Aldrich
3,5-Dimethoxyphenol	99.0 %	Aldrich
4-Fluorophenylmagnesium bromide	1.0 M in THF	Aldrich
4-Methoxyphenylmagnesium bromide	0.5 M in THF	Aldrich
Acetone	>99.0 %	Aldrich
Aluminium trichloride	98.0%	BDH
Chloroform	99.0-99.4 %	Aldrich
Cyanuric chloride	>99.5 %	Aldrich
Dichloromethane	>99.0 %	Aldrich
Diethyl 2-bromo-2-methylmalonate	98.0 %	Aldrich
Diethyl ether	>99.0 %	Aldrich
Diethyl iminodiacetate	98.0 %	Aldrich
Diethyl methylmalonate	99.0 %	Aldrich
Dimethyl-5-aminoisophthalate	98.0 %	Aldrich
Epibromohydrin	98.0 %	Aldrich
Ethyl acetate	99.5 %	Aldrich
Ethylene glycol	99.8 %	Univar Ltd
Hexane	>97.0 %	Aldrich
Hydrochloric acid	37.0 %	Aldrich
Lithium aluminium hydride	95.0 %	Aldrich
Manganese(II) acetate tetrahydrate	>99.0 %	Aldrich
Methanol	99.7 %	Aldrich
Methyl 4-hydroxybenzoate	>99.0 %	Aldrich
<i>N,N</i> -Diisopropylethylamine	>99.0 %	Aldrich
<i>N,N</i> -Dimethylformamide	>99.8 %	Aldrich
Phenylmagnesium bromide	1.0 M in THF	Aldrich
Phloroglucinol	>99.0 %	Aldrich
Potassium iodide	>99.5 %	Aldrich
Potassium sodium tartrate	99.0 %	Aldrich
Resorcinol	>99.0 %	Aldrich
Sodium carbonate	99.5 %	Fisher
Sodium chloride	100.0 %	GPR
Sodium hydride	60.0 % in oil	Aldrich
Sodium hydroxide	99.0 %	VWR
Sodium sulfate	99.0 %	Fisher
Tetrahydrofuran	99.9 %	Aldrich
Toluene	>99.3 %	Aldrich

Table 3.1 - List of solvents and reagents used

Anhydrous THF, diethyl ether, hexane and DCM were obtained from an SPS solvent drying system. The solvents and reagents listed above were used as received, without any further purification.

3.1.2 Equipment

A Perkin Elmer Spectrum One Fourier Transform Infrared (FT-IR) spectrometer was used to record FT-IR spectra. The spectra were recorded using Attenuated Total Reflectance (ATR) within the range 400 to 4000 cm^{-1} .

Nuclear magnetic resonance (NMR) spectra were recorded on Bruker DPX 400 and DRX 500 instruments in the NMR Laboratory at the University of Strathclyde, for ^1H , ^{13}C and ^{19}F nuclei. The chemical shifts (δ) are quoted in part per million (ppm), relative to the residual proton resonances of the solvent, and coupling constants (J values) in Hz. Multiplicities are abbreviated as: s, singlet; d, doublet; t, triplet; q, quartet; m, multiplet for the ^1H NMR spectra. In cases where superimposition of signals occurred, the signals were reported as a multiplet (m). CDCl_3 and d_6 -DMSO were used as NMR solvents.

High resolution mass spectrometry (HRMS) was carried out by a member of staff in the Strathclyde Institute of Pharmacy and Biomedical Sciences (SIPBS). HRMS was performed using a Thermo Scientific-Exactive Orbitrap Mass Spectrometer. Methanol was used as the solvent and the scan range was 75-1200 m/z.

Gas chromatography mass spectrometry (GCMS) was carried out using an Agilent Technologies 7890A GCMS with a RESTEK RXi-5Sil MS column. Samples were dissolved in CHCl_3 and helium was used as the gas carrier at a flow rate of 1 mL/min. The ions were produced by electron ionisation (EI) using a nitrogen laser at 337 nm.

UV-Visible absorption spectra were acquired using a Photonics CCD array UV-VIS spectrophotometer with a 1 mm pathlength quartz cell. DMSO and CHCl_3 were used as solvents and the scan range was 290-500 nm.

Thermogravimetric analysis (TGA) of UVA monomers were performed by a member of staff at the University of Strathclyde using a Perkin Elmer TGA 7. Approximately 10 mg of sample was heated in air at a rate of 10 °C/min from 40 °C to 500 °C.

Uncorrected melting points were determined in capillary tubes using a Gallenkamp Griffin Melting Point Apparatus.

3.1.3 Synthesis of Ultraviolet Absorber Monomers (UVAMs)

3.1.3.1 Grignard Reactions

2,4-Dichloro-6-phenyl-1,3,5-triazine (1)

1 M Phenylmagnesium bromide in THF (110 mL, 11.00 mmol) was added dropwise to a solution of cyanuric chloride **1.90** (20.00 g, 10.84 mmol) in anhydrous THF (300 mL) under nitrogen, whilst maintaining the temperature at 0 °C. Once the addition was complete, the mixture was stirred at 0 °C for 4 hours and poured into 10 % v/v aqueous HCl (200 mL). The THF was removed under reduced pressure and the organic product was extracted with CHCl₃ (3×150 mL). The organic layer was combined and washed with water (2×150 mL) and brine (100 mL), dried over anhydrous sodium sulfate and the solvent was removed under reduced pressure. The crude product was purified by grinding into a fine powder, suspending and washing using MeOH (3×100 mL). This yielded a white powder which was dried at 70 °C *in vacuo* (60 mbar). **1** (15.67 g, 64 %, Figure 3.1).

HRMS: Found m/z 226.0121 (M+H)⁺; Calculated m/z 225.9933

M. pt. Expected: 118-120 °C;¹²⁶ Found: 118-120 °C

FT-IR: $\bar{\nu}$ / cm⁻¹: 3030 (C-H stretch, aromatic), 1523, 1494 (C=N stretch, conjugated)

¹H NMR (400 MHz, CDCl₃) δ : 7.52-7.56 (m, 2H, H₂), 7.65-7.69 (m, 1H, H₁), 8.50-8.52 (m, 2H, H₃)

¹³C NMR (100 MHz, CDCl₃) δ : 129.3 (C₃), 130.1 (C₂), 132.9 (C₄), 134.9 (C₁), 172.3 (C₅), 175.1 (C₆)

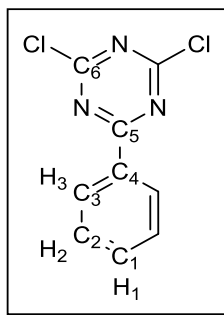


Fig.3.1 – Chemical structure of 1

2-Chloro-4,6-diphenyl-1,3,5-triazine (2)

1 M Phenylmagnesium bromide in THF (250 mL, 0.25 mol) was added dropwise to a solution of cyanuric chloride **1.90** (20.00 g, 0.11 mol) in anhydrous THF (300 mL) under nitrogen, whilst maintaining the temperature at 0 °C. Once the addition was complete, the mixture was stirred at room temperature for 16 hours and poured into cold 10 % v/v aqueous HCl (200 mL). The THF was removed under reduced pressure and the organic product was extracted with CHCl₃ (3×150 mL). The organic layer was washed with water (2×150 mL) and brine (100 mL), dried over anhydrous sodium sulfate and the solvent removed under reduced pressure to give a purple/red coloured solid. The crude product was purified by grinding into a fine powder, suspending and washing using MeOH (3×100 mL). This yielded a white powder which was dried at 70 °C *in vacuo* (60 mbar). **2** (19.07 g, 67 %, Figure 3.2).

HRMS: Found *m/z* 268.0635 (M+H)⁺; Calculated *m/z* 268.0642

M. pt. Expected: 139 - 140 °C;¹²⁷ Found: 137 - 139 °C

FT-IR: $\bar{\nu}$ / cm⁻¹: 3049 (C-H stretch, aromatic), 1537, 1490 (C=N stretch, conjugated)

¹H NMR (500 MHz, CDCl₃) δ : 7.54-7.58 (**m**, 4H, H₂), 7.64 (**m**, 2H, H₁), 8.62-8.64 (**m**, 4H, H₃)

¹³C NMR (100 MHz, CDCl₃) δ : 129.0 (C₃), 129.6 (C₂), 133.8 (C₁), 134.6 (C₄), 172.4 (C₆), 173.6 (C₅)

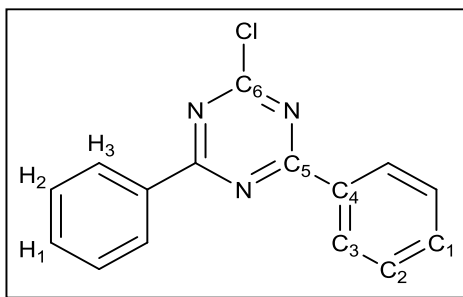


Fig.3.2 – Chemical structure of 2

2-([1,1'-Biphenyl]-4-yl)-4,6-dichloro-1,3,5-triazine (3)

0.5 M 4-Biphenylmagnesium bromide in THF (5.00 mL, 2.45 mmol) was added dropwise to a solution of cyanuric chloride **1.90** (0.45 g, 2.45 mmol) in anhydrous THF (25 mL) under nitrogen, whilst maintaining the temperature at 0 °C. Once the addition was complete, the mixture was stirred at 0 °C for 4 hours and poured into 10 % v/v aqueous HCl (25 mL). The THF was removed under reduced pressure and the organic product was extracted with CHCl₃ (2×50 mL). The organic phase was separated, washed with water (2×50 mL) and dried over anhydrous sodium sulfate. The solvent was removed under reduced pressure and the crude product was purified by grinding into a fine powder, suspending and washing using MeOH (3×50 mL). This yielded a white powder which was dried at 70 °C *in vacuo* (60 mbar). **3** (0.28 g, 38 %, Figure 3.3).

HRMS: Found *m/z* 302.0242 (M+H)⁺; Calculated *m/z* 302.0246

M. pt. Expected: 160-161 °C;¹²⁸ Found: 159-160 °C

FT-IR: $\bar{\nu}$ / cm⁻¹: 3034 (C-H stretch, aromatic), 1525, 1475 (C=N stretch, conjugated)

¹H NMR (500 MHz, CDCl₃) δ : 7.43 (m, 1H, H₁), 7.48-7.51 (m, 2H, H₂), 7.69-7.67 (m, 2H, H₃), 7.77 (d, *J* = 8.6 Hz, 2H, H₄), 8.57 (d, *J* = 8.6 Hz, 2H, H₅)

¹³C NMR (100 MHz, CDCl₃) δ : 127.3 (C₃), 127.7 (C₆), 128.6 (C₁), 129.0 (C₂), 130.5 (C₇), 131.4 (C₄), 139.6 (C₅), 147.5 (C₈), 172.0 (C₉), 174.6 (C₁₀)

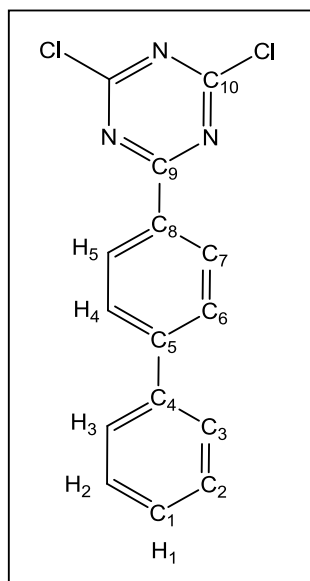


Fig.3.3 – Chemical Structure of 3

2,4-Bis([1,1'-biphenyl]-4-yl)-6-chloro-1,3,5-triazine (4)

0.5 M 4-Biphenylmagnesium bromide in THF (50.00 mL, 25.00 mmol) was added dropwise to a stirred solution of cyanuric chloride **1.90** (1.53 g, 8.33 mmol) in anhydrous THF (100 mL) under nitrogen, whilst maintaining the temperature at 0 °C. Once the addition was complete, the mixture was stirred for 16 hours at 50 °C and poured into 10 % v/v aqueous HCl (100 mL). The THF was removed under reduced pressure and the organic product was extracted with CHCl₃ (2×50 mL). The organic layer was washed with water (2×50 mL) and brine (50 mL), and dried over anhydrous sodium sulfate. The solvent was removed under reduced pressure and purified by grinding into a fine powder, suspending and washing using MeOH (3×100 mL). The white coloured powder was dried at 70 °C *in vacuo* (60 mbar). **4** (2.00 g, 57 %, Figure 3.4).

HRMS: Found m/z 420.1263 [M+H]⁺; Calculated m/z 420.1262

M. pt. Found: 164-167 °C

FT-IR: $\bar{\nu}$ / cm⁻¹: 3035, 3034 (C-H stretch, aromatic), 1526, 1489 (C=N stretch, conjugated)

^1H NMR (400 MHz, CDCl_3) δ : 7.43-7.47 (m, 2H, H₁), 7.51-7.54 (m, 4H, H₂), 7.71-7.73 (m, 4H, H₃), 7.82 (d, J = 8.5 Hz, 4H, H₄), 8.73 (d, J = 8.5 Hz, 4H, H₅)

^{13}C NMR (100 MHz, CDCl_3) δ : 126.8 (C₃), 127.0 (C₆), 127.8 (C₁), 128.5 (C₂), 129.5 (C₇), 132.8 (C₄), 139.5 (C₅), 145.8 (C₈), 171.6 (C₁₀), 172.6 (C₉)

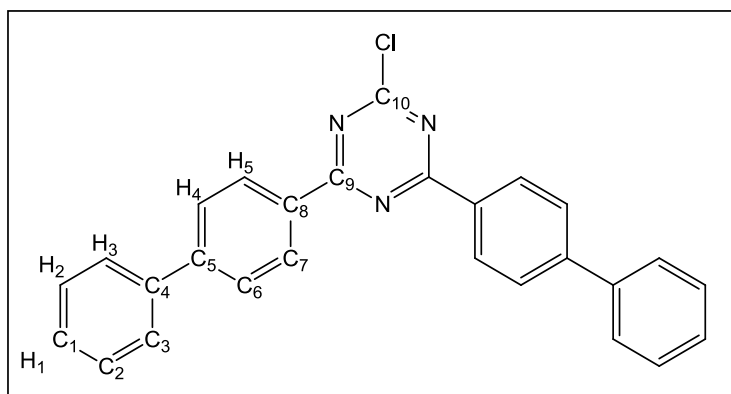


Fig.3.4 - Chemical structure of 4

2,4-Dichloro-6-(4-fluorophenyl)-1,3,5-triazine (5)

1 M 4-Fluorophenylmagnesium bromide in THF (10 mL, 0.01 mol) was added dropwise to a stirred solution of cyanuric chloride **1.90** (1.84 g, 0.01 mol) in anhydrous THF (40 mL) under nitrogen, whilst maintaining the temperature at 0 °C. Once the addition was complete, the mixture was stirred for 3 hours at 0 °C and poured into cold 10 % v/v aqueous HCl (100 mL). The THF was removed under reduced pressure and the organic product was extracted with CHCl_3 (2×100 mL). The organic layer was washed with water (2×50 mL) and brine (50 mL), dried over anhydrous sodium sulfate and the solvent removed under reduced pressure. The crude solid was purified by grinding into a fine powder, suspending and washing using MeOH (3×100 mL). The white coloured product was dried at 40 °C *in vacuo* (60 mbar). **5** (0.96 g, 39 %, Figure 3.5).

GC-MS: Found m/z 244.0 $[\text{M}+\text{H}]^+$; Calculated m/z 244.0

M. pt. Expected: 112-115 °C;¹²⁹ Found: 114-115 °C

FT-IR: $\bar{\nu}$ / cm^{-1} : 3113, 3080 (C-H stretch, aromatic), 1508, 1479 (C=N stretch, conjugated)

^1H NMR (400 MHz, CDCl_3) δ : 7.20-7.26 (m, 2H, H₁), 8.54-8.59 (m, 2H, H₂)

^{13}C NMR (100 MHz, CDCl_3) δ : 115.5 (d, J = 22 Hz, C₂), 128.3 (d, J = 3 Hz, C₄), 132.1 (d, J = 9 Hz, C₃), 166.1 (d, J = 254 Hz, C₁), 171.6 (C₅), 171.2 (C₆)

^{19}F NMR (400 MHz, CDCl_3) δ : -102.3 (m, 1F, F)

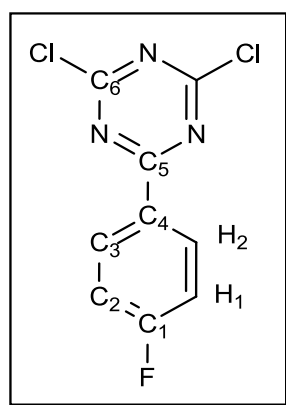


Fig.3.5 – Chemical structure of 5

2-Chloro-4,6-bis(4-fluorophenyl)-1,3,5-triazine (6)

1 M 4-Fluorophenylmagnesium bromide in THF (30 mL, 0.03 mol) was added dropwise to a stirred solution of cyanuric chloride **1.90** (1.84 g, 0.01 mol) in anhydrous THF (30 mL) under nitrogen, whilst maintaining the temperature at 0 °C. Once the addition was complete, the mixture was stirred for 16 hours at room temperature and then poured into cold 10 % v/v aqueous HCl (50 mL). The THF was removed under reduced pressure and the organic product was extracted with CHCl_3 (2×50 mL). The organic layer was washed with water (2×50 mL) and brine (50 mL), dried over anhydrous sodium sulfate and the solvent removed under reduced pressure. The crude solid was purified by grinding into a fine powder, suspending and washing using MeOH (3×100 mL). The white coloured product was dried at 40 °C *in vacuo* (60 mbar). **6** (1.52 g, 50 %, Figure 3.6).

HRMS: Found m/z 304.0448 $[\text{M}+\text{H}]^+$; Calculated m/z 304.0448

M. pt. Expected: 177-180 °C;¹²⁹ Found: 176-178 °C

FT-IR: $\bar{\nu}$ / cm^{-1} : 3116, 3072 (C-H stretch, aromatic), 1531, 1492 (C=N stretch, conjugated)

^1H NMR (400 MHz, CDCl_3) δ : 7.19-7.26 (m, 4H, H₁), 8.61-8.66 (m, 4H, H₂)

^{13}C NMR (100 MHz, CDCl_3) δ : 115.5 (d, J = 22 Hz, C₂), 129.9 (d, J = 3 Hz, C₄), 131.3 (d, J = 9 Hz, C₃), 166.0 (d, J = 254 Hz, C₁), 171.6 (C₆), 171.8 (C₅)

^{19}F NMR (400 MHz, CDCl_3) δ : -104.7 (m, 2F, F)

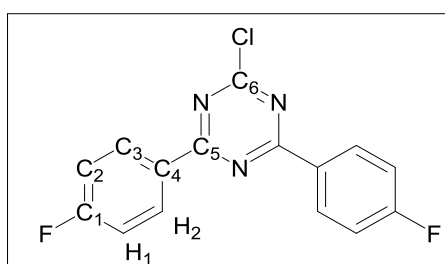


Fig.3.6 – Chemical structure of 6

2,4-Dichloro-6-(4-methoxyphenyl)-1,3,5-triazine (7)

0.5 M 4-Methoxyphenylmagnesium bromide in THF (20 mL, 0.01 mol) was added to a stirred solution of cyanuric chloride **1.90** (1.84 g, 0.01 mol) in anhydrous THF (25 mL) under nitrogen, whilst maintaining the temperature at 0 °C. Once the addition was complete, the reaction mixture was stirred at 0 °C for 4 hours and then poured into cold 10 % v/v aqueous HCl (50 mL). The THF was removed under reduced pressure and the organic product was extracted with CHCl_3 (2×50 mL). The organic layer was washed with water (2×100 mL), brine (100 mL), dried over anhydrous sodium sulfate and the solvent removed under reduced pressure. The crude solid was purified by grinding into a fine powder, suspending and washing using MeOH (3×100 mL). The white coloured product was dried at 40 °C *in vacuo* (60 mbar). **7** (1.20 g, 47 %, Figure 3.7).

HRMS: Found m/z 256.0036 [M]⁺; Calculated m/z 256.0039

M. pt. Expected: 137-138 °C;¹¹⁴ Found: 137-138 °C

FT-IR: $\bar{\nu}$ / cm⁻¹: 3078 (C-H stretch, aromatic), 2974, 2937 (C-H stretch, aliphatic), 1516, 1477 (C=N stretch, conjugated), 1244 (C-O stretch)

¹H NMR (500 MHz, CDCl₃) δ : 3.92 (s, 3H, H₁), 7.01 (d, J = 9.1 Hz, 2H, H₂), 8.47 (d, J = 9.1 Hz, 2H, H₃)

¹³C NMR (125 MHz, CDCl₃) δ : 55.7 (C₁), 114.5 (C₃), 125.1 (C₅), 132.3 (C₄), 165.2 (C₂), 171.6 (C₆), 174.2 (C₇)

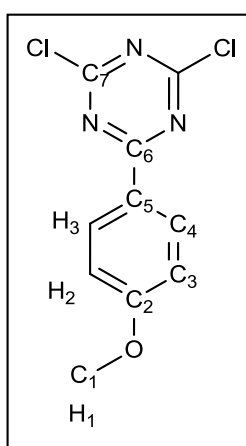


Fig.3.7 – Chemical structure of 7

2-Chloro-4,6-bis(4-methoxyphenyl)-1,3,5-triazine (8)

0.5 M 4-Methoxyphenylmagnesium bromide in THF (45 mL, 25.00 mmol) was added to a stirred solution of cyanuric chloride **1.90** (1.84 g, 10.00 mmol) in anhydrous THF (25 mL) under nitrogen, whilst maintaining the temperature at 0 °C. Once the addition was complete, the reaction mixture was stirred at room temperature for 16 hours and poured into cold 10 % v/v aqueous HCl (100 mL). The THF was removed under reduced pressure and the organic product was extracted with CHCl₃ (2×50 mL). The organic layer was washed with water (2×100 mL) and brine (50 mL), dried over anhydrous sodium sulfate and the solvent removed under reduced pressure. The crude solid was purified by grinding into a fine powder, suspending and washing

using MeOH (3×100 mL). The white coloured product was dried at 40 °C *in vacuo* (60 mbar). **8** (1.57 g, 48 %, Figure 3.8).

HRMS: Found m/z 328.0848 [M+H]⁺; Calculated m/z 328.0847

M. pt. Expected: 195-197 °C;¹³⁰ Found: 194-195 °C

FT-IR: $\bar{\nu}$ / cm⁻¹: 3017 (C-H stretch, aromatic), 2973, 2935, 2839 (C-H stretch, aliphatic), 1516, 1489 (C=N stretch, conjugated), 1241 (C-O stretch)

¹H NMR (500 MHz, CDCl₃) δ : 3.92 (s, 6H, H₁), 7.01 (d, J = 9.0 Hz, 4H, H₂), 8.47 (d, J = 9.0 Hz, 4H, H₃)

¹³C NMR (125 MHz, CDCl₃) δ : 55.5 (C₁), 114.1 (C₃), 127.0 (C₅), 131.4 (C₄), 164.1 (C₂), 171.7 (C₇), 172.6 (C₆)

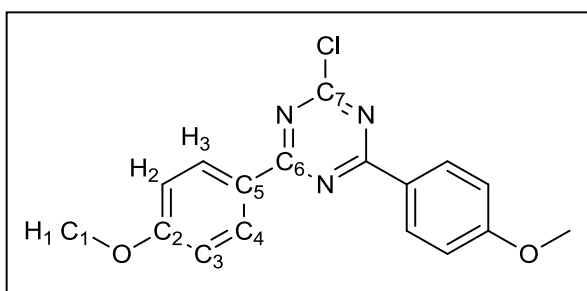


Fig.3.8 – Chemical structure of 8

3.1.3.2 Amine and Alcohol Nucleophile Reactions

Diethyl 2,2'-((4,6-dichloro-1,3,5-triazin-2-yl)azanediyl)diacetate (9)

A solution of cyanuric chloride **1.90** (2.00 g, 10.56 mmol) in acetone (50 mL) was stirred at 0 °C. To this, a solution of diethyl iminodiacetate **3.1** (1.99 g, 10.56 mmol) in acetone (30 mL) was added over a period of 30 mins. An aqueous NaOH solution (0.25 M) was added dropwise until the mixture was neutralised, stirred at 0 °C for 2 hours and subsequently filtered whilst cold. The white coloured powder was washed with water (100 mL) and dried at 70 °C *in vacuo* (<1 mbar). No further purification was necessary and the crude product was used in the subsequent step. **9** (3.25 g, 89 %, Figure 3.9).

HRMS: Found m/z 337.0465 $[M+H]^+$; Calculated m/z 337.0465

M. pt. Found: 120-122 °C

FT-IR: $\bar{\nu}$ / cm^{-1} : 2987 (C-H stretch, aliphatic), 1737 (C=O stretch, ester), 1483, 1471 (C=N stretch, conjugated)

^1H NMR (400 MHz, CDCl_3) δ : 1.20 (t, $J = 7.1$ Hz, 6H, H_1), 4.17 (q, $J = 7.1$ Hz, 4H, H_2), 4.53 (s, 4H, H_3)

^{13}C NMR (100 MHz, CDCl_3) δ : 13.6 (C_1), 49.0 (C_4), 61.3 (C_2), 165.4 (C_5), 167.6 (C_3), 170.0 (C_6)

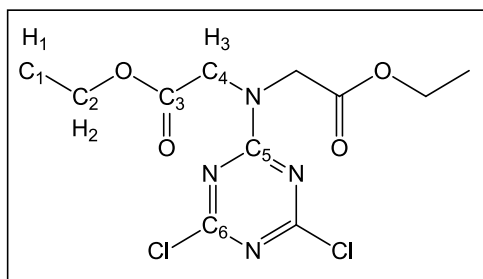


Fig.3.9 – Chemical structure of 9

Dimethyl 4,4'-((6-chloro-1,3,5-triazine-2,4-diyl)bis(oxy))dibenzoate (10)

A solution of cyanuric chloride **1.90** (3.00 g, 16.27 mmol) in acetone (150 mL) was stirred at 0 °C. To this, a solution mixture of *N,N*-diisopropylethylamine (DIPEA) (4.21 g, 32.54 mmol) and methyl 4-hydroxybenzoate **3.2** (4.95 g, 32.54 mmol) in acetone (50 mL) was added over a period of 45 mins. The reaction was left to stir at room temperature for 16 hours. The solvent was removed under reduced pressure and the residue was purified by grinding into a fine powder, suspending and washing using MeOH (3×100 mL). The white coloured solid was dried at 40 °C *in vacuo* (<1 mbar). **10** (4.30 g, 69 %, Figure 3.10).

GC-MS: Found m/z 417.10 $(M+H)^+$; Expected m/z 416.79

M. pt. Found: 188 °C

FT-IR: $\bar{\nu}$ / cm^{-1} : 2958 (C-H stretch, aliphatic), 1720 (C=O stretch, ester), 1528, 1504 (C=N stretch, conjugated), 1277, 1251 (C-O stretch)

Elemental microanalysis: Expected: C, 54.9; H, 3.4; N, 10.1. Found: C, 54.9; H, 3.3; N, 10.3

^1H NMR (400 MHz, CDCl_3) δ : 3.94 (s, 6H, H_1), 7.23 (AA'BB' system, $J = 8.9, 2.3$ Hz, 4H, H_3), 8.09 (AA'BB' system, $J = 8.9, 2.3$ Hz, 4H, H_2)

^{13}C NMR (100 MHz, CDCl_3) δ : 51.8 (C_1), 120.9 (C_5), 128.1 (C_3), 131.0 (C_4), 154.1 (C_6), 165.5 (C_2), 171.5 (C_7), 173.5 (C_8)

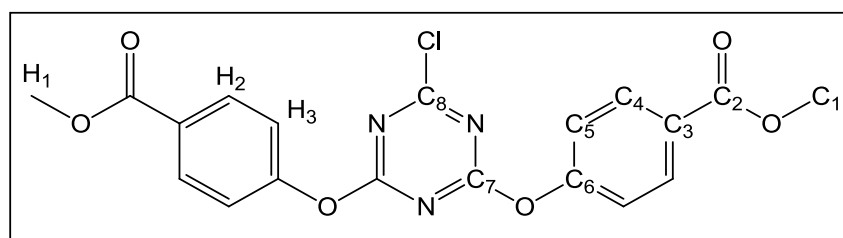


Fig.3.10 – Chemical structure of 10

3.1.3.3 Friedel-Crafts Reactions

4-(4,6-Diphenyl-1,3,5-triazin-2-yl)benzene-1,3-diol (11)

AlCl_3 (1.91 g, 14.60 mmol) was added to a suspension of 2-chloro-4,6-diphenyl-1,3,5-triazine **2** (3.00 g, 11.20 mmol) and resorcinol **1.136** (1.49 g, 13.50 mmol) in 1,2-dichlorobenzene (250 mL) and stirred at 130 °C for 16 hours under nitrogen. The mixture was cooled to room temperature and quenched with 10 % v/v aqueous HCl (150 mL). After stirring at room temperature for 1 hour, the red coloured precipitate was collected by filtration, washed with water (150 mL) and dried at 70 °C *in vacuo* (60 mbar). No further purification was required and the crude product was used in the subsequent step. **11** (3.03 g, 78 %, Figure 3.11).

M. pt. Expected: 275 - 275.5 °C;¹³¹ Found: 272 °C

HRMS: Found m/z 342.1235 ($\text{M}+\text{H}$)⁺; Calculated m/z 342.1237

UV λ_{\max} (0.1 mM in DMSO): 343 nm ($\epsilon = 24,000 \text{ cm}^{-1} \text{ M}^{-1}$)

FT-IR: $\bar{\nu}$ / cm^{-1} : 3150-3400 (O-H stretch), 3057 (C-H stretch, aromatic), 1508 (C=N stretch, conjugated), 1519, 1504 (C=N stretch, conjugated)

^1H NMR (500 MHz, DMSO- d_6) δ : 6.38 (**d**, $J = 2.0$ Hz, 1H, H₆), 6.53 (**dd**, $J = 9.0, 2.0$ Hz, 1H, H₅), 7.63-7.65 (**m**, 4H, H₂) 7.69-7.72 (**m**, 2H, H₁), 8.48 (**d**, $J = 9.0$ Hz, 1H, H₄), 8.52-8.54 (**m**, 4H, H₃), 10.48 (**s**, 1H, H₈), 13.22 (**s**, 1H, H₇)

^{13}C NMR (100 MHz, DMSO- d_6) δ : 103.5 (C₁₁), 109.36 (C₉), 109.44 (C₇), 129.0 (C₃), 129.5 (C₂), 132.0 (C₈), 133.7 (C₁), 135.2 (C₄), 164.2 (C₁₀ or C₁₂), 164.8 (C₁₀ or C₁₂), 170.0 (C₅), 171.1 (C₆)

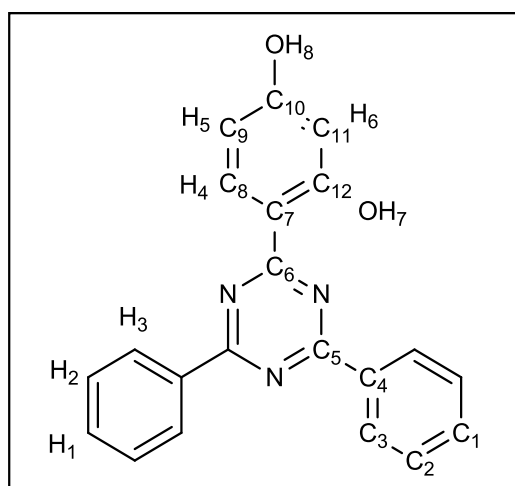


Fig.3.11 – Chemical structure of 11

2-(4,6-Diphenyl-1,3,5-triazin-2-yl)benzene-1,3,5-triol (12)

Phloroglucinol **1.159** (0.4664 g, 3.70 mmol) and 2-chloro-4,6-diphenyl-1,3,5-triazine **2** (0.66 g, 2.47 mmol) were added to a 1:4 mixture of anhydrous DCM and anhydrous diethyl ether (25 ml). AlCl_3 (0.4931 g, 3.70 mmol) catalyst was added and the mixture was refluxed for 16 hours under nitrogen. The solvent was removed under reduced pressure and the solid was suspended in 10 % v/v aqueous HCl (25 mL). The suspension was transferred to a centrifuge tube and spun at 3400 rpm for 5 minutes. The supernatant was removed and the pellet was re-suspended and spun at 3400 rpm for 5 minutes in distilled water (25 mL) and the supernatant removed. The crude

product was collected by filtration and dried at 70 °C *in vacuo* (60 mbar). No further purification was required and the crude product was used in the subsequent step. **12** (0.79 g, 60 %, Figure 3.12).

HRMS: Found m/z 356.1046 (M-H)⁻; Calculated m/z 356.1041

M. pt. Found: 244-245 °C

FT-IR: $\bar{\nu}$ / cm^{-1} : 3150-3500 (O-H stretch), 3026 (C-H stretch, aromatic), 1508, 1479 (C=N stretch, conjugated), 1282 (C-O stretch)

UV λ_{max} (0.1 mM in DMSO): 330 nm ($\epsilon = 33,000 \text{ cm}^{-1} \text{ M}^{-1}$)

TGA (Air): Weight loss at 300 °C (2.80 %); Onset temperature (372 °C)

¹H NMR (400 MHz, DMSO) δ : 5.94 (s, 2H, H₅), 7.66-7.70 (m, 4H, H₂), 7.70-7.76 (m, 2H, H₁), 8.40 (d, $J = 7.3 \text{ Hz}$, 4H, H₃), 10.57 (s, 1H, H₆), 13.57 (s, 2H, H₄)

¹³C NMR (100 MHz, DMSO) δ : 95.6 (C₉), 95.7 (C₇), 128.5 (C₃), 129.3 (C₂), 133.79 (C₁), 133.82 (C₄), 164.2 (C₈), 165.0 (C₁₀), 168.3 (C₅), 170.5 (C₆)

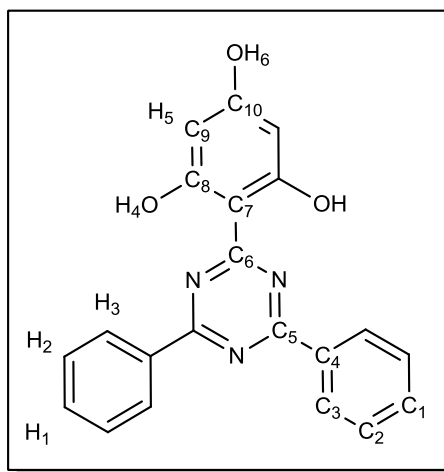


Fig.3.12 – Chemical structure of **12**

4-(4,6-Di([1,1'-biphenyl]-4-yl)-1,3,5-triazin-2-yl)benzene-1,3-diol (13**)**

2,4-Bis([1,1'-biphenyl]-4-yl)-6-chloro-1,3,5-triazine **4** (2.00 g, 4.76 mmol), resorcinol **1.136** (0.63 g, 5.72 mmol) and AlCl₃ (0.83 g, 6.19 mmol) were added to 1,2-

dichlorobenzene (100 mL) and stirred at 130 °C for 16 hours under nitrogen. The mixture was cooled to room temperature, 10 % v/v aqueous HCl (200 mL) was added and the suspension was stirred at room temperature for 30 minutes. The precipitate was collected by filtration and washed with water (100 mL). The red coloured crude product was dried in a 70 °C *in vacuo* (60 mbar). No further purification was required and the crude product was used in the subsequent step. **13** (1.51 g, 64 %, Figure 1.13).

HRMS: Found m/z 494.1862 (M+H)⁺; Calculated m/z 494.1863

M. pt. Found: 264-266 °C

FT-IR: $\bar{\nu}$ / cm⁻¹: 2900-3550 (O-H stretch), 3057, 3030 (C-H stretch, aromatic), 1506 (C=N stretch, conjugated), 1254 (C-O stretch)

UV λ_{\max} (0.1 mM in DMSO): 322 nm ($\epsilon = 60,000 \text{ cm}^{-1} \text{ M}^{-1}$)

TGA (Air): Weight loss at 300 °C (7.76 %); Onset temperature (336 °C)

¹H NMR (400 MHz, DMSO-d₆) δ : 6.40 (**d**, J = 2.3 Hz, 1H, H₉), 6.55 (**dd**, J = 8.9, 2.3 Hz, 1H, H₇), 7.46 (**t**, J = 7.3 Hz, 2H, H₁), 7.51-7.56 (**m**, 4H, H₂), 7.79 (**m**, 4H, H₃), 7.93 (**d**, J = 8.5 Hz, 4H, H₄), 8.50 (**d**, J = 8.9 Hz, 1H, H₆), 8.60 (**d**, J = 8.5 Hz, 4H, H₅), 10.51 (**s**, 1H, H₈), 13.29 (**s**, 1H, H₁₀)

¹³C NMR (100 MHz, CDCl₃) δ : 103.0 (C₁₅), 108.9 (C₁₃), 109.0 (C₁₁), 127.0 (C₃), 127.2 (C₆), 128.4 (C₁), 129.08 (C₂), 129.11 (C₇), 131.5 (C₁₂), 133.6 (C₄), 138.9 (C₅), 144.6 (C₈), 163.8 (C₁₄ or C₁₆), 164.3 (C₁₄ or C₁₆), 169.1 (C₉), 170 (C₁₀)

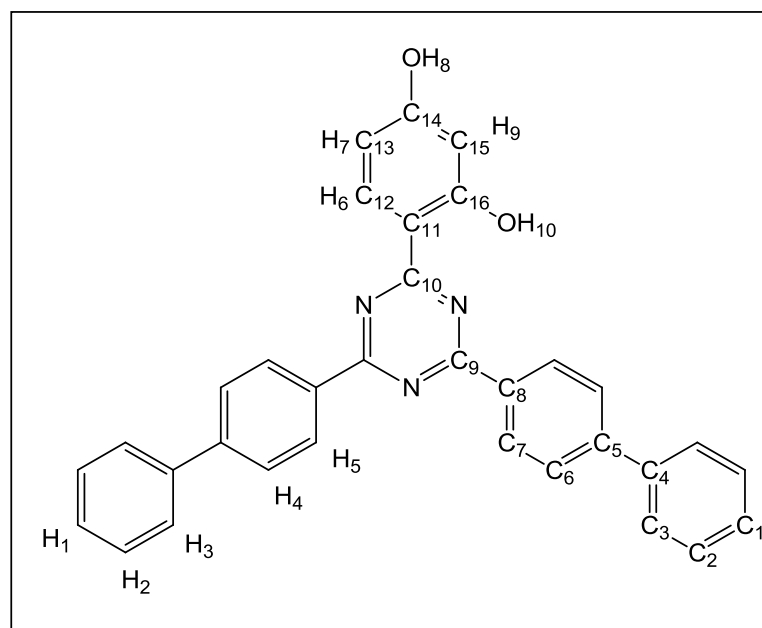


Fig.3.13 – Chemical structure of 13

4-(4,6-Diphenyl-1,3,5-triazin-2-yl)naphthalene-1,3-diol (14)

AlCl_3 (0.30 g, 2.24 mmol) was added to 1,3-dihydroxynaphthalene **3.3** (0.36 g, 2.24 mmol) and 2-chloro-4,6-diphenyl-1,3,5-triazine **2** (0.50 g, 1.87 mmol) in anhydrous 1,2-dichloroethane (20 mL) and the mixture was stirred at reflux temperature for 16 hours under nitrogen. The solvent was removed under reduced pressure and the residue was suspended in 10 % v/v aqueous HCl (80 mL). The suspension was stirred at room temperature for 15 mins and ultrasonicated at room temperature for a further 15 mins. The solid was collected by filtration and washed with water (100 mL). The crude solid was purified by grinding into a fine powder, suspending and washing with MeOH (30 mL). The orange coloured product was dried at 70 °C *in vacuo* (60 mbar). **14** (0.25 g, 34 %, Figure 3.14)

HRMS: Found m/z 392.1390 $[\text{M}+\text{H}]^+$; Calculated m/z 392.1405

M. pt. Found: 286-289 °C

FT-IR: $\bar{\nu}$ / cm^{-1} : 3200-3400 (O-H stretch), 3047 (C-H stretch, aromatic), 1510 (C=N stretch, conjugated), 1145 (C-O stretch)

UV λ_{max} (0.1 mM in DMSO): 394 nm ($\epsilon = 21,000 \text{ cm}^{-1} \text{ M}^{-1}$)

TGA (Air): Weight loss at 300 °C (1.47 %); Onset temperature (313 °C)

^1H NMR (400 MHz, CDCl_3) δ : 6.63 (s, 1H, H₅), 7.38-7.42 (m, 1H, H₉), 7.65-7.70 (m, 5H, H₈ and H₂), 7.70-7.75 (m, 2H, H₁), 8.19 (m, 1H, H₁₀), 8.56 (m, 4H, H₃), 9.62 (m, 1H, H₇), 11.36 (s, 1H, H₆), 14.81 (s, 1H, H₄)

^{13}C NMR (100 MHz, CDCl_3) δ : 100.8 (C₉), 102.0 (C₇), 121.4 (C₁₁), 122.6 (C₁₆), 122.8 (C₁₅), 125.7 (C₁₃), 128.5 (C₃), 128.6 (C₁₄), 129.2 (C₂), 133.2 (C₁), 133.9 (C₁₂), 135.0 (C₄), 160.0 (C₈ or C₁₀), 165.6 (C₈ or C₁₀), 169.2 (C₅), 171.6 (C₆)

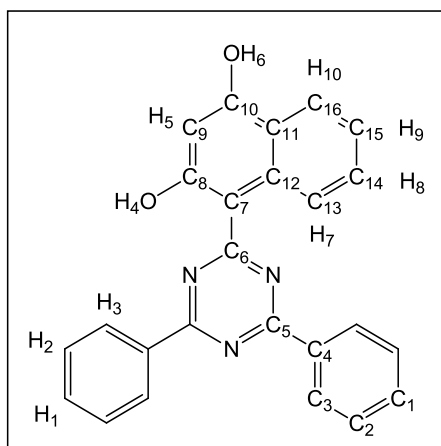


Fig.3.14 – Chemical structure of 14

4-(4,6-Bis(4-fluorophenyl)-1,3,5-triazin-2-yl)benzene-1,3-diol (15)

AlCl_3 (0.13 g, 0.99 mmol) was added to a suspension of 2-chloro-4,6-bis(4-fluorophenyl)-1,3,5-triazine **6** (0.25 g, 0.82 mmol) and resorcinol **1.136** (0.11 g, 0.99 mmol) in 1,2-dichlorobenzene (10 mL) and the mixture was stirred at 130 °C for 3 hours under nitrogen. The reaction mixture was cooled to room temperature and 10 % v/v aqueous HCl (30 mL) was added and stirred for 30 mins. The pink coloured precipitate was collected by filtration, washed with water (50 mL) and dried at 70 °C *in vacuo* (60 mbar). No further purification was required and the pink coloured solid was used in the subsequent step. **15** (0.26 g, 84 %, Figure 3.15).

HRMS: Found m/z 376.0909 $[\text{M}-\text{H}]^-$; Calculated m/z 376.0903

M. pt. Expected: >300 °C.¹²⁸ Found: 333-335 °C

FT-IR: $\bar{\nu}$ / cm^{-1} : 3250-3500 (O-H stretch), 3072 (C-H stretch, aromatic), 1519, 1504 (C=N stretch, conjugated), 1142 (C-O stretch)

UV λ_{max} (0.1 mM in DMSO): 342 nm ($\epsilon = 21,000 \text{ cm}^{-1} \text{ M}^{-1}$)

TGA (Air): Weight loss at 300 °C (4.78 %); Onset temperature (325 °C)

^1H NMR (500 MHz, DMSO- d_6) δ : 6.32 (**d**, $J = 2.4$ Hz, 1H, H₆), 6.46 (**dd**, $J = 8.8, 2.4$ Hz, 1H, H₄), 7.39 (**m**, 4H, H₁), 8.37 (**d**, $J = 8.8$ Hz, 1H, H₃), 8.48-8.50 (**m**, 4H, H₂), 10.45 (**s**, 1H, H₅), 12.99 (**s**, 1H, H₇)

^{13}C NMR (125 MHz, DMSO- d_6) δ : 103.5 (C₁₁), 109.27 (C₉), 109.32 (C₇), 116.5 (**d**, $J = 23$ Hz, C₂), 129.1 (**d**, $J = 3$ Hz, C₄), 131.6 (**d**, $J = 10$ Hz, C₃), 132.0 (C₈), 164.2 (C₁₀ or C₁₂), 164.8 (C₁₀ or C₁₂), 165.1 (**d**, $J = 245$ Hz, C₁), 168.9 (C₅), 171.0 (C₆)

^{19}F NMR (400 MHz, DMSO) δ : -106.1 (**m**, 2F, F)

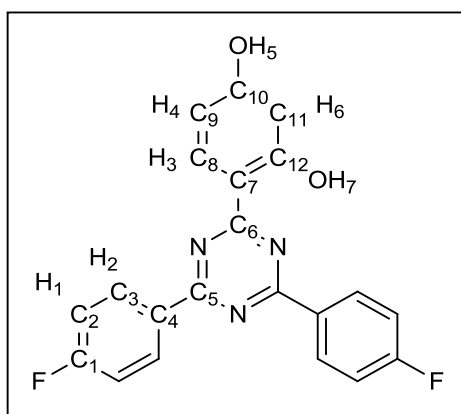


Fig.3.15 – Chemical structure of 15

4-(4,6-Bis(4-methoxyphenyl)-1,3,5-triazin-2-yl)benzene-1,3-diol (16)

AlCl_3 (0.12 g, 9.2 mmol) was added to a suspension of 2-chloro-4,6-bis(4-methoxyphenyl)-1,3,5-triazine **8** (0.25 g, 0.76 mmol) and resorcinol **1.136** (0.10 g, 0.92 mmol) in 1,2-dichlorobenzene (10 mL) and the reaction mixture was stirred at 130 °C for 16 hours under nitrogen. The reaction mixture was cooled to room temperature and 10 % v/v aqueous HCl (30 mL). The suspension was spun at 1000 rpm for 5 min and the supernatant was removed. The solid residue was collected by

filtration, washed with water (100 mL) and dried at 70 °C *in vacuo* (60 mbar). No further purification was necessary and the red coloured crude solid was used in the subsequent step. **16** (0.33 g, 90 %, Figure 3.16).

HRMS: Found m/z 400.1307 (M-H)⁻; Calculated m/z 400.1303

M. pt. Expected: 251-252 °C;¹³² Found: 253-255 °C

FT-IR: $\bar{\nu}$ / cm^{-1} : 2800-3500 (O-H stretch), 3076 (C-H stretch, aromatic), 2837 (C-H stretch, aliphatic), 1504 (C=N stretch, conjugated), 1145 (C-O stretch)

UV λ_{max} (0.1 mM in DMSO): 318 nm ($\epsilon = 53,000 \text{ cm}^{-1} \text{ M}^{-1}$)

TGA (Air): Weight loss at 300 °C (2.56 %); Onset temperature (333 °C)

¹H NMR (500 MHz, DMSO- d_6) δ : 3.87 (s, 6H, H₁), 6.36 (d, $J = 2.2 \text{ Hz}$, 1H, H₇), 6.49 (dd, $J = 8.8, 2.2 \text{ Hz}$, 1H, H₅), 7.13 (d, $J = 8.9 \text{ Hz}$, 4H, H₂), 8.42-8.45 (d, $J = 8.8 \text{ Hz}$, 1H, H₄), 8.44 (d, $J = 8.9 \text{ Hz}$, 4H, H₃) 10.42 (s, 1H, H₆), 13.40 (s, 1H, H₈)

¹³C NMR (125 MHz, DMSO- d_6) δ : 56.0 (C₁), 103.5 (C₁₂), 109.1 (C₁₀), 109.6 (C₈), 114.9 (C₃), 127.5 (C₅), 130.9 (C₄), 131.8 (C₉), 163.9 (C₂), 164.2 (C₁₁ or C₁₃), 164.5 (C₁₁ or C₁₃), 169.2 (C₆), 170.7 (C₇)

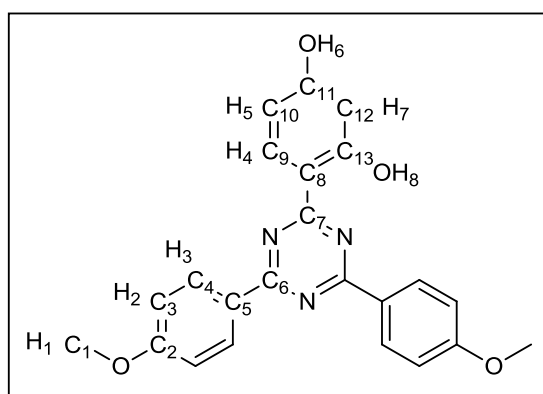


Fig.3.16 – Chemical structure of **16**

4,4'-(6-Phenyl-1,3,5-triazine-2,4-diyl)bis(benzene-1,3-diol) (17)

A mixture of 2,4-dichloro-6-phenyl-1,3,5-triazine **1** (8.00 g, 0.035 mol) and resorcinol **1.136** (7.99 g, 0.073 mol) in anhydrous 1,2-dichloroethane (250 mL) was warmed to 70 °C under nitrogen. Once the resorcinol **1.136** had dissolved, the reaction mixture was cooled to 40 °C and AlCl₃ (9.68 g, 0.073 mol) was added. The mixture was heated to 55 °C, and a dark red coloured precipitate formed after 1 hour which prevented stirring. The reaction was kept at 55 °C without stirring for a further 16 hours. The mixture was cooled to room temperature, water (200 mL) was added and the supernatant removed. The solid residue remaining in the reaction flask was suspended in hot MeOH/water (50/50, v/v, 250 mL) and ultrasonicated at 55 °C for 1 hour. The yellow coloured solid was collected by filtration and washed with MeOH (100 mL) and dried at 70 °C *in vacuo* (60 mbar). No further purification was necessary and the yellow coloured crude solid was used in the subsequent step. **17** (8.97 g, 68 %, Figure 3.17).

HRMS: Found m/z 374.1132 (M+H)⁺; Calculated m/z 374.1135

M. pt. Expected: >300 °C;¹³³ Found: 335-338 °C

FT-IR: $\bar{\nu}$ / cm⁻¹: 3200-3350 (O-H stretch), 3020 (C-H stretch, aromatic), 1508 (C=N stretch, conjugated), 1101 (C-O stretch)

UV λ_{\max} (0.1 mM in DMSO): 352 nm ($\epsilon = 36,000 \text{ cm}^{-1} \text{ M}^{-1}$)

TGA (Air): Weight loss at 300 °C (0.27 %); Onset temperature (415 °C)

¹H NMR (500 MHz, DMSO) δ : 6.36 (**d**, J = 2.3 Hz, 2H, H₇), 6.51 (**dd**, J = 8.8, 2.3 Hz, 2H, H₅), 7.62-7.65 (**m**, 2H, H₂), 7.71 (**t**, J = 7.3 Hz, 1H, H₁), 8.27 (**d**, J = 8.8 Hz, 2H, H₄), 8.33 (**d**, J = 7.3 Hz, 2H, H₃), 10.49 (**s**, 2H, H₆), 13.03 (**s**, 2H, H₈)

¹³C NMR (100 MHz, DMSO) δ : 103.6 (C₉), 109.3 (C₁₁), 109.4 (C₇), 128.7 (C₃), 129.7 (C₂), 131.9 (C₁₂), 133.8 (C₁), 134.8 (C₄), 164.2 (C₈ or C₁₀), 164.8 (C₈ or C₁₀), 168.3 (C₅), 169.8 (C₆)

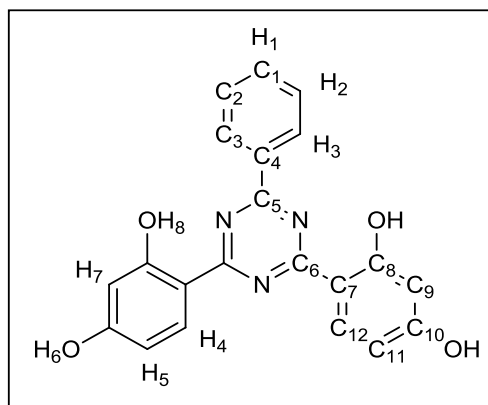


Fig.3.17 – Chemical structure of 17

4,4'-(6-(4-Methoxyphenyl)-1,3,5-triazine-2,4-diyl)bis(benzene-1,3-diol) (18)

AlCl_3 (1.19 g, 8.92 mmol) was added to a solution of 2,4-dichloro-6-(4-methoxyphenyl)-1,3,5-triazine **7** (1.00 g, 3.90 mmol) and resorcinol **1.136** (0.99 g, 9.00 mmol) in 1,2-dichlorobenzene (25 mL) and the mixture was stirred at 130 °C for 1 hour under nitrogen. A precipitate formed which was broken up using a glass rod and the reaction mixture was stirred at 130 °C for 16 hours. The mixture was cooled to room temperature, 10 % v/v aqueous HCl (30 mL) was added and stirred for 30 mins. The suspension was spun in a centrifuge (2000 rpm, 2 mins) and the supernatant was removed. The residue was resuspended in water (30 mL), spun in a centrifuge (2000 rpm, 2 mins) and the supernatant was removed. The solid residue was collected by filtration, washed with water (100 mL) and dried at 70 °C *in vacuo* (60 mbar). The crude brown coloured solid was purified by dissolving in hot DMF (10 mL) and precipitating the product with cold water (20 mL). The precipitate was collected by filtration, washed with water (100 mL) and the yellow coloured solid was dried at 70 °C *in vacuo* (60 mbar). **18** (1.12 g, 71 %, Figure 3.18).

HRMS: Found m/z 404.1245 ($\text{M}+\text{H}^+$); Calculated m/z 404.1241

M. pt. Expected: >360 °C;¹³⁴ Found: >360 °C

FT-IR: $\bar{\nu}$ / cm^{-1} : 2900-3600 (O-H stretch), 3022 (C-H stretch, aromatic), 2850 (C-H stretch, aliphatic), 1506 (C=N stretch, conjugated), 1165 (C-O stretch)

UV λ_{\max} (0.1 mM in DMSO): 343 nm ($\epsilon = 46,000 \text{ cm}^{-1} \text{ M}^{-1}$)

TGA (Air): Weight loss at 300 °C (3.17 %); Onset temperature (354 °C)

^1H NMR (400 MHz, DMSO- d_6) δ : 3.88 (s, 3H, H₁), 6.36 (d, J = 2.3 Hz, 2H, H₅), 6.50 (dd, J = 8.8, 2.3 Hz, 2H, H₇), 7.16 (d, J = 9.0 Hz, 2H, H₂), 8.23-8.28 (m, 4H, H₈ and H₃), 10.46 (s, 2H, H₆), 13.35 (s, 2H, H₄)

^{13}C NMR (100 MHz, DMSO- d_6) δ : 55.6 (C₁), 103.1 (C₁₀), 108.78 (C₁₂), 108.82 (C₈), 114.6 (C₃), 126.2 (C₅), 130.2 (C₁₃), 131.2 (C₄), 163.6 (C₂), 163.7 (C₉ or C₁₁), 164.2 (C₉ or C₁₁), 167.1 (C₆), 169.1 (C₇)

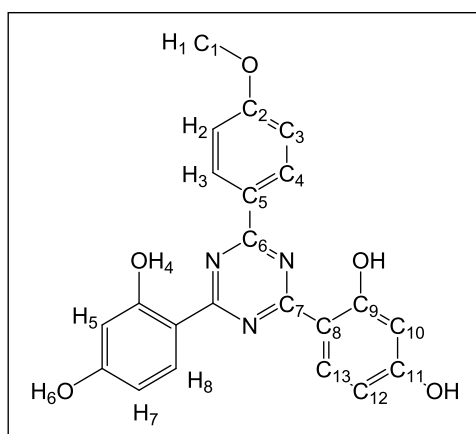


Fig.3.18 – Chemical structure of 18

4,4',4''-(1,3,5-Triazine-2,4,6-triyl)tris(benzene-1,3-diol) (19)

AlCl_3 (11.25 g, 84.37 mmol) was added to cyanuric chloride **1.90** (5.00 g, 27.10 mmol) and resorcinol **1.136** (9.25 g, 84.01 mmol) in 1,2-dichloroethane (250 mL) and the mixture was stirred at reflux temperature for 16 hours under nitrogen. A precipitate formed overnight which prevented stirring, so a glass rod was used to break the solid up and the reaction was stirred at reflux for an additional 4 hours. The suspension was cooled to room temperature, added slowly to cold water (150 mL) and stirred at room temperature for 1 hour. The solid was collected by filtration, washed with water (100 mL) and dried *in vacuo* at 70 °C (60 mbar). The brown/yellow solid was recrystallised from DMF to afford a bright yellow coloured solid which was washed

suspended in water (200 mL) and stirred at room temperature for 3 hours. The off white coloured precipitate was collected by filtration, washed with water (100 mL) and dried at 70 °C *in vacuo* (<1 mbar). The crude product was purified by flash column chromatography on silica gel (100 % CHCl₃, R_f value for **20** in CHCl₃ = 0.33). The solvent was removed under reduced pressure and the white coloured solid was dried at 70 °C *in vacuo* (<1 mbar). **20** (10.50 g, 86 %, Figure 3.20).

HRMS: Found m/z 409.0928 [M-H]⁻; Calculated m/z 409.0920

M. pt. Found: 164-166 °C

FT-IR: $\bar{\nu}$ / cm⁻¹: 3412 (O-H narrow stretch), 2995 (C-H stretch, aliphatic), 1743, 1726 (C=O stretch, ester), 1517, 1504 (C=N stretch, conjugated), 1230, 1205 (C-O stretch)

UV λ_{\max} (0.1 mM in DMSO): 334 nm (ϵ = 19,000 cm⁻¹ M⁻¹)

TGA (Air): Weight loss at 300 °C (11.00 %); Onset temperatures (197 and 329 °C)

¹H NMR (400 MHz, DMSO) δ : 1.21 (apparent **q**, J = 6.9 Hz, 6H, H₁), 4.13-4.19 (**m**, 4H, H₂), 4.52 (apparent **d**, J = 4.2 Hz, 4H, H₃), 6.30 (**d**, J = 2.3 Hz, 1H, H₅), 6.45 (**dd**, J = 2.3, 8.9 Hz, 1H, H₇), 8.05 (**d**, J = 8.9 Hz, 1H, H₄), 10.57 (**s**, 1H, H₆), 12.02 (**s**, 1H, H₈)

¹³C NMR (100 MHz, DMSO-d₆) δ : 14.0 (C₁), 50.4 (C₄ or C₁₄), 50.9 (C₄ or C₁₄), 60.9 (C₂), 102.9 (C₁₂), 107.7 (C₈), 109.0 (C₁₀), 131.5 (C₉), 163.3 (C₁₁ or C₁₃), 163.7 (C₁₁ or C₁₃), 164.6 (C₅), 167.4 (C₇), 168.25 (C₃ or C₁₅), 168.31 (C₃ or C₁₅), 170.7 (C₆)

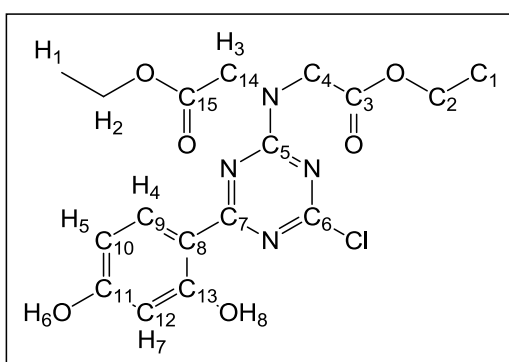


Fig.3.20 – Chemical structure of **20**

Diethyl 2,2'-((4,6-bis(2-hydroxy-4,6-dimethoxyphenyl)-1,3,5-triazin-2-yl)azanediyl)diacetate (21)

AlCl₃ (0.59 g, 4.45 mmol) was added to a mixture of diethyl 2,2'-((4,6-dichloro-1,3,5-triazin-2-yl)azanediyl)diacetate **9** (0.50 g, 1.48 mmol) and 3,5-dimethoxyphenol **1.134** (0.69 g, 4.45 mmol) in 1,2-dichloroethane (25 mL) and stirred at reflux temperature for 16 hours under nitrogen. The solvent was removed under reduced pressure. The residue was suspended in water (50 mL) and stirred at room temperature for 30 mins. The solid was collected by filtration, washed with water (50 mL) and dried at 70 °C *in vacuo* (60 mbar). The crude product was purified by flash column chromatography on silica gel (100 % CHCl₃, R_f value for **21** in CHCl₃ = 0.28). The solvent was removed under reduced pressure and the beige coloured solid was dried at 70 °C *in vacuo* (60 mbar). **21** (0.42 g, 30 %, Figure 3.21).

HRMS: Found m/z 573.2197 (M+H)⁺; Calculated m/z 573.2202

M. pt. Found: 175-176 °C

FT-IR: $\bar{\nu}$ / cm⁻¹: 2958, 2937 (C-H stretch, aliphatic), 1744 (C=O stretch, ester) 1549 (C=N stretch, conjugated), 1204, 1156, 1106 (C-O stretch)

UV λ_{\max} (0.1 mM in DMSO): 327 nm (ϵ = 35,000 cm⁻¹ M⁻¹)

TGA (Air): Weight loss at 300 °C (2.79 %); Onset temperatures (325 °C)

¹H NMR (400 MHz, CDCl₃) δ : 1.28 (t, J = 7.1 Hz, 6H, H₁), 3.82 (s, 6H, H₆ or H₈), 3.90 (s, 6H, H₆ or H₈), 4.24 (q, J = 7.1 Hz, 4H, H₂), 4.52 (s, 4H, H₃), 6.02 (d, J = 2.4 Hz, 2H, H₅), 6.15 (d, J = 2.4 Hz, 2H, H₇), 14.38 (s, 2H, H₄)

¹³C NMR (100 MHz, CDCl₃) δ : 14.1 (C₁), 49.8 (C₄), 55.3 (C₁₃ or C₁₄), 55.6 (C₁₃ or C₁₄), 61.5 (C₂), 91.5 (C₁₁), 94.1 (C₉), 101.1 (C₇), 161.7 (C₅), 162.9 (C₈ or C₁₀ or C₁₂), 164.6 (C₈ or C₁₀ or C₁₂), 166.0 (C₈ or C₁₀ or C₁₂), 168.4 (C₆), 169.1 (C₃)

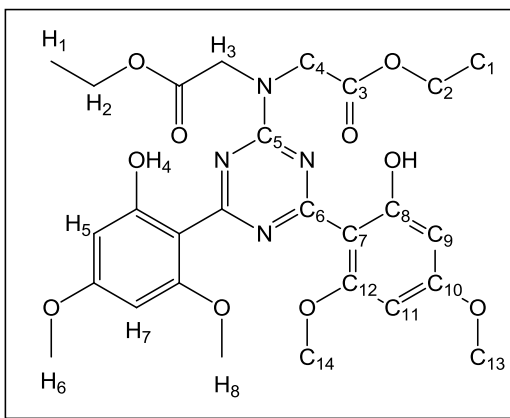


Fig.3.21 – Chemical structure of 21

Dimethyl 4,4'-((6-(2,4-dihydroxyphenyl)-1,3,5-triazine-2,4-diyl)bis(oxy))dibenzoate (22)

AlCl_3 (0.96 g, 7.2 mmol) was added to a mixture of dimethyl 4,4'-((6-chloro-1,3,5-triazine-2,4-diyl)bis(oxy))dibenzoate **10** (1.00 g, 2.40 mmol) and resorcinol **1.136** (0.79 g, 7.2 mmol) in 1,2-dichloroethane (50 mL) and stirred at reflux temperature for 16 hours under nitrogen. The solvent was removed under reduced pressure. The residue was suspended in 10 % v/v aqueous HCl (50 mL) and stirred at room temperature for 2 hours. The white coloured solid was collected by filtration and purified by grinding into a fine powder, suspending and washing using MeOH (50 mL). The white coloured solid was dried at 70 °C *in vacuo* (60 mbar). **22** (0.83 g, 71 %, Figure 3.22).

HRMS: Found m/z 488.1105 (M-H)⁻; Calculated m/z 488.1099

M. pt. Found: 192-193 °C

FT-IR: $\bar{\nu}$ / cm^{-1} : 2800-3300 (O-H stretch), 3068, 3010 (C-H stretch, aromatic), 2953 (C-H stretch, aliphatic), 1722 (C=O stretch, ester), 1556, 1537 (C=N stretch, conjugated), 1209, 1278 (C-O stretch)

UV λ_{max} (0.1 mM in DMSO): 335 nm ($\epsilon = 24,000 \text{ cm}^{-1} \text{ M}^{-1}$)

TGA (Air): Weight loss at 300 °C (21.34 %); Onset temperatures (236 °C)

^1H NMR (400 MHz, DMSO- d_6) δ : 3.89 (s, 6H, H₁), 6.21 (d, J = 2.2 Hz, 1H, H₅), 6.39 (dd, J = 8.9, 2.2 Hz, 1H, H₇), 7.50 (d, J = 8.7 Hz, 4H, H₃), 7.86 (d, J = 8.9 Hz, 1H, H₈), 8.09 (d, J = 8.7 Hz, 4H, H₂), 10.62 (s, 1H, H₆), 11.60 (s, 1H, H₄)

^{13}C NMR (100 MHz, DMSO- d_6) δ : 52.3 (C₁), 79.1 (C₁₁), 102.9 (C₁₃), 108.0 (C₁₄), 109.1 (C₉), 122.1 (C₅), 127.6 (C₃), 131.1 (C₄), 154.9 (C₆), 163.3 (C₁₀ or C₁₂), 164.8 (C₁₀ or C₁₂), 165.7 (C₂), 170.6 (C₇), 173.5 (C₈)

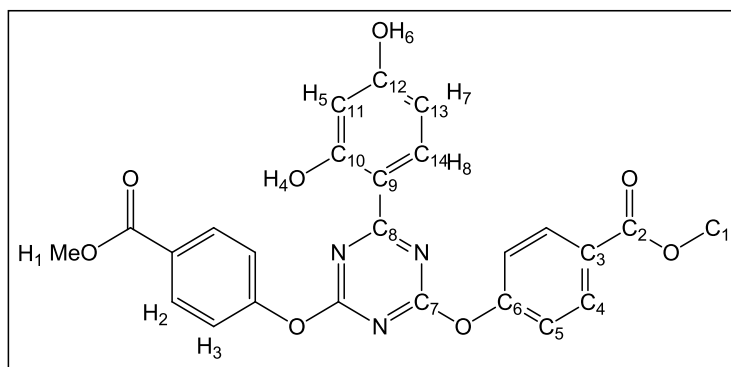


Fig.3.22 – Chemical structure of 22

3.1.3.4 Incorporation of Polymerisable Functional Groups

Diethyl 2-(6-bromohexyl)-2-methylmalonate (23)

NaH (3.00 g, 0.75 mol) in a 60 % mineral oil suspension was added to anhydrous THF (1 L) and stirred at 0 °C under nitrogen. To this, a solution of diethyl methylmalonate **3.4** (10.00 g, 57.40 mmol) in anhydrous THF (100 mL) was added dropwise over a period of 1 hour. Once the addition was complete, the reaction was stirred for 30 minutes and 1,6-dibromohexane **3.5** (55.00 g, 0.20 mol) added in one portion. The reaction was then stirred for 16 hours at room temperature. 1M aqueous NaOH (200 mL) was added to the reaction mixture and the organic product was extracted using ethyl acetate (2×100 mL). The organic phases were combined, washed with brine (100 mL), dried with anhydrous sodium sulfate and the solvent removed under reduced pressure. The colourless crude product was purified by flash column chromatography on silica gel (100 % hexane, switching to 2.5 % ethyl acetate in hexane, R_f value for **23** in 2.5 % ethyl acetate in hexane = 0.24). The solvent was

removed under reduced pressure and the colourless oil was dried at room temperature *in vacuo* (60 mbar). **23** (14.51 g, 75 %, Figure 3.23).

HRMS: Found m/z 337.1009 ($M(\text{Br}^{79})+\text{H}^+$), 339.0987 ($M(\text{Br}^{81})+\text{H}^+$); Calculated m/z 337.1002 and 339.0990

FT-IR: $\bar{\nu}$ / cm^{-1} : 2980, 2935, 2858 (C-H stretch, aliphatic), 1728 (C=O stretch, ester), 1249, 1109 (C-O stretch)

^1H NMR (400 MHz, CDCl_3) δ : 1.25 (t, $J = 7.1$ Hz, 6H, H_1), 1.38 (s, 3H, H_3), 1.23-1.39 (m, 6H, $\text{H}_5, \text{H}_6, \text{H}_7$), 1.42-1.48 (m, 2H, H_8), 1.81-1.88 (m, 2H, H_4) 3.39 (t, $J = 8.5$ Hz, 2H, H_9), 4.18 (q, $J = 7.1$ Hz, 4H, H_2)

^{13}C NMR (100 MHz, CDCl_3) δ : 13.4 (C_1), 19.2 (C_5), 23.5 (C_{11}), 27.3 (C_8 or C_9), 28.4 (C_8 or C_9), 32.1 (C_7 or C_{10}), 33.1 (C_7 or C_{10}), 34.8 (C_6), 53.0 (C_4), 60.5 (C_2), 171.8 (C_3)

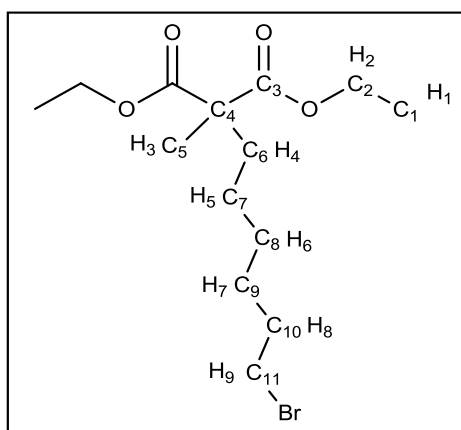


Fig.3.23 – Chemical structure of **23**

Diethyl 2-(6-(4-(4,6-diphenyl-1,3,5-triazin-2-yl)-3-hydroxyphenoxy)hexyl)-2-methylmalonate (24)

A solution of 4-(4,6-diphenyl-1,3,5-triazin-2-yl)benzene-1,3-diol **11** (15.26 g, 44.72 mmol) and Na_2CO_3 (9.48 g, 89.43 mmol) in DMF (200 mL) was stirred at 70 °C. To this, a solution of diethyl 2-(6-bromohexyl)-2-methylmalonate **23** (15.08 g, 44.72 mmol) in anhydrous DMF (100 mL) was added slowly, and once the addition was complete, the mixture was heated at 110 °C for 16 hours. The mixture was cooled

and the solvent was removed under reduced pressure. Toluene/acetone (7/3, v/v) (350 mL) was added to the residue and the organic salts were removed by filtration. The solvent was removed under reduced pressure and the crude product was suspended in MeOH (150 mL) for 24 hours, filtered and washed with MeOH (100 mL). The cream coloured solid was dried at 70 °C *in vacuo* (60 mbar) and then purified by flash column chromatography on silica gel (100% DCM, R_f value for **24** in DCM = 0.35). The solvent was removed under reduced pressure and the yellow coloured solid was dried at 70 °C *in vacuo* (60 mbar). **24** (16.20 g, 60 %, Figure 3.24).

HRMS: Found m/z 598.2914 (M+H)⁺; Calculated m/z 598.2912

M. pt. Found: 109 °C

FT-IR: $\bar{\nu}$ / cm⁻¹: 3031 (C-H stretch, aromatic), 2945, 2850 (C-H stretch, aliphatic), 1728 (C=O stretch, ester), 1508 (C=N stretch, conjugated), 1259, 1182 (C-O stretch)

UV λ_{\max} (0.1 mM in CHCl₃): 341 nm (ϵ = 26,000 cm⁻¹ M⁻¹)

TGA (Air): Weight loss at 300 °C (0.59 %); Onset temperature (365 °C)

¹H NMR (500 MHz, CDCl₃) δ : 1.27 (**t**, J = 7.1 Hz, 6H, H₁₆), 1.40 (**s**, 3H, H₁₄), 1.30-1.56 (**m**, 6H, H₁₀, H₁₁ and H₁₂), 1.79-1.91 (**m**, 4H, H₉ and H₁₃), 4.02 (**t**, J = 6.5 Hz, 2H, H₈), 4.20 (**q**, J = 7.1 Hz, 4H, H₁₅), 6.50 (**d**, J = 2.4 Hz, 1H, H₆), 6.57 (**dd**, J = 11.0, 2.4 Hz, 1H, H₅), 7.55-7.58 (**m**, 4H, H₂), 7.60-7.63 (**m**, 2H, H₁), 8.58-8.60 (**m**, 5H, H₃ and H₄), 13.52 (**s**, 1H, H₇)

¹³C NMR (100 MHz, CDCl₃) δ : 14.3 (C₂₃), 20.1 (C₂₀), 24.4 (C₁₅ or C₁₆), 26.0 (C₁₅ or C₁₆), 29.2 (C₁₄ or C₁₇), 29.8 (C₁₄ or C₁₇), 35.7 (C₁₈), 53.9 (C₁₉), 61.3 (C₂₂), 68.3 (C₁₃), 101.9 (C₁₁), 108.4 (C₉), 110.8 (C₇), 129.0 (C₂) 129.1 (C₃), 131.5 (C₈), 133.1 (C₁), 135.6 (C₄), 164.6 (C₁₀ or C₁₂), 165.3 (C₁₀ or C₁₂), 171.5 (C₅ and C₆), 172.7 (C₂₁)

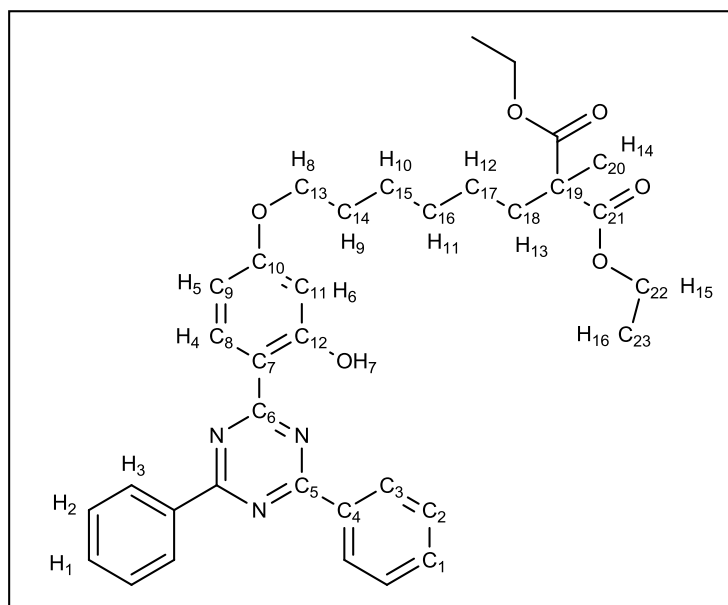


Fig.3.24 – Chemical structure of **24**

2-(6-(4-(4,6-Diphenyl-1,3,5-triazin-2-yl)-3-hydroxyphenoxy)hexyl)-2-methylpropane-1,3-diol (25**)**

A suspension of LiAlH_4 (0.04 g, 1.01 mmol) in anhydrous THF (5 mL) was stirred at 0 °C under nitrogen atmosphere. To this, a solution of diethyl 2-(6-(4-(4,6-diphenyl-1,3,5-triazin-2-yl)-3-hydroxyphenoxy)hexyl)-2-methylmalonate **24** (0.20 g, 0.39 mmol) in anhydrous THF (5 mL) was added slowly. The mixture was then stirred at room temperature for one hour and then refluxed for a further two hours. The reaction was left stirring overnight at room temperature and was then quenched with water (0.039 mL), 10 % v/v aqueous NaOH (0.078 mL) and water (0.117 mL) at 0 °C. The reaction mixture was stirred for two hours at room temperature and then filtered through a pad of Celite, washing with THF (20 mL). The filtrate was dried with anhydrous sodium sulfate, filtered and the solvent was removed under reduced pressure. The crude product was purified by flash column chromatography on silica gel (100 % DCM, switching to 2.5 %, 5 % and 10 % MeOH in DCM, R_f value for **25** in 10 % MeOH in DCM = 0.39). The solvent was removed under reduced pressure and the purified white powder was dried overnight at 70 °C *in vacuo* (60 mbar). **25** (109 mg, 52 %, Figure 3.25).

HRMS: Found m/z 514.2703 ($M+H$)⁺; Calculated m/z 514.2700

M. pt. Found: 143 – 145 °C

FT-IR: $\bar{\nu}$ / cm^{-1} : 3150-3350 (O-H stretch), 2937 (C-H stretch, aliphatic), 1510 (C=N stretch, conjugated)

UV λ_{max} (0.1 mM in CHCl_3): 342 nm ($\epsilon = 22,000 \text{ cm}^{-1} \text{ M}^{-1}$)

TGA (Air): Weight loss at 300 °C (3.10 %); Onset temperature (392 °C)

^1H NMR (500 MHz, CDCl_3) δ : 0.85 (s, 3H, H_{14}), 1.35-1.43 (m, 6H, H_{10} , H_{11} , H_{12}), 1.48-1.56 (m, 2H, H_{13}) 1.79-1.86 (m, 2H, H_9), 2.50 (s, 2H, H_{16}) 3.56 (m, 4H, H_{15}), 4.03 (t, $J = 8.2 \text{ Hz}$, 2H, H_8), 6.52 (d, $J = 3.1 \text{ Hz}$, 1H, H_6), 6.58 (dd, $J = 11.2, 3.1 \text{ Hz}$, 1H, H_5), 7.54-7.58 (m, 4H, H_2), 7.62 (m, 2H, H_1), 8.57-8.64 (m, 5H, H_3 , H_4), 13.51 (s, 1H, H_7)

^{13}C NMR (100 MHz, CDCl_3) δ : 18.0 (C_{20}), 22.7 (C_{15} or C_{16}), 25.5 (C_{15} or C_{16}), 28.6 (C_{14} or C_{17}), 29.8 (C_{14} or C_{17}), 33.4 (C_{18}), 38.3 (C_{19}), 67.7 (C_{13}), 70.2 (C_{21}), 101.3 (C_{11}), 107.8 (C_9), 110.1 (C_7), 128.3 (C_2) 128.4 (C_3), 130.8 (C_8), 132.4 (C_1), 135.6 (C_4), 163.8 (C_{10} or C_{12}), 164.6 (C_{10} or C_{12}), 170.8 (C_5 and C_6)

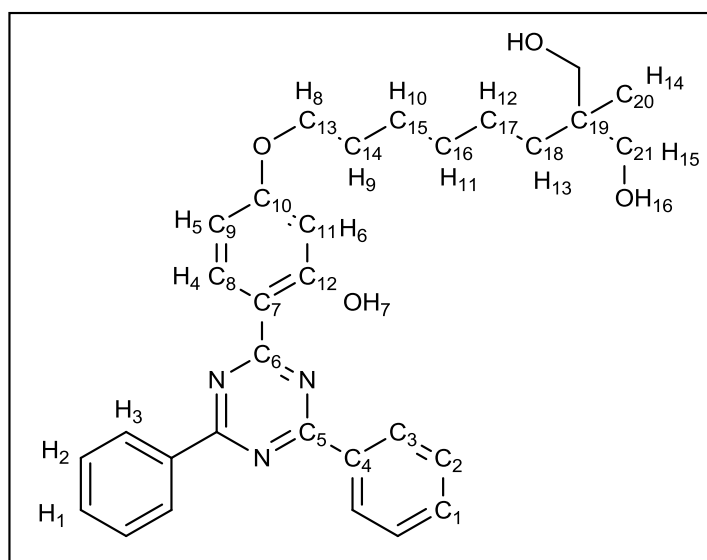


Fig.3.25 – Chemical structure of 25

2-(6-(4-(4,6-Diphenyl-1,3,5-triazin-2-yl)-3-hydroxyphenoxy)hexyl)-2-methylmalonic acid (26)

Diethyl 2-(6-(4-(4,6-diphenyl-1,3,5-triazin-2-yl)-3-hydroxyphenoxy)hexyl)-2-methylmalonate **24** (2.59 g, 4.33 mmol) was dissolved in DCM (5 mL) and added to MeOH (45 mL). To this, a solution of 3 N NaOH in MeOH (400 mL) was added and the mixture stirred at room temperature for 16 hours. The reaction was monitored by TLC for the disappearance of the ester starting material. The solvent was removed under reduced pressure and the residue was diluted with water (100 mL). The aqueous solution was extracted with diethyl ether (25 mL) to remove any unreacted ester. The aqueous phase was then acidified to pH 2-3 using 20 % v/v aqueous HCl and extracted with diethyl ether (3x25 mL). The combined organic layers were washed with water (2x50 mL), brine (50 mL), dried over anhydrous sodium sulfate and the solvent removed under reduced pressure. The crude product was purified by grinding into a fine powder, suspending and washing with cold DCM (50 mL). The purified yellow coloured solid was dried at 70 °C *in vacuo* (60 mbar). **26** (1.84 g, 78 %, Figure 3.26).

HRMS: Found m/z 542.2289 (M+H)⁺; Calculated m/z 542.2286

M. pt. Found: 110-112 °C

FT-IR: $\bar{\nu}$ / cm⁻¹: 2600-3300 (weak and broad, O-H stretch), 2937 (C-H stretch, aliphatic), 1705 (C=O stretch), 1508 (C=N stretch, conjugated)

UV λ_{\max} (0.1 mM in DMSO): 342 nm (ϵ = 21,000 cm⁻¹ M⁻¹)

TGA (Air): Weight loss at 300 °C (11.64 %); Onset temperatures (181 and 324 °C)

¹H NMR (500 MHz, DMSO) δ : 1.20-1.43 (m, 6H, H₁₀, H₁₁, H₁₂), 1.24 (s, 3H, H₁₄), 1.66-1.75 (m, 4H, H₉, H₁₃), 3.96 (t, J = 6.6 Hz, 2H, H₈), 6.43 (d, J = 2.5 Hz, 1H, H₆), 6.56 (dd, J = 9.0, 2.5 Hz, 1H, H₅), 7.61-7.64 (m, 4H, H₂), 7.71 (m, 2H, H₁), 8.45 (d, J = 9.0 Hz, 1H, H₄), 8.50 (m, 4H, H₃), 12.59 (s, 2H, H₁₅), 13.22 (s, 1H, H₇)

^{13}C NMR (100 MHz, DMSO) δ : 20.2 (C₂₀), 24.4 (C₁₅ or C₁₆), 25.7 (C₁₅ or C₁₆), 28.9 (C₁₄ or C₁₇), 29.6 (C₁₄ or C₁₇), 35.6 (C₁₈), 53.2 (C₁₉), 68.3 (C₁₃), 102.0 (C₁₁), 108.6 (C₉), 110.3 (C₇), 129.0 (C₂), 129.5 (C₃), 131.5 (C₈), 133.7 (C₁), 135.1 (C₄), 164.2 (C₁₀ or C₁₂), 165.1 (C₁₀ or C₁₂), 169.1 (C₅), 171.0 (C₆), 174.2 (C₂₁)

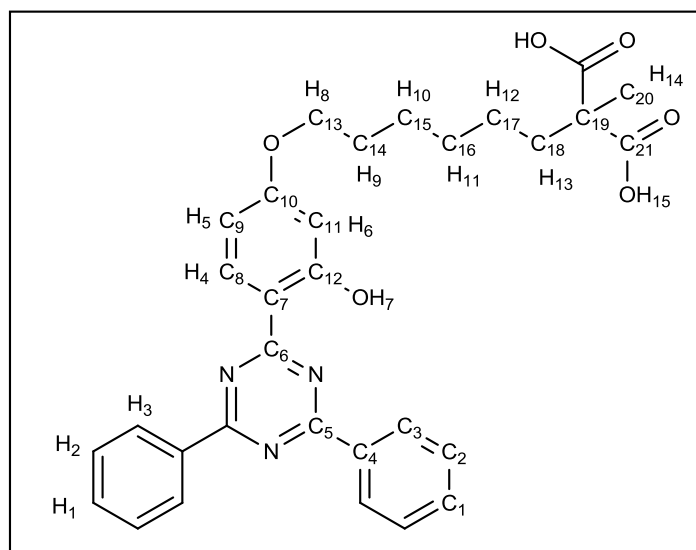


Fig.3.26 – Chemical structure of 26

Bis(2-hydroxyethyl) 2-(6-(4-(4,6-diphenyl-1,3,5-triazin-2-yl)-3-hydroxyphenoxy)hexyl)-2-methyl malonate (27)

Diethyl 2-(6-(4-(4,6-diphenyl-1,3,5-triazin-2-yl)-3-hydroxyphenoxy)hexyl)-2-methylmalonate **24** (5.04 g, 8.42 mmol), ethylene glycol (170.00 g, 2.70 mol) and Mn(OAc)₂·4H₂O (0.15 g 0.61 mmol) were added to a round-bottomed flask which was fitted with a Dean Stark trap. The reaction mixture was stirred at reflux temperature for 3 hours under nitrogen, then cooled to 100 °C and poured into cold distilled water (200 mL). The suspension was kept in a fridge at 3 °C for 3 hours and the precipitate was collected by filtration. The crude product was washed with water (150 mL) and dried at 70 °C *in vacuo* (60 mbar). (2.72 g, 51 % yield). 1.50 g of crude product was used in the polycondensation process. Purification of the remaining crude product was achieved by flash column chromatography on silica gel (100 % DCM, switching to 5 % MeOH in DCM, R_f value of **27** in 5 % MeOH in DCM = 0.32). The solvent was

removed under reduced pressure and the off-white coloured solid was dried at 70 °C *in vacuo* (60 mbar). **27** (0.43 g, 8 %, Figure 3.27).

HRMS: Found m/z 630.3211 (M+H)⁺; Calculated m/z 630.3209

M. pt. Found: 122-123 °C

FT-IR: $\bar{\nu}$ / cm^{-1} : 3200-3500 (O-H stretch), 2927, 2854 (C-H stretch, aliphatic), 1730, 1712 (C=O stretch, ester groups), 1506 (C=N stretch, conjugated), 1257, 1157 (C-O stretch)

UV λ_{max} (0.1 mM in DMSO): 342.0 nm ($\epsilon = 22,000 \text{ cm}^{-1} \text{ M}^{-1}$)

TGA (Air): Weight loss at 300 °C (1.13 %); Onset temperature (373 °C)

¹H NMR (400 MHz, CDCl₃) δ : 1.47 (s, 3H, H₁₄), 1.19-1.40 (m, 6H, H₁₀, H₁₁, H₁₂), 1.79-1.84 (m, 2H, H₉), 1.91-1.95 (m, 2H, H₁₃), 3.25 (s, 2H, H₁₇), 3.81-3.83 (m, 4H, H₁₆), 3.99 (t, 2H, J = 6.5 Hz, H₈), 4.29 (t, J = 3.7 Hz, 4H, H₁₅), 6.48 (d, J = 2.4 Hz, 1H, H₆), 6.56 (dd, J = 9.0, 2.4 Hz, 1H, H₅), 7.54-7.57 (m, 4H, H₂), 7.60 (m, 2H, H₁), 8.55-8.59 (m, 5H, H₃, H₄), 13.49 (s, 1H, H₇)

¹³C NMR (100 MHz, CDCl₃) δ : 20.1 (C₂₀), 24.2 (C₁₅ or C₁₆), 25.8 (C₁₅ or C₁₆), 29.0 (C₁₄ or C₁₇), 29.5 (C₁₄ or C₁₇), 35.6 (C₁₈), 53.7 (C₁₉), 60.8 (C₂₃), 66.8 (C₂₂), 68.1 (C₁₃), 101.7 (C₁₁), 108.2 (C₉), 110.6 (C₇), 128.8 (C₂), 128.9 (C₃), 131.3 (C₈), 132.9 (C₁), 135.4 (C₄), 164.3 (C₁₀ or C₁₂), 165.0 (C₁₀ or C₁₂), 171.2 (C₅ and C₆), 172.7 (C₂₁)

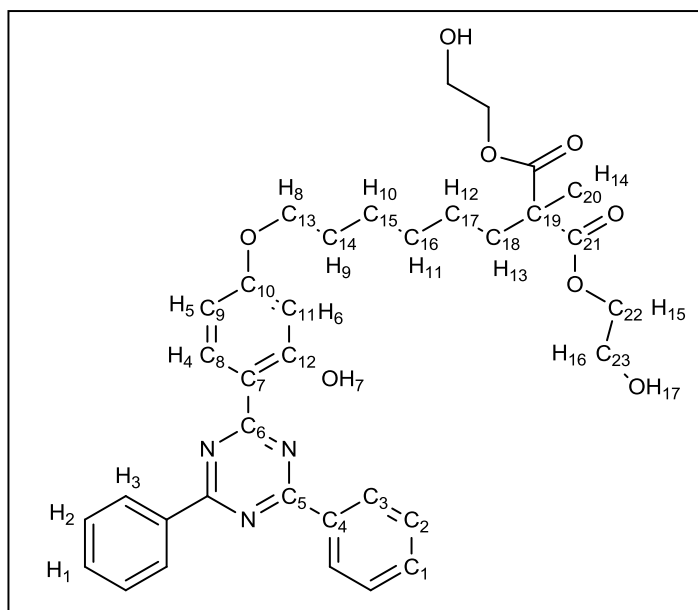


Fig.3.27 – Chemical structure of 27

2-Hydroxyethyl 8-(4-(4,6-diphenyl-1,3,5-triazin-2-yl)-3-hydroxyphenoxy)-2-methyl octanoate (28)

2-(6-(4-(4,6-Diphenyl-1,3,5-triazin-2-yl)-3-hydroxyphenoxy)hexyl)-2-methylmalonic acid **26** (1.5 g, 2.77 mmol), ethylene glycol (170.00 g, 2.70 mol) and Mn(OAc)₂·4H₂O (0.15 g 0.61 mmol) were added to a round-bottomed flask which was fitted with a Dean-Stark trap. The reaction flask was heated at reflux temperature for 3 hours under nitrogen, then cooled to 100 °C and poured into cold distilled water (200 mL). The suspension was kept in a fridge at 3 °C for 1 hour and the precipitate was collected by filtration. The crude product was washed with water (100 mL) and dried at 70 °C *in vacuo* (60 mbar). (0.75 g, 50 % yield). 0.26 g of crude product was used in the polycondensation process. Purification of the remaining crude product was achieved by flash column chromatography on silica gel (100 % DCM, R_f value for **28** in DCM = 0.24). The solvent was removed under reduced pressure and the off-white coloured solid was dried at 70 °C *in vacuo* (60 mbar). **28** (0.37 g, 25 %, Figure 3.28).

HRMS: Found m/z 542.2652 (M+H)⁺; Calculated m/z 542.2655

M. pt. Found: 145-147 °C

FT-IR: $\bar{\nu}$ / cm^{-1} : 3150-3500 (O-H stretch), 2934, 2858 (C-H stretch, aliphatic), 1724 (C=O stretch, ester groups), 1529, 1508 (C=N stretch, conjugated), 1257, 1120 (C-O stretch)

UV λ_{max} (0.1 mM in CHCl_3): 342 nm ($\epsilon = 23,000 \text{ cm}^{-1} \text{ M}^{-1}$)

TGA (Air): Weight loss at 300 °C (0.91 %); Onset temperature (346 °C)

^1H NMR (500 MHz, CDCl_3) δ : 1.19 (**d**, $J = 8.7 \text{ Hz}$, 3H, H_{14}), 1.32-1.54 (**m**, 6H, H_{10} , H_{11} , H_{12}), 1.67-1.86 (**m**, 5H, H_{13} , H_9 , H_{18}), 2.49-2.53 (**m**, 1H, H_{15}), 3.83-3.86 (**m**, 2H, H_{17}), 4.04 (**t**, $J = 8.2 \text{ Hz}$, 2H, H_8), 4.22-4.24 (**m**, 2H, H_{16}), 6.52 (**d**, $J = 3.1 \text{ Hz}$, 1H, H_6), 6.59 (**dd**, $J = 11.2, 3.1 \text{ Hz}$, 1H, H_5), 7.55-7.59 (**m**, 4H, H_2), 7.60 (**m**, 2H, H_1), 8.60-8.62 (**m**, 5H, H_3 , H_4), 13.51 (**s**, 1H, H_7)

^{13}C NMR (100 MHz, CDCl_3) δ : 17.2 (C_{20}), 26.1 (C_{15} or C_{16}), 27.3 (C_{15} or C_{16}), 29.2 (C_{14} or C_{17}), 29.4 (C_{14} or C_{17}), 33.9 (C_{18}), 38.9 (C_{19}), 61.2 (C_{23}), 66.6 (C_{22}), 68.3 (C_{13}), 101.9 (C_{11}), 108.2 (C_9), 110.9 (C_7), 129.0 (C_2), 129.1 (C_3), 131.6 (C_8), 133.2 (C_1), 135.4 (C_4), 164.6 (C_{10} or C_{12}), 165.3 (C_{10} or C_{12}), 171.6 (C_5 and C_6), 177.2 (C_{21})

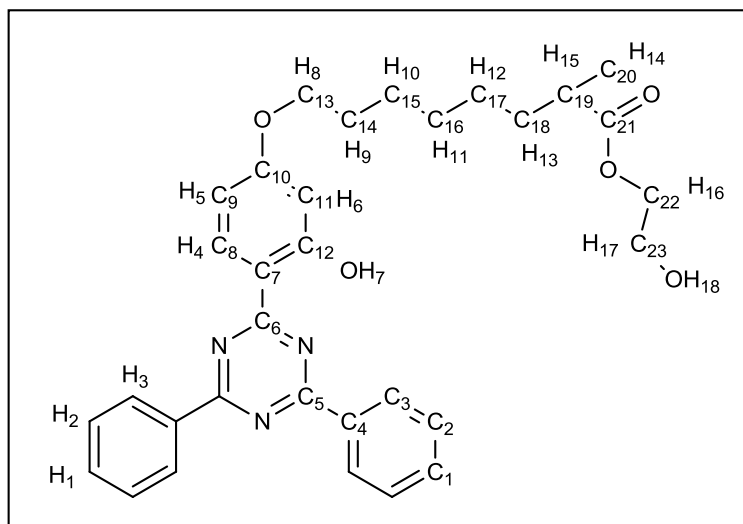


Fig.3.28 – Chemical structure of 28

Diethyl 2-(4-(4,6-diphenyl-1,3,5-triazin-2-yl)-3-hydroxyphenoxy)-2-methylmalonate (29)

A mixture of 4-(4,6-diphenyl-1,3,5-triazin-2-yl)benzene-1,3-diol **11** (0.25 g, 0.73 mmol) and Na₂CO₃ (0.15 g, 1.46 mmol) in DMF (20 mL) was heated to 70 °C. A solution of diethyl 2-bromo-2-methylmalonate **3.6** (0.20 g, 0.81 mmol) in DMF (10 mL) was added slowly, and once the addition was complete the mixture was heated at 110 °C overnight. The mixture was filtered whilst hot, the solvent was removed from the filtrate under reduced pressure and the residue was redissolved in ethyl acetate/MeOH (8/2, v/v, 50 mL). The organic layer was washed with 5 % v/v aqueous acetic acid (25 mL), 0.25 M aqueous NaHCO₃ (25 mL) and brine (25 mL). The solvent was dried using sodium sulfate and removed under reduced pressure. The crude product was suspended in MeOH (40 mL), filtered and the off-white coloured powder was dried at 70 °C *in vacuo* (60 mbar). **29** (0.23 g, 60.5 %, Figure 3.29).

HRMS: Found m/z 514.1976 (M+H)⁺; Calculated m/z 514.1973

M. pt. Found: 122-124 °C

FT-IR: $\bar{\nu}$ / cm⁻¹: 3031 (C-H stretch, aromatic), 2981 (C-H stretch, aliphatic), 1755, 1735 (C=O stretch, ester), 1525, 1508 (C=N stretch, conjugated), 1271, 1139 (C-O stretch)

UV λ_{\max} (0.1 mM in CHCl₃): 340 nm (ϵ = 19,000 cm⁻¹ M⁻¹)

TGA (Air): Weight loss at 300 °C (0.81 %); Onset temperature (342 °C)

¹H NMR (500 MHz, CDCl₃) δ : 1.31 (**t**, J = 7.1 Hz, 6H, H₁₀), 1.92 (**s**, 3H, H₈), 4.33 (**q**, J = 7.1 Hz, 4H, H₉), 6.61 (**d**, J = 2.5 Hz, 1H, H₆), 6.66 (**dd**, J = 8.9, 2.5 Hz, 1H, H₅), 7.57-7.60 (**m**, 4H, H₂), 7.65 (**m**, 2H, H₁), 8.63-8.65 (**m**, 5H, H₃, H₄), 13.45 (**s**, 1H, H₇)

¹³C NMR (100 MHz, CDCl₃) δ : 14.0 (C₁₇), 20.8 (C₁₄), 62.5 (C₁₆), 82.6 (C₁₃), 106.5 (C₁₁), 110.6 (C₉), 112.5 (C₇), 128.9 (C₂), 129.0 (C₃), 131.2 (C₈), 133.1 (C₁), 135.3 (C₄), 160.7 (C₁₀), 163.7 (C₁₂), 168.3 (C₁₅), 170.6 (C₆), 171.2 (C₅)

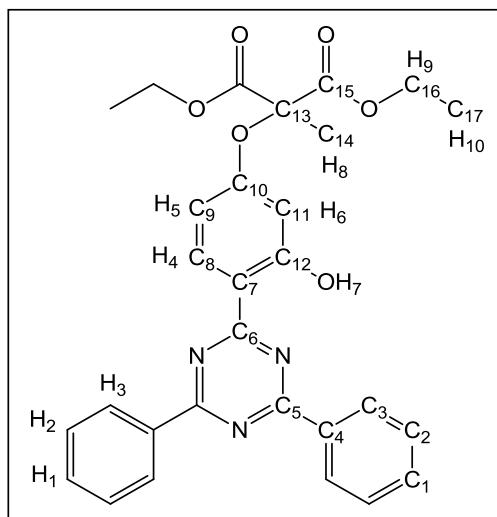


Fig.3.29 – Chemical structure of 29

Diethyl 2-(4-(4,6-di([1,1'-biphenyl]-4-yl)-1,3,5-triazin-2-yl)-3-hydroxyphenoxy)-2-methylmalonate (30)

A solution of 4-(4,6-di([1,1'-biphenyl]-4-yl)-1,3,5-triazin-2-yl)benzene-1,3-diol **13** (0.50 g, 1.01 mmol) and Na₂CO₃ (0.22 g, 2.02 mmol) in DMF (50 mL) was stirred at 70 °C for 1 hour. A solution of diethyl 2-bromo-2-methylmalonate **3.6** (0.31 g, 1.22 mmol) in DMF (50 mL) was added dropwise, and once the addition was complete the mixture was stirred at 110 °C for 16 hours. The mixture was filtered whilst hot and the solvent was removed under reduced pressure. The residue was redissolved in toluene/acetone (7/3, v/v, 100 mL) and filtered to remove inorganic salts. The solvent was removed under reduced pressure and the residue was suspended in MeOH (20 mL) and filtered. The crude product was purified by flash column chromatography on silica gel (100 % CHCl₃, R_f value for **30** in CHCl₃ = 0.42). The solvent was removed under reduced pressure and the red coloured solid was dried at 70 °C *in vacuo* (60 mbar). **30** (0.40 g, 59 %, Figure 3.30).

HRMS: Found m/z 666.2600 (M+H)⁺; Calculated m/z 666.2599

M. pt. Found: 150-151 °C

FT-IR: $\bar{\nu}$ / cm⁻¹: 3091 (C-H stretch, aromatic), 2947, 2896 (C-H stretch, aliphatic), 1722, 1708 (C=O stretch, ester), 1508 (C=N stretch, conjugated), 1245, 1157 (C-O stretch)

UV λ_{\max} (0.1 mM in CHCl₃): 323 nm ($\epsilon = 75,000 \text{ cm}^{-1} \text{ M}^{-1}$)

TGA (Air): Weight loss at 300 °C (1.29 %); Onset temperature (326 °C).

¹H NMR (500 MHz, CDCl₃) δ : 1.31 (**t**, $J = 7.1 \text{ Hz}$, 6H, H₁₂), 1.93 (**s**, 3H, H₁₀), 4.35 (**q**, $J = 7.1 \text{ Hz}$, 4H, H₁₁), 6.63 (**d**, $J = 2.5 \text{ Hz}$, 1H, H₈), 6.68 (**dd**, $J = 8.9, 2.5 \text{ Hz}$, 1H, H₇), 7.43 (**m**, 2H, H₁), 7.50-7.53 (**m**, 4H, H₂), 7.71 (**m**, 4H, H₃), 7.81 (**m**, 4H, H₄), 8.65 (**d**, $J = 8.9 \text{ Hz}$, 1H, H₆), 8.65-8.70 (**m**, 4H, H₅), 13.53 (**s**, 1H, H₉)

¹³C NMR (100 MHz, CDCl₃) δ : 13.5 (C₂₁), 20.33 (C₁₈), 62.0 (C₂₀), 82.2 (C₁₇), 106.0 (C₁₅), 110.1 (C₁₃), 112.1 (C₁₁), 126.8 (C₃), 127.0 (C₆), 127.7 (C₁), 128.5 (C₂), 129.0 (C₇), 130.7 (C₁₂), 133.7 (C₄), 139.6 (C₅), 145.3 (C₈), 160.2 (C₁₄), 163.2 (C₁₆), 167.8 (C₁₉), 170.7 (C₉ and C₁₀)

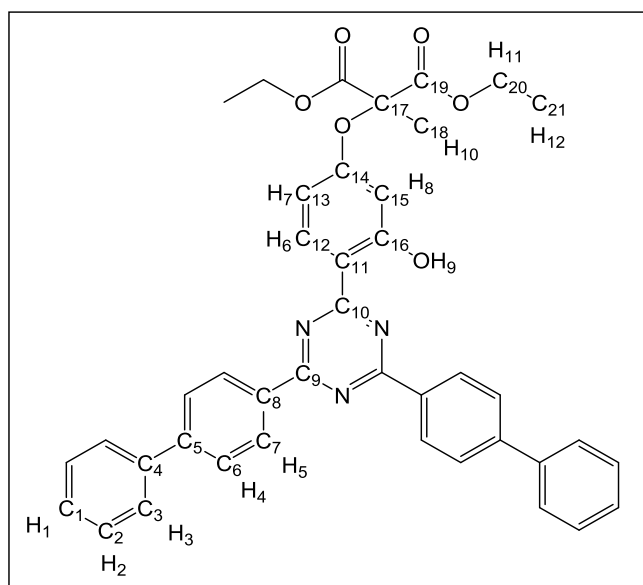


Fig.3.30 – Chemical structure of 30

2-(4,6-Diphenyl-1,3,5-triazin-2-yl)-5-(oxiran-2-ylmethoxy)phenol (31)

A solution of 4-(4,6-diphenyl-1,3,5-triazin-2-yl)benzene-1,3-diol **11** (0.25 g, 0.73 mmol) and Na₂CO₃ (0.16 g, 1.46 mmol) in anhydrous DMF (20 mL) was stirred at 70 °C. To this, a solution of epibromohydrin **3.7** (0.20 g, 1.46 mmol) in anhydrous DMF (5 mL) was added and the mixture was stirred at 110 °C for 16 hours. The reaction mixture was filtered whilst hot and the solvent was removed under reduced

pressure. The residue was suspended in toluene/acetone (7/3, v/v, 70 mL), filtered to remove salts and the solvent was removed under reduced pressure. The crude product was purified by flash column chromatography on silica gel (100 % CHCl₃, R_f value for **31** in CHCl₃ = 0.25). The solvent was removed under reduced pressure and the light yellow coloured solid was dried at 70 °C *in vacuo* (60 mbar). **31** (0.12 g, 41 %, Figure 3.31).

HRMS: Found m/z 456.1209 (M+COOH)⁺; Calculated m/z 456.1201

M. pt. Expected: 186 °C;¹³⁵ Found: 187-189 °C

FT-IR: $\bar{\nu}$ / cm⁻¹: 3250-3500 (O-H stretch), 3089, 3064 (C-H stretch, aromatic), 2926 (C-H stretch, aliphatic), 1508 (C=N stretch, conjugated), 1259 (C-O epoxide stretch)

UV λ_{\max} (0.1 mM in DMSO): 342 nm (ϵ = 21,000 cm⁻¹ M⁻¹)

TGA (Air): Weight loss at 300 °C (9.83 %); Onset temperature (204 and 342 °C)

¹H NMR (400 MHz, DMSO-d₆) δ : 4.20-4.24 (**m**, 1H, H₁₁ or H₁₂), 3.26-4.30 (**m**, 1H, H₁₁ or H₁₂), 4.38-4.42 (**m**, 1H, H₉ or H₈), 4.67 (apparent **t**, J = 8.6 Hz, 1H, H₉ or H₈), 5.15-5.19 (**m**, 1H, H₁₀), 6.43 (**s**, 1H, H₆), 6.54 (**d**, J = 8.8 Hz, 1H, H₅), 7.55-7.58 (**m**, 4H, H₂), 7.65 (**m**, 2H, H₁), 8.37-8.41 (**m**, 5H, H₃ and H₄), 13.17 (**s**, 1H, H₇)

¹³C NMR (100 MHz, DMSO-d₆) δ : 66.4 (C₁₃), 68.1 (C₁₅), 75.1 (C₁₄), 102.3 (C₁₁), 108.4 (C₉), 111.0 (C₇), 128.9 (C₃), 129.4 (C₂), 131.6 (C₈), 133.7 (C₁), 134.9 (C₄), 155.3 (C₁₀), 164.0 (C₁₂), 169.8 (C₅), 170.8 (C₆)

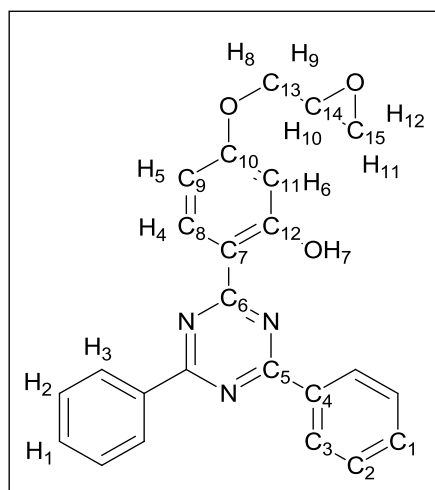


Fig.3.31 – Chemical structure of 31

3-[4-(4,6-Diphenyl-1,3,5-triazin-2-yl)-3-hydroxyphenoxy]-1,2-propanediol
(32)

Method 1

A solution of 2-(4,6-diphenyl-1,3,5-triazin-2-yl)-5-(oxiran-2-ylmethoxy)phenol **31** (0.10 g, 0.25 mmol) in THF (5 mL) was stirred at room temperature. To this, 0.4 M aqueous H₂SO₄ (5 mL) was added and the solution refluxed for 16 hours. The THF was removed under reduced pressure and the precipitate was collected by filtration and washed with water (20 mL). The crude product was purified by flash column chromatography on silica gel (100 % CHCl₃, switching to 10 % MeOH in CHCl₃, R_f value for **32** in 10 % MeOH in CHCl₃ = 0.35). The solvent was removed under reduced pressure and the yellow coloured solid was dried at 70 °C *in vacuo* (60 mbar). **32** (0.81 g, 75 %, Figure 3.32).

Method 2

A mixture of 4-(4,6-diphenyl-1,3,5-triazin-2-yl)benzene-1,3-diol **11** (1.50 g, 4.39 mmol), Na₂CO₃ (1.40 g, 13.18 mmol) and KI (1.10 g, 6.59 mmol) in DMF (100 mL) was stirred at 70 °C. To this, a solution of 3-chloropropane-1,2-diol **3.8** (1.95 g, 17.58 mmol) in DMF (50 mL) was added and stirred at 110 °C for 3 days. The mixture was filtered whilst hot and the solvent removed under reduced pressure. The residue

was suspended in water (75 mL) and stirred at room temperature for 30 mins. The solid was collected by filtration and washed with water (50 mL). The crude solid was purified by flash column chromatography on silica gel (10 % MeOH in CHCl₃, R_f value for **32** in 10 % MeOH in CHCl₃ = 0.35). The solvent was removed under reduced pressure and the yellow coloured solid was dried at 70 °C *in vacuo* (60 mbar). **32** (1.35 g, 75 %, Figure 3.32).

HRMS: Found m/z 416.1611 (M+H)⁺; Calculated m/z 416.1605

M. pt. Found: 203-205 °C

FT-IR: $\bar{\nu}$ / cm⁻¹: 3100-3400 (O-H stretch), 3060 (C-H stretch, aromatic), 2954, 2921, 2896 (C-H stretch, aliphatic), 1511 (C=N stretch, conjugated), 1355, 1262 (C-O stretch)

UV λ_{\max} (0.1 mM in DMSO): 342 nm (ϵ = 24,000 cm⁻¹ M⁻¹)

TGA (Air): Weight loss at 300 °C (2.26 %); Onset temperature (312 °C)

¹H NMR (400 MHz, DMSO-d₆) δ : 3.48 (**m**, 2H, H₁₁), 3.80-3.87 (**m**, 1H, H₁₀), 3.93-3.97 (**m**, 1H, H₈ or H₉), 4.07-4.11 (**m**, 1H, H₈ or H₉), 4.72 (**t**, J = 5.7 Hz, 1H, H₁₂), 5.02 (**d**, J = 5.2 Hz, 1H, H₁₃), 6.50 (**d**, J = 2.5 Hz, 1H, H₆), 6.62 (**dd**, J = 9.0, 2.5 Hz, 1H, H₅), 7.63-7.66 (**m**, 4H, H₂), 7.72 (**m**, 2H, H₁), 8.52-8.56 (**m**, 5H, H₃ and H₄), 13.31 (**s**, 1H, H₇)

¹³C NMR (100 MHz, DMSO-d₆) δ : 62.5 (C₁₅), 69.8 (C₁₄), 70.0 (C₁₃), 101.7 (C₁₁), 108.3 (C₉), 109.9 (C₇), 128.5 (C₃), 129.1 (C₂), 131.1 (C₈), 133.3 (C₁), 134.6 (C₄), 163.7 (C₁₀ or C₁₂), 164.8 (C₁₀ or C₁₂), 169.6 (C₅), 170.5 (C₆)

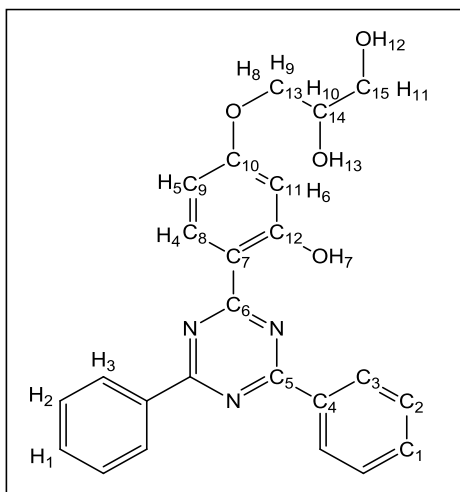


Fig.3.32 - Chemical structure of 32

3-[4-(4,6-Diphenyl-1,3,5-triazin-2-yl)-3,5-dihydroxyphenoxy]-1,2-propanediol (33)

A mixture of 4-(4,6-diphenyl-1,3,5-triazin-2-yl)benzene-1,3-diol **11** (1.50 g, 4.20 mmol), Na₂CO₃ (1.55 g, 14.70 mmol) and KI (1.22 g, 7.36 mmol) in DMF (100 mL) was stirred at 70 °C. To this, a solution of 3-chloropropane-1,2-diol **3.8** (2.09 g, 18.9 mmol) in DMF (50 mL) was added and stirred at 110 °C for 5 days. The mixture was filtered whilst hot and the solvent removed under reduced pressure. The residue was suspended in 10 % v/v aqueous HCl (50 mL) and stirred at room temperature for 30 mins. The solid was collected by filtration and washed with water (50 mL). The crude solid was dissolved in hot DMF (10 mL) and cooled to room temperature. To this, MeOH (70 mL) was added to form a precipitate which was collected by filtration and washed with MeOH (30 mL). The red coloured solid was dried at 70 °C *in vacuo* (60 mbar). **33** (1.23 g, 68 %, Figure 3.33).

HRMS: Found m/z 432.1560 (M+H)⁺; Calculated m/z 432.1554

M. pt. Found: 236-238 °C

FT-IR: $\bar{\nu}$ / cm⁻¹: 3100-3500 (O-H stretch), 3058 (C-H stretch, aromatic), 2900 (C-H stretch, aliphatic), 1511 (C=N stretch, conjugated), 1152 (C-O stretch)

UV λ_{\max} (0.1 mM in DMSO): 327 nm ($\epsilon = 34,000 \text{ cm}^{-1} \text{ M}^{-1}$)

TGA (Air): Weight loss at 300 °C (3.61 %); Onset temperature (329 °C).

^1H NMR (400 MHz, DMSO- d_6) δ : 3.46 (**d**, $J = 5.5$ Hz, 2H, H₉), 3.78-3.81 (**m**, 1H, H₈), 3.86-3.90 (**m**, 1H, H₆ or H₇), 4.01-4.04 (**m**, 1H, H₆ or H₇), 4.71 (**s**, 1H, H₁₀), 4.99 (**s**, 1H, H₁₁), 6.00 (**s**, 2H, H₅), 7.63-7.67 (**m**, 4H, H₂), 7.74 (**m**, 2H, H₁), 8.36 (**m**, 4H, H₃), 13.53 (**s**, 2H, H₄)

^{13}C NMR (100 MHz, DMSO- d_6) δ : 62.6 (C₁₃), 69.7 (C₁₂), 70.0 (C₁₁), 94.5 (C₉), 96.6 (C₇), 128.5 (C₃), 129.3 (C₂), 133.7 (C₁), 133.8 (C₄), 164.0 (C₁₀), 165.3 (C₈), 168.4 (C₅), 170.5 (C₆)

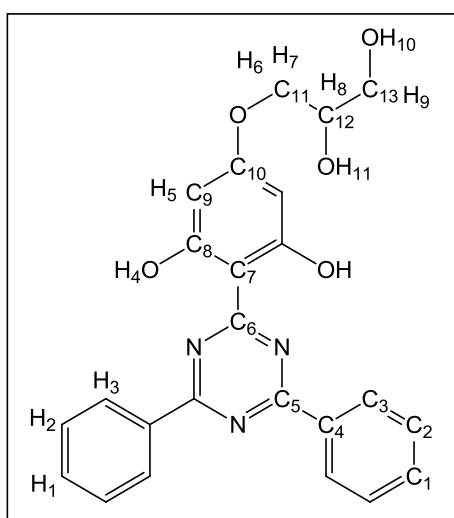


Fig.3.33 – Chemical structure of 33

3-{4-[4,6-Bis(4-biphenyl)-1,3,5-triazin-2-yl]-3,5-dihydroxyphenoxy}-1,2-propanediol (34)

A mixture of 4-(4,6-di([1,1'-biphenyl]-4-yl)-1,3,5-triazin-2-yl)benzene-1,3-diol **13** (0.25 g, 0.51 mmol), Na₂CO₃ (0.16 g, 1.52 mmol) and KI (0.13 g, 0.77 mmol) in DMF (10 mL) was stirred at 70 °C. To this, a solution of 3-chloropropane-1,2-diol **3.8** (0.23 g, 2.04 mmol) in DMF (5 mL) was added and stirred at 110 °C for 3 days. The mixture was filtered whilst hot and the solvent was removed under reduced pressure. The residue was suspended in 10 % v/v aqueous HCl (15 mL) and stirred at room temperature for 30 mins. The solid was collected by filtration and washed with water (30 mL). The crude solid was purified by flash column chromatography on silica gel

(10 % MeOH in CHCl₃, Rf value for **34** in 10 % MeOH in CHCl₃ = 0.40). The solvent was removed under reduced pressure and the red coloured solid was dried at 70 °C *in vacuo* (60 mbar). **34** (0.17 g, 59 %, Figure 3.34).

HRMS: Found m/z 568.2242 (M+H)⁺; Calculated m/z 568.2231

M. pt. Found: 251-252 °C

FT-IR: $\bar{\nu}$ / cm⁻¹: 3000-3600 (O-H stretch), 3030 (C-H stretch, aromatic), 2926 (C-H stretch, aliphatic), 1506 (C=N stretch, conjugated), 1260 (C-O stretch)

UV λ_{\max} (0.1 mM in DMSO): 323 nm (ϵ = 74,000 cm⁻¹ M⁻¹)

TGA (Air): Weight loss at 300 °C (3.29 %); Onset temperature (346 °C).

¹H NMR (500 MHz, DMSO-d₆) δ : 3.47-3.49 (**m**, 2H, H₁₃), 3.81-3.86 (**m**, 1H, H₁₂), 3.92-3.95 (**m**, 1H, H₁₀ or H₁₁), 4.05-4.08 (**m**, 1H, H₁₀ or H₁₁), 4.73 (**t**, J = 5.6 Hz, 1H, H₁₄), 5.02 (**d**, J = 5.2 Hz, 1H, H₁₅), 6.47 (**d**, J = 2.4 Hz, 1H, H₈), 6.61 (**dd**, J = 8.9, 2.4 Hz, 1H, H₇), 7.43 (**m**, 2H, H₁), 7.48-7.51 (**m**, 4H, H₂), 7.71 (**m**, 4H, H₃), 7.84 (**d**, J = 8.5 Hz, 4H, H₄), 8.44 (**d**, J = 8.9 Hz, 1H, H₆), 8.59 (**d**, J = 8.5 Hz, 4H, H₅), 13.24 (**s**, 1H, H₉)

¹³C NMR (100 MHz, DMSO-d₆) δ : 63.1 (C₁₉), 70.3 (C₁₈), 70.4 (C₁₇), 102.1 (C₁₅), 108.6 (C₁₃), 110.4 (C₁₁), 127.4 (C₃), 127.6 (C₆), 128.8 (C₁), 129.5 (C₂), 130.0 (C₇), 131.5 (C₁₂), 133.9 (C₄), 139.4 (C₅), 145.1 (C₈), 164.1 (C₁₄ or C₁₆), 165.2 (C₁₄ or C₁₆), 169.6 (C₉), 170.9 (C₁₀)

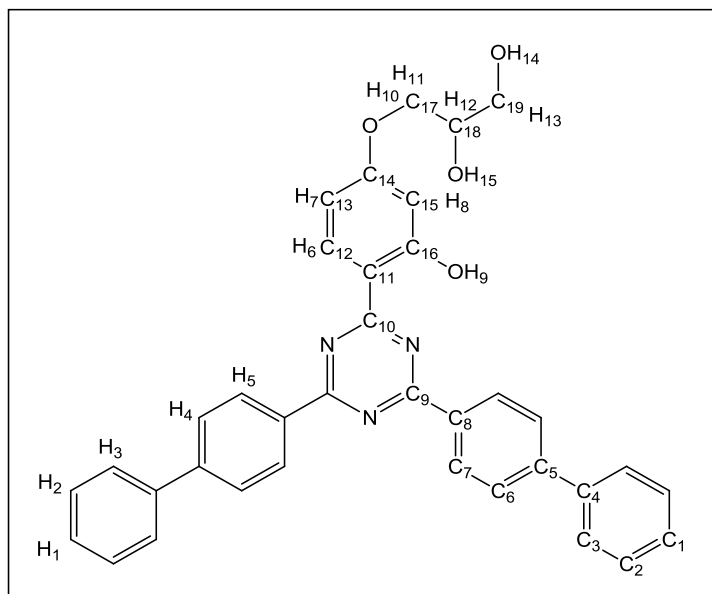


Fig.3.34 – Chemical structure of 34

3-(4-(4,6-Bis(4-fluorophenyl)-1,3,5-triazin-2-yl)-3-hydroxyphenoxy)propane-1,2-diol (35)

A mixture of 4-(4,6-bis(4-fluorophenyl)-1,3,5-triazin-2-yl)benzene-1,3-diol **15** (1.00 g, 2.65 mmol), KI (0.68 g, 4.10 mmol) and Na₂CO₃ (0.84 g, 7.93 mmol) in DMF (75 mL) was stirred at 70 °C. To this, a solution of 3-chloropropane-1,2-diol **3.8** (1.16 g, 10.49 mmol) in DMF (25 mL) was added and stirred at 110 °C for 16 hours. The mixture was filtered whilst hot and the solvent removed under reduced pressure. DMF (5 mL) was added to the residue followed by 5 % v/v aqueous HCl (50 mL). The precipitate was collected by filtration and washed with water (40 mL). The crude solid was purified by flash column chromatography on silica gel (10 % MeOH in CHCl₃, R_f value for **35** in 10 % MeOH in CHCl₃ = 0.37). The solvent was removed under reduced pressure and the yellow coloured solid was dried at 70 °C *in vacuo* (60 mbar). **35** (0.84 g, 70 %, Figure 3.35).

HRMS: Found m/z 450.1278 (M-H)⁻; Calculated m/z 450.1271

M. pt. Found: 182-185 °C

FT-IR: $\bar{\nu}$ / cm^{-1} : 3100-3400 (O-H stretch), 2932 (C-H stretch, aliphatic), 1530, 1504 (C=N stretch, conjugated), 1264, 1236, 1227 (C-O stretch)

UV λ_{max} (0.1 mM in DMSO): 342 nm ($\epsilon = 21,000 \text{ cm}^{-1} \text{ M}^{-1}$)

TGA (Air): Weight loss at 300 °C (4.07 %); Onset temperature (319 °C)

^1H NMR (400 MHz, DMSO- d_6) δ : 3.48 (**m**, 2H, H₁₀), 3.82-3.87 (**m**, 1H, H₉), 3.91-3.95 (**m**, 1H, H₇ or H₈), 4.05-4.08 (**m**, 1H, H₇ or H₈), 4.74 (**t**, $J = 5.6 \text{ Hz}$, 1H, H₁₁), 5.04 (**d**, $J = 5.1 \text{ Hz}$, 1H, H₁₂), 6.41 (**d**, $J = 2.4 \text{ Hz}$, 1H, H₅), 6.56 (**dd**, $J = 9.0, 2.4 \text{ Hz}$, 1H, H₄), 7.35-7.39 (**m**, 4H, H₁), 8.35 (**d**, $J = 9.0 \text{ Hz}$, 1H, H₃), 8.34-8.45 (**m**, 4H, H₂), 12.99 (**s**, 1H, H₆)

^{13}C NMR (100 MHz, DMSO- d_6) δ : 62.6 (C₁₅), 69.8 (C₁₄), 70.0 (C₁₃), 101.6 (C₁₁), 108.1 (C₉), 109.7 (C₇), 116.0 (**d**, $J = 22 \text{ Hz}$, C₂), 130.8 (**d**, $J = 3 \text{ Hz}$, C₄), 131.1 (**d**, $J = 9 \text{ Hz}$, C₃), 132.4 (C₈), 163.6 (C₁₀ or C₁₂), 164.8 (C₁₀ or C₁₂), 165.0 (**d**, $J = 254 \text{ Hz}$, C₁), 168.3 (C₅), 170.3 (C₆)

^{19}F NMR (400 MHz, DMSO) δ : -106.2 (**m**, 2F, F)

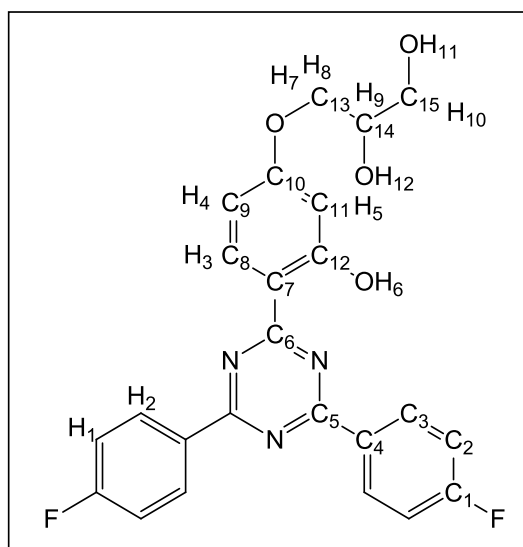


Fig.3.35 – Chemical structure of 35

3-(4-(4,6-Bis(4-methoxyphenyl)-1,3,5-triazin-2-yl)-3-hydroxyphenoxy)propane-1,2-diol (36)

A mixture of 4-(4,6-bis(4-methoxyphenyl)-1,3,5-triazin-2-yl)benzene-1,3-diol **16** (0.25 g, 0.62 mmol), Na₂CO₃ (0.23 g, 2.18 mmol) and KI (0.16 g, 0.90 mmol) in DMF (20 mL) was stirred at 70 °C. To this, a solution of 3-chloropropane-1,2-diol **3.8** (0.31 g, 2.80 mmol) in DMF (5 mL) was added and stirred at 110 °C for 7 days. The mixture was filtered whilst hot and more than 50 % of the solvent removed under reduced pressure. 5 % v/v aqueous HCl (50 mL) was added to the residue and the precipitate collected by filtration, washing with deionised water (50 mL). The crude solid was purified by flash column chromatography on silica gel (10 % MeOH in CHCl₃, R_f value for **36** in 10 % MeOH in CHCl₃ = 0.33). The solvent was removed under reduced pressure and the red coloured solid was dried at 70 °C *in vacuo* (60 mbar). **36** (0.19 g, 64 %, Figure 3.36).

HRMS: Found m/z 476.1821 (M+H)⁺; Calculated m/z 476.1816

M. pt. Found: 182-185 °C

FT-IR: $\bar{\nu}$ / cm⁻¹: 3050-3400 (O-H stretch), 3030 (C-H stretch, aromatic), 2954, 2928, 2837 (C-H stretch, aliphatic), 1504 (C=N stretch, conjugated), 1256, 1174 (C-O stretch)

UV λ_{\max} (0.1 mM in DMSO): 321 nm (ϵ = 55,000 cm⁻¹ M⁻¹)

TGA (Air): Weight loss at 300 °C (5.66 %); Onset temperature (310 °C).

¹H NMR (400 MHz, DMSO-d₆) δ : 3.47-3.51 (**m**, 2H, H₁₁), 3.84-3.86 (**m**, 1H, H₁₀), 3.88 (**s**, 6H, H₁), 3.93-3.97 (**m**, 1H, H₈ or H₉), 4.07-4.11 (**m**, 1H, H₈ or H₉), 4.71 (**t**, J = 5.3 Hz, 1H, H₁₂), 5.01 (**d**, J = 4.9 Hz, 1H, H₁₃), 6.49 (**d**, J = 2.4 Hz, 1H, H₆), 6.62 (**dd**, J = 8.9, 2.4 Hz, 1H, H₅), 7.12 (**d**, J = 7.1 Hz, 4H, H₂), 8.41-8.47 (**m**, 5H, H₃ and H₄), 13.41 (**s**, 1H, H₇)

¹³C NMR (100 MHz, DMSO-d₆) δ : 56.0 (C₁), 63.1 (C₁₆), 70.3 (C₁₅), 70.5 (C₁₄), 102.2 (C₁₂), 108.5 (C₁₀), 110.6 (C₈), 114.9 (C₃), 127.4 (C₅), 131.0 (C₄), 131.5 (C₉), 163.9 (C₂), 164.1 (C₁₁ or C₁₃), 165.0 (C₁₁ or C₁₃), 169.3 (C₆), 170.6 (C₇)

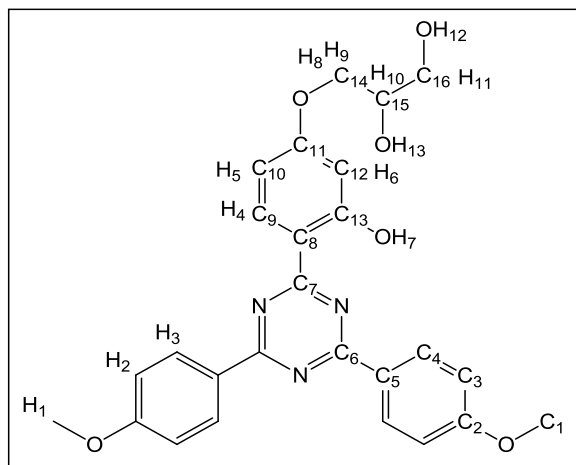


Fig.3.36 – Chemical structure of 36

6,6'-(6-Phenyl-1,3,5-triazine-2,4-diyl)bis(3-(2-hydroxyethoxy)phenol) (37)

A mixture of 4,4'-(6-phenyl-1,3,5-triazine-2,4-diyl)bis(benzene-1,3-diol) **17** (3.00 g, 8.04 mmol) and Na₂CO₃ (4.26 g, 40.20 mmol) in DMF (200 mL) was heated to 70 °C whilst stirring. A solution of 2-bromoethanol **3.9** (2.50 g, 20.00 mmol) in DMF (100 mL) was added slowly. Once the addition was complete, the mixture was stirred at 110 °C for 16 hours. The mixture was cooled to 70 °C and a second solution of 2-bromoethanol **3.9** (2.50 g, 20.00 mmol) in DMF (100 mL) was added dropwise. Once the addition was complete, the mixture was stirred at 110 °C for an additional 16 hours. The mixture was filtered whilst hot, the solvent removed under reduced pressure and the residue was redissolved in ethyl acetate/MeOH (8/2, v/v, 100 mL). The organic layer was washed with 5 % v/v aqueous acetic acid (50 mL), 0.25 M aqueous NaHCO₃ (50 mL) and brine (50 mL). The organic layer was dried using sodium sulfate and the solvent removed under reduced pressure. The light yellow solid was suspended in MeOH (25 mL), filtered and dried at 70 °C *in vacuo* (60 mbar). **37** (1.50 g, 41 %, Figure 3.37).

HRMS: Found m/z 462.1660 (M+H)⁺; Calculated m/z 462.1660

M. pt. Found: 222-225 °C

FT-IR: $\bar{\nu}$ / cm⁻¹: 3150-3400 (O-H stretch), 2921, 2879 (C-H stretch, aliphatic), 1537, 1508 (C=N stretch, conjugated), 1290, 1232 (C-O stretch)

UV λ_{\max} (0.1 mM in DMSO): 349 nm ($\epsilon = 37,000 \text{ cm}^{-1} \text{ M}^{-1}$)

TGA (Air): Weight loss at 300 °C (1.74 %); Onset temperature (388 °C)

^1H NMR (400 MHz, DMSO) δ : 3.73-3.77 (m, 4H, H₉), 4.06 (t, J = 4.8 Hz, 4H, H₈), 4.93 (t, J = 5.6 Hz, 2H, H₁₀), 6.51 (d, J = 2.4 Hz, 2H, H₆), 6.62 (dd, J = 9.0, 2.4 Hz, 2H, H₅), 7.63-7.67 (m, 2H, H₂), 7.73 (m, 1H, H₁), 8.31-8.36 (m, 4H, H₃, H₄), 13.03 (s, 2H, H₇)

^{13}C NMR (100 MHz, DMSO) δ : 59.3 (C₁₄), 69.9 (C₁₃), 101.8 (C₁₁), 108.2 (C₇), 109.8 (C₉), 128.1 (C₃), 129.2 (C₂), 131.0 (C₈), 133.4 (C₁), 134.1 (C₄), 163.5 (C₁₀ or C₁₂), 164.7 (C₁₀ or C₁₂), 167.8 (C₆), 169.1 (C₅)

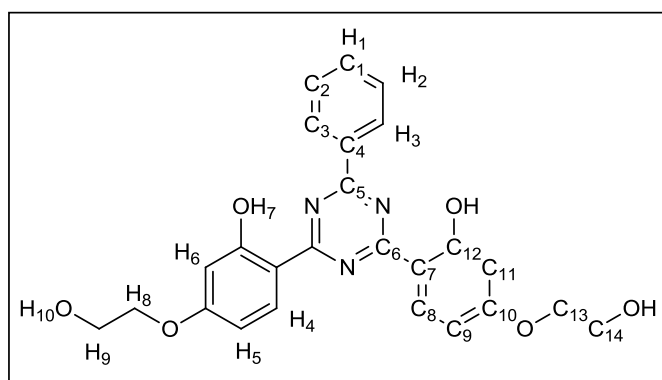


Fig.3.37 – Chemical structure of 37

6,6'-(6-Phenyl-1,3,5-triazine-2,4-diyl)bis(3-((9-hydroxynonyl)oxy)phenol)
(38)

A mixture of 4,4'-(6-phenyl-1,3,5-triazine-2,4-diyl)bis(benzene-1,3-diol) **17** (2.00 g, 5.40 mmol) and Na₂CO₃ (2.27 g, 21.60 mmol) in DMF (150 mL) was heated to 70 °C whilst stirring. A solution of 9-bromo-1-nonanol **3.10** (3.01 g, 13.50 mmol) in DMF (100 mL) was added slowly. Once the addition was complete, the mixture was stirred at 110 °C for 16 hours. The mixture was filtered whilst hot, the solvent removed under reduced pressure and the residue was redissolved in CHCl₃ (100 mL). The organic layer was washed with 5 % v/v aqueous acetic acid (30 mL), 0.25 M aqueous NaHCO₃ (30 mL) and brine (50 mL). The organic layer was dried over sodium sulfate and the solvent removed under reduced pressure. The crude product was suspended in MeOH (25 mL), filtered and dried at 70 °C *in vacuo* (60 mbar). The crude product

was purified by flash column chromatography on silica gel (100 % CHCl₃, switching to 10% MeOH, R_f value for **38** in 10 % MeOH in CHCl₃ = 0.8). The solvent was removed under reduced pressure and the yellow coloured solid was dried at 70 °C *in vacuo* (60 mbar). **38** (1.01 g, 28 %, Figure 3.38).

HRMS: Found m/z 658.3851 (M+H)⁺; Calculated m/z 658.3851

M. pt. Found: 128-130 °C

FT-IR: $\bar{\nu}$ / cm⁻¹: 3100-3500 (O-H stretch), 2922, 2850 (C-H stretch, aliphatic), 1504 (C-O stretch, phenol), 1533, 1504 (C=N stretch, conjugated), 1290, 1234 (C-O stretch)

UV λ_{\max} (0.1 mM in CHCl₃): 357 nm (ϵ = 37,000 cm⁻¹ M⁻¹)

TGA (Air): Weight loss at 300 °C (0 %); Onset temperature (411 °C)

¹H NMR (500 MHz, CDCl₃) δ : 1.36-1.62 (m, 26H, H₁₀, H₁₁, H₁₂, H₁₃, H₁₄, H₁₅ and H₁₇), 1.78-1.83 (m, 4H, H₉), 3.64-3.67 (t, J = 6.8 Hz, 4H, H₁₆), 3.99 (t, J = 6.6 Hz, 4H, H₈), 6.46 (d, J = 2.4 Hz, 2H, H₆), 6.52 (dd, J = 9.0, 2.4 Hz, 2H, H₅), 7.53-7.56 (m, 2H, H₂), 7.62 (m, 1H, H₁), 8.35 (broad s, 4H, H₄, H₃), 13.38 (s, 2H, H₇)

¹³C NMR (100 MHz, CDCl₃) δ : 25.7, 26.0, 29.3, 29.4, 29.5, (C₁₅, C₁₆, C₁₇, C₁₈ or C₁₉), 29.1 (C₁₄ or C₂₀), 32.8 (C₁₄ or C₂₀), 63.1 (C₂₁), 68.3 (C₁₃), 101.8 (C₁₁), 108.6 (C₇), 110.0 (C₉), 128.7 (C₃), 129.0 (C₂), 131.2 (C₈) 133.3 (C₁), 134.3 (C₄), 164.6 (C₁₀ or C₁₂), 165.5 (C₁₀ or C₁₂). No signals for C₅ and C₆ in HMBC.

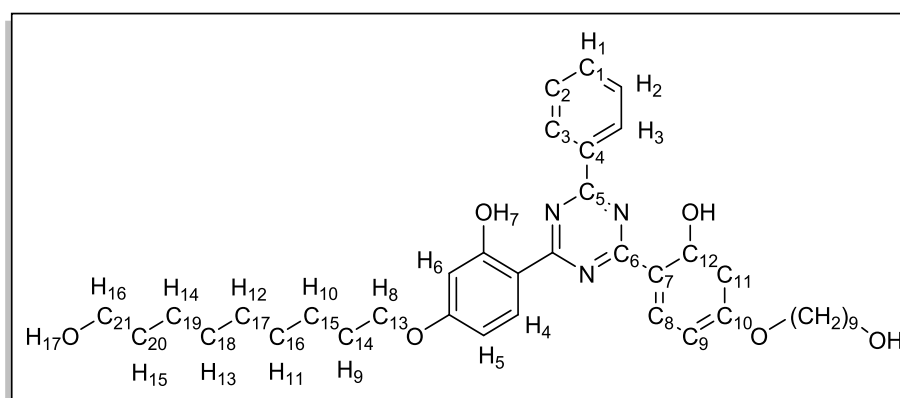


Fig.3.38 – Chemical structure of **38**

6,6'-(6-(4-Methoxyphenyl)-1,3,5-triazine-2,4-diyl)bis(3-(2-hydroxyethoxy)phenol) – (39)

A solution of 4,4'-(6-(4-methoxyphenyl)-1,3,5-triazine-2,4-diyl)bis(benzene-1,3-diol) **18** (0.25 g, 0.62 mmol) and Na₂CO₃ (0.20 g, 1.86 mmol) in DMF (15 mL) was stirred at 70 °C. To this, a solution of 2-bromoethanol **3.9** (0.23 g, 1.86 mmol) in DMF (5 mL) was added and the reaction mixture was stirred at 110 °C for 16 hours. The mixture was filtered whilst hot and the solvent removed under reduced pressure. The residue was suspended in 10 % v/v aqueous HCl (75 mL), ultrasonicated for 20 mins and stirred at room temperature for a further 10 mins. The suspension was spun in a centrifuge (2000 rpm, 2 mins) and the supernatant removed. The residue was resuspended in water (20 mL), the solid collected by filtration and washed with more water (30 mL). The light brown coloured solid was dried at 70 °C *in vacuo* (60 mbar). **39** (0.20 g, 66 %, Figure 3.39).

HRMS: Found m/z 492.1772 (M+H)⁺; Calculated m/z 492.1765

M. pt. Expected: 155-158 °C;¹³⁴ Found: 157-158 °C

FT-IR: $\bar{\nu}$ / cm⁻¹: 3100-3500 (O-H stretch), 2935 (C-H stretch, aliphatic), 1535, 1502 (C=N stretch, conjugated), 1255, 1170 (C-O stretch)

UV λ_{\max} (0.1 mM in CHCl₃): 342 nm (ϵ = 46,000 cm⁻¹ M⁻¹)

TGA (Air): Weight loss at 300 °C (1.36 %); Onset temperature (331°C)

¹H NMR (400 MHz, DMSO-d₆) δ : 3.73-3.76 (m, 4H, H₉), 3.87 (s, 3H, H₁), 4.02 (t, J = 5.7 Hz, 4H, H₈), 4.96 (t, J = 5.5 Hz, 2H, H₁₀), 6.43 (d, J = 2.4 Hz, 2H, H₅), 6.56 (dd, J = 9.0, 2.4 Hz, 2H, H₆), 7.11 (d, J = 9.0 Hz, 2H, H₂), 8.15-8.18 (m, 4H, H₃, H₇), 13.1 (s, 2H, H₄)

¹³C NMR (100 MHz, DMSO-d₆) δ : 56.1 (C₁), 59.9 (C₁₄), 70.4 (C₁₅), 102.2 (C₁₀), 108.6 (C₈), 108.2 (C₁₂), 115.0 (C₃), 126.6 (C₅), 130.4 (C₄), 131.3 (C₁₃), 163.7 (C₂), 164.1 (C₉ or C₁₁), 165.1 (C₉ or C₁₁), 167.6 (C₆), 169.4 (C₇)

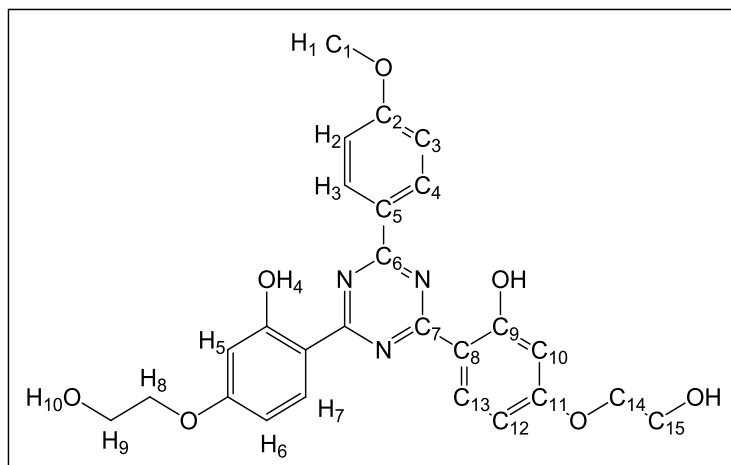


Fig.3.39 – Chemical structure of 39

2-(4,6-Diphenyl-1,3,5-triazin-2-yl)-5-(2-hydroxyethoxy)benzene-1,3-diol (40)

A solution of 2-(4,6-diphenyl-1,3,5-triazin-2-yl)benzene-1,3,5-triol **12** (3.00 g, 8.40 mmol) and Na₂CO₃ (1.78 g, 16.80 mmol) in DMF (100 mL) was stirred at 70 °C. To this, a solution of 2-bromoethanol **3.9** (2.10 g, 16.80 mmol) in DMF (50 mL) was added and the mixture was stirred at 110 °C for 16 hours. The mixture was filtered whilst hot and the solvent was removed under reduced pressure. The residue was suspended in water (100 mL), ultrasonicated for 10 mins and stirred at room temperature for 30 mins. The solid was collected by filtration and washed with water (100 mL). The light yellow coloured solid was dried overnight at 70 °C *in vacuo* (60 mbar). **40** (3.20 g, 95 %, Figure 3.40).

HRMS: Found *m/z* 402.1452 (M+H)⁺; Calculated *m/z* 402.1448

M. pt. Found: 245-248 °C

FT-IR: $\bar{\nu}$ / cm⁻¹: 3150-3400 (O-H stretch), 2931, 2875 (C-H stretch, aliphatic), 1537, 1514 (C=N stretch, conjugated), 1330, 1172 (C-O stretch)

UV λ_{\max} (0.1 mM in DMSO): 327 nm (ϵ = 33,000 cm⁻¹ M⁻¹)

TGA (Air): Weight loss at 300 °C (5.65 %); Onset temperature (314 °C)

^1H NMR (500 MHz, DMSO- d_6) δ : 3.69-3.71 (m, 2H, H₇), 3.96 (t, J = 4.9 Hz, 2H, H₆), 4.89 (t, J = 5.5 Hz, 1H, H₈), 5.98 (s, 2H, H₅), 7.63-7.66 (m, 4H, H₂), 7.72 (t, J = 7.3 Hz, 2H, H₁), 8.34 (d, J = 7.3 Hz, 4H, H₃), 13.51 (s, 1H, H₄)

^{13}C NMR (100 MHz, DMSO- d_6) δ : 59.8 (C₁₂), 70.3 (C₁₁), 95.0 (C₉), 97.1 (C₇), 129.0 (C₃), 129.8 (C₂), 134.2 (C₄), 134.3 (C₁), 164.5 (C₈), 165.8 (C₁₀), 168.9 (C₅), 171.0 (C₆)

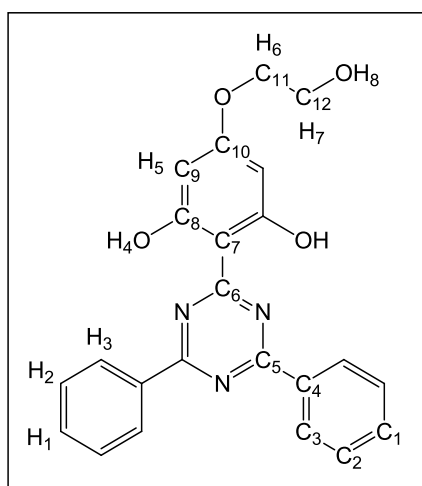


Fig.3.40 – Chemical structure of 40

2-(4,6-Bis(4-fluorophenyl)-1,3,5-triazin-2-yl)-5-(2-hydroxyethoxy)phenol (41)

A mixture of 4-(4,6-bis(4-fluorophenyl)-1,3,5-triazin-2-yl)benzene-1,3-diol **15** (0.25 g, 0.66 mmol) and Na_2CO_3 (0.14 g, 1.32 mmol) in DMF (20 mL) was stirred at 70 °C. To this, a solution of 2-bromoethanol **3.9** (0.17 g, 1.32 mmol) in DMF (5 mL) was added and stirred at 110 °C for 16 hours. The mixture was filtered whilst hot and the solvent was removed under reduced pressure. DMF (5 mL) was added to the residue followed by 5 % v/v aqueous HCl (50 mL), and the precipitate was collected by filtration, washing with water (40 mL). The crude solid was purified by flash column chromatography on silica gel (10 % MeOH in CHCl_3 , R_f value for **41** in 10 % MeOH in CHCl_3 = 0.38) and the solvent was removed under reduced pressure. The yellow coloured solid was dried at 70 °C *in vacuo* (60 mbar). **41** (0.23 g, 83 %, Figure 3.41).

HRMS: Found m/z 420.1175 (M-H)⁻; Calculated m/z 420.1165

M. pt. Found: 220-222 °C

FT-IR: $\bar{\nu}$ / cm^{-1} : 3150-3450 (O-H stretch), 3081 (C-H stretch, aromatic), 2934 (C-H stretch, aliphatic), 1506 (C=N stretch, conjugated), 1260 (C-O stretch)

UV λ_{max} (0.1 mM in DMSO): 345 nm ($\epsilon = 19,000 \text{ cm}^{-1} \text{ M}^{-1}$)

TGA (Air): Weight loss at 300 °C (8.59 %); Onset temperature (309 °C)

^1H NMR (400 MHz, DMSO- d_6) δ : 3.74-3.76 (**m**, 2H, H₈), 4.04 (**t**, J = 4.8 Hz, 2H, H₇), 4.92 (**s**, 1H, H₉), 6.45 (**d**, J = 2.5 Hz, 1H, H₅), 6.57 (**dd**, J = 9.0, 2.5 Hz, 1H, H₄), 7.37-7.42 (**m**, 4H, H₁), 8.40 (**d**, J = 9.0 Hz, 1H, H₃), 8.47-8.51 (**m**, 4H, H₂), 13.02 (**s**, 1H, H₆)

^{13}C NMR (100 MHz, DMSO- d_6) δ : 59.4 (C₁₄), 69.9 (C₁₃), 101.5 (C₁₁), 108.1 (C₉), 109.7 (C₇), 116.0 (**d**, J = 22Hz, C₂), 130.8 (C₄), 131.1 (**d**, J = 9 Hz, C₃), 132.4 (C₈), 163.6 (C₁₀ or C₁₂), 164.7 (C₁₀ or C₁₂), 165.0 (**d**, J = 254 Hz, C₁), 168.3 (C₅), 170.3 (C₆)

^{19}F NMR (400 MHz, DMSO) δ : -106.3 (**m**, 2F, F)

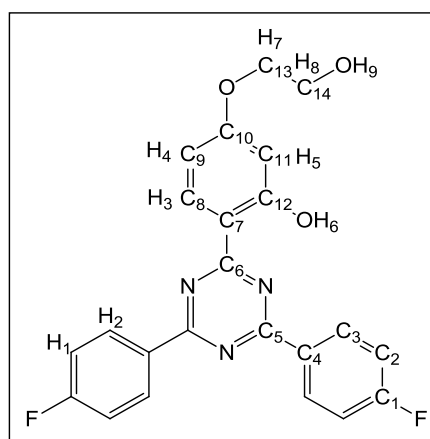


Fig.3.41 – Chemical structure of 41

2-(4,6-Bis(4-methoxyphenyl)-1,3,5-triazin-2-yl)-5-(2-hydroxyethoxy)phenol (42)

A solution of 4-(4,6-bis(4-methoxyphenyl)-1,3,5-triazin-2-yl)benzene-1,3-diol **16** (0.25 g, 0.62 mmol) and Na_2CO_3 (0.13 g, 1.25 mmol) in DMF (20 mL) was stirred at 70 °C. To this, a solution of 2-bromoethanol **3.9** (0.16 g, 1.25 mmol) in DMF (5 mL) was added and the mixture was stirred at 110 °C for 16 hours. The reaction mixture was filtered whilst hot and the solvent was removed under reduced pressure. The

residue was suspended in water (30 mL), stirred for 1 hour at room temperature and filtered. The brown coloured solid was resuspended in acetone (5 mL), collected by filtration and washed with acetone (10 mL). The beige coloured solid was dried overnight at 70 °C *in vacuo* (60 mbar). **42** (0.17 g, 61 %, Figure 3.42).

HRMS: Found m/z 446.1716 (M+H)⁺; Calculated m/z 446.1721

M. pt. Found: 121-123 °C

FT-IR: $\bar{\nu}$ / cm⁻¹: 3100-3400 (O-H stretch), 3005 (C-H stretch, aromatic), 2931, 2835 (C-H stretch, aliphatic), 1500 (C=N stretch, conjugated), 1251, 1170 (C-O stretch)

UV λ_{\max} (0.1 mM in DMSO): 322 nm ($\epsilon = 61,000$ cm⁻¹ M⁻¹)

TGA (Air): Weight loss at 300 °C (1.71 %); Onset temperature (339 °C)

¹H NMR (400 MHz, DMSO-d₆) δ : 3.72-3.75 (m, 2H, H₉), 3.87 (s, 6H, H₁), 4.04 (t, J = 4.8 Hz, 2H, H₈), 4.91 (t, J = 5.2 Hz, 1H, H₁₀), 6.47 (d, J = 2.3 Hz, 1H, H₆), 6.59 (dd, J = 9.0, 2.3 Hz, 1H, H₅), 7.10 (d, J = 8.9 Hz, 4H, H₂), 8.39-8.44 (m, 5H, H₃ and H₄), 13.4 (s, 1H, H₇)

¹³C NMR (100 MHz, DMSO-d₆) δ : 55.5 (C₁), 59.4 (C₁₅), 69.9 (C₁₄), 101.5 (C₁₂), 107.9 (C₁₀), 110.0 (C₈), 114.3 (C₃), 126.9 (C₅), 130.4 (C₄), 130.9 (C₉), 163.3 (C₂), 163.6 (C₁₁ or C₁₃), 164.4 (C₁₁ or C₁₃), 168.6 (C₆), 170.0 (C₇)

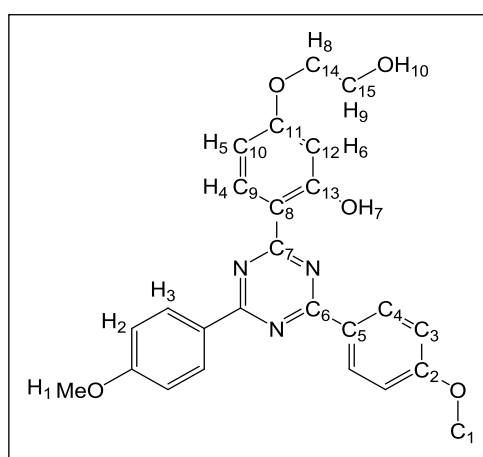


Fig.3.42 – Chemical structure of **42**

3.2 Results and Discussion

3.2.1 Synthesis of UVAMs

The synthetic starting point for the UVAMs was cyanuric chloride **1.90**. Grignard and Friedel-Crafts chemistry were employed successfully to deliver tri-aryl 1,3,5-triazines with one or more IMHBs. Thereafter, polymerisable moieties were successfully installed *via* nucleophilic substitution. An alternative strategy to Grignard chemistry focused on generating mono- and di-aryl triazine UVAMs with amine/ether-triazine bonds. This was done using the inexpensive substrates methyl 4-hydroxybenzoate **3.2** and diethyl iminodiacetate **3.1**, and subsequently introducing resorcynyl moieties using Friedel-Crafts reactions.

An alternative to Friedel-Crafts chemistry is Suzuki coupling which offers superior regioselectivity and is compatible with more complex reagents. The main drawbacks are the cost of reagents and palladium catalyst which becomes particularly expensive on larger industrial scales. Grignard chemistry was preferred over lithium halogen exchange since the reagents are easier to handle and less strict control of temperature was required for the Grignard reagents. Since one of the main goals was to synthesise industrially viable UVAMs, the study used Friedel-Crafts chemistry and Grignard chemistry exclusively.

3.2.1.1 Grignard Reactions

Compounds **1-8** were synthesised using a wide range of Grignard reagents (Figures 3.44 and 3.45). 4-Fluorophenylmagnesium bromide and 4-methoxyphenylmagnesium bromide were used to investigate the effects of electron-donating and electron-withdrawing groups on the UV absorbance profile. The position of the methoxy group on the aryl ring was crucial to ensure electron donation into the triazine system (Figure 3.43). Unlike a methoxy group positioned *ortho* and *para* to the triazine ring, a *meta*-positioned methoxy group is unable to donate electrons into the triazine ring. The more complex Grignard reagents were more expensive, in particular 4-biphenylmagnesium bromide which was £103 for 50 mL. This categorically ruled out the scale-up of the biphenyl triazine UVAMs, but this

was an extremely important reagent used to investigate the effects of greatly increasing the conjugation on the spectroscopic properties of UVAMs.

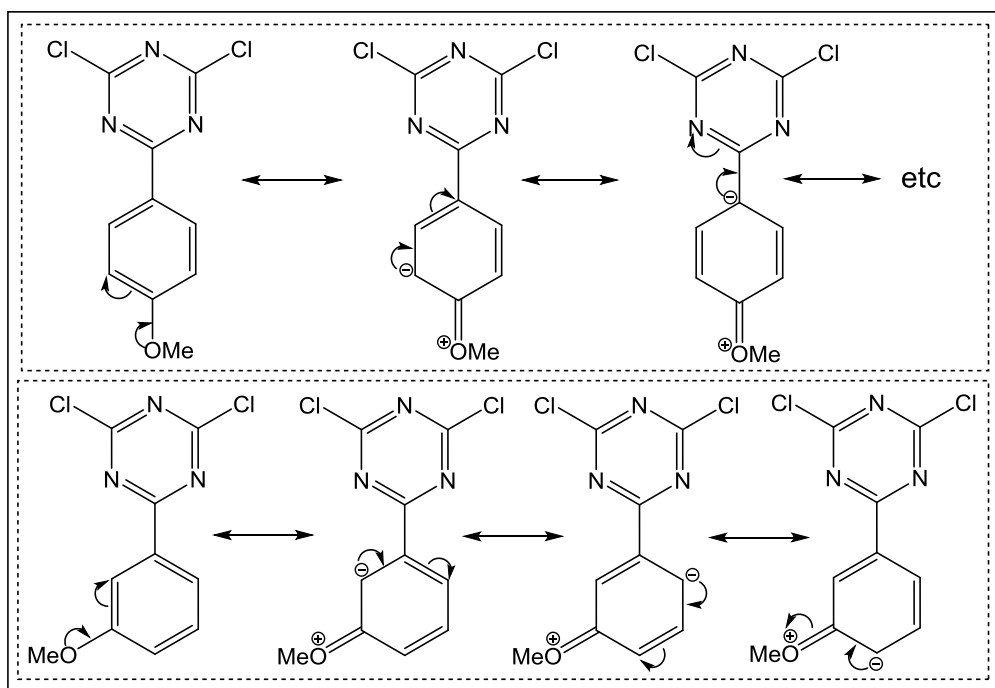


Fig.3.43 – Comparison of resonance structures of methoxyphenyl-1,3,5-triazine with methoxy group in the *ortho* and *para* position

A key aspect of the Grignard reactions was controlling the reaction temperature to selectively displace the chlorines. The first chlorine displacement was highly exothermic and required slow addition of the Grignard reagent whilst maintaining the reaction temperature at 0 °C. For the synthesis of the mono-substituted triazines **1**, **3**, **5** and **7**, the reaction was stirred at 0 °C and quenched by pouring the entire reaction mixture into cold 10 % aqueous HCl (Figure 3.44). Furthermore, stoichiometric amounts of Grignard reagents were employed as a precaution against yielding di-substituted by-products.

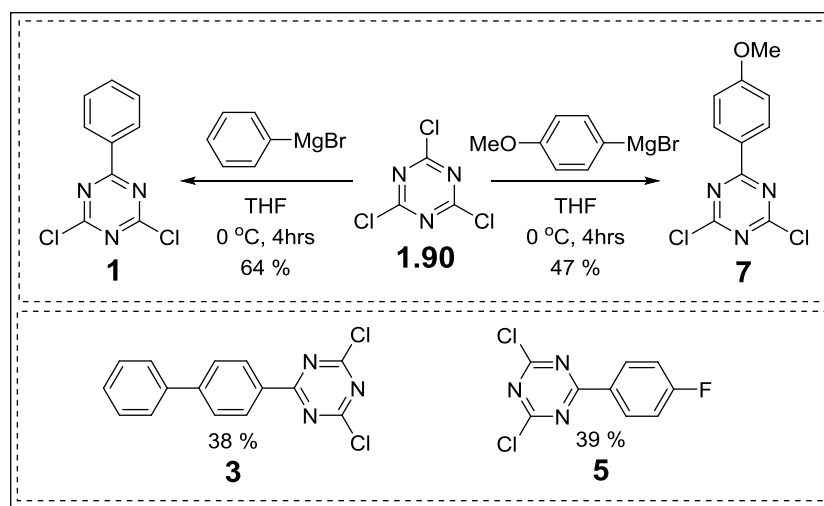


Fig.3.44 – Synthesis of **1** and **7** and the chemical structures of **3** and **5**

To obtain di-substituted compounds **2**, **6** and **8**, slight excesses of the Grignard reagents were used and the reaction mixtures were stirred overnight at room temperature (Figure 3.45). The synthesis of **4** at room temperature resulted in mixtures of mono- and di-substituted products, which were particularly difficult to separate by recrystallisation and flash column chromatography. This was circumvented by following a synthetic method from Tyler and co-workers¹³⁶ who employed a 3:1 excess of 4-biphenylmagnesium bromide to cyanuric chloride **1.90** and stirred the reaction mixture at 50 °C overnight. Purifying compounds **1-8** by recrystallisation was ineffective and led to an unnecessary loss of product. Alternatively, suspending and washing with methanol was found to be the most efficient method of purification.

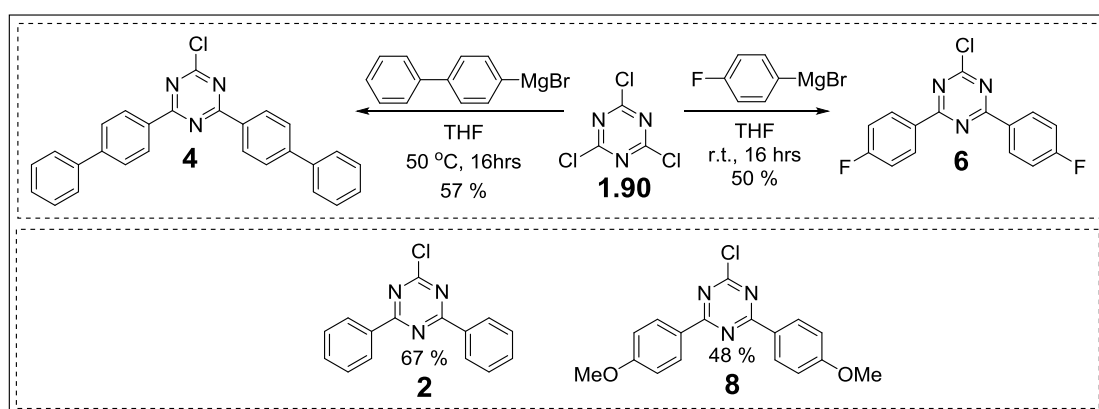


Fig.3.45 – Synthesis of **4** and **6**, chemical structures and yields of **2** and **8**

3.2.1.2 Amine and Alcohol Nucleophile Reactions

With the aim of developing UVAMs that were beyond the protection of BASF intellectual property, it was decided to incorporate polymerisable ester functionality using amine and alcohol nucleophiles. The BASF patents describe exclusively tri-aryl 1,3,5-triazine monomers thus it was logical to investigate the potential of mono-/di-aryl UVAMs with nitrogen/oxygen atoms bonded to the heterocycle. The inexpensive diethyl iminodiacetate **3.1** and methyl 4-hydroxybenzoate **3.2** were identified as suitable amine and alcohol nucleophiles for the task in hand.

Compound **9** was synthesised using stoichiometric amounts of amine and cyanuric chloride **1.90** at 0 °C, using a method similar to that described by Bhat and Pandey (Figure 3.46).⁹⁵ The HCl produced, as a by-product, was neutralised by the addition of aqueous NaOH. Compound **10** was synthesised using stoichiometric amounts of DIPEA and methyl 4-hydroxybenzoate **3.2**. Once the first chlorine substitution took place at 0 °C, the second chlorine was displaced overnight at room temperature. The use of a non-nucleophilic base such as DIPEA was crucial to deprotonate the phenol group without nucleophilically attacking the cyanuric chloride **1.90**.

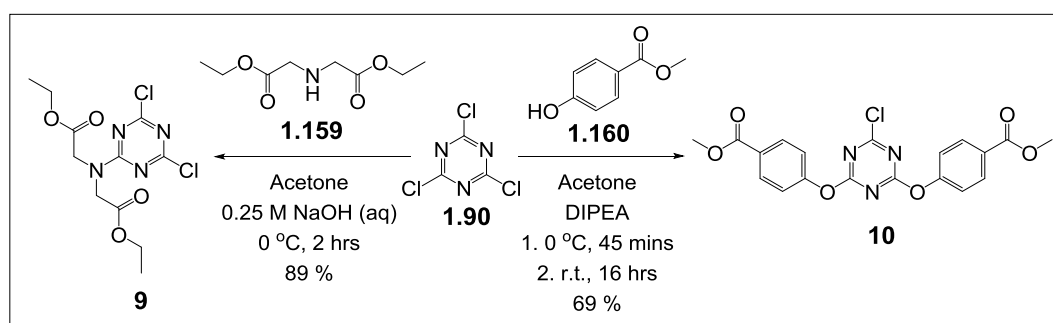


Fig.3.46 – Synthesis of **9** and **10**

The ¹H NMR spectrum of **10** exhibited extra resonances of coupling for H₂ and H₃ at 8.09 and 7.23 ppm, respectively, which is typical for 1,4-disubstituted aromatic ring (Figure 3.47). The H₂ protons are chemically equivalent but they are magnetically inequivalent and they couple to both H₃ protons differently. This results in extra resonances on either side of the intense doublet from a H₂,H₂',H₃,H₃' system of resonances.

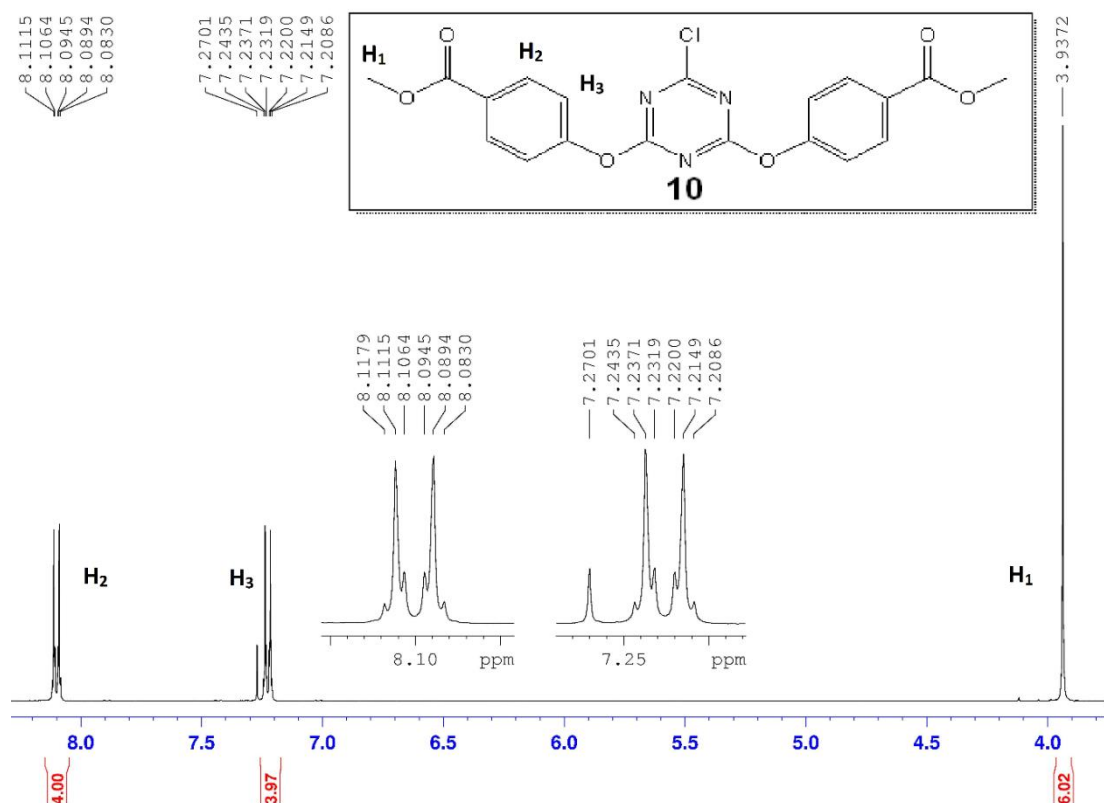


Fig.3.47 – ¹H NMR spectrum of **10**

Using diethyl iminodiacetate **3.1** and methyl 4-hydroxybenzoate **3.2** was an effective way of incorporating polymerisable ester groups onto the triazine ring. This strategy provided a good opportunity to install resorcinol **1.136**, phloroglucinol **1.159** or 3,5-dimethoxyphenol **1.134** by Friedel-Crafts chemistry and yield UVAMs in two synthetic steps. Furthermore, this synthetic route was a cheaper and less hazardous alternative to Grignard chemistry.

3.2.1.3 Friedel-Crafts Reactions

The Friedel-Crafts substitution of chlorine atoms on a triazine ring proceeded through a mechanism similar to that of Friedel-Crafts acylation. The mechanism begins with the dissociation of a chloride ion forming a carbocation which is stabilised by the adjacent electronegative nitrogen atoms (Figure 3.48). It is also worth noting that on approach of the Lewis acid, the aluminium atom may bind to a nitrogen atom of the heterocyclic ring. The carbocation is then attacked nucleophilically by a suitable

aromatic substrate such as resorcinol. The final stage involves the loss of a proton to restore aromaticity to the ring, generating HCl as a by-product.

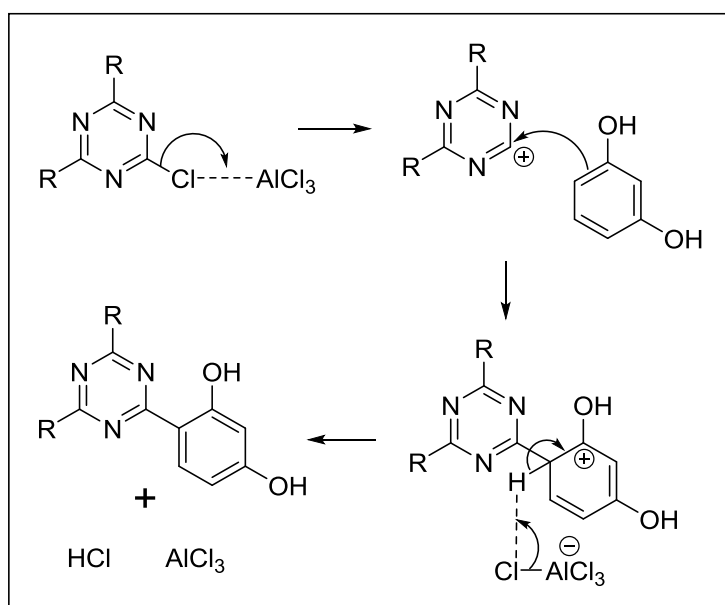


Fig.3.48 – Mechanism of Friedel-Crafts reaction between a 1,3,5-triazine and resorcinol

The Friedel-Crafts reactions were all carried out using AlCl₃ as a catalyst, in quantities never less than stoichiometric amounts due to formation of complexes with the substrate and product. Compounds **11**, **13**, **15**, **16**, and **18** were synthesised in 1,2-dichlorobenzene as solvent at 130 °C using a method similar to that reported by Bojinov and co-workers (Figure 3.49).^{81-87,137} These reactions generally required overnight stirring, but the reaction to obtain **15** was complete within 3 hours. One possible explanation for this was that the electronegative fluorine atoms increase the electrophilicity of the triazine carbon atoms. The final stage involved the addition of 10 % aqueous HCl to liberate the desired product from the Lewis acid complexes. Compounds **16** and **18** produced thick suspensions after the addition of aqueous acid which prevented stirring and which filtered extremely slowly. To counteract this, the suspensions were spun in a centrifuge to remove the supernatant liquids, resuspended in water and filtered. Purification of compounds **11**, **13**, **15** and **16** was not required, with the crude products sufficiently pure for the subsequent steps. Compound **18** was purified by precipitation from hot DMF using cold water.

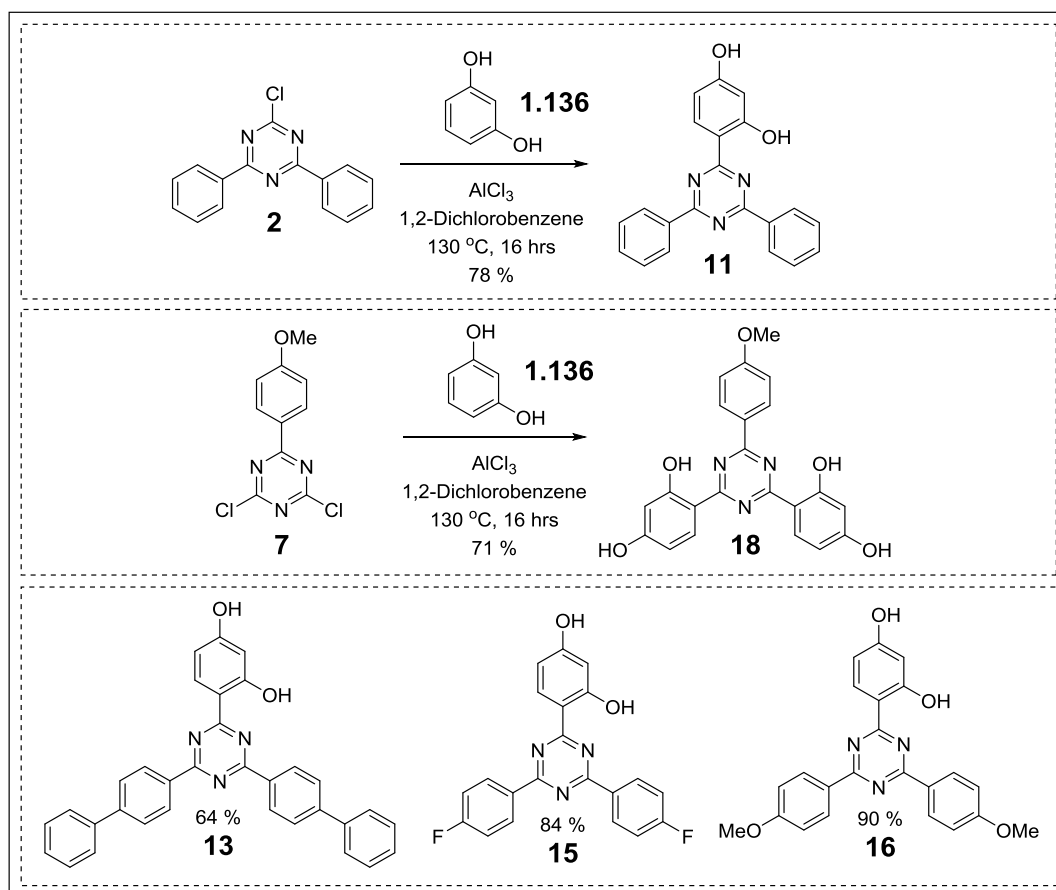


Fig.3.49 – Synthesis of 11 and 18, and chemical structures of 13, 15 and 16

One must consider the reason for not generating by-products from the Friedel-Crafts alkylation of 1,2-dichlorobenzene and the aryl nucleophiles. This may suggest that the Lewis acid forms an adduct with the basic nitrogen atoms, making the dissociation of the chloride ion from the heterocycle more favourable in comparison to 1,2-dichlorobenzene. In addition to this, the nitrogen atoms are electronegative and they can bear negative charge which further facilitates substitution on the 1,3,5-triazine (Figure 3.50).

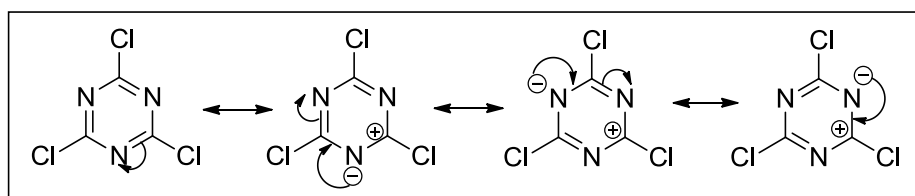


Fig.3.50 – Resonance structures of cyanuric chloride 1.90

Compound **19**, an electron-rich UV absorber with three IMHBs, was synthesised following a method similar to that of Eisler and Conn which claimed to purify the crude product by centrifuging in water and thoroughly washing in diethyl ether (Figure 3.51).¹¹⁶ This method of purification was found to be ineffective, and a more efficient method of purification was found which involved recrystallising using DMF. Unfortunately, compound **19** could not be elaborated into a UVAM using the experimental methods outlined by Bolle and co-workers⁹¹ which involved 2-bromoethanol **3.9** or ethylene carbonate. These reactions yielded mixtures of mono-, di- and tri-functional products which were inseparable by recrystallisation or flash column chromatography.

1,3-Dihydroxynaphthalene **3.3** was used to synthesise **14** to investigate the effect of increasing the conjugation on the same aryl ring which bears the IMHB. After the addition of 10 % aqueous HCl, the mixture required ultrasonication since stirring failed to break up the solid. The ¹H NMR spectrum of **14** showed a large chemical shift of 14.81 ppm for the phenolic proton *ortho* to the triazine ring from the strong IMHB deshielding the phenolic hydrogen nuclei.

After stirring the reaction mixture of **17** for 1 hour at 55 °C, a solid precipitate formed in the bottom of the flask. This hard solid residue was thought to be a Lewis acid complex with the desired product. The most effective way of liberating the final product was to ultrasonicate in a mixture of MeOH/water (1/1, v/v) at 55 °C for 1 hour. The red coloured solid formed a yellow suspension and the solid was collected by filtration without the need for purification.

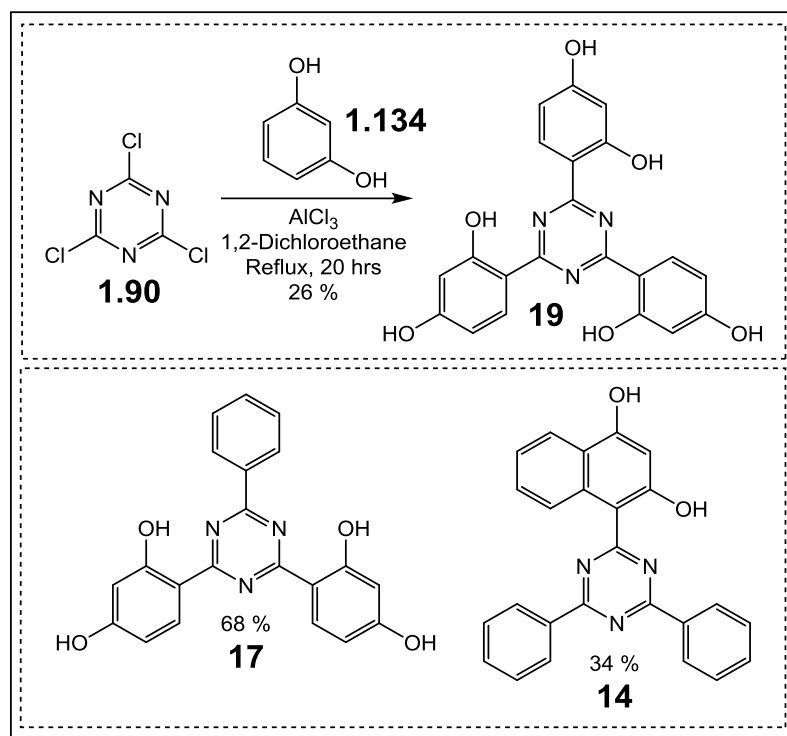


Fig.3.51 – Synthesis of **19**, and the chemical structures of **14** and **17**

Developing UVAMs in two synthetic steps was possible by elaborating **9** and **10** using Friedel-Crafts chemistry. An aryl nucleophile that was particularly interesting was 3,5-dimethoxyphenol **1.134** due to the two electron-donating methoxy groups. Unfortunately, the reaction between 3,5-dimethoxyphenol **1.134** and **10** was unsuccessful and the reaction of 3,5-dimethoxyphenol **1.134** with **9** gave **21** in low yield (Figure 3.52). This was disappointing, since it was expected that the electron rich 3,5-dimethoxyphenol **1.134** would displace favourably the remaining two chlorines. Discerning that steric hindrance may play a role between the two substrates, the temperature and reaction time were increased but with no improvements the yield of **21**. The phenolic proton of **21** showed a high chemical shift in the ^1H NMR spectrum which indicated deshielding from a strong IMHB.

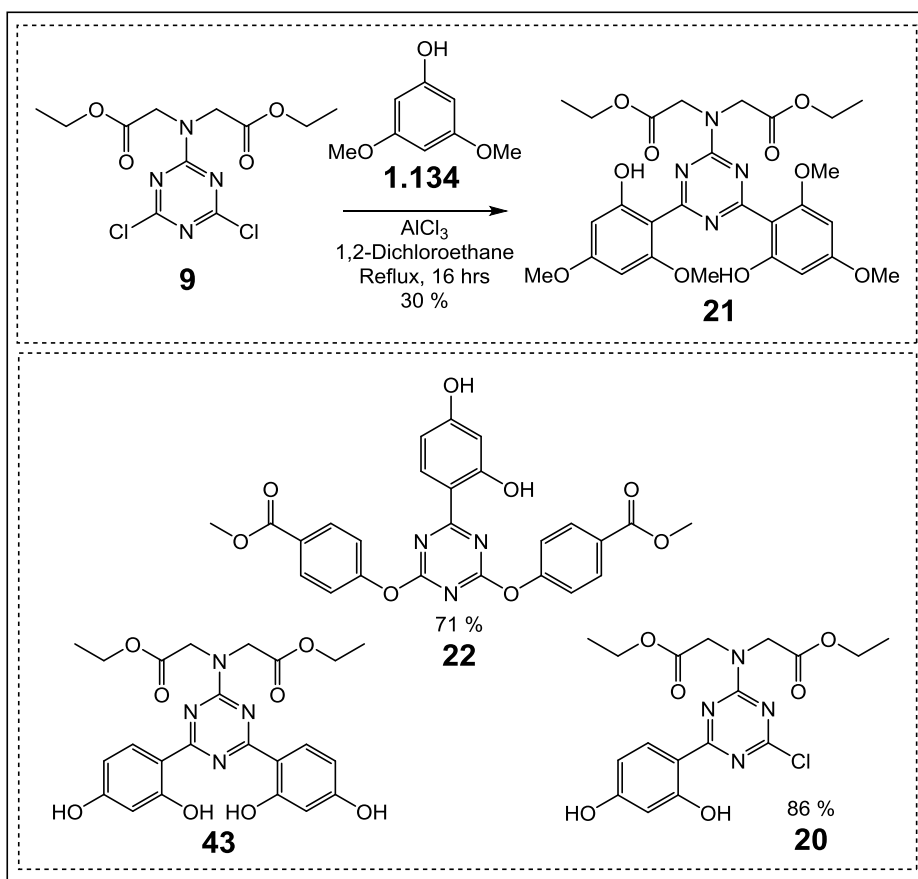


Fig.3.52 – Synthesis of **21**, and the chemical structures of **20** and **22**

For the reaction that yielded **20**, the initial target was the tri-substituted derivative **43** (Figure 3.52). After stirring at reflux temperature in 1,2-dichloroethane overnight, mass spectrometry analysis of the crude sample showed signals for **20** and **43**. The two products were separated by flash column chromatography, with **20** obtained in 86 % yield and **43** in 2 % yield. When comparing the ^1H NMR spectra of **20** and **43**, the phenolic proton H_8 was shifted further downfield in **43** due to the stronger IMHB (Figure 3.53). The ^1H NMR spectrum of **20** exhibited extra resonances of splitting for H_1 , H_2 and H_3 due to the geometrical differences between these protons. Similarly, two signals were observed in the ^{13}C NMR spectrum of **20** for each of the aliphatic carbon nuclei. The extra resonances were believed to be caused from the restricted rotation between the imino nitrogen and triazine carbon bond, which was thought to have a double bond nature from the donation of the nitrogen lone pair. Additionally, the FT-IR spectrum of **20** displayed two C=O stretches at 1743 and 1726 cm^{-1} .

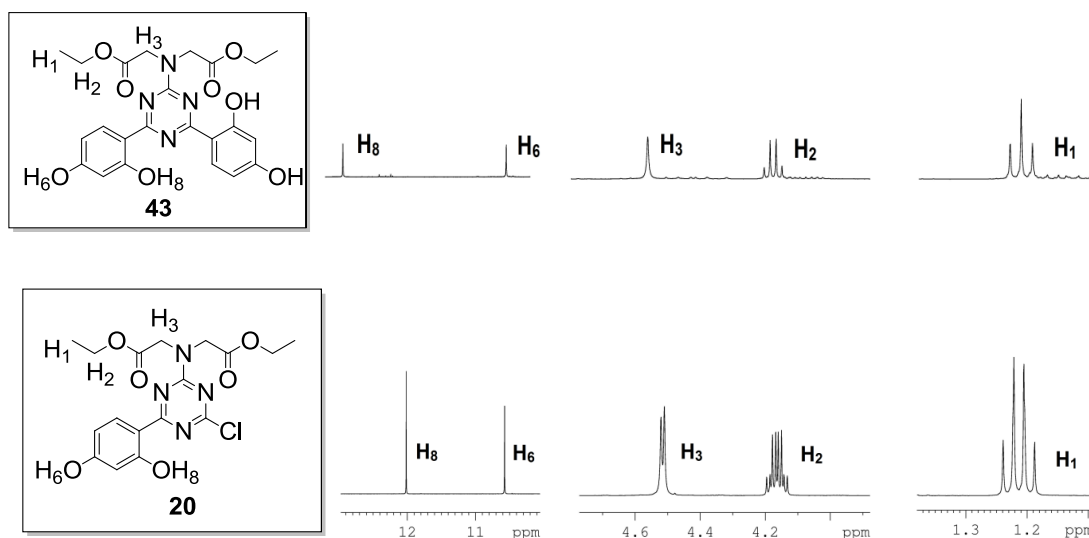


Fig.3.53 – H₁, H₂, H₃, H₆ and H₈ signals in the ¹H NMR Spectra of 20 and 43

Phloroglucinol **1.159** was an interesting nucleophile that was used in the synthesis of **12**. As touched on in the Introduction, Eisler and Conn¹¹⁶ generated **1.142** by stirring phloroglucinol **1.159**, aluminium trichloride and cyanuric chloride **1.90** in a 1:4 mixture of DCM and diethyl ether at 40 °C overnight (Figure 3.54). A similar method was used to synthesise **12**, but stirring at 40 °C overnight resulted in an approximately 50:50 mixture of desired product and unreacted starting material. All of the starting material was reacted by stirring the reaction mixture at reflux temperature overnight.

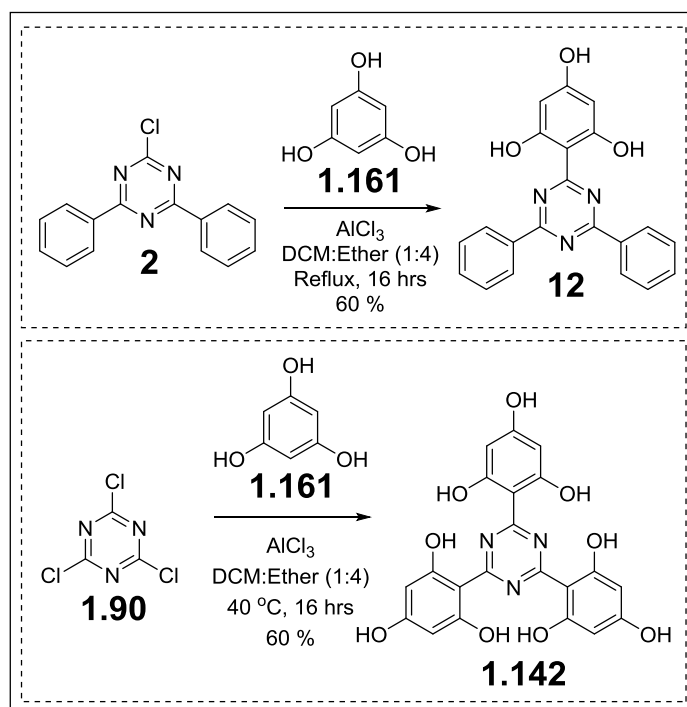


Fig.3.54 – Synthesis of **12** and **1.142**¹¹⁶

There were a number of potential UV absorbing targets that could not be prepared successfully using aryl nucleophiles **3.11-16** in Friedel-Crafts reactions (Figure 3.55). After employing these substrates at reflux temperatures for between 1-3 days, only the starting materials were retrieved upon work up. The idea for using **3.11**, **3.12** and **3.13** was inspired by a paper from Turro and co-workers⁶³ who reported that sterically bulky groups were responsible for protecting the IMHB from intermolecular polar interactions. Although it was understandable that the sterically encumbered **3.11** was unsuccessful in substituting onto a triazine ring, it was surprising that the less bulky **3.12** and **3.13** were similarly unreactive. Compounds **3.15** and **3.16** were used in an attempt to increase conjugation on the resorcinyl ring and investigate the effect of electron-withdrawing groups. Compound **3.16** was particularly interesting because this could have potentially generated a powerful UV absorbing derivative bearing a 2-(2-hydroxyphenyl)-1,3,5-triazine (TA) and a 2-hydroxybenzophenone (BP) chromophore on the same triazine. Further highlighting the unpredictable nature of the Friedel-Crafts reaction was the unsuccessful substitution of **3.14** which was considered to be a strong and regioselective nucleophile. Suzuki coupling would be a

more effective method to install these aryl nucleophiles than Friedel-Crafts chemistry as the former method is more regioselective and less affected by other substituents on the ring.

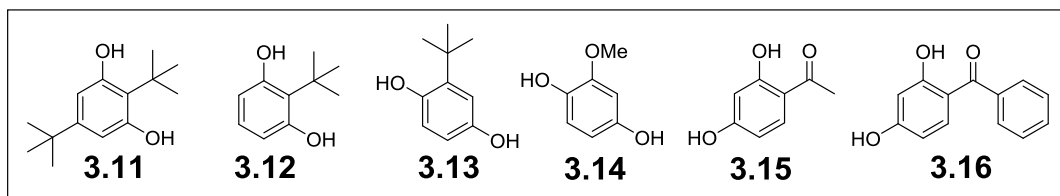


Fig.3.55 – Chemical structures of aromatic nucleophiles 3.11, 3.12, 3.13, 3.14, 3.15 and 3.16

3.2.1.4 Incorporation of Polymerisable Functional Groups

The relevant patents published over the last 30 years, mainly by BASF, include a vast array of polymerisable UVAMs. However, the polymerisable derivatives of Tinuvin 1577 **1.10** and Tinuvin 1600 **3.17** were mono-functional chain stoppers which turned attention to bifunctional monomers as a means to exploit a weakness in prior art.^{80,90,91}

The first aim of this study was to create bifunctional monomers of UV absorber **11** to generate bifunctional polymerisable UVAMs which mimicked the UV profile of Tinuvin 1577 **1.10**. A convergent synthesis strategy was devised to incorporate a malonate group onto **11** (Figure 3.56). Accordingly, the malonate derivate **23** was synthesised by reacting 1,6-dibromohexane **3.5** with diethyl methylmalonate **3.4** under basic conditions. The presence of the methyl group on the carbanion prevented intramolecular cyclisation of **23**. To reduce the probability of generating a di-substituted by-product, a dilute solution of diethyl methylmalonate **3.4** was used (0.057 M) and, additionally, 3.5 equivalents of 1,6-dibromohexane **3.5** were added in one portion. Unreacted diethyl methylmalonate **3.4** was removed by washing the organic phase with aqueous NaOH. NMR and mass spectroscopy showed no evidence of di-substitution, and the isotope pattern from the mass spectrum confirmed the presence of the bromine atom.

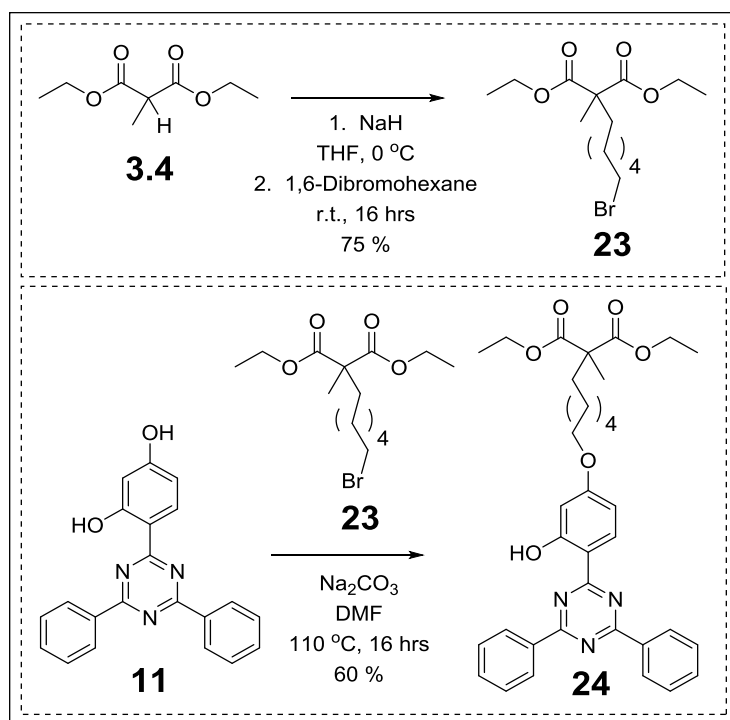


Fig.3.56 – Synthesis of 23 and 24

For the synthesis of UVAM **24**, UV absorber **11** was reacted with **23** under basic conditions (Figure 3.56). The phenolic group in the *para* position with respect to the triazine ring of **11** was deprotonated under basic conditions and this phenoxide anion nucleophilically attacked the bromomalonate. The *ortho* phenol remained unchanged due to its lower acidity and the protection provided by the IMHB. LC-MS and NMR spectroscopy displayed no evidence of substitution of the *ortho* phenol. The ¹H and ¹³C NMR spectra were assigned using heteronuclear single quantum coherence spectroscopy (HSQC), but an interesting observation was two ‘missing’ ¹³C NMR signals. One very weak quaternary carbon signal (C₄) at 135.6 ppm was identified using heteronuclear multiple bond correlation (HMBC) NMR spectroscopy (Figure 3.57). The second ‘missing’ signal was associated with the three triazine carbons (C₅ and C₆) being magnetically equivalent appearing as one signal at 171.5 ppm.

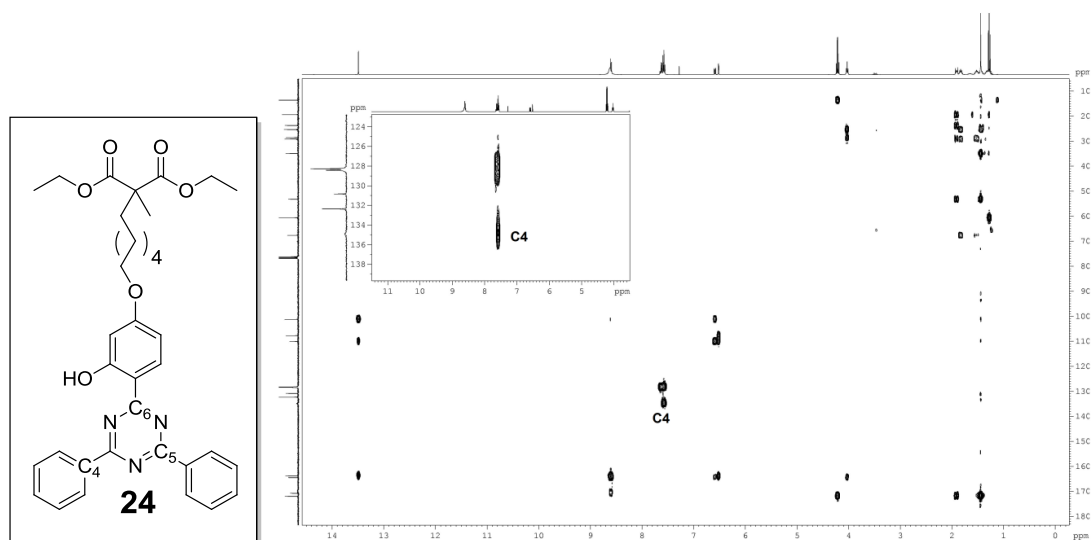


Fig.3.57 - HMBC spectrum of UVAM 4 showing a weak quaternary signal for C₄ at 135.6 ppm

The malonate group of **24** was elaborated to yield UVAMs **25-28** using a variety of synthetic reagents. A powerful reducing reagent, LiAlH₄, was used for the reduction of the malonate group to generate UVAM **25** (Figure 3.58). The low yield was first thought to be due to the basic work-up, however an acidic work-up failed to generate more product. TLC showed evidence of a polar by-product and the ¹H NMR spectrum of this by-product showed the absence of a phenolic proton. It was believed that the highly electropositive lithium ion was breaking the intramolecular hydrogen bond and forming a stable aluminium complex. A reagent that could be called upon to liberate the product from the aluminium complex would be potassium sodium tartrate.¹³⁸ Potassium sodium tartrate acts as an excellent ligand for aluminium and effectively releases the product by breaking up the aluminium emulsion.

UVAM **26** was synthesised by hydrolysing the ester groups of **24** into the corresponding carboxylic acid groups by a saponification reaction. A methanolic NaOH solution was applied to convert the malonate ester into the sodium salt which was subsequently protonated to yield the dicarboxylic acid product **26**.

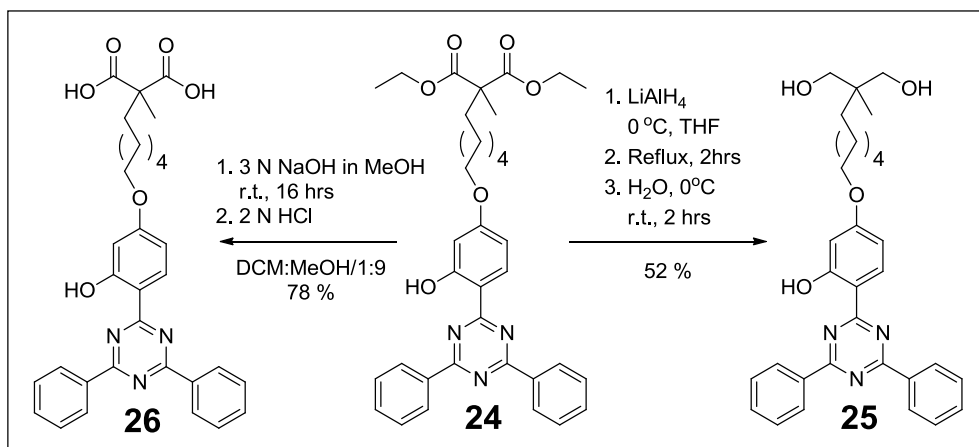


Fig.3.58 – Synthesis of 26 and 25

Glycolisation reactions of diester **24** and dicarboxylic acid **26** were performed using manganese(II) acetate tetrahydrate catalyst with a high excess of ethylene glycol **1.2** (Figure 3.59). The catalyst forms a complex with the donor oxygen atom of the carbonyl group, which increases the susceptibility of the carbonyl group to nucleophilic attack. Ethylene glycol **1.2** then nucleophilically attacks the more electrophilic carbon to form a tetrahedral intermediate **3.18** which collapses to generate the glycolised **27** or **28** and expel ethanol or water. The glycolisation of diacid **26** generated the mono-glycolised UVAM **28** due to decarboxylation of the malonic acid group at the reflux temperature of ethylene glycol. The loss of CO₂ was observed in the thermogravimetric analysis (TGA) of **26** which showed 9.6 % weight loss at 183 °C, which compared well with the 8.1 % theoretical weight loss.

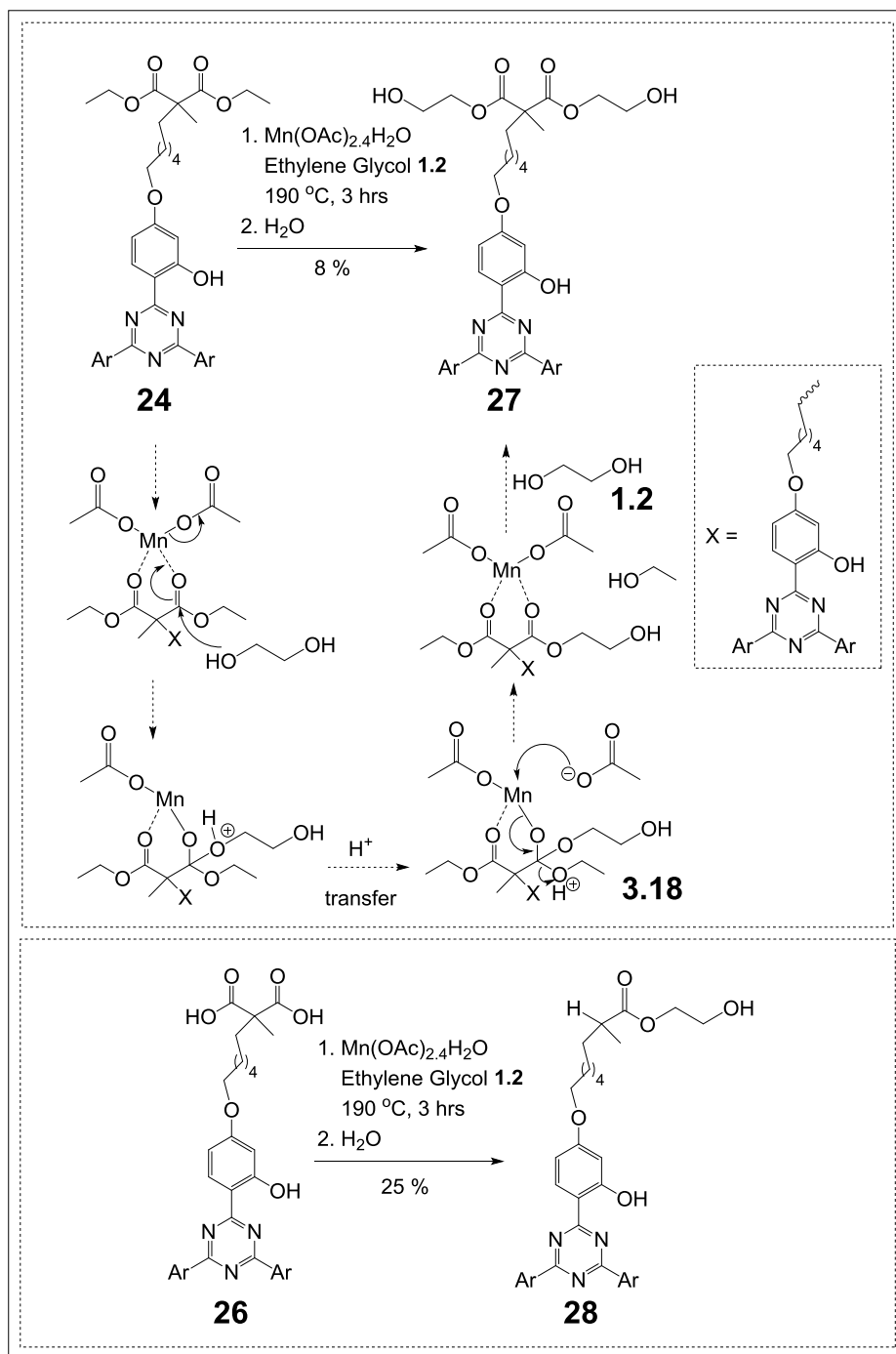


Fig.3.59 – Synthesis of **27** and **28**. Mechanism of glycolisation reaction

The crude product from the synthesis of **27** contained mono-glycolised by-product and unreacted diester **24** which could be separated by flash column chromatography. Increasing the reaction time might be the most effective way to increase the yield of the di-glycolated product, however this must be accompanied with larger excess of ethylene glycol **1.2** to prevent the generation of oligomers (Figure 3.60).

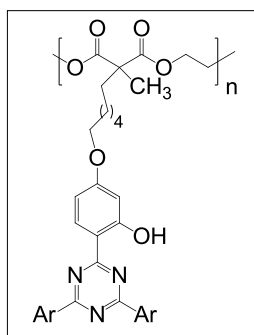


Fig.3.60 – Structure of polymerised **27**, a by-product during the glycolisation of **24**

UVAMs **29** and **30** were synthesised using the commercially available 2-bromo-2-methylmalonate **3.6** (Figure 3.61). This was a more streamlined route to obtain UVAM derivatives of Tinuvin 1577 **1.10** compared to the synthetic pathway of UVAMs **24-28**. The FT-IR spectra of **27**, **29** and **30** displayed two C=O stretch bands in the 1730 cm^{-1} region. This was commonly observed for a wide range of malonate compounds due to symmetric and asymmetric vibration couplings of the two stretching vibrations.¹³⁹

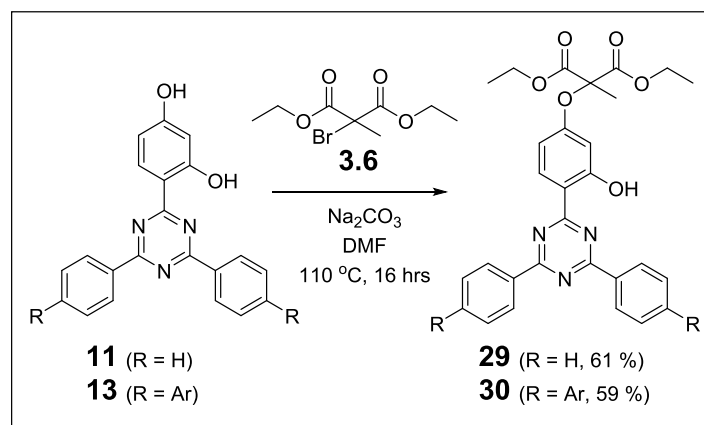


Fig.3.61 – Synthesis of **29** and **30**

UVAM **32** was synthesised using two different methods, the first being a simple reaction involving **11** and 3-chloropropane-1,2-diol **3.8** (Figure 3.62). The second was a two-step process involving the substitution of epibromohydrin **3.7** and subsequent opening of the epoxide ring in **31** *via* acid catalysis. The epibromohydrin **3.7** method evolved after unsuccessfully trying to substitute glycidol, with the idea of opening the epoxide ring during nucleophilic attack from the phenoxide anion. The alternative

was the epibromohydrin **3.7** reaction which installs an epoxide group that is opened up using acid catalysis. The overall yield of the two-step epoxide process to generate **32** was 30 %. This was significantly lower in comparison to the 75 % yield for the single step reaction using **11** and 3-chloropropane-1,2-diol **3.8**. A 4:1 molar excess of 3-chloropropane-1,2-diol **3.8** to **11** had to be employed along with potassium iodide to compensate for the slow rate of substitution. Even with this excess of reagent and presence of KI, the duration of the reaction had to be increased to 3 days. Reaction temperatures above 110 °C had a detrimental effect on the yield of **32** and gave a darker coloured product which was suspected to be from the substitution of the phenol *ortho* to the triazine ring.

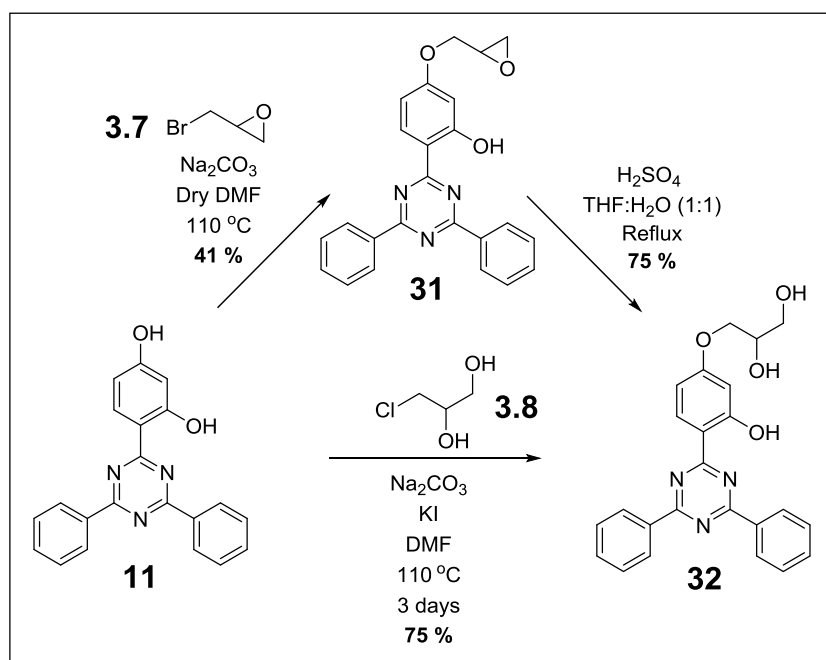


Fig.3.62 – Synthesis of **32** using epibromohydrin and 3-chloropropane-1,2-diol

HSQC analysis of **31** showed that H₁₀ was bonded to C₁₄, whilst H₈ and H₉ were both on C₁₃, and H₁₁ and H₁₂ were bonded to C₁₅ (Figure 3.63). It was thought that the phenol ether would deshield H₈ and H₉ to a greater extent compared to the deshielding experienced by H₁₁ and H₁₂ from the epoxide oxygen atom. Therefore H₈ and H₉ were assigned to the signals that were further downfield. Interestingly, the signal for H₈ and H₉ at 4.65 ppm was an apparent triplet rather than an expected pair of doublet of doublets.

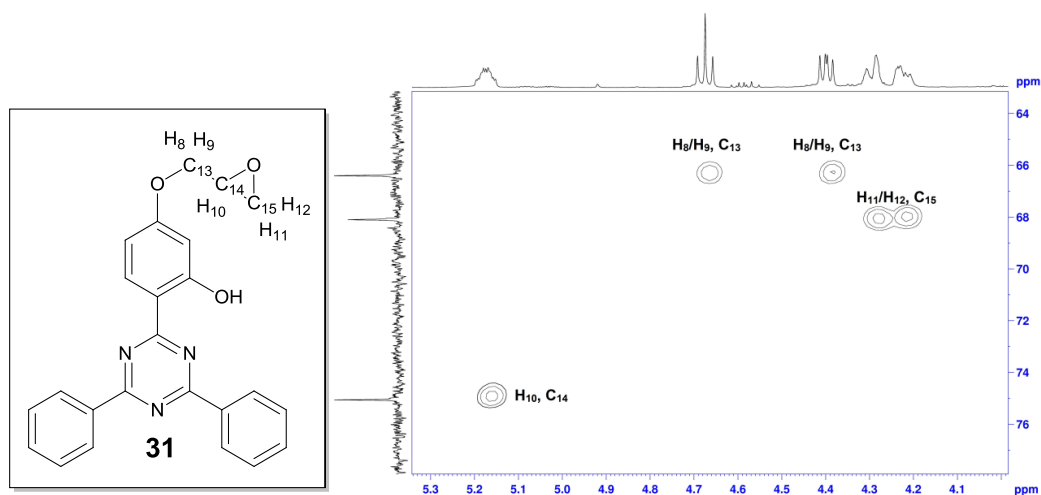


Fig.3.63 – HSQC of **31** used to assign H₈-H₁₂ and C₁₃, C₁₄ and C₁₅

HSQC and Correlation Spectroscopy (COSY) were used to assign the protons and carbons in the aliphatic region of **32** (Figure 3.64). The ¹H NMR spectrum of **32** showed H₁₂ as a triplet and H₁₃ as a doublet due to coupling with H₁₁ and H₁₀, respectively. Discrete signals for aliphatic hydroxyl protons, with observable coupling to nearby protons, were commonly observed when using deuterated DMSO. The formation of strong hydrogen bonds with the OH groups slows down intermolecular proton exchange which allows coupling to adjacent protons.

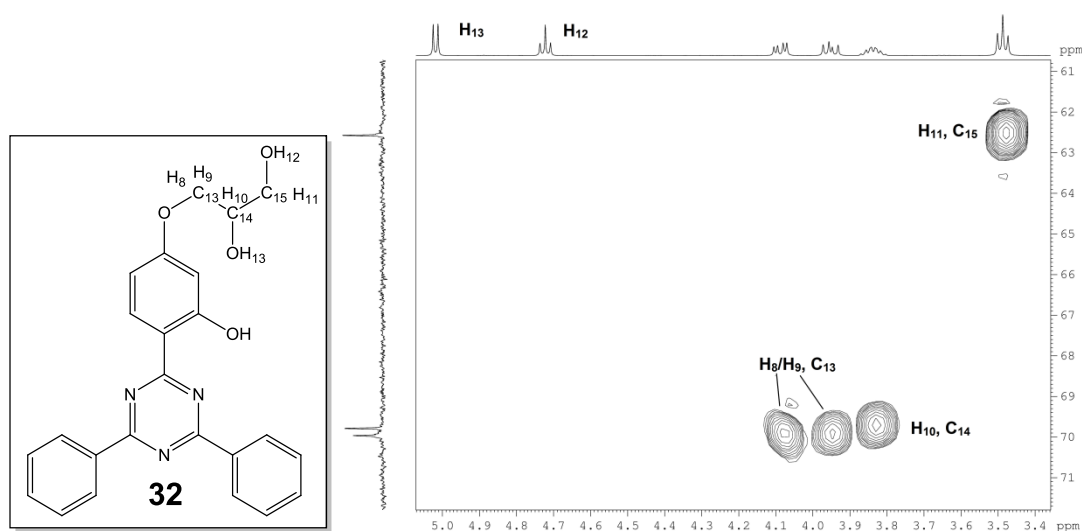


Fig.3.64 – HSQC of **32** used to assign H₈, H₉, H₁₂, H₁₃, C₁₃, C₁₄ and C₁₅

Compounds **33-36** were also synthesised using 3-chloropropane-1,2-diol **3.8**, with the duration of the reactions ranging from between 1 to 7 days (Figure 3.65). All were

purified by flash column chromatography, apart from **33** which was purified by precipitating the product out of hot DMF using MeOH.

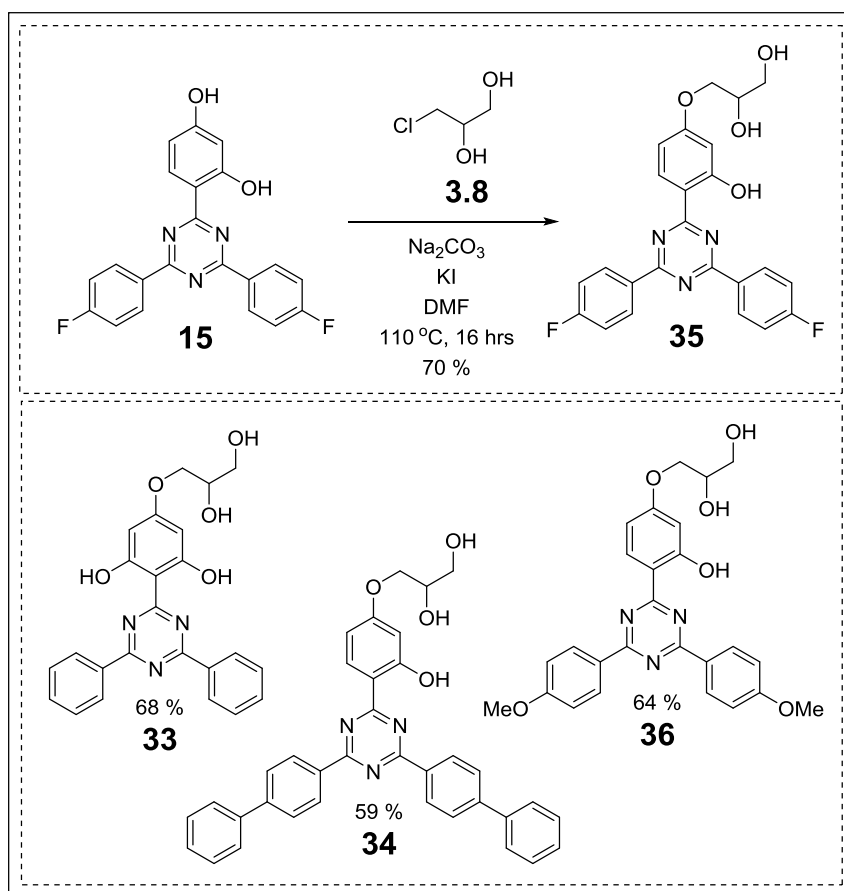


Fig.3.65 - Synthesis of **35** and the chemical structures of **33**, **34** and **36**

37 and **39** were synthesised by reacting 2-bromoethanol **3.9** with **17** and **18**, respectively (Figure 3.66). A second addition of 2-bromoethanol **3.9** was required to ensure all of the *para* positioned phenols of **17** had been reacted. 9-Bromo-1-nonanol **3.10** was chosen to synthesise UVAM **38** to investigate the effect of long aliphatic chain hydroxyl groups on the level of incorporation and glass transition temperature (T_g) upon copolymerisation. Most of the weak quaternary signals in the ^{13}C NMR spectrum of **38** were detected by HMBC except for both triazine carbons which were absent even in concentrated solutions. Compounds **37** and **39** were protected by BASF in a patent by Bolle and co-workers,⁹¹ however **37** had been disclosed in an expired patent by Dennenberger⁷⁷ which allowed freedom to operate.

UVAM **37** played a big role in this study due to the freedom to operate, relative ease of synthesis and strong UV absorbance within the 290-400 nm.

UVAMs **40**, **41** and **42** were synthesised to investigate the effect of polymerising monofunctional UVAMs, in particular looking at the molecular weight of the copolymers and the level of incorporation (Figure 3.66). Bojinov⁸¹⁻⁸⁷ found that the degree of incorporation of the polymerisable stabiliser was higher for monomers with a second polymerisable group, albeit vinyl groups for free radical polymerisation. Bojinov concluded that compounds with two unsaturated vinyl groups were superior photostabilisers compared to monofunctional species. Since a large number of UVAMs protected by BASF were monofunctional, it was imperative to examine if bifunctional monomers were more effective with regards to obtaining higher levels of incorporation or higher molecular weight polymers in step-growth polymerisations.

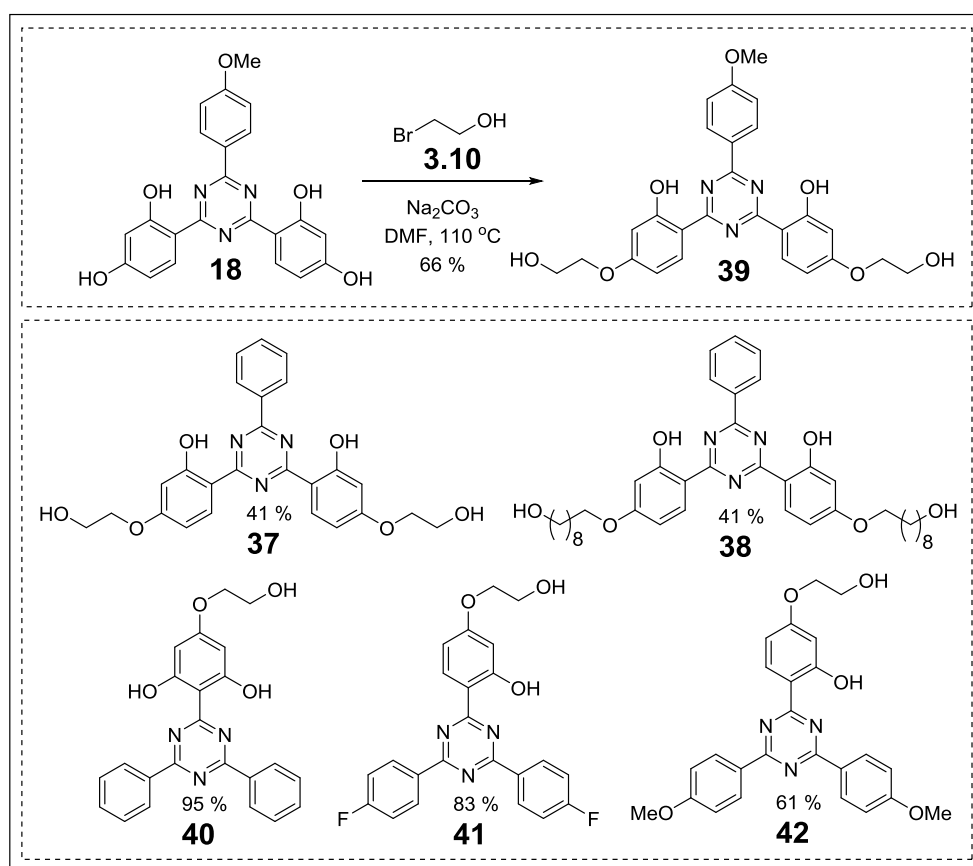


Fig.3.66 – Synthesis of **39** and the chemical structures of **37**, **38**, **40**, **41** and **42**

3.2.2 UV Spectra of UVAMs

The UV profiles of UVAMs **24-29** and **32** were found to be very similar to that of Tinuvin 1577 **1.10** (Figure 3.67 and Figure 3.68). These UVAMs have the same chromophoric structure, with the structural diversity being restricted to the aliphatic chain. One would expect blue- or red-shifts to be observed only when influencing the electronic delocalisation of the aromatic moieties and/or by increasing the number of IMHBs. Therefore, installing the polymerisable moieties solely on the aliphatic chain was an effective way to mimic the UV behaviour of Tinuvin 1577 **1.10**. The higher wavelength band is ascribed to the π - π^* intramolecular charge transfer transition and the lower wavelength band was attributed to localised π - π^* transitions.⁶⁷

Although DMSO is a polar solvent which is known to disturb the IMHBs of 2-hydroxybenzophenone (BP) and 2-(hydroxyphenyl)benzotriazole (BT) UV absorbers,⁶³ there was no experimental evidence of this having an effect on the UV absorption curve of these 2-(2-hydroxyphenyl)-1,3,5-triazine (TA) monomers due to their more robust IMHBs.

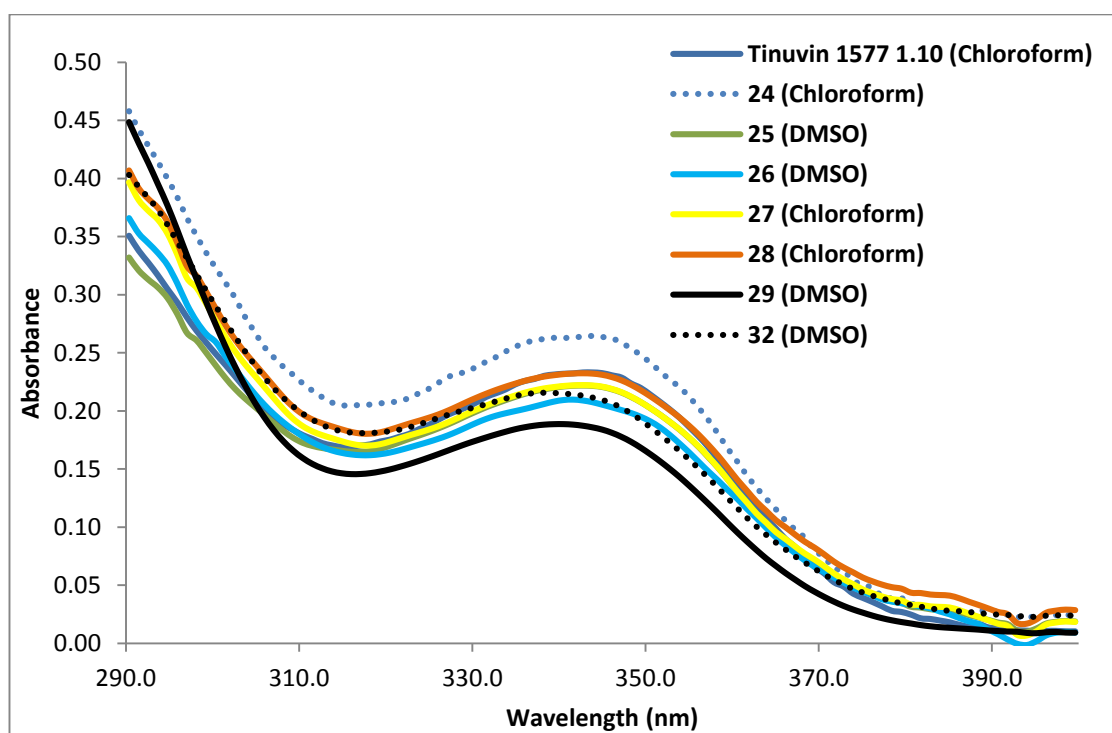


Fig.3.67 – UV spectra of 0.1 mM solutions of UVAMs 24, 25, 26, 27, 28, 29, 32 and Tinuvin 1577 1.10

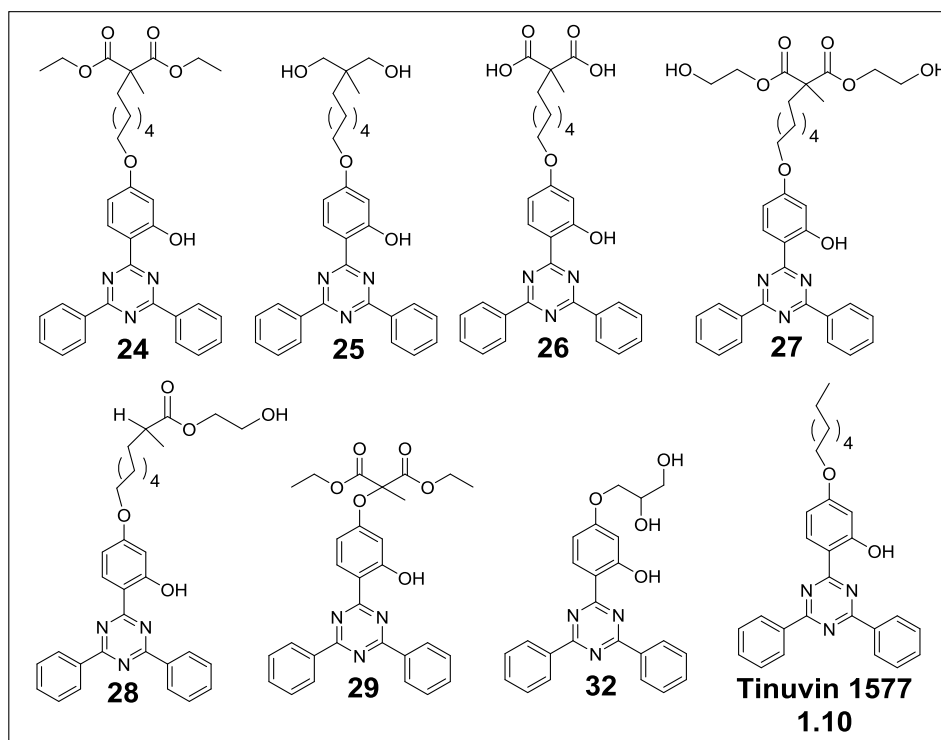


Fig.3.68 – Chemical structures of UVAMs 24, 25, 26, 27, 28, 29, 32 and Tinuvin 1577 1.10

Increasing the conjugation and the number of π bonds reduced the energy gap required for electron promotion. A red-shift is commonly observed since reducing the energy needed for excitation increases the wavelength of light. The most conjugated UVAMs **30** and **34** were the most powerful UV absorbers in this study (Figure 3.69 and Figure 3.70). The biphenyl bearing **30** and **34** mimicked the UV profile of the powerful and expensive UV absorbing commercial additive, Tinuvin 1600 **3.17**, another example of the UV profile remaining the same by installing polymerisable functional groups on the aliphatic chain. The biphenyl groups caused a red-shift in the π - π^* band which overlapped with the π - π^* charge transfer transition. In the case of **14**, the presence of the 1,3-dihydroxy naphthalene moiety results in a large red-shift of the π - π^* charge transfer band into the visible region. Absorbance in the visible region is undesirable as it produces a brown colour upon copolymerisation, therefore **14** was not elaborated into a UVAM.

The effect of an electron-donating methoxy group and an electron-withdrawing fluorine group were investigated by comparing the UV absorbance curves of **35** and

36 with Tinuvin 1577 **1.10**. When comparing the UV spectra of **36** and Tinuvin 1577 **1.10**, the electron-donating methoxy groups caused a red-shift in the π - π^* transitions and increased the molar absorptivity. Keck and co-workers^{52,60,64} have reported that electron-donating functional groups increase the basicity of the nitrogen triazine atoms which in turn strengthens the IMHB and contributes to the increase in extinction coefficient. The inductive effect of the fluorine atoms had little influence on the UV profile of **35**. In contrast to the methoxy functional groups, the fluorine atoms may marginally weaken the strength of the IMHB. An IMHB that is too weak is susceptible to disruption in polar environments, however the Keck group postulated that an IMHB which is too powerful is unfavourable and can hinder the radiationless deactivation by impeding the twisting vibration between the aryl and heterocyclic moieties. It is therefore important to recognise the potential of decreasing the strength of the IMHB, especially if this is achievable without damaging the UV absorbance of the UVAM.

Comparing the UV curve of **33** to Tinuvin 1577 **1.10** illustrates the increase in absorbance that is observed when an additional IMHB is introduced. An additional IMHB on the same aryl ring caused a blue-shift and an increase in the molar extinction coefficient of the π - π^* charge transfer transition. Keck^{52,60,64} postulated that this transition relied heavily on the planarity of the orientation and an additional IMHB further reinforces this conformation to give an increase in the molar absorptivity. However, having two IMHBs on the same aryl ring raises questions as to what affect this would have on the ESIPT and radiationless deactivation process. If an IMHB is too strong then this inhibits the twisting vibration and radiationless deactivation, therefore it would be fair to assume that the twisting vibration would be inhibited to a greater extent by an additional IMHB. Furthermore, Shizuka⁶⁰ postulated that the excited molecule undergoes *cis-trans* isomerisation post intramolecular proton transfer to prevent reverse intramolecular proton transfer, however one would expect the second IMHB to hinder the 180 ° rotation of the triazine-aryl bond. The situation whereby both IMHBs undergo intramolecular proton transfer is unlikely since this would disrupt the aromaticity of the molecule.

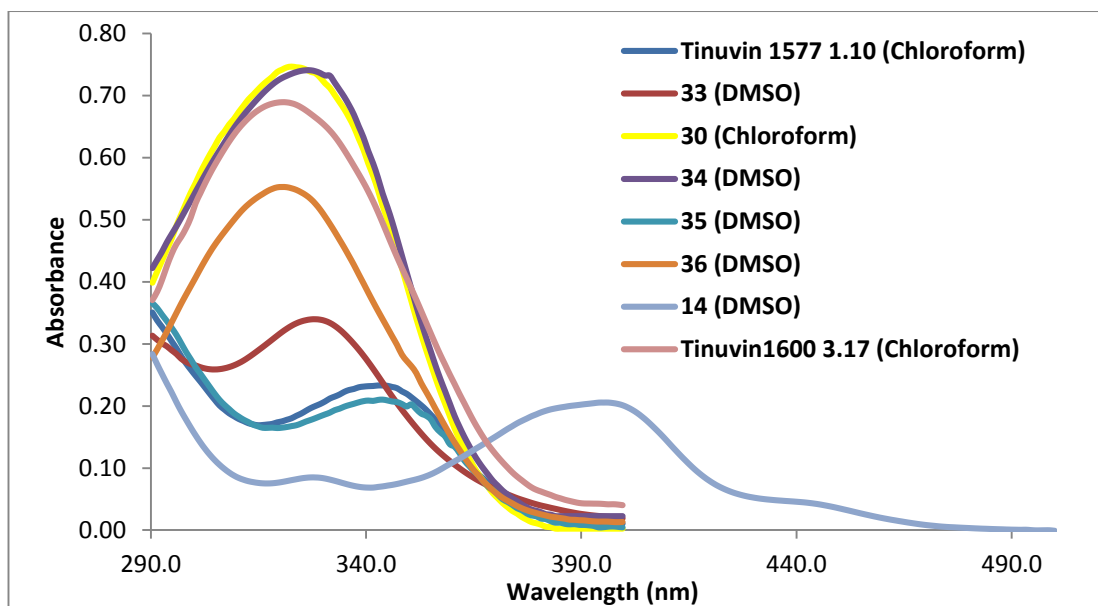


Fig.3.69 – UV spectra of 0.1 mM solutions of UVAMs 33, 30, 34, 35, 36, 14, Tinuvin 1577 1.10 and Tinuvin 1600

3.17

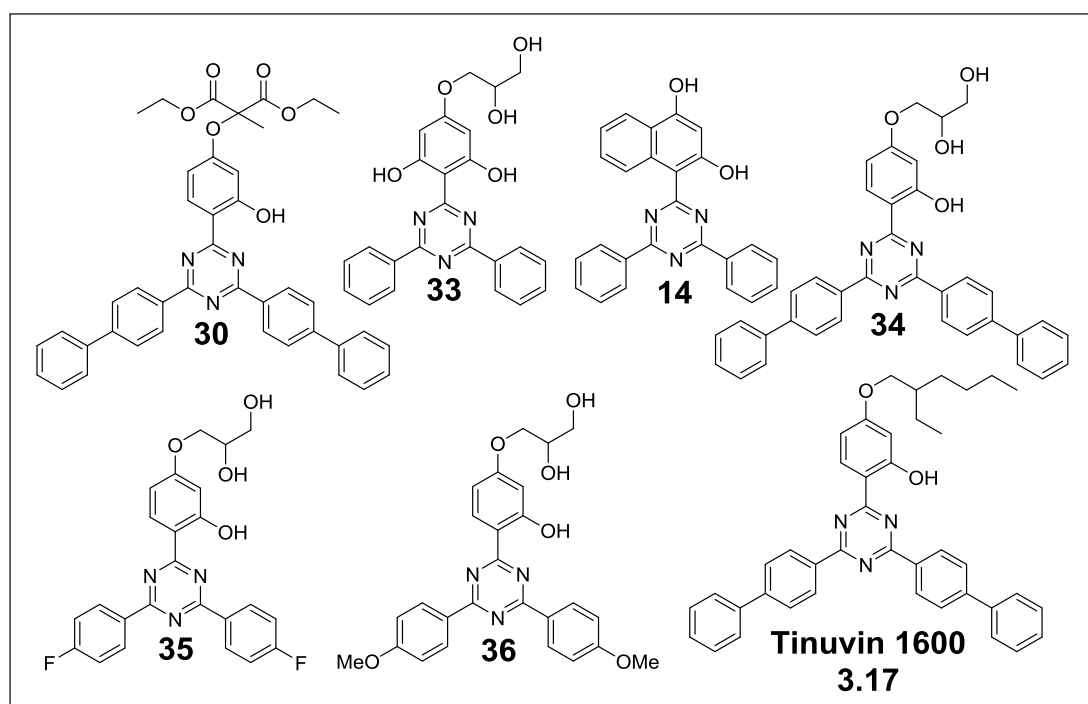


Fig.3.70 – Chemical structures of UVAMs 33, 30, 34, 35, 36, 14 and Tinuvin 1600

In summary, UVAMs **37**, **38** and **39** had larger molar extinction coefficients than Tinuvin 1577 **1.10** throughout the 290-400 nm region. Increasing the number of resorcinylic moieties and the number of IMHBs caused a red-shift in both π - π^* and charge transfer transitions. The tri-resorcinylic **19** exhibited the highest extinction

coefficient in the long UV wavelength region due to the 3 IMHBs (Figure 3.71 and Figure 3.72). A slight red-shift was observed for **38** with long aliphatic hydroxyl chains in comparison to the UV curve of **37** which had shorter polymerisable chains. UVAM **39** had a higher molar absorptivity between 310-350 nm than **37** and **38**, with the methoxy group causing a blue-shift in the charge transfer transition and a red-shift in the π - π^* transition resulting in an overlap. Dobashi^{55,56} discovered a clear relationship between the photostabilising effect and the maximum wavelength of absorption (λ_{max}) of the UVA. Dobashi demonstrated that BP and BT ultraviolet absorbers with higher λ_{max} were the superior photostabilisers. If the same is true for TA derivatives and absorbance at longer wavelengths enhances the photostabilising effect then this further highlights the potential of **37**, **38** and **39**. Furthermore, these UVAMs would be more adept at preventing the fluorescent by-products during PET degradation which are formed by deeply penetrating low energy, high wavelength UV light.^{33,34}

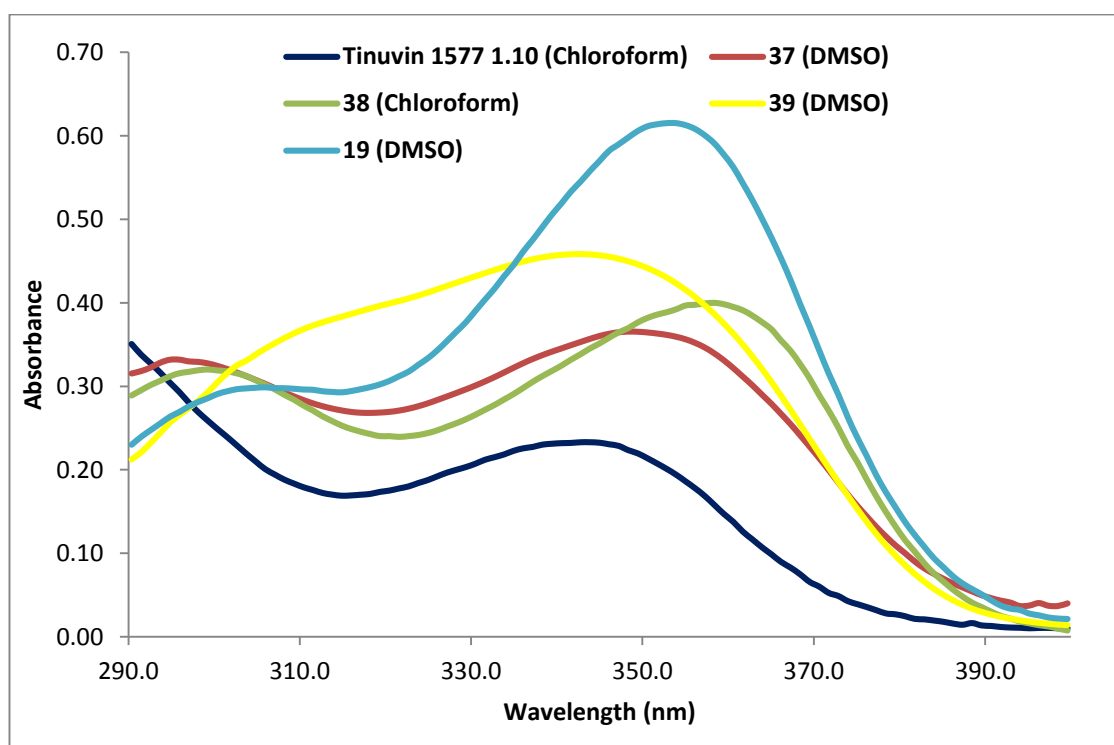


Fig.3.71 – UV Spectra of 0.1 mM solutions of 19, 37, 38, 39 and Tinuvin 1577 1.10

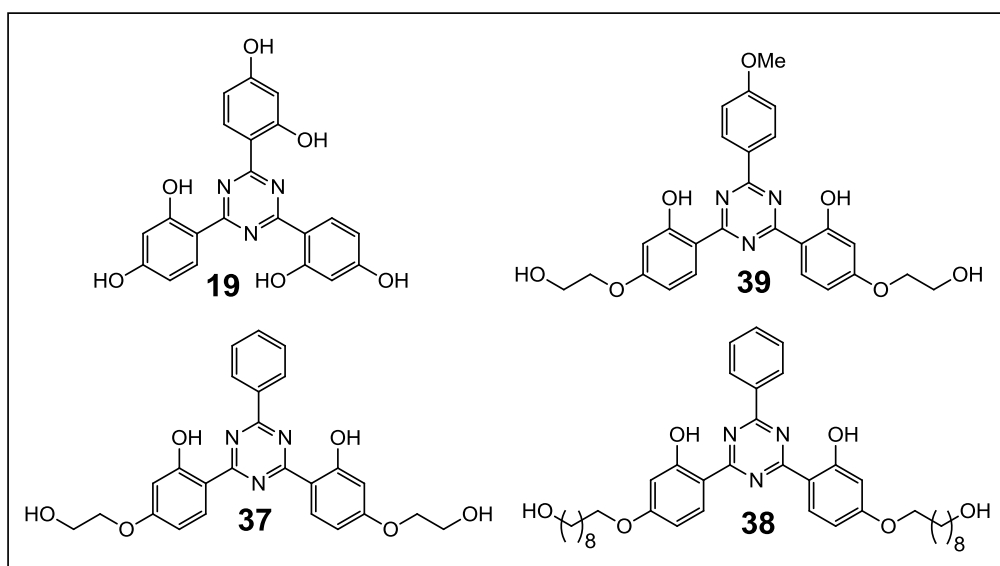


Fig.3.72 – Chemical structures of 19, 37, 38 and 39

When comparing the UV spectra of monofunctional and bifunctional derivatives, it is clear to see that monofunctional UVAMs **40**, **41** and **42** have the same UV profiles as those of the bifunctional derivatives, **33**, **35** and **36**, respectively (Figure 3.73 and Figure 3.74). Therefore, the UV spectra of the copolymers can be compared to illustrate the level of incorporation and the molar extinction coefficients.

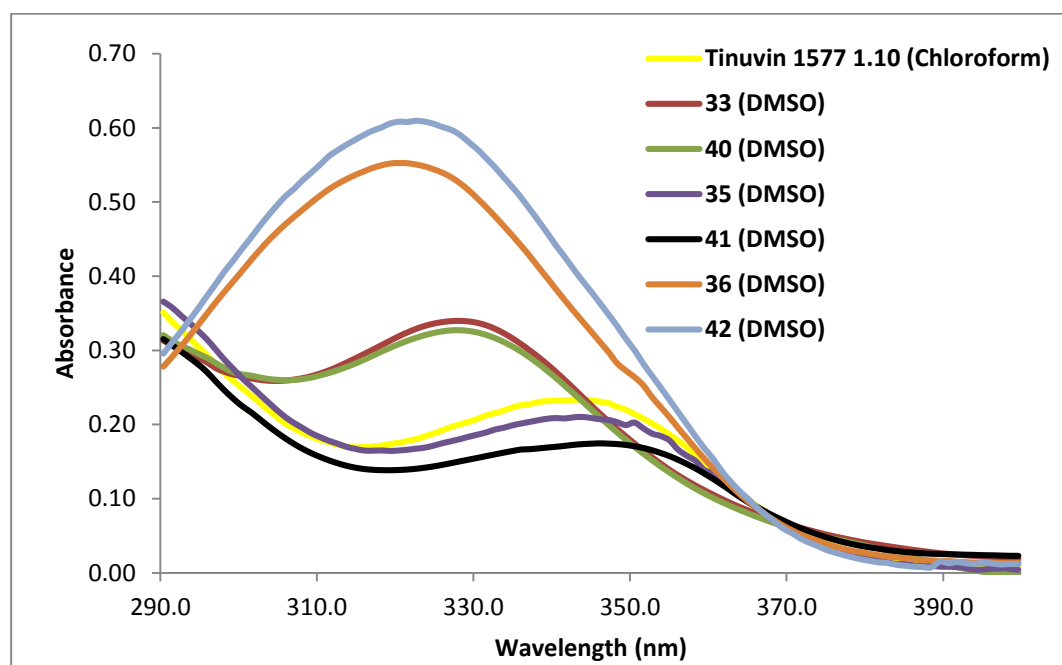


Fig.3.73 – UV spectra of 0.1 mM solutions of 33, 35, 36, 40, 41, 42 and Tinuvin 1577 1.10

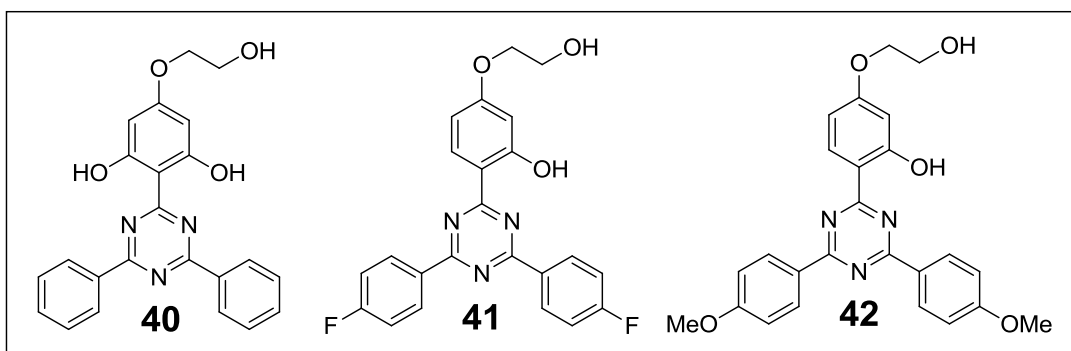


Fig.3.74 – Chemical structures of 40, 41 and 42

The UV spectra of **20**, **21** and **22** showed a blue shift for the π - π^* charge transfer band (Figure 3.75 and Figure 3.76). The less conjugated **20** and **22** displayed lower molar extinction coefficients for the π - π^* band with respect to the tri-aryl Tinuvin 1577 **1.10**. As seen previously, the methoxy groups greatly increase the molar absorption of **21** and cause a red-shift in the π - π^* transition. The UV absorbance curve of **22** showed an expected lower molar absorption than Tinuvin 1577 **1.10**. The commercial additive greatly outperformed the mono-aryl UVAM **20**, with Tinuvin 1577 **1.10** showing higher molar extinction coefficients across the entire 290-400 nm range. UVAM **21** exhibited a stronger molar absorption than the commercial additive at wavelengths between 300-350 nm, however Tinuvin 1577 **1.10** was superior at wavelengths below 300 nm and above 350 nm.

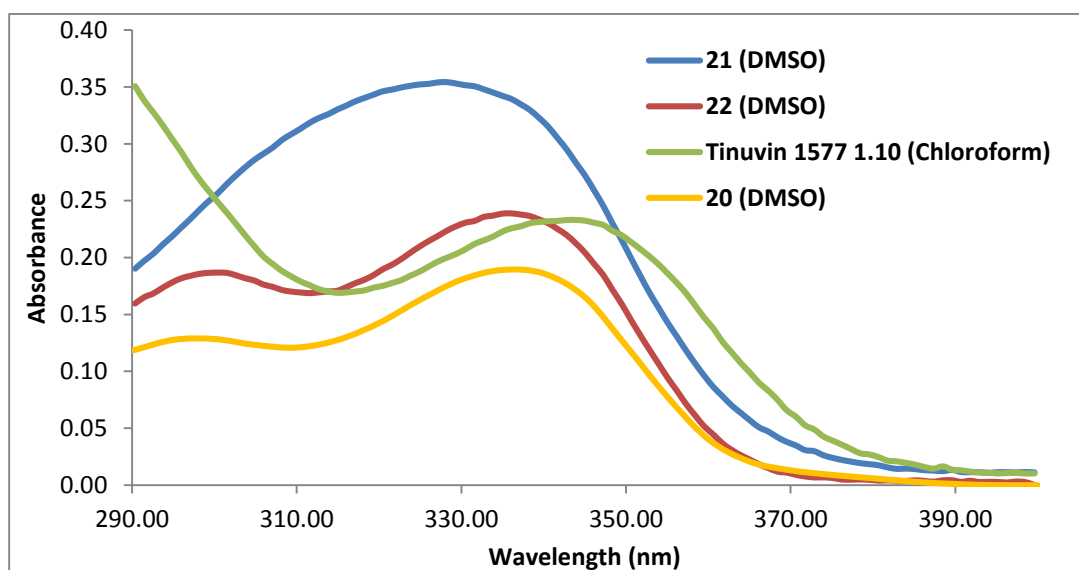


Fig.3.75 – UV spectra of 0.1 mM solutions of 20, 21, 22 and Tinuvin 1577 1.10

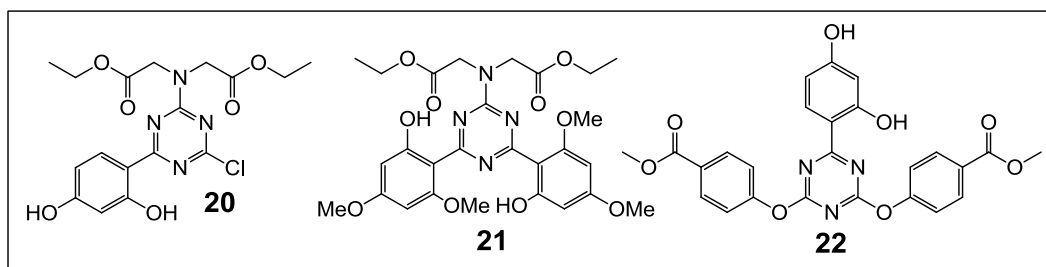


Fig.3.76 – Chemical structures of UVAM 20, 21 and 22

3.2.3 Thermal Analysis of UVAMs

Thermogravimetric analyses were carried out in air, increasing the temperature at a rate of 10 °C/min. PET and PEI are typically processed at 285 °C in industry, thus the thermal stability of UVAMs at such a high processing temperature is an important characteristic. The onset of degradation was calculated by differentiating the percentage weight loss curve. UVAMs with insufficient thermal stability would result in less active ingredient residing in the polymer and lower levels of UV protection.

UVAMs **24**, **27**, **28** and **29** displayed superior thermal stability compared to Tinuvin 1577 **1.10** at 300 °C (Table 3.2 and Figure 3.77). UVAMs **24**, **25** and **27** exhibited the highest onset temperature amongst the Tinuvin 1577 **1.10** derivative UVAMs. All the UVAMs in this table, except for **26** and **31**, demonstrated adequate thermal stability at 285 °C.

<i>Compound</i>	<i>Weight loss at 300 °C (%)</i>	<i>Onset temperature (°C)</i>
Tinuvin 1577 1.10	2.0	340
24	0.6	365
25	3.1	392
26	11.6	181 and 324
27	1.1	373
28	0.9	346
29	0.8	342
31	9.8	204 and 342
32	2.3	312

Table 3.2 - Percentage weight loss at 300 °C and the onset temperatures of UVAMs 24-29, 31, 32 and Tinuvin 1577 1.10

The ~8 % loss of weight for UVAM **31** at an onset of 204 °C was believed to be from the decomposition or rearrangement of the epoxide ring. UVAM **26** had a

significantly higher percentage weight loss due to the release of CO₂ from decarboxylation which took place at 181 °C and contributed to 9.6 % of the weight loss, which is comparable to the 8.1 % calculated weight loss of CO₂ from **26**. Once decarboxylation takes place, the mono-carboxylic acid UVAM is stable until 324 °C.

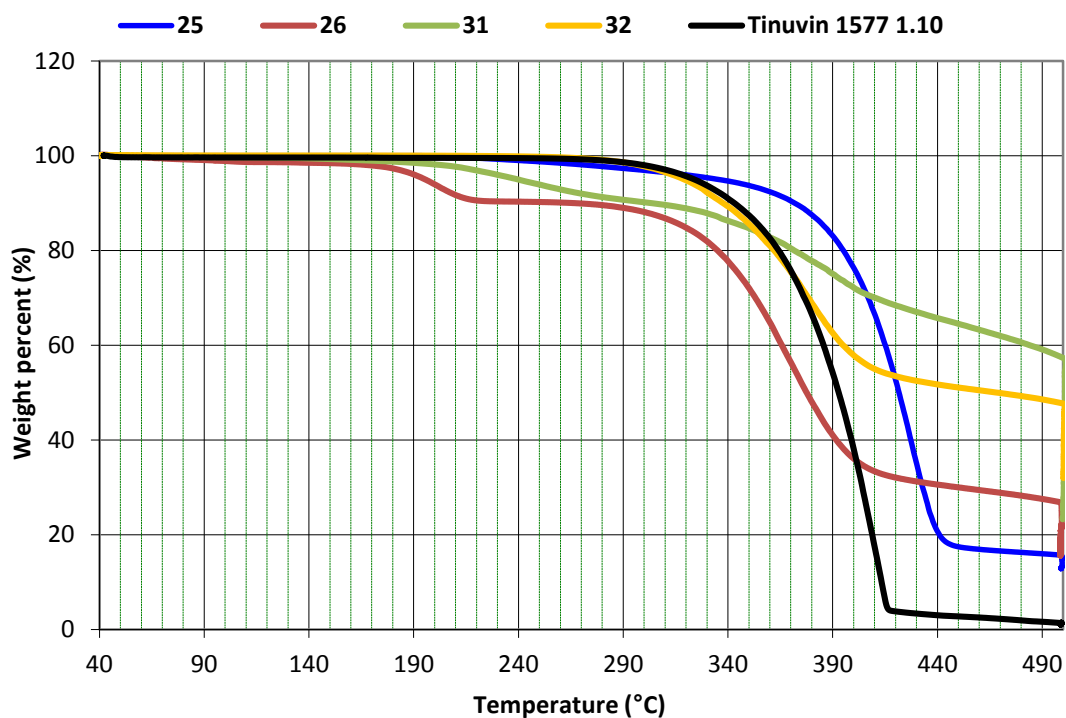


Fig.3.77 - TGA plots of UVAM 25, 26, 31, 32 and Tinuvin 1577 1.10 showing the percentage weight loss between 40 – 500 °C

UVAMs containing propanediol or glycol polymerisable moieties showed sufficient thermal stability for future 285 °C copolymerisations, however all except for **42** displayed inferior thermal resistance in comparison to Tinuvin 1577 **1.10** (Table 3.3 and Figure 3.78). Since the precursors were generally more thermally stable, the loss of weight up to 300 °C could be attributed to the thermal degradation of the polymerisable fragments. This would favour introducing the UVAMs in the beginning of the polymerisation and raising the temperature of a copolymerisation gradually, allowing the UVAMs to chemically tether to the polymer backbone before degradation ensues. UVAM **41** exhibited a loss of 2.9 % at 120 °C which was accredited to residual solvent and which contributed to the 8.6 % weight loss after 300 °C.

<i>Compound</i>	<i>Weight loss at 300 °C (%)</i>	<i>Onset temperature (°C)</i>
Tinuvin 1577 1.10	2.0	340
33	3.6	329
34	3.3	346
35	4.1	319
36	5.7	310
40	5.6	314
41	8.6	309
42	1.7	339

Table 3.3 - Percentage weight loss at 300 °C and the onset temperatures of UVAMs 33-36, 40-42 and Tinuvin

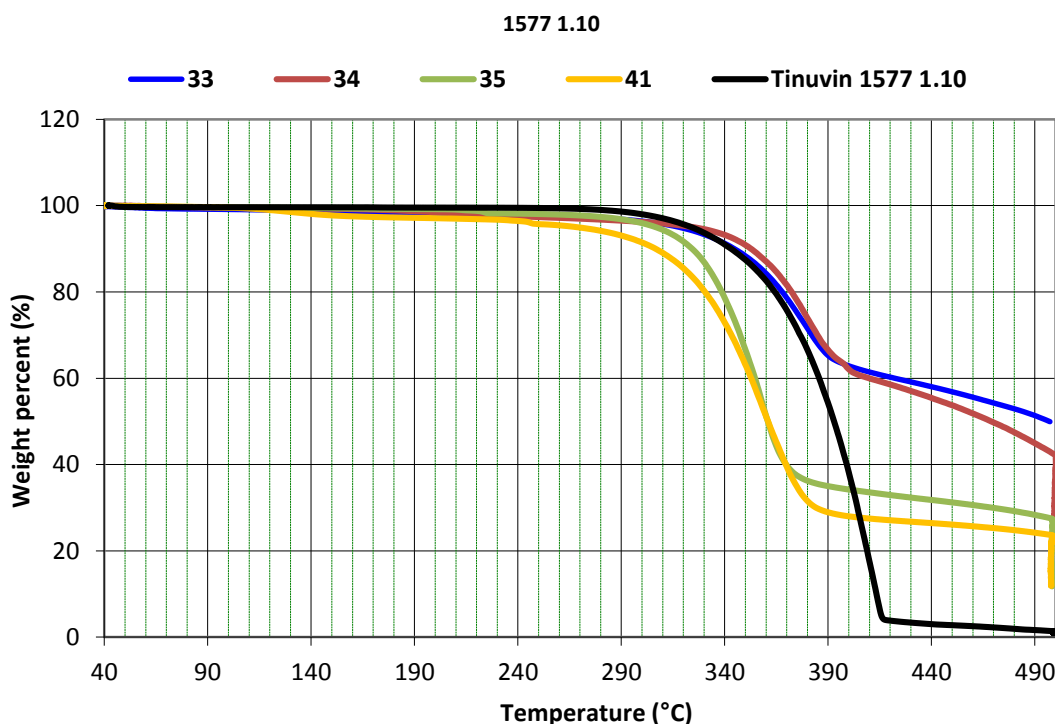


Fig.3. 78 - TGA plots of UVAM 33, 34, 35, 41 and Tinuvin 1577 1.10 showing the percentage weight loss between 40 – 500 °C

Increasing the number of resorcinol moieties and IMHBs increased the thermal stability of the compounds. UVAMs **37** and **38** contained two resorcinol moieties and displayed superior stability at high temperatures compared to Tinuvin 1577 **1.10**, whereas **39** had similar resistance to the commercial additive (Table 3.4 and Figure 3.79). UVAM **38** displayed no weight loss after 300 °C which may be due to the increased stability of long chain polymerisable functional groups. Tri-resorcinol **19** had the highest onset temperature of all the compounds in this study, further strengthening the idea that increasing the number of resorcinols and IMHBs

enhances the thermal robustness of the tri-aryl UVAMs. The TGA curve of **19** showed a 3.8 % loss after 60 °C which was due to solvent remaining from recrystallisation.

<i>Compound</i>	<i>Weight loss at 300 °C (%)</i>	<i>Onset temperature (°C)</i>
Tinuvin 1577 1.10	2.0	340
19	5.1	454
37	1.7	388
38	0	411
39	1.4	331

Table 3.4 - Percentage weight loss at 300 °C and the onset temperatures of **19**, **37**, **38**, **39** and Tinuvin 1577 1.10

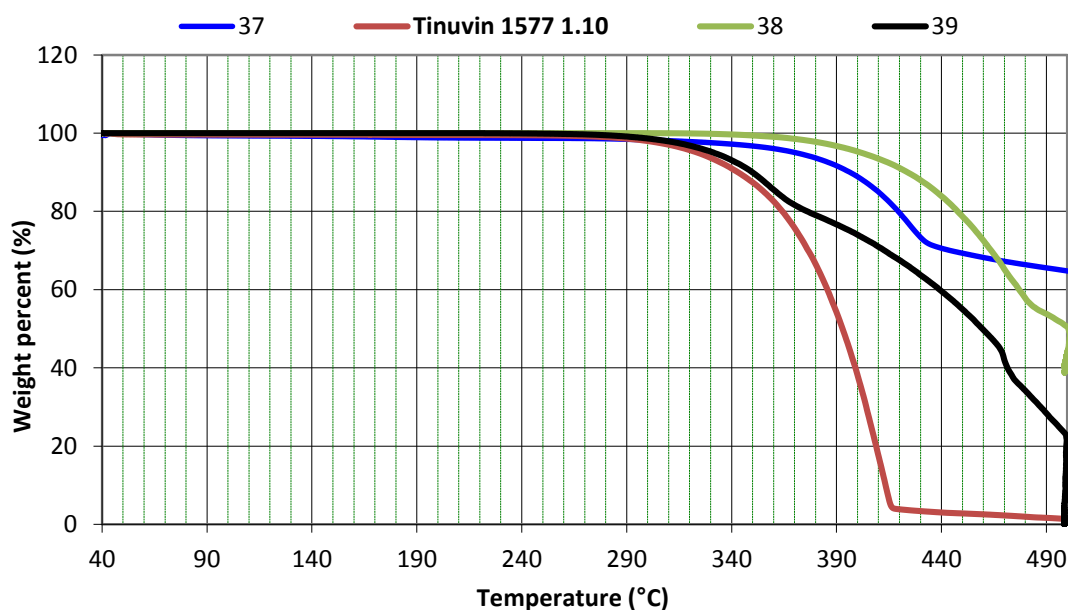


Fig.3.79 - TGA of UVAMs **37**, **38**, **39** and Tinuvin 1577 1.10 showing the percentage weight loss 40 – 500 °C

The TGA curve of **20** showed a weight reduction of roughly 10 % after an onset of 197 °C which may be from the loss of chlorine (Table 3.5 and Figure 3.80). The remaining compound was seemingly stable at higher temperatures, however the PEI copolymer of **20** showed evidence of thermal degradation. The major disadvantage of UVAMs with ether-triazine bonds was the lack of thermal stability at temperatures required for PET processing. For this reason, the design and synthesis of UVAM targets with ether-triazine bonds were disregarded. Although TGA analysis showed that **21** demonstrated thermal stability similar to Tinuvin 1577 **1.10**, a very low level of incorporation after copolymerisation into PEI is ascribed to thermal deterioration of the stabilising monomer.

<i>Compound</i>	<i>Weight loss at 300 °C (%)</i>	<i>Onset temperature (°C)</i>
Tinuvin 1577 1.10	2.0	340
20	11.0	197 and 329
21	2.8	325
22	21.3	236

Table 3.5 - Percentage weight loss at 300 °C and the onset temperatures of UVAMs 20, 21 and 22 and Tinuvin

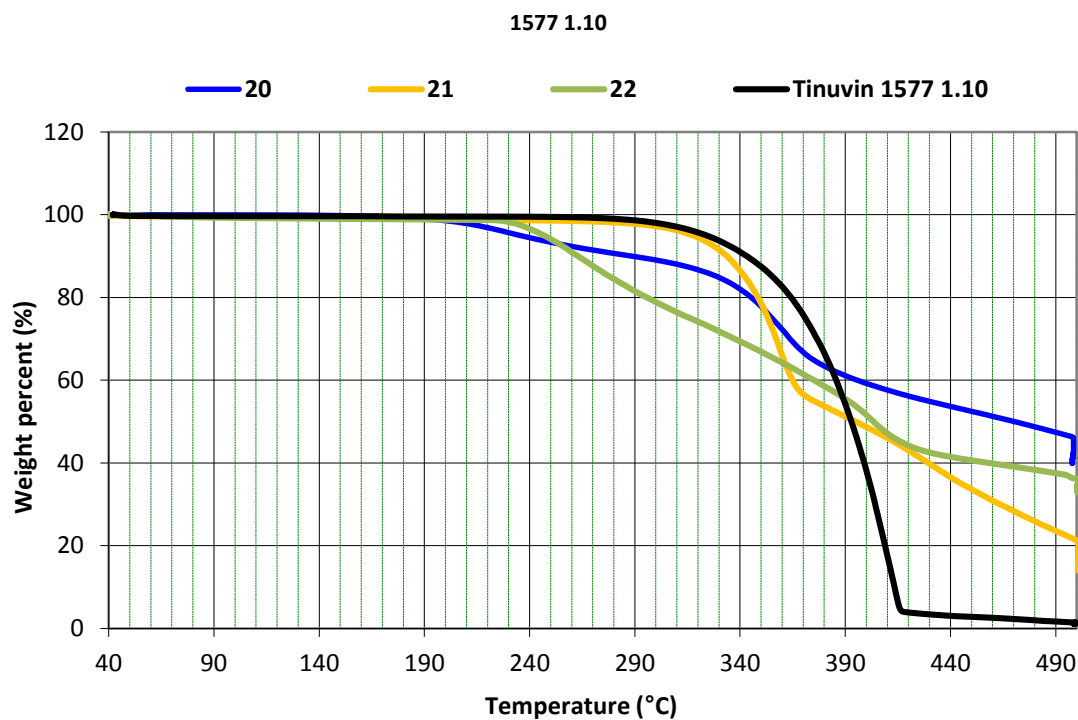


Fig.3.80 - TGA of UVAM 20, 21, 22 and Tinuvin 1577 1.10 showing the percentage weight loss between 40 – 500 °C

3.3 Conclusions

Novel ultraviolet absorber monomers (UVAMs) were synthesised successfully from cyanuric chloride **1.90** as a synthetic starting point. Grignard and Friedel-Crafts chemistry were employed to successfully construct the core chromophore structures. Polymerisable moieties for step-growth polymerisations were installed using a wide range of synthetic reactions.

The structures of UVAMs that were based on the chromophore of Tinuvin 1577 **1.10** mimicked the UV profile of the commercial additive. This was achievable simply through chemically altering the aliphatic chain with polymerisable moieties. A similar strategy was used to synthesise UVAMs **30** and **34** which mimicked the UV profile of the powerful commercial additive, Tinuvin 1600 **3.17**. UVAMs with alternative chromophoric structures were designed and synthesised to deliver UVAMs with superior UV absorption properties in comparison to Tinuvin 1577 **1.10**. A wider and stronger UV absorbance was generally observed when increasing the number of IMHBs, electron density and conjugation of the chromophores. Most of the UVAMs exhibited sufficient thermal stability, which is important from the point of view of polymer processing which is carried out at elevated temperatures. In particular, UVAMs **25**, **37** and **38** displayed impressive thermal stability with high onset temperatures for decomposition.

Novel mono- and di-aryl triazine UVAMs with ether-triazine and amine-triazine bonds were synthesised successfully to examine the potential of inexpensive monomers which were not protected by intellectual property. The UV absorbance of **21** showed a stronger absorbance in comparison to Tinuvin 1577 **1.10** between the 300-350 nm wavelength range. The main drawback of these mono-aryl and di-aryl UVAMs was that they were insufficiently stable at high polymer processing temperatures. The tri-aryl triazine systems were more thermally robust and possessed stronger IMHBs.

Chapter 4 - Poly(ethylene isophthalate)

Copolymers

4.1 Experimental

UVAMs were firstly copolymerised into poly(ethylene isophthalate) (PEI) to prove that the polymerisable stabilisers could be incorporated successfully into the polymer chain. The amorphous copolymers were soluble in organic solvents which allowed for purification and analysis using UV and NMR spectroscopy. This was an effective screening strategy to ultimately select which UVAMs to copolymerise with poly(ethylene terephthalate) (PET).

4.1.1 Reagents

Reagent	Purity	Supplier
Antimony trioxide	>99.65 %	SICA
<i>Bis</i> (2-Hydroxyethyl)isophthalate (BHEI)	-	Synthesised at DTF
Chloroform	99.0-99.4%	Aldrich
Methanol	99.7%	Aldrich
Poly(ethylene isophthalate)	-	Synthesised at DTF

Table 4.1 - List of solvents and reagents used

4.1.2 Equipment

The polymers in this study were synthesised in a polycondensation (PC) rig at DuPont Teijin Films, Wilton, UK (Appendix, Figure 7.1). The equipment included a polycondensation head, stirrer guide, air stirrer, delivery side-arm, distillate tube inside an ice-filled Dewar flask, thermocouples and optical revolution counter. The system was connected to a gas and vacuum manifold.

Nuclear magnetic resonance (NMR) spectra were recorded on Bruker DPX 400 and DRX 500 instruments in the NMR Laboratory at the University of Strathclyde for ^1H nuclei. The chemical shifts (δ) are quoted in part per million (ppm), relative to the residual proton resonances of the NMR solvent, and coupling constants (J values) in Hz. Multiplicities are abbreviated as s, singlet; d, doublet; t, triplet; q, quartet; m, multiplet for the ^1H NMR spectra. In cases where superimposition of signals occurred, the signals were reported as multiplet (m). CDCl_3 was used as a solvent. The phenolic and aromatic protons of polymerised UVAMs were integrated in the ^1H NMR spectra to calculate the actual wt. % and mol. % incorporation values.

Matrix-assisted laser desorption/ionisation (MALDI) spectrometry was carried out in the MS Laboratory at the University of Strathclyde using a Shimadzu Biotech Axima-CFR MALDI-TOF. 10 mg of sample was dissolved in 1 mL of CHCl_3 and no matrix was used.

UV-Visible absorption spectra were acquired using a Photonics CCD array UV-VIS spectrophotometer with a 1 mm pathlength quartz cell. 10 mg of sample was dissolved in 1 mL of CHCl_3 .

Differential scanning calorimetry (DSC) analysis of polymer samples was carried out at DuPont Teijin Films (DTF) using a 6000 Enhanced Single-Furnace DSC. The samples were heated from $-20\text{ }^\circ\text{C}$ to $310\text{ }^\circ\text{C}$ at a rate of $20\text{ }^\circ\text{C}/\text{min}$, cooled back to $-20\text{ }^\circ\text{C}$ at a rate of $50\text{ }^\circ\text{C}/\text{min}$ and then reheated to $310\text{ }^\circ\text{C}$ at a rate of $20\text{ }^\circ\text{C}/\text{min}$.

Molecular weight determination of polymers using gel permeation chromatography (GPC) was carried out at Intertek on a Viscotek GPC Max instrument with refractive index detection. The samples were dissolved in hexafluoroisopropanol (HFIP) and passed through PLgel HFIP Gel Column at a flow rate of $0.7\text{ mL}/\text{min}$ at $40\text{ }^\circ\text{C}$.

4.1.3 Synthesis of Poly(ethylene isophthalate) (PEI) Copolymers

4.1.3.1 Poly(EI-co-UVAM) Copolymers

A stirred slurry of *bis*(2-hydroxyethyl)isophthalate (BHEI) **4.1** was pre-heated at $90\text{ }^\circ\text{C}$ for 30 mins. Once the viscosity of the slurry had reduced sufficiently, the slurry was poured into a polycondensation (PC) tube. To this, **UVAM** and Sb_2O_3 (0.15 g, 0.52 mmol) were added and the PC tube was scored lightly on the stem using a Stanley blade, to ensure safe extrusion, and clamped inside a heating block. The PC tube was fitted with a polycondensation head, stirrer guide, air stirrer, delivery side-arm, distillate tube inside an ice-filled Dewar flask, thermocouples, optical revolution counter and connected to a gas manifold. The temperature was raised using a control box to $200\text{ }^\circ\text{C}$ over 35 mins under a nitrogen purge. The air stirrer was then started with a pressure of 8.5 psi and the nitrogen purge was then stopped, with the system now under vacuum (approximately 950 mbar). The pressure was reduced

gradually to less than 10 mbar as the temperature was increased to 285-290 °C at a rate of 1 °C/min, with the stirrer speed reaching between 165-175 rpm. After stirring at 285-290 °C for 30 mins, the vacuum was slowly replaced with a nitrogen purge. A hammer and chisel was used to break the stem of the PC rig tube, and the synthesised copolymer was extruded and quenched into an ice-water bath. The copolymer lace formed was left to dry in air.

A 10 % w/v solution of crude polymer in chloroform was filtered through a cotton wool plug and added dropwise into cold methanol, ensuring a 1:10 v/v ratio of chloroform to methanol. The precipitate which formed was filtered and washed with chloroform/methanol (1:10). The precipitate was dried at 40 °C *in vacuo* (60 mbar) for 1 hour and this process was repeated twice more.

Poly(EI-co-25) (P1)

Copolymer	UVAM 25 mass (g)	BHEI 4.1 mass (g)	UVAM 25 in the feed		UVAM 25 in copolymer	
			Wt %	Mol %	Wt %	Mol %
P1	0.40	40	0.99	0.49	1.06	0.40

Table 4.2 – Theoretical and actual UVAM 25 loading in P1

Yield = 67 %

DSC: T_g = 67.0 °C

GPC: M_w = 40,900; M_n = 16,500; M_w/M_n = 2.5

¹H NMR (500 MHz, CDCl₃) δ: 1.26 (s, 0.0113H, H₅), 4.67 (s, 4H, H₄), 6.50 (s, 0.0029H, H₇), 6.55-6.57 (m, 0.0034H, H₆), 7.50 (t, J = 7.8 Hz, 1H, H₂), 8.21 (d, J = 7.8 Hz, 2H, H₁), 8.69 (s, 1H, H₃), 13.48 (s, 0.0040H, H₈)

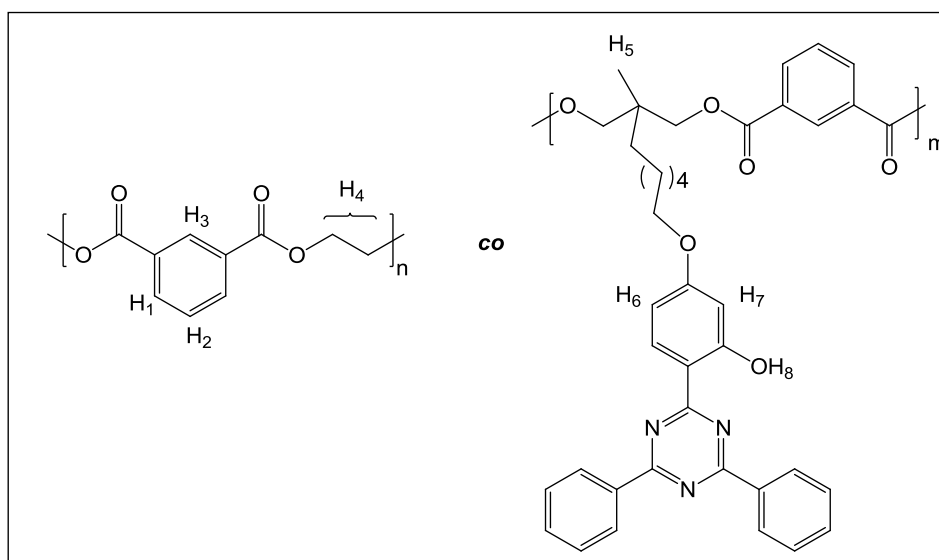


Fig. 4.1 - Structure of P1

Poly(EI-co-27) (P2)

Copolymer	UVAM 27	BHEI 4.1	UVAM 27 in the feed		UVAM 27 in copolymer	
	mass (g)	mass (g)	Wt %	Mol %	Wt %	Mol %
P2	1.50	75.00	1.96	0.80	1.72	0.53

Table 4.3 – Theoretical and actual UVAM 27 loading in P2

Yield = 72 %

DSC: T_g = 63.7 °C

GPC: M_w = 24,100; M_n = 7,000; M_w/M_n = 3.5

¹H NMR (400 MHz, CDCl₃) δ: 4.68 (s, 4H, H₄), 6.47-6.59 (m, 0.0132H, H₅ and H₆), 7.50 (t, J = 7.8 Hz, 1H, H₂), 8.21 (d, J = 7.8 Hz, 2H, H₁), 8.69 (s, 1H, H₃), 13.48 (s, 0.0053H, H₇)

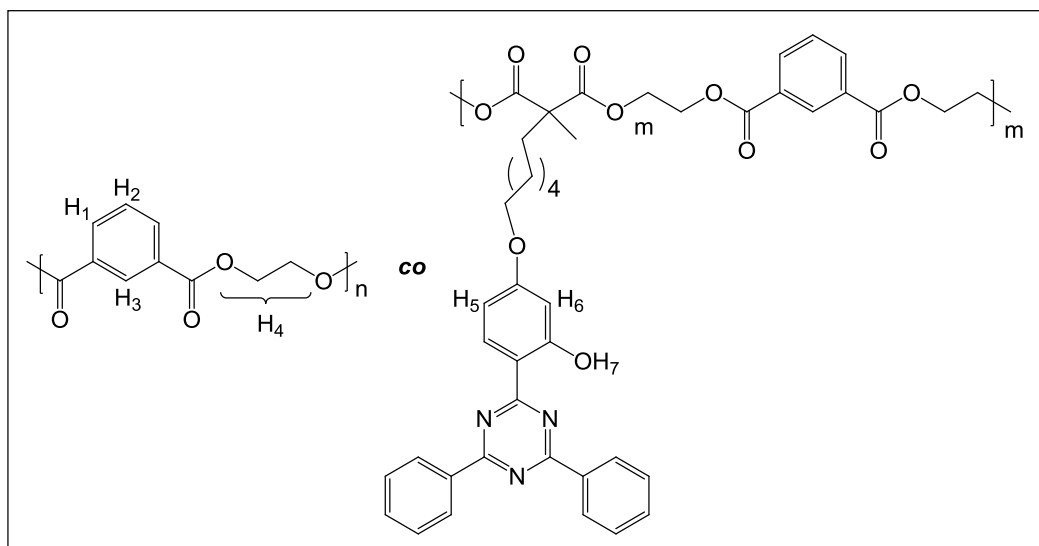


Fig. 4.2 – Structure of P2

Poly(EI-co-28) (P3)

Copolymer	UVAM 28	BHEI 4.1	UVAM 28 in the feed		UVAM 28 in copolymer	
	mass (g)	mass (g)	Wt %	Mol %	Wt %	Mol %
P3	0.26	40.00	0.65	0.31	0.73	0.26

Table 4.4 - Theoretical and actual UVAM 28 loading in P3

Yield = 60 %

DSC: T_g = 66.0 °C

GPC: M_w = 35,500; M_n = 13,600; M_w/M_n = 2.6

¹H NMR (500 MHz, CDCl₃) δ: 4.68 (s, 4H, H₄), 6.51-6.59 (m, 0.0040H, H₅ and H₆), 7.50 (t, J = 7.8 Hz, 1H, H₂), 8.21 (d, J = 7.8 Hz, 2H, H₁), 8.69 (s, 1H, H₃), 13.49 (s, 0.0026H, H₇)

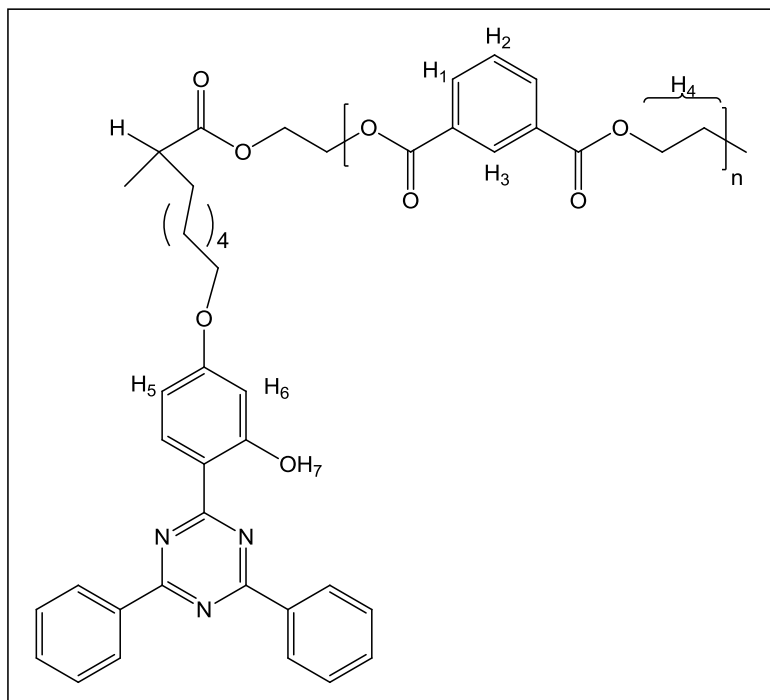


Fig. 4.3 – Structure of P3

Poly(EI-co-29) (P4)

Copolymer	UVAM 29	BHEI 4.1	UVAM 29 in the feed		UVAM 29 in copolymer	
	mass (g)	mass (g)	Wt %	Mol %	Wt %	Mol %
P4	0.40	39.61	1.00	0.50	0.90	0.34

Table 4.5 - Theoretical and actual UVAM 29 loading in P4

Yield = 56 %

DSC: Tg = 66.3 °C

GPC: Mw = 43,100; Mn = 17,200; Mw/Mn = 2.5

¹H NMR (400 MHz, CDCl₃) δ: 1.69 (s, 0.0110H, H₅), 6.44 (d, J = 2.4 Hz, 0.0031H, H₇), 6.55 (dd, J = 8.9, 2.5 Hz, 0.0031H, H₆), 4.68 (s, 4H, H₄), 7.50 (t, J = 7.8 Hz, 1H, H₂), 8.21 (dd, J = 7.8, 1.5 Hz, 2H, H₁), 8.69 (s, 1H, H₃), 13.28 (s, 0.0034H, H₈)

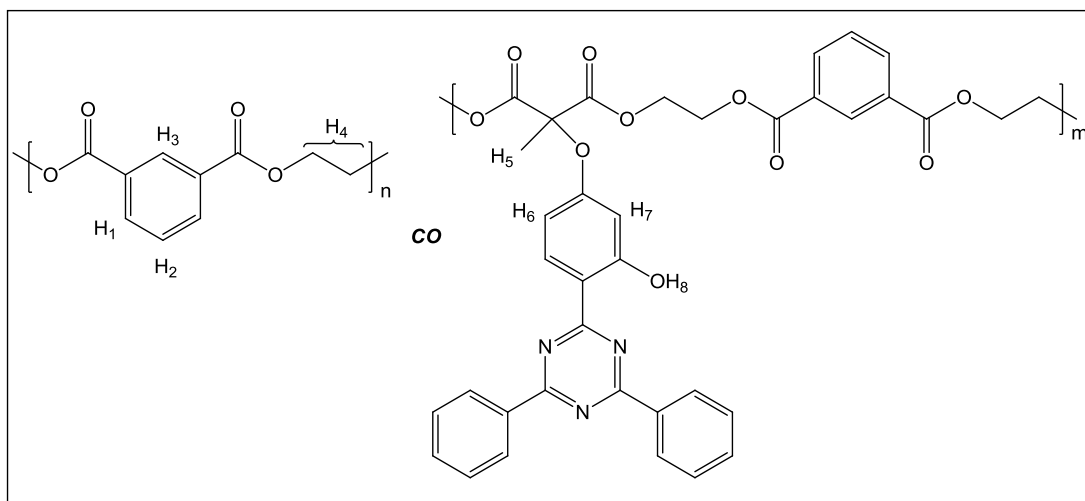


Fig. 4.4 – Structure of P4

Poly(EI-co-32) (P5)

Copolymer	UVAM 32	BHEI 4.1	UVAM 32 in the feed		UVAM 32 in copolymer	
	mass (g)	mass (g)	Wt %	Mol %	Wt %	Mol %
P5	0.40	39.60	1.00	0.62	0.91	0.42

Table 4.6 - Theoretical and actual UVAM 32 loading in P5

Yield = 76 %

DSC: T_g = 67.1 °C

GPC: M_w = 38,500; M_n = 14,400; M_w/M_n = 2.7

¹H NMR (400 MHz, CDCl₃) δ: 4.68 (s, 4H, H₄), 6.60 (d, J = 2.5 Hz, 0.0035H, H₆), 6.62-6.65 (m, 0.0037H, H₅), 7.50 (t, J = 7.8 Hz, 1H, H₂), 8.21 (dd, J = 7.8, 1.7 Hz, 2H, H₁), 8.69 (s, 1H, H₃), 13.46 (s, 0.0042H, H₇)

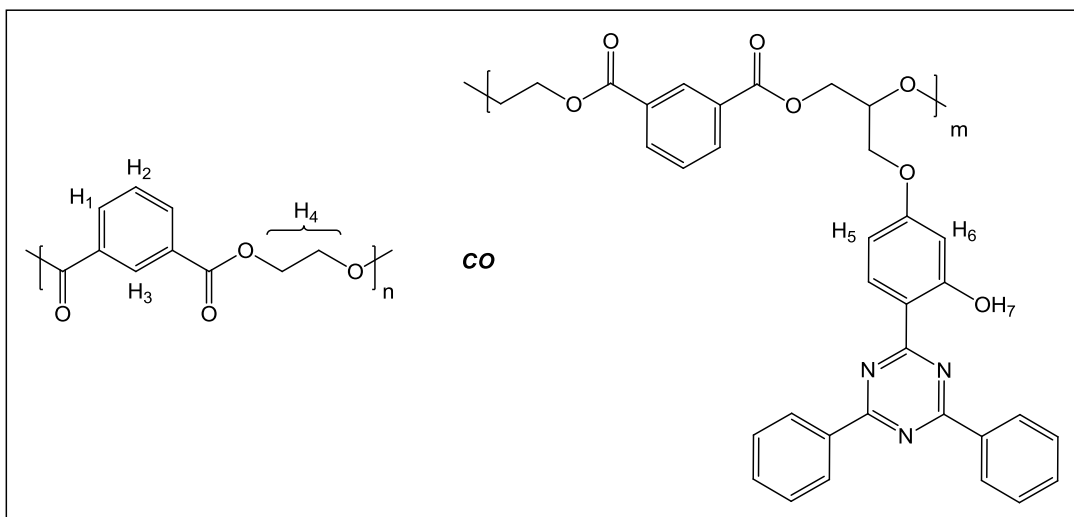


Fig. 4.5 – Structure of P5

Poly(EI-co-33) (P6)

Copolymer	UVAM 33	BHEI 4.1	UVAM 33 in the feed		UVAM 33 in copolymer	
	mass (g)	mass (g)	Wt %	Mol %	Wt %	Mol %
P6	0.40	40.10	1.00	0.60	0.80	0.36

Table 4.7 - Theoretical and actual UVAM 33 loading in P6

Yield = 66 %

DSC: T_g = 67.5 °C

GPC: M_w = 54,200; M_n = 16,000; M_w/M_n = 3.4

¹H NMR (400 MHz, CDCl₃) δ: 4.68 (s, 4H, H₄), 6.16 (s, 0.0078H, H₅), 7.50 (t, J = 7.8 Hz, 1H, H₂), 8.21 (dd, J = 7.8, 1.7 Hz, 2H, H₁), 8.69 (s, 1H, H₃), 13.67 (s, 0.0072H, H₆)

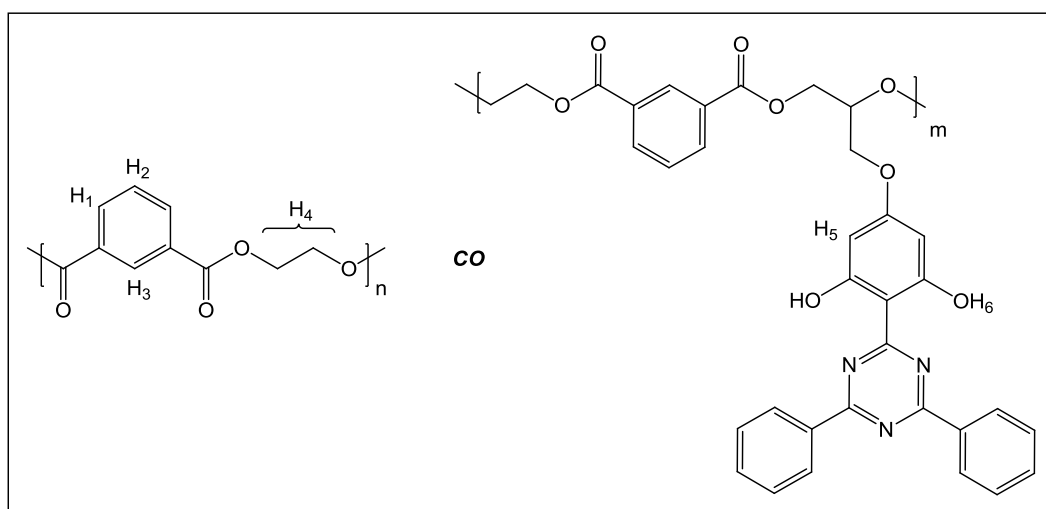


Fig. 4.6 – Structure of P6

Poly(EI-co-34) (P7)

Copolymer	UVAM 34 mass (g)	BHEI 4.1 mass (g)	UVAM 34 in the feed Wt %	UVAM 34 in the feed Mol %	UVAM 34 in copolymer Wt %	UVAM 34 in copolymer Mol %
P7	0.40	39.70	1.00	0.45	0.94	0.32

Table 4.8- Theoretical and actual UVAM 34 loading in P7

Yield = 89 %

DSC: Tg = 66.8 °C

GPC: Mw = 33,300; Mn = 12,200; Mw/Mn = 2.7

$^1\text{H NMR}$ (400 MHz, CDCl_3) δ : 4.68 (s, 4H, H₄), 6.61-6.67 (m, 0.0035H, H₅ and H₆), 7.50 (t, J = 7.8 Hz, 1H, H₂), 8.21 (dd, J = 7.8, 1.6 Hz, 2H, H₁), 8.69 (s, 1H, H₃), 13.54 (s, 0.0032H, H₇)

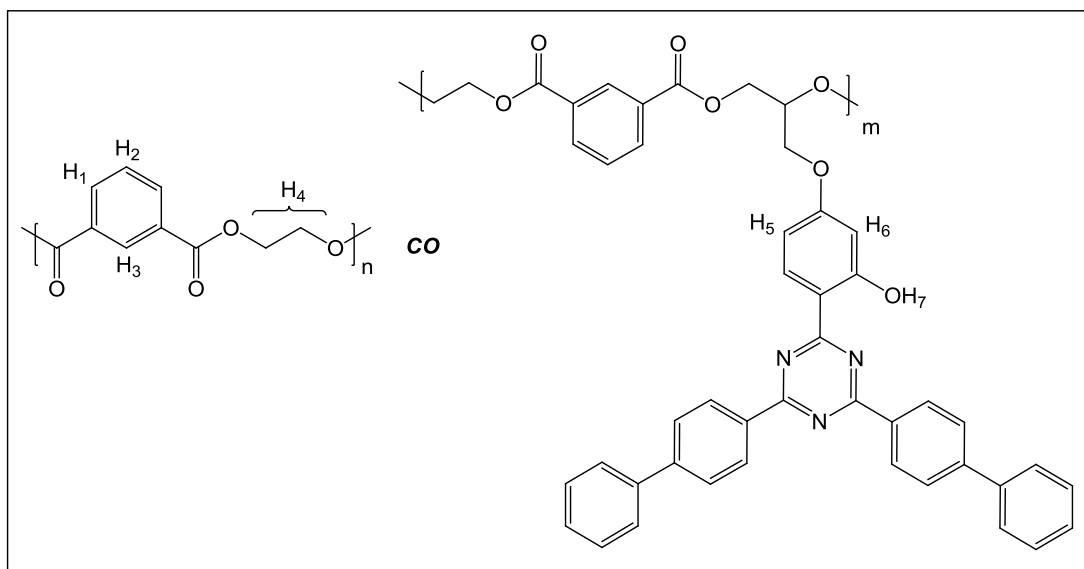


Fig. 4.7 – Structure of P7

Poly(EI-co-35) P8

Copolymer	UVAM 35	BHEI 4.1	UVAM 35 in the feed		UVAM 35 in copolymer	
	mass (g)	mass (g)	Wt %	Mol %	Wt %	Mol %
P8	0.40	39.60	1.00	0.57	1.31	0.56

Table 4.9 - Theoretical and actual UVAM 35 loading in P8

Yield = 56 %

DSC: T_g = 66.6 °C

GPC: M_w = 51,000; M_n = 11,800; M_w/M_n = 4.3

¹H NMR (400 MHz, CDCl₃) δ: 4.68 (s, 4H, H₄), 6.58 (d, J = 2.4 Hz, 0.0040H, H₆), 6.62-6.65 (m, 0.0039H, H₅) 7.50 (t, J = 7.8 Hz, 1H, H₂), 8.21 (dd, J = 7.8, 1.6 Hz, 2H, H₁), 8.69 (s, 1H, H₃), 13.33 (s, 0.0056H, H₇)

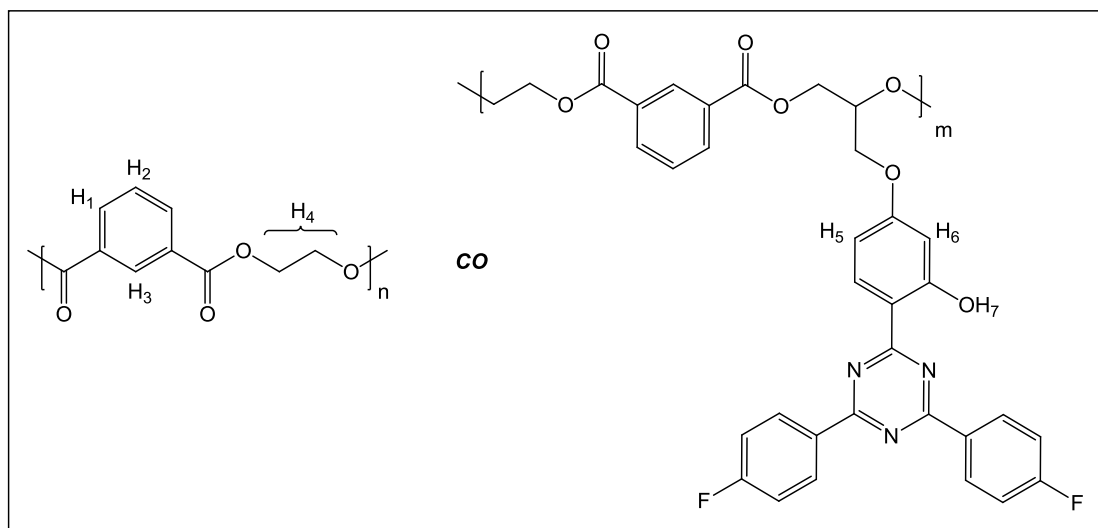


Fig. 4.8 – Structure of P8

Poly(EI-co-36) (P9)

Copolymer	UVAM 36	BHEI 4.1	UVAM 36 in the feed		UVAM 36 in copolymer	
	mass (g)	mass (g)	Wt %	Mol %	Wt %	Mol %
P9	0.40	39.70	1.00	0.54	0.89	0.36

Table 4.10 - Theoretical and actual UVAM 36 loading in P9

Yield = 63 %

DSC: T_g = 65.8 °C

GPC: M_w = 55,000; M_n = 14,200; M_w/M_n = 3.9

¹H NMR (400 MHz, CDCl₃) δ: 4.68 (s, 4H, H₄), 6.58 (d, J = 2.2 Hz, 0.0024H, H₆), 6.62 (dd, J = 9.0, 2.2 Hz, 0.0024H, H₅), 7.50 (t, J = 7.8 Hz, 1H, H₂), 8.21 (dd, J = 7.8, 1.7 Hz, 2H, H₁), 8.69 (s, 1H, H₃), 13.69 (s, 0.0036H, H₇)

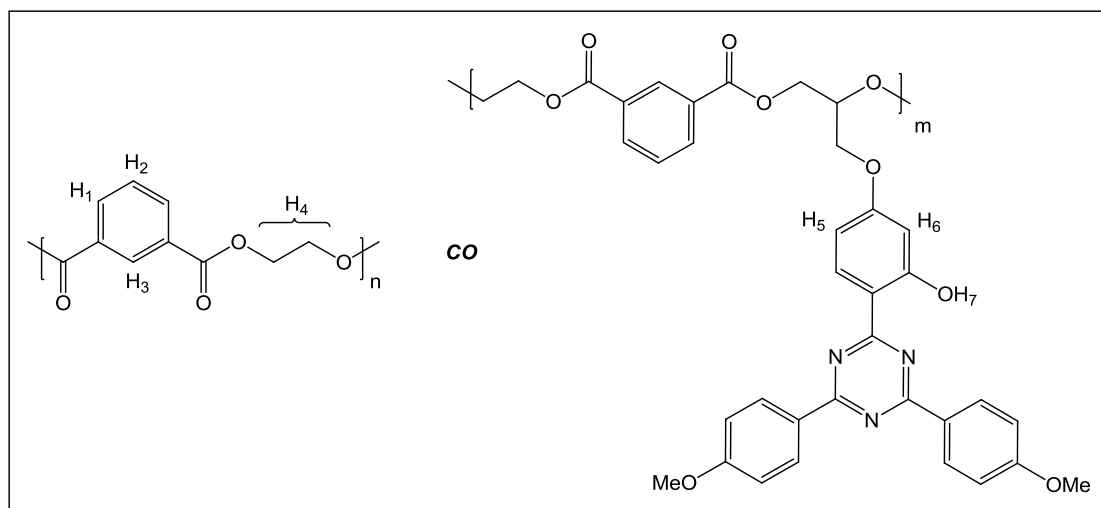


Fig. 4.9 – Structure of P9

Poly(EI-co-37[1 wt %]) (P10)

Copolymer	UVAM 37	BHEI 4.1	UVAM 37 in the feed		UVAM 37 in copolymer	
	mass (g)	mass (g)	Wt %	Mol %	Wt %	Mol %
P10	0.50	49.50	1.00	0.57	0.67	0.28

Table 4.11 - Theoretical and actual UVAM 37 loading in P10

Yield = 53 %

DSC: Tg = 68.3 °C

GPC: Mw = 107,000; Mn = 28,500; Mw/Mn = 3.8

¹H NMR (400 MHz, CDCl₃) δ: 4.68 (s, 4H, H₄), 6.56-6.58 (m 0.0058H, H₆) 6.63 (d, J = 8.0 Hz, 0.0060H, H₅), 7.50 (t, J = 7.8 Hz, 1H, H₂), 8.21 (dd, J = 7.8, 1.7 Hz, 2H, H₁), 8.69 (s, 1H, H₃), 13.38 (s, 0.0056H, H₇)

Poly(EI-co-37[2 wt %]) (P11)

Copolymer	UVAM 37	BHEI 4.1	UVAM 37 in the feed		UVAM 37 in copolymer	
	mass (g)	mass (g)	Wt %	Mol %	Wt %	Mol %
P11	1.00	49.00	2.00	1.12	1.68	0.70

Table 4.12 - Theoretical and actual UVAM 37 loading in P11

Yield = 46 %

DSC: Tg = 67.5 °C

GPC: Mw = 85,700; Mn = 24,400; Mw/Mn = 3.6

¹H NMR (400 MHz, CDCl₃) δ: 4.68 (s, 4H, H₄), 6.55-6.57 (m, 0.0143H, H₆) 6.63 (d, J = 8.2 Hz, 0.0138H, H₅), 7.50 (t, J = 7.8 Hz, 1H, H₂), 8.21 (dd, J = 7.8, 1.7 Hz, 2H, H₁), 8.69 (s, 1H, H₃), 13.38 (s, 0.0139H, H₇)

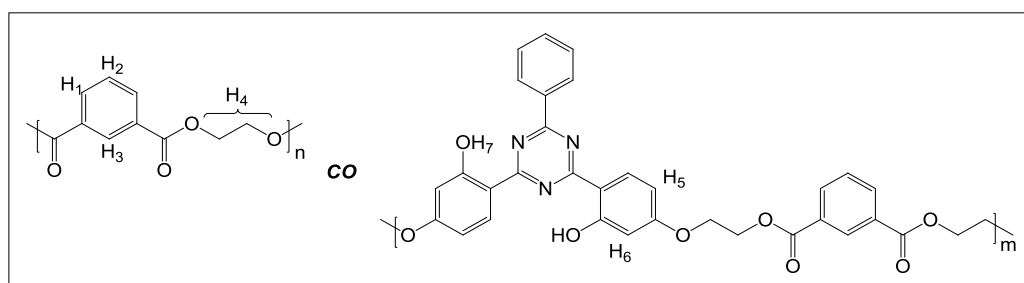


Fig. 4.10 – Structure of P10 and P11

Poly(EI-co-38) (P12)

Copolymer	UVAM 38	BHEI 4.1	UVAM 38 in the feed		UVAM 38 in copolymer	
	mass (g)	mass (g)	Wt %	Mol %	Wt %	Mol %
P12	0.93	95.00	0.97	0.38	0.51	0.15

Table 4.13 - Theoretical and actual UVAM 38 loading in P12

Yield = 71 %

DSC: Tg = 57.6 °C

GPC: Mw = 45,700; Mn = 15,900; Mw/Mn = 2.9

$^1\text{H NMR}$ (400 MHz, CDCl_3) δ : 4.69 (s, 4H, H₄), 6.52-6.60 (m, 0.0062H, H₅ and H₆) 7.51 (s, 1H, H₂), 8.21 (s, 2H, H₁), 8.70 (s, 1H, H₃), 13.43 (s, 0.0030H, H₇)

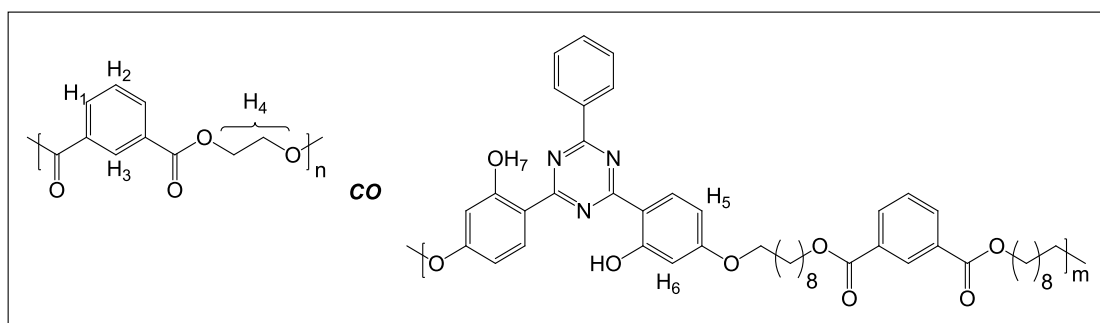


Fig. 4.11 – Structure of P12

Poly(EI-co-39) (P13)

<i>Copolymer</i>	<i>UVAM 39</i>	<i>BHEI 4.1</i>	<i>UVAM 39 in the feed</i>		<i>UVAM 39 in copolymer</i>	
	<i>mass (g)</i>	<i>mass (g)</i>	<i>Wt %</i>	<i>Mol %</i>	<i>Wt %</i>	<i>Mol %</i>
P13	0.40	39.60	1.00	0.52	0.51	0.20

Table 4.14 - Theoretical and actual UVAM 39 loading in P13

Yield = 66 %

DSC: T_g = 69.2 °C

GPC: M_w = 67,000; M_n = 18,100; M_w/M_n = 3.7

¹H NMR (400 MHz, CDCl₃) δ: 4.68 (s, 4H, H₄), 6.56 (d, J = 2.1 Hz, 0.0043H, H₆) 6.63 (d, J = 9.0 Hz, 0.0044H, H₅), 7.50 (t, J = 7.8 Hz, 1H, H₂), 8.21 (dd, J = 7.8, 1.7 Hz, 2H, H₁), 8.69 (s, 1H, H₃), 13.49 (s, 0.0039H, H₇)

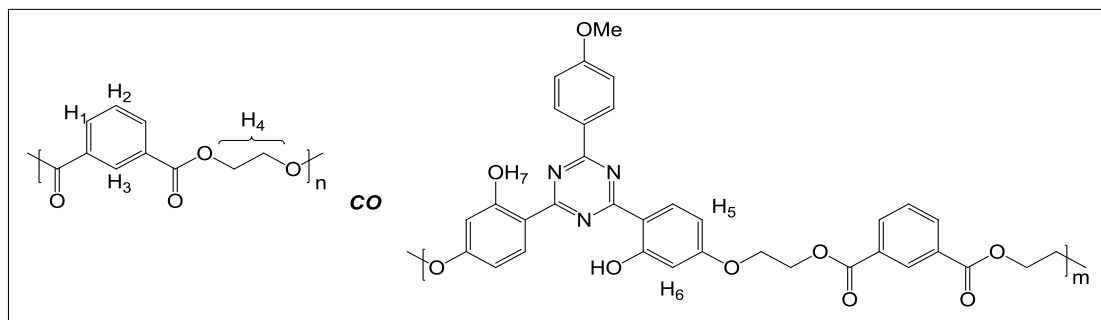


Fig. 4.12 – Structure of P13

Poly(EI-co-40) (P14)

Copolymer	UVAM 40	BHEI 4.1	UVAM 40 in the feed		UVAM 40 in copolymer	
	mass (g)	mass (g)	Wt %	Mol %	Wt %	Mol %
P14	0.70	69.30	1.00	0.65	0.73	0.34

Table 4.15 - Theoretical and actual UVAM 40 loading in P14

Yield = 86 %

DSC: Tg = 65.1 °C

GPC: Mw = 23,700; Mn = 7,900; Mw/Mn = 3.0

¹H NMR (500 MHz, CDCl₃) δ: 4.68 (s, 4H, H₄), 6.16 (s, 0.0060H, H₅), 7.50 (t, J = 7.8 Hz, 1H, H₂), 8.21 (d, J = 7.8 Hz, 2H, H₁), 8.69 (s, 1H, H₃), 13.63 (s, 0.0068H, H₆)

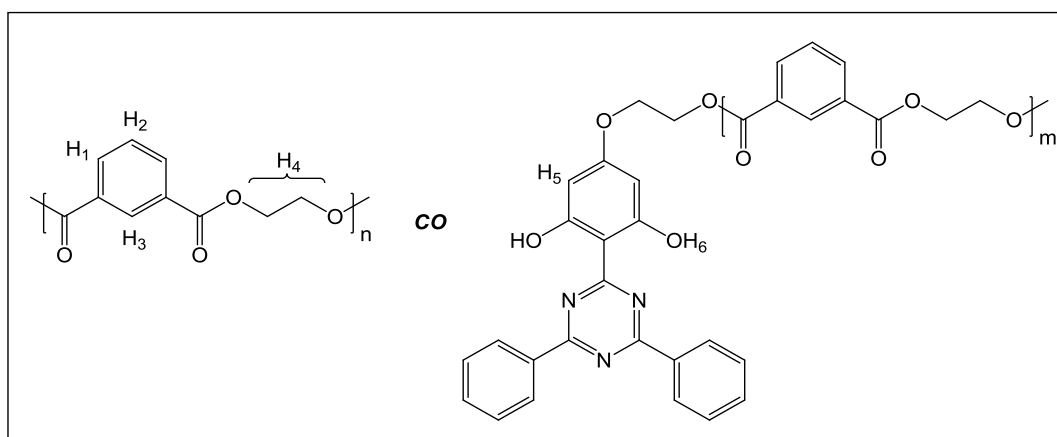


Fig. 4.13 – Structure of P14

Poly(EI-co-41) (P15)

<i>Copolymer</i>	<i>UVAM 41</i>	<i>BHEI 4.1</i>	<i>UVAM 41 in the feed</i>		<i>UVAM 41 in copolymer</i>	
	<i>mass (g)</i>	<i>mass (g)</i>	<i>Wt %</i>	<i>Mol %</i>	<i>Wt %</i>	<i>Mol %</i>
P15	0.40	39.50	1.00	0.61	0.88	0.40

Table 4.16 - Theoretical and actual UVAM 41 loading in P15

Yield = 66 %

DSC: T_g = 66.1 °C

GPC: M_w = 21,000; M_n = 7,800; M_w/M_n = 2.6

¹H NMR (400 MHz, CDCl₃) δ: 4.68 (s, 4H, H₄), 6.58 (s, 0.0033H, H₆), 6.62-6.65 (m, 0.0035H, H₅), 7.50 (t, J = 7.8 Hz, 1H, H₂), 8.21 (dd, J = 7.8, 1.7 Hz, 2H, H₁), 8.69 (s, 1H, H₃), 13.35 (s, 0.0040H, H₇)

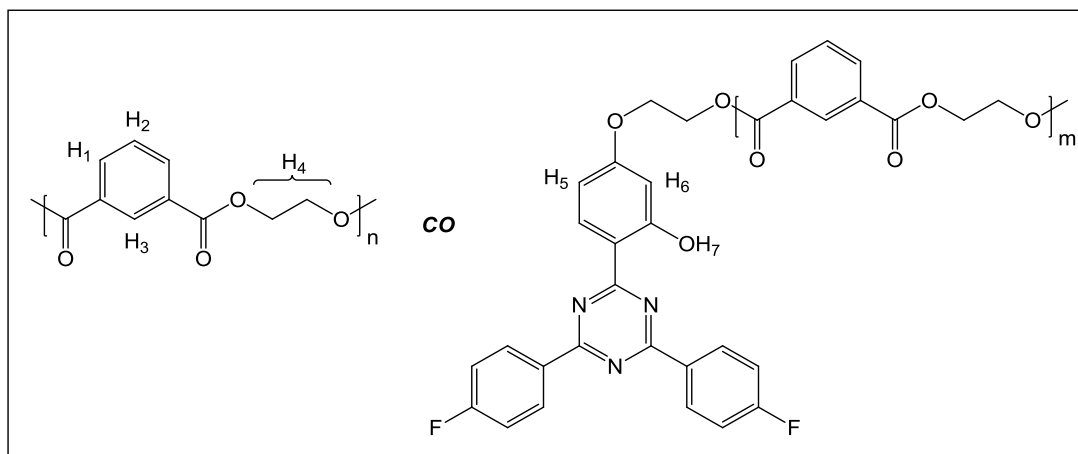


Fig. 4.14 – Structure of P15

Poly(EI-co-42) (P16)

Copolymer	UVAM 42	BHEI 4.1	UVAM 42 in the feed		UVAM 42 in copolymer	
	mass (g)	mass (g)	Wt %	Mol %	Wt %	Mol %
P16	0.40	39.50	1.00	0.56	0.97	0.41

Table 4.17 - Theoretical and actual UVAM 42 loading in P16

Yield = 83 %

DSC: Tg = 66.1 °C

GPC: Mw = 44,900; Mn = 12,900; Mw/Mn = 3.5

^1H NMR (400 MHz, CDCl_3) δ : 4.68 (s, 4H, H₄), 6.57 (d, J = 1.9 Hz, 0.0030H, H₆), 6.62 (dd, J = 7.1, 1.9 Hz, 0.0030H, H₅), 7.50 (t, J = 7.8 Hz, 1H, H₂), 8.21 (dd, J = 7.8, 1.7 Hz, 2H, H₁), 8.69 (s, 1H, H₃), 13.71 (s, 0.0041H, H₇)

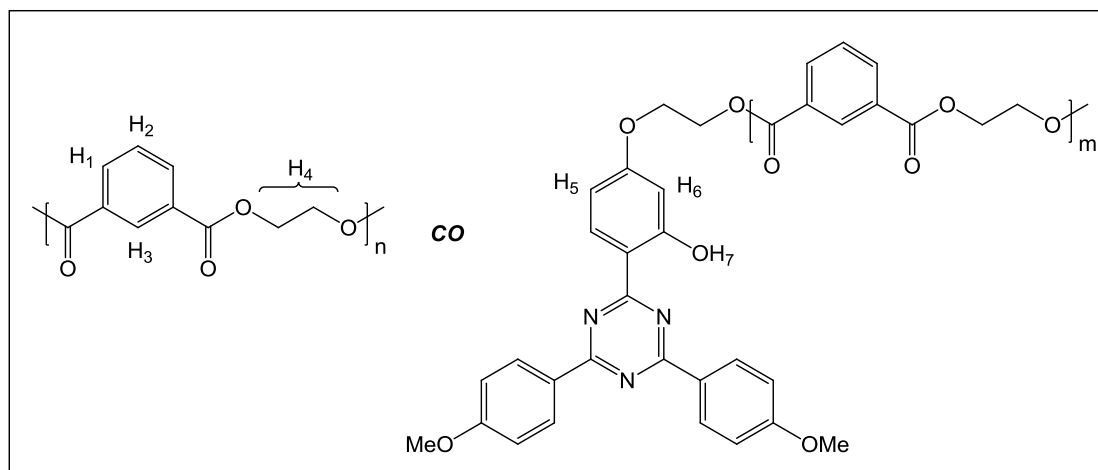


Fig. 4.15 – Structure of P16

Poly(EI-co-20) (P17)

Copolymer	UVAM 20 mass (g)	BHEI 4.1 mass (g)	UVAM 20 in the feed		UVAM 20 in copolymer	
			Wt %	Mol %	Wt %	Mol %
P17	0.35	35.00	1.00	0.61	0.20	0.10

Table 4.18 - Theoretical and actual UVAM 20 loading in P17

Yield = 60 %

DSC: Tg = 68.8 °C

GPC: Mw = 59,400; Mn = 16,800; Mw/Mn = 3.5

^1H NMR (400 MHz, CDCl_3) δ : 4.68 (s, 4H, H₄), 6.45-6.57 (m, 0.0020H, H₅ and H₆), 7.50 (t, J = 7.8 Hz, 1H, H₂), 8.21 (dd, J = 7.8, 1.7 Hz, 2H, H₁), 8.69 (s, 1H, H₃)

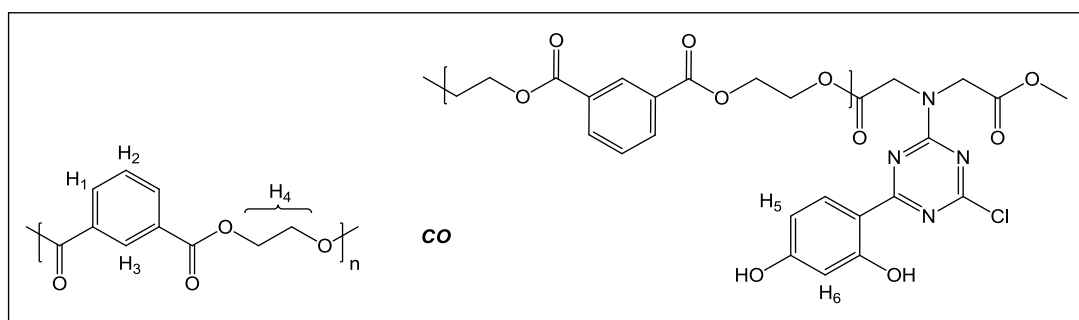


Fig. 4.16 – Structure of P17

Poly(EI-co-21) (P18)

Copolymer	UVAM 21	BHEI 4.1	UVAM 21 in the feed		UVAM 21 in copolymer	
	mass (g)	mass (g)	Wt %	Mol %	Wt %	Mol %
P18	0.30	29.60	1.00	0.45	0.26	0.09

Table 4.19 – Theoretical and actual UVAM 21 loading in P18

Yield = 45 %

DSC: Tg = 66.0 °C

GPC: Mw = 64,900; Mn = 18,500; Mw/Mn = 3.5

¹H NMR (400 MHz, CDCl₃) δ4.68 (s, 4H, H₄), 6.06-6.10 (m, 0.0035H, H₅ and H₆), 7.50 (t, J = 7.8 Hz, 1H, H₂), 8.21 (dd, J = 7.8, 1.7 Hz, 2H, H₁), 8.69 (s, 1H, H₃)

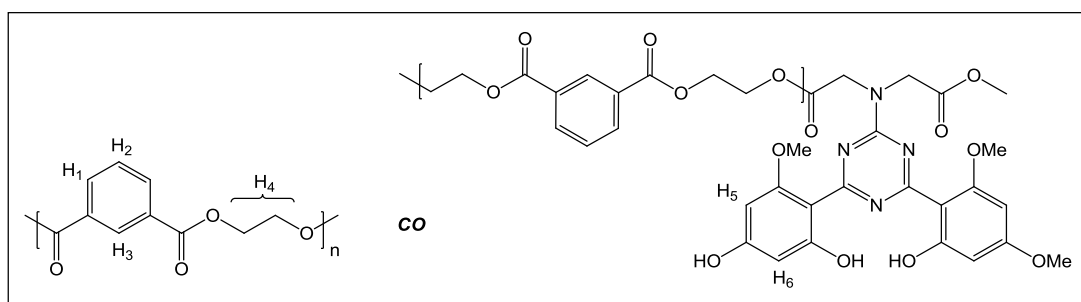


Fig. 4.17 – Structure of P18

4.1.3.2 Poly(EI-co-UVAM-co-UVAM) Copolymers

Poly(EI-co-32-co-37) (P19)

Copolymer	UVAM 32 mass (g)	BHEI 4.1 mass (g)	UVAM 32 in the feed Wt %	UVAM 32 in the feed Mol %	UVAM 32 in copolymer Wt %	UVAM 32 in copolymer Mol %
P19	0.35	69.0	0.50	0.30	0.47	0.22

Table 4.20 – Theoretical and actual UVAM 32 loading in P19

Copolymer	UVAM 37 mass (g)	BHEI 4.1 mass (g)	UVAM 37 in the feed Wt %	UVAM 37 in the feed Mol %	UVAM 37 in copolymer Wt %	UVAM 37 in copolymer Mol %
P19	0.35	69.0	0.50	0.28	0.24	0.10

Table 4.21 – Theoretical and actual UVAM 37 loading in P19

Yield = 90 %

DSC: T_g = 64.6 °C

GPC: M_w = 36,700; M_n = 13,700; M_w/M_n = 2.7

¹H NMR (400 MHz, CDCl₃) δ: 4.69 (s, 4H, H₄), 6.57-6.65 (m, 0.0081H, H₅, H₆, H₈ and H₉), 7.51 (t, J = 7.8 Hz, 1H, H₂), 8.22 (dd, J = 7.8, 1.7 Hz, 2H, H₁), 8.70 (s, 1H, H₃), 13.38 (s, 0.0019H, H₇), 13.46 (s, 0.0022H, H₁₀)

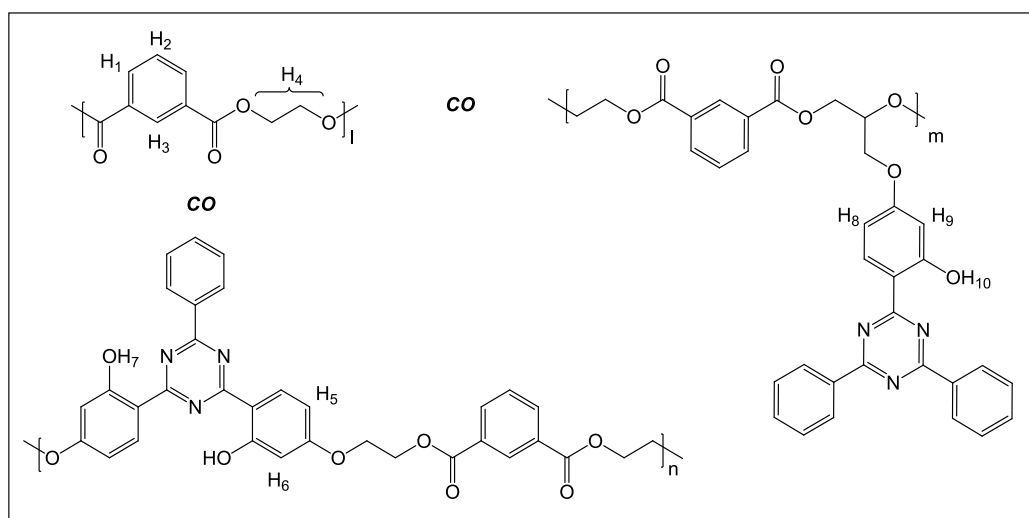


Fig. 4.18 – Structure of P19

Poly(EI-co-33-co-37) (P20)

Copolymer	UVAM 33 mass (g)	BHEI 4.1 mass (g)	UVAM 33 in the feed		UVAM 33 in copolymer	
			Wt %	Mol %	Wt %	Mol %
P20	0.25	48.50	0.50	0.30	0.45	0.20

Table 4.22 – Theoretical and actual UVAM 33 loading in P20

Copolymer	UVAM 37 mass (g)	BHEI 4.1 mass (g)	UVAM 37 in the feed		UVAM 37 in copolymer	
			Wt %	Mol %	Wt %	Mol %
P20	0.25	48.50	0.50	0.30	0.25	0.11

Table 4.23 – Theoretical and actual UVAM 37 loading in P20

Yield = 66 %

DSC: T_g = 66.8 °C

GPC: M_w = 35,700; M_n = 13,200; M_w/M_n = 2.7

¹H NMR (400 MHz, CDCl₃) δ: 4.68 (s, 4H, H₄), 6.17 (s, 0.0027H, H₈), 6.57 (d, J = 2.3 Hz, 0.0022H, H₆), 6.63 (dd, J = 9.1, 2.3 Hz, 0.0022H, H₅), 7.50 (t, J = 7.8 Hz, 1H, H₂), 8.21 (dd, J = 7.8, 1.7 Hz, 2H, H₁), 8.69 (s, 1H, H₃), 13.38 (s, 0.0022H, H₇), 13.63 (s, 0.0040H, H₉)

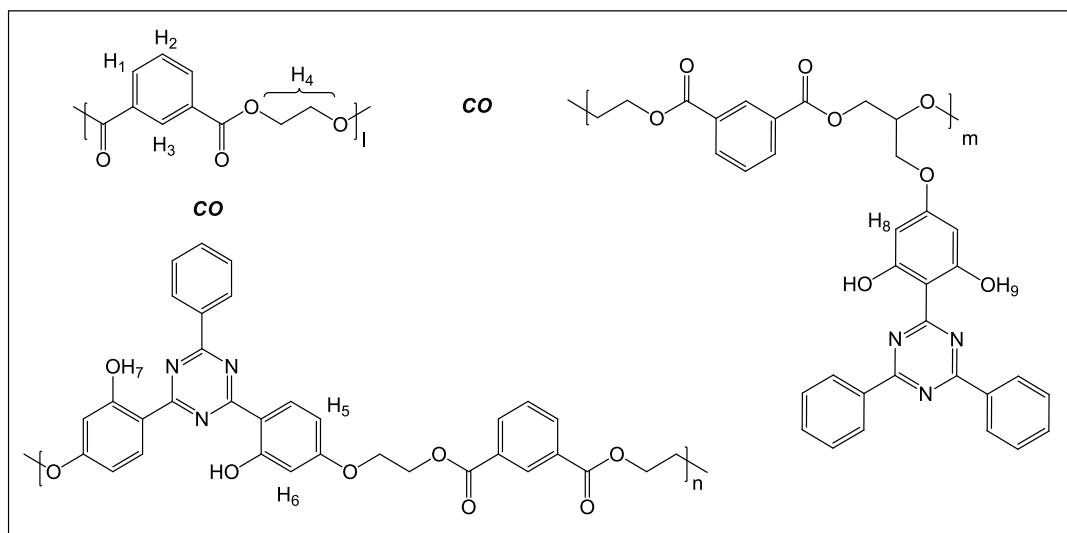


Fig. 4.19 – Structure of P20

Poly(EI-co-36-co-37) (P21)

Copolymer	UVAM 36	BHEI 4.1	UVAM 36 in the feed		UVAM 36 in copolymer	
	mass (g)	mass (g)	Wt %	Mol %	Wt %	Mol %
P21	0.20	39.50	0.50	0.27	0.42	0.17

Table 4.24 – Theoretical and actual UVAM 36 loading in P21

Copolymer	UVAM 37	BHEI 4.1	UVAM 37 in the feed		UVAM 37 in copolymer	
	mass (g)	mass (g)	Wt %	Mol %	Wt %	Mol %
P21	0.20	39.50	0.50	0.28	0.24	0.10

Table 4.25 – Theoretical and actual UVAM 37 loading in P21

Yield = 56 %

DSC: Tg = 68.5 °C

GPC: Mw = 42,000; Mn = 13,500; Mw/Mn = 3.1

¹H NMR (400 MHz, CDCl₃) δ: 4.68 (s, 4H, H₄), 6.57-6.64 (m, 0.0101H, H₅, H₆, H₈ and H₉)
7.50 (t, J = 7.8 Hz, 1H, H₂), 8.22 (dd, J = 7.8, 1.7 Hz, 2H, H₁), 8.69 (s, 1H, H₃), 13.40 (s, 0.0020H, H₇), 13.69 (s, 0.0017H, H₁₀)

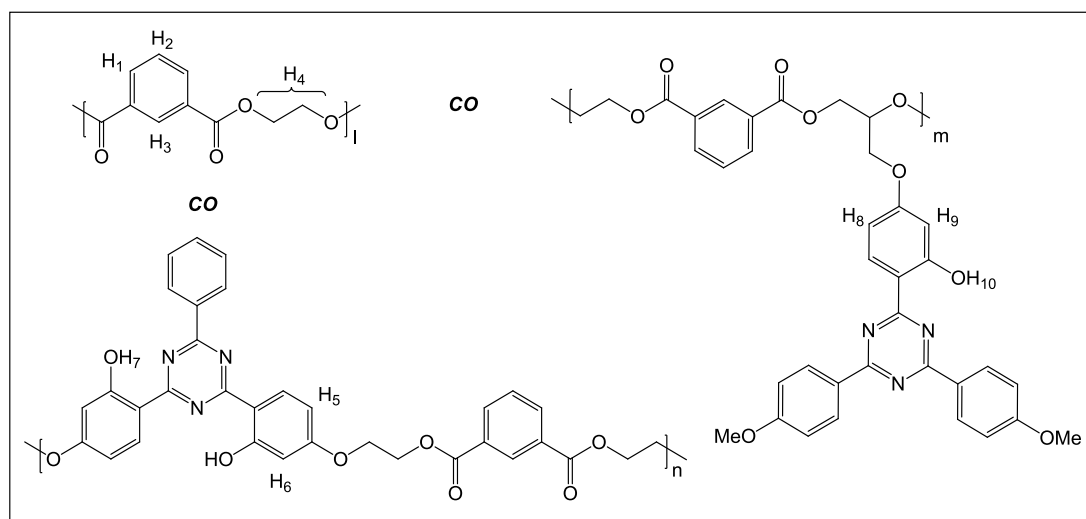


Fig. 4.20 – Structure of P21

Poly(EI-co-32-co-36) (P22)

Copolymer	UVAM 32 mass (g)	BHEI 4.1 mass (g)	UVAM 32 in the feed		UVAM 32 in copolymer	
			Wt %	Mol %	Wt %	Mol %
P22	0.20	39.50	0.50	0.30	0.50	0.23

Table 4.26 – Theoretical and actual UVAM 32 loading in P22

Copolymer	UVAM 36 mass (g)	BHEI 4.1 mass (g)	UVAM 36 in the feed		UVAM 36 in copolymer	
			Wt %	Mol %	Wt %	Mol %
P22	0.20	39.50	0.50	0.27	0.30	0.12

Table 4.27 – Theoretical and actual UVAM 36 loading in P22

Yield = 70 %

DSC: Tg = 68.4 °C

GPC: Mw = 52,000; Mn = 17,800; Mw/Mn = 2.9

¹H NMR (400 MHz, CDCl₃) δ: 4.68 (s, 4H, H₄), 6.59-6.65 (m, 0.0064H, H₅, H₆, H₈ and H₉), 7.50 (t, J = 7.8 Hz, 1H, H₂), 8.21 (dd, J = 7.8, 1.7 Hz, 2H, H₁), 8.69 (s, 1H, H₃), 13.48 (s, 0.0023H, H₇), 13.70 (s, 0.0012H, H₁₀)

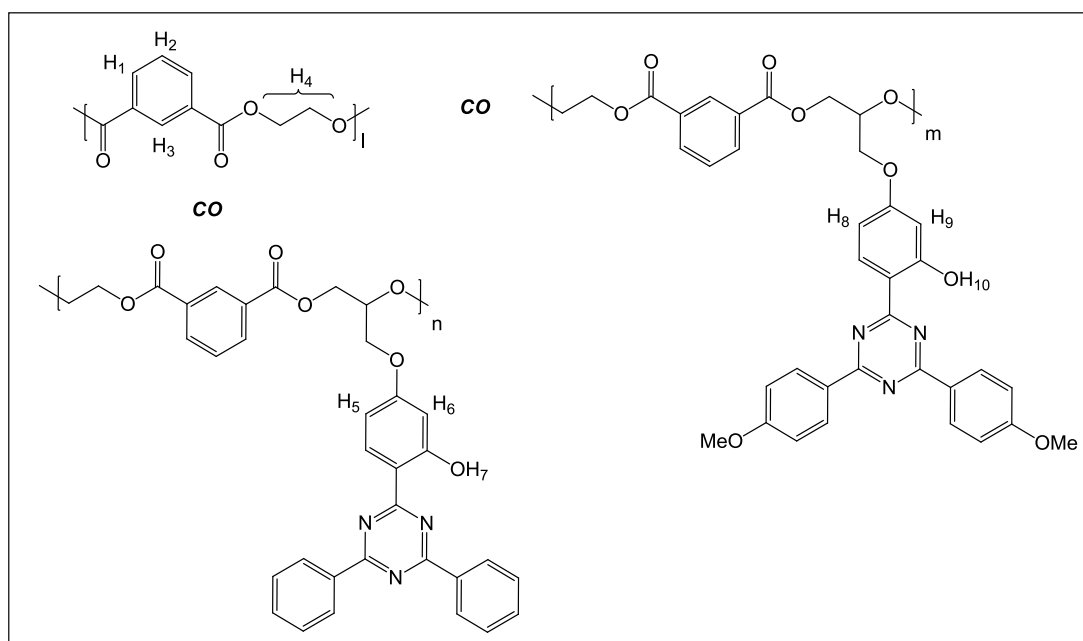


Fig. 4.21 – Structure of P22

Poly(EI-co-36-co-39) (P23)

Copolymer	UVAM 36	BHEI 4.1	UVAM 36 in the feed		UVAM 36 in copolymer	
	mass (g)	mass (g)	Wt %	Mol %	Wt %	Mol %
P23	0.20	39.60	0.50	0.26	0.44	0.18

Table 4.28 – Theoretical and actual UVAM 36 loading in P23

Copolymer	UVAM 39	BHEI 4.1	UVAM 39 in the feed		UVAM 39 in copolymer	
	mass (g)	mass (g)	Wt %	Mol %	Wt %	Mol %
P23	0.20	39.60	0.50	0.27	0.24	0.10

Table 4.29 – Theoretical and actual UVAM 39 loading in P23

Yield = 56 %

DSC: Tg = 65.6 °C

GPC: Mw = 62,600; Mn = 17,100; Mw/Mn = 3.7

¹H NMR (400 MHz, CDCl₃) δ: 4.68 (s, 4H, H₄), 6.55-6.63 (m, 0.0065H, H₅, H₆, H₈ and H₉)
7.50 (t, J = 7.8 Hz, 1H, H₂), 8.22 (dd, J = 7.8, 1.7 Hz, 2H, H₁), 8.69 (s, 1H, H₃), 13.48 (s, 0.0019H, H₇), 13.69 (s, 0.0018H, H₁₀)

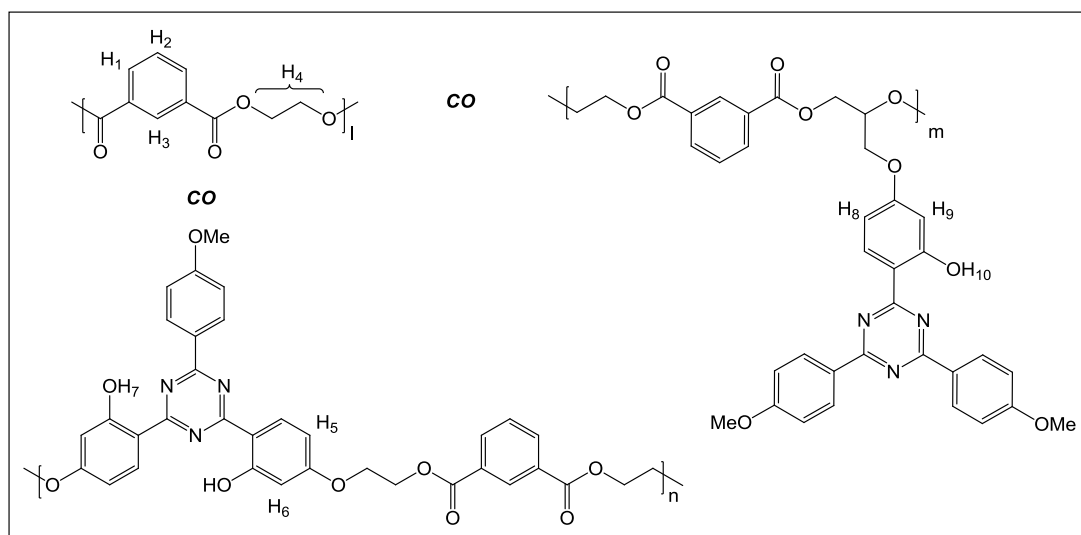


Fig. 4.22 – Structure of P23

Poly(EI-co-35-co-36) (P24)

Copolymer	UVAM 35	BHEI 4.1	UVAM 35 in the feed		UVAM 35 in copolymer	
	mass (g)	mass (g)	Wt %	Mol %	Wt %	Mol %
P24	0.20	39.80	0.50	0.28	0.40	0.17

Table 4.30 – Theoretical and actual UVAM 35 loading in P24

Copolymer	UVAM 36	BHEI 4.1	UVAM 36 in the feed		UVAM 36 in copolymer	
	mass (g)	mass (g)	Wt %	Mol %	Wt %	Mol %
P24	0.20	39.80	0.50	0.27	0.25	0.10

Table 4.31 – Theoretical and actual UVAM 36 loading in P24

Yield = 73 %

DSC: Tg = 66.4 °C

GPC: Mw = 46,600; Mn = 15,100; Mw/Mn = 3.0

¹H NMR (400 MHz, CDCl₃) δ: 4.68 (s, 4H, H₄), 6.59-6.65 (m, 0.0038H, H₅, H₆, H₈ and H₉)
7.50 (t, J = 7.8 Hz, 1H, H₂), 8.22 (dd, J = 7.8, 1.7 Hz, 2H, H₁), 8.69 (s, 1H, H₃), 13.33 (s, 0.0017H, H₇), 13.69 (s, 0.0010H, H₁₀)

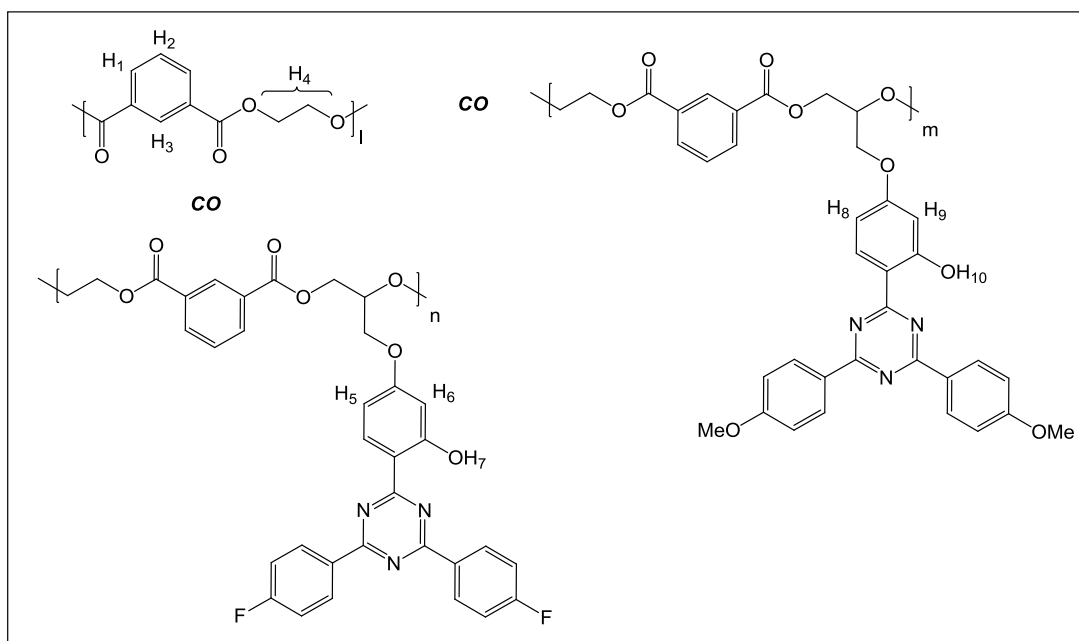


Fig. 4.23 – Structure of P24

Poly(EI-co-37-co-40) (P25)

Copolymer	UVAM 37	BHEI 4.1	UVAM 37 in the feed		UVAM 37 in copolymer	
	mass (g)	mass (g)	Wt %	Mol %	Wt %	Mol %
P25	0.30	56.50	0.50	0.28	0.24	0.10

Table 4.32 – Theoretical and actual UVAM 37 loading in P25

Copolymer	UVAM 40	BHEI 4.1	UVAM 40 in the feed		UVAM 40 in copolymer	
	mass (g)	mass (g)	Wt %	Mol %	Wt %	Mol %
P25	0.30	56.50	0.50	0.33	0.33	0.16

Table 4.33 – Theoretical and actual UVAM 40 loading in P25

Yield = 68 %

DSC: Tg = 65.8 °C

GPC: Mw = 39,700; Mn = 12,000; Mw/Mn = 3.3

¹H NMR (400 MHz, CDCl₃) δ: 4.68 (s, 4H, H₄), 6.16 (s, 0.0024H, H₈), 6.57-6.64 (m, 0.0024H, H₅ and H₆), 7.50 (t, J = 7.8 Hz, 1H, H₂), 8.21 (dd, J = 7.8, 1.7 Hz, 2H, H₁), 8.69 (s, 1H, H₃), 13.37 (s, 0.0020H, H₇), 13.63 (s, 0.0032H, H₉)

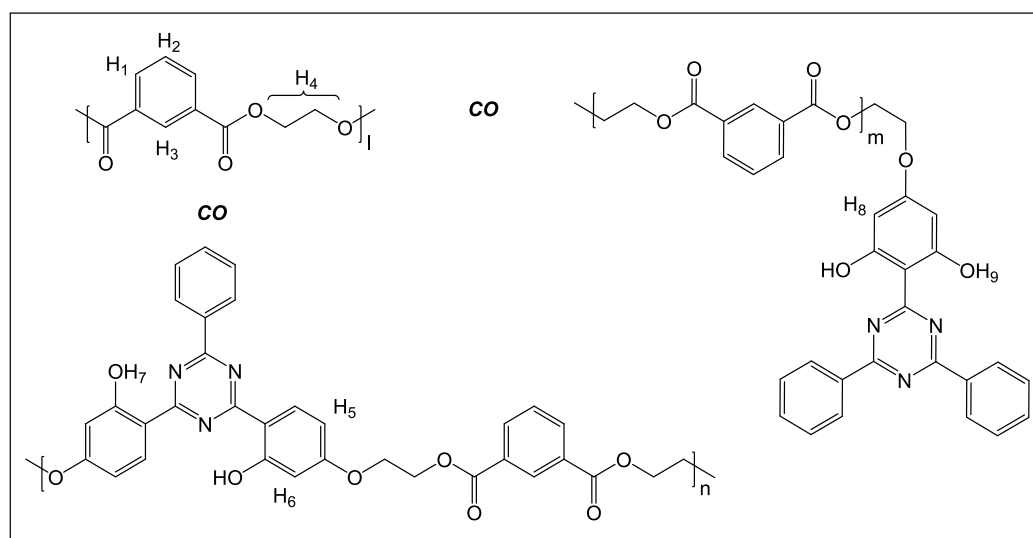


Fig. 4.24 – Structure of P25

Poly(EI-co-37-co-42) (P26)

Copolymer	UVAM 37	BHEI 4.1	UVAM 37 in the feed		UVAM 37 in copolymer	
	mass (g)	mass (g)	Wt %	Mol %	Wt %	Mol %
P26	0.20	39.60	0.50	0.27	0.19	0.08

Table 4.34 – Theoretical and actual UVAM 37 loading in P26

Copolymer	UVAM 42	BHEI 4.1	UVAM 42 in the feed		UVAM 42 in copolymer	
	mass (g)	mass (g)	Wt %	Mol %	Wt %	Mol %
P26	0.30	39.60	0.50	0.28	0.57	0.25

Table 4.35 – Theoretical and actual UVAM 42 loading in P26

Yield = 86 %

DSC: Tg = 68.1 °C

GPC: Mw = 36,200; Mn = 11,200; Mw/Mn = 3.2

¹H NMR (400 MHz, CDCl₃) δ: 4.68 (s, 4H, H₄), 6.57-6.64 (m, 0.0057H, H₅, H₆, H₈ and H₉)
7.50 (t, J = 7.8 Hz, 1H, H₂), 8.22 (dd, J = 7.8, 1.7 Hz, 2H, H₁), 8.69 (s, 1H, H₃), 13.40 (s, 0.0017H, H₇), 13.69 (s, 0.0025H, H₁₀)

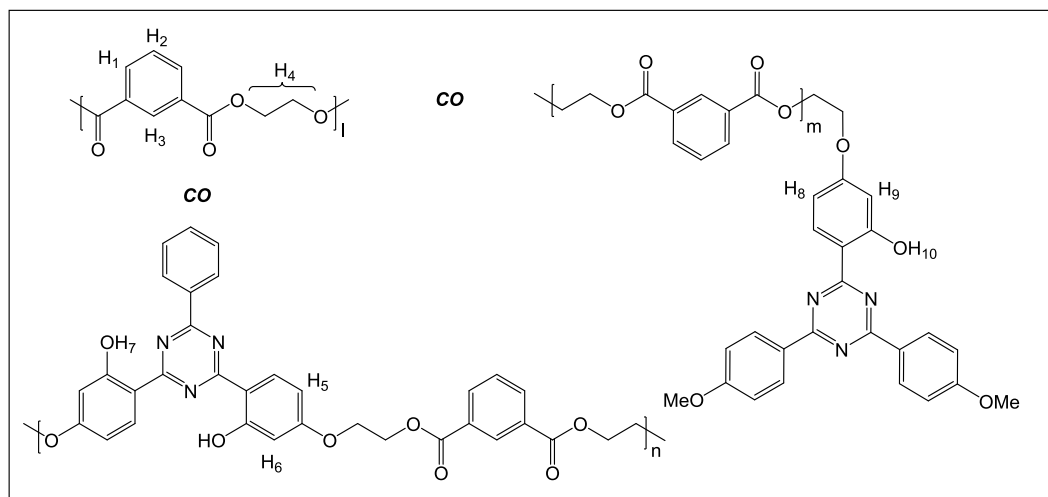


Fig. 4.25 – Structure of P26

4.2 Results and Discussion

The polymers in this study were synthesised in a PC rig at DuPont Teijin Films (Appendix, Figure 7.1). BHEI **4.1** was selected in preference to *bis*(2-hydroxyethyl)terephthalate) (BHET, **1.4**) since PEI is readily soluble in organic solvents and this facilitates both polymer purification and analysis by solution state NMR and UV spectroscopy. A significant increase in viscosity was not observed during the synthesis of the fully amorphous PEI, unlike poly(ethylene terephthalate) (PET) synthesis whereby the stirrer revolution rate drops by 30-40 rpm due to the crystallisation of the PET chains. Therefore PEI was cast after stirring at temperatures between 285-290 °C *in vacuo* (<10 mbar) for 30 minutes.

The presence of UVAMs in the PEI copolymers were observed in the ¹H NMR and UV spectra of the purified copolymers which was clear evidence of successful copolymerisation. With any unreacted monomer having been removed through purification of the copolymers by precipitation, the actual mol % of UVAMs in the purified copolymers was obtained by integrating the phenolic protons on the UVAM with respect to the aromatic protons on the polymer backbone. The filtrates produced during purification by precipitation were analysed by MALDI which detected no traces of unreacted UVAMs.

In certain cases a change in chemical shift was observed in the ¹H NMR spectrum of the copolymer with respect to the spectrum of the monomeric UVAMs. From comparing the ¹H NMR spectrum of **P1** with that of UVAM **5**, the signal assigned to the methyl group (H₅) was shifted slightly downfield by 0.2 ppm (Figure 4.26). The presence of crude UVAM **27** was responsible for lots of signals within the 1-2 ppm region of the ¹H NMR spectrum of **P2** and it is for this reason that the methyl protons could not be accurately assigned.

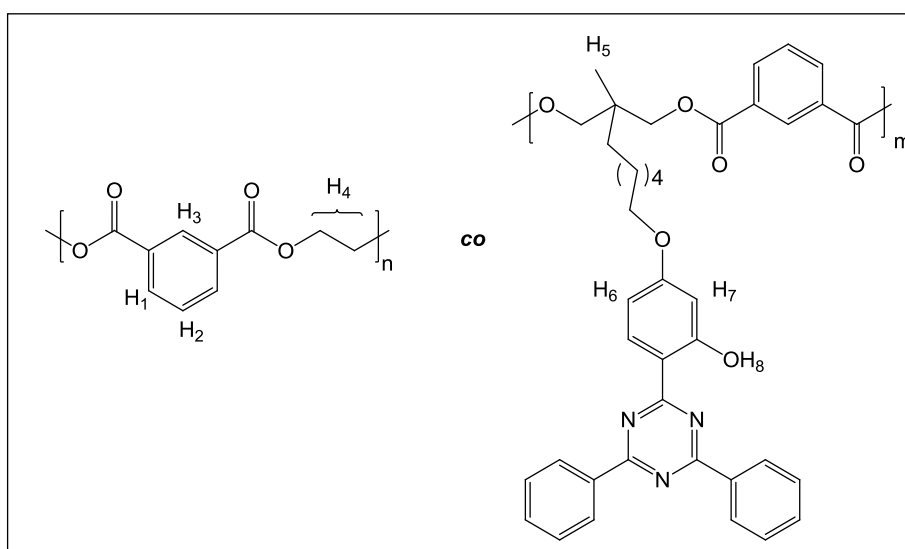
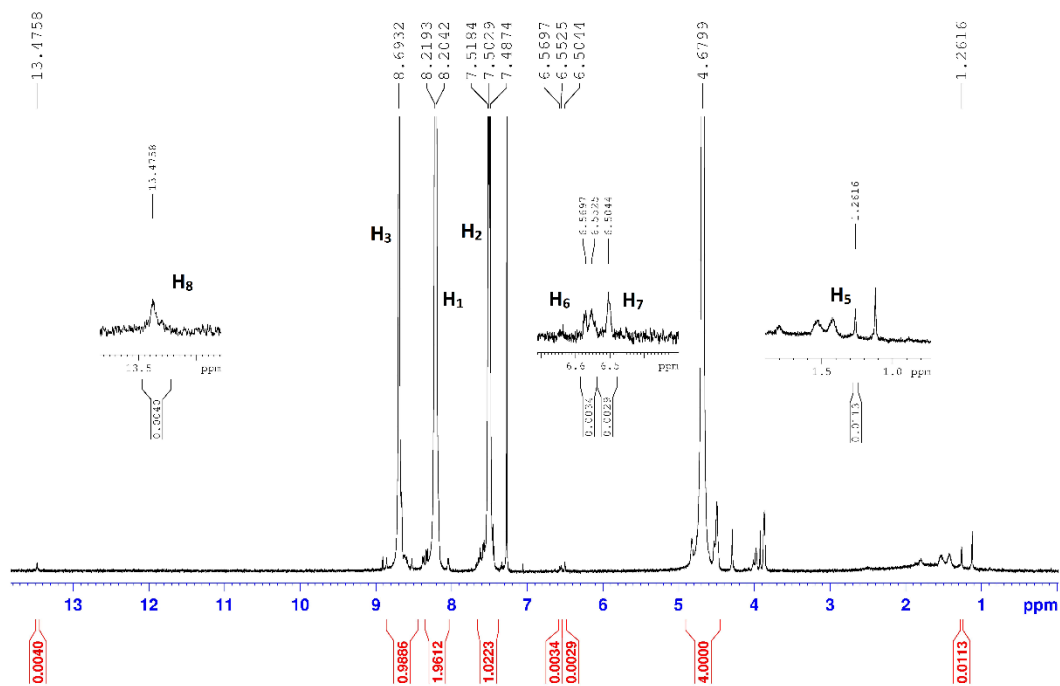


Fig. 4.26 – ^1H NMR spectrum (upper) and chemical structure (lower) of P1

There were a number of circumstances whereby the signals which undergo a change in chemical shift were masked under the polymeric signals. Nonetheless, for the copolymerisations involving UVAMs with polymerisable alcohol moieties on short aliphatic chains (**P5-P11**, **P13-P16** and **P19-P26**) a change in chemical shift was observed for the phenolic resorcinyl protons.

The mono- and di-aryl triazine UVAMs possess weak IMHBs and were unstable at polymerisation temperatures. The ^1H NMR spectra of the crude and purified samples of **P17** and **P18** contained no signals for the phenolic protons of UVAMs **20** and **21**, respectively. This was suspected to be caused by the disruption of the IMHB within the polymer matrix. Shizuka and Kramer have reported that the strength of the IMHB increases with the number of aryl rings connected to the triazine core.^{52,59} The actual mol % values for **20** and **21** were calculated by integrating the aromatic protons of the UVAMs in the ^1H NMR spectra of **P17** and **P18**, respectively. The very low levels of incorporation suggested a large loss of UVAM from thermal degradation.

Copolymers **P19-P26** were synthesised to investigate a 'cocktail' strategy. The aim was to copolymerise two different UVAMs into the same polymer chain to achieve a broader UV coverage within the 290-400 nm region. There is evidence in the literature which has reported the 'synergistic effect' of employing UV absorbers and hindered amine light stabilisers (HALS) simultaneously.^{66,82,140} Dobashi¹⁴¹ examined the interaction of two 2-hydroxybenzophenone (BP) UV absorbers, claiming that a synergism was possible when two UVA possessed maximum absorption in the range of UV-A (320-400 nm) and UV-B (290-320 nm). In an instance when the short wavelength absorber fails to deactivate *via* a radiationless pathway and fluoresces, the emission can be absorbed by the long wavelength absorber. With this in mind, the aim of this study was to achieve a similar synergistic effect using two different UVAMs.

Kramer and co-workers^{64,79} showed that polymerised 2-(2-hydroxyphenyl)-1,3,5-triazine (TA) derivatives emitted more phosphorescence and fluorescence than admixed TA additives due to the more packed arrangement of the polymerised TA increasing the activation energy of the radiationless deactivation. This emitted light can further degrade the polymer if the wavelengths falls within the ultraviolet spectrum. Simply having long wavelength UVAMs such as **37** or **39** absorbing any harmful fluorescent light emitted from the short wavelength UVAMs such as **32** or **36**

can provide a synergistic system. The cocktail strategy is a way in which this problem can be overcome, and could be a novel route to securing intellectual property.

4.2.1 UV analysis of PEI Copolymers

The UV spectra of the purified copolymers were acquired at a concentration of 10 mg/mL. The comparison of the purified copolymer UV spectra to that of the PEI control showed the presence of successfully polymerised UVAMs. Most of the copolymers were of a light brown or light yellow colour which alluded to some degradation of the UVAMs and/or the protrusion of absorbance into the visible region. UV spectra of the purified copolymers confirmed that this was in most cases due to absorbance in the visible region.

UVAMs with the same chromophore as Tinuvin 1577 **1.10** were copolymerised with BHEI **4.1** to give **P1-P5**, and the copolymers exhibited similar UV profiles with λ_{\max} in the region of 340-343 nm (Figure 4.27). The UV spectra of **P1-P5** showed no protrusion into the visible region, however absorbance levels between 370-400 nm were very weak. Work carried out by Sankey and Raine at DuPont Teijin Films (DTF) demonstrated that UV light above 340 nm was responsible for the formation of fluorescent material at depths of at least 450 μm in stacked PET systems and at 250 μm in thick films.⁴⁶ Therefore, UVAMs **25**, **27-29** and **32** (Figure 4.28) would be less effective in preventing the formation of fluorescent products from photodegradation at long wavelengths. **P2** was synthesised using the highest UVAM loading in the feed and the UV spectrum displayed the highest molar extinction coefficient coupled with a slight red shift in comparison to the other copolymers shown in Figure 4.27.

Out of the polymers which had 1 wt % of UVAM in the feed (**P1**, **P4** and **P5**), the highest molar absorptivity was exhibited by **P5**. **P5** displayed a considerably higher molar absorptivity in comparison to **P1**, despite containing similar levels of incorporated UVAM. **P4** also exhibited a higher molar extinction coefficient than **P1**, regardless of the former containing less incorporated UVAM.

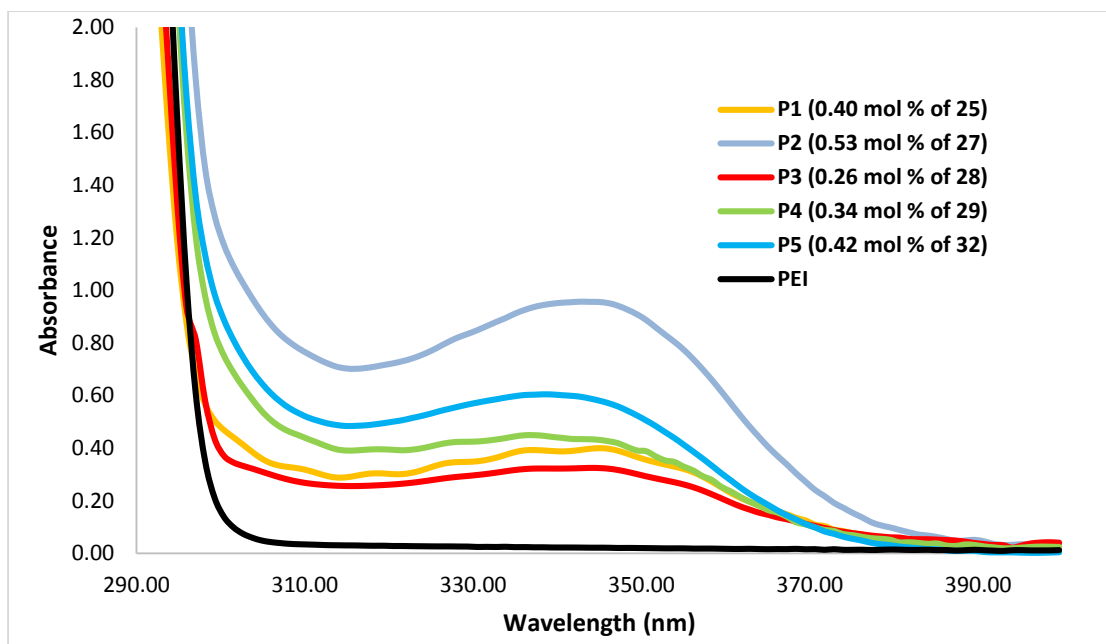


Fig. 4.27 – UV Spectra of P1, P2, P3, P4, P5 and PEI in CHCl_3 (10 mg/mL)

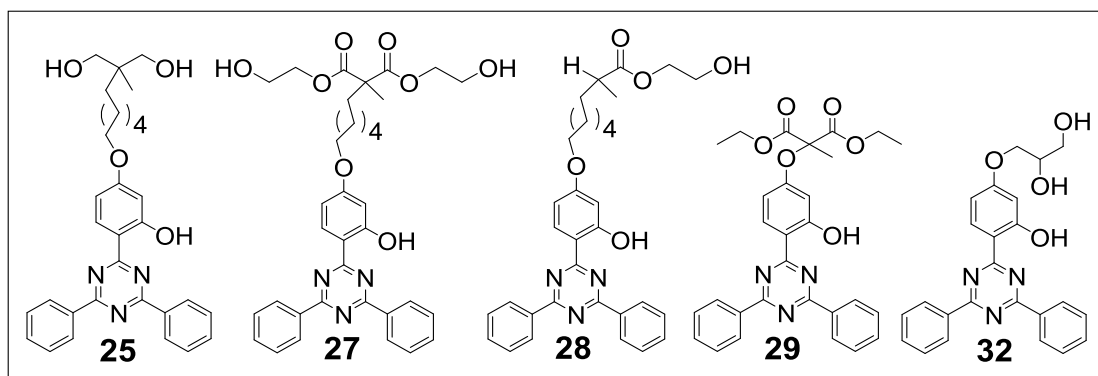


Fig. 4.28 – Chemical structures of UVAMs 25, 27, 28, 29 and 32

UVAMs **33**, **34** and **36** (Figure 4.30) had chromophores different to that of Tinuvin 1577 **1.10**, and the copolymers **P6**, **P7** and **P9** displayed superior molar absorptivity at wavelengths 290-400 nm in comparison to **P1-P5** (Figure 4.29). Despite the fluorinated aryl rings, **35** mimicked the UV profile of Tinuvin 1577 **1.10**, and for that reason the copolymer **P8** had an identical UV profile to that of **P1-P5**. The copolymer with the highest molar absorptivity was **P9**, which contained 0.36 mol % of polymerised UVAM **36**, surprisingly outperforming **P7** which contained 0.30 mol % of the more powerful UVAM **34**. Wavelengths between 310-315 nm are critical for polymer degradation, leading to the production of COOH end groups in the bulk,

front and rear surface of polymer films.^{29,42,43} Therefore UVAMs **34** and **36** possess great potential for combating UV degradation, specifically chain scissions and formation of acid end groups. No significant red- or blue-shifts were observed when comparing the λ_{max} of **P6-P9** to that of the free monomers; however, they did display slight protrusion into the visible region which explained the light yellow/brown colour of the polymers. UVAM **33** contained two IMHBs and the UV spectrum of **P6** showed an increased absorbance at wavelengths above 365 nm in comparison to **P7**, **P8** and **P9**. This shows that **33** is more adept at protecting the polymer from the formation of fluorescent mono-/di-hydroxyterephthalate by-products caused by deeply penetrating low energy UV light.

The ¹H NMR spectra of **P17** and **P18** showed low levels of UVAMs **20** and **21** incorporated into the polymer. The main reason for this was that these two UVAMs are unstable at polymerisation temperatures. Phenolic signals were absent in the ¹H NMR spectra of crude and purified **P17** and **P18**, which suggested that the phenolic moieties of **20** and **21** were taking part in the polymerisation. It is evident that tri-aryl triazines possess stronger IMHBs and are more thermally robust in comparison to **20** and **21**. These mono-aryl and di-aryl triazine UVAMs may be suitable for polymerisations with less harsh processing conditions, however it is convincingly clear that UVAMs **20** and **21** do not possess the key attributes required for effective use as UVAMs in PEI or PET processing.

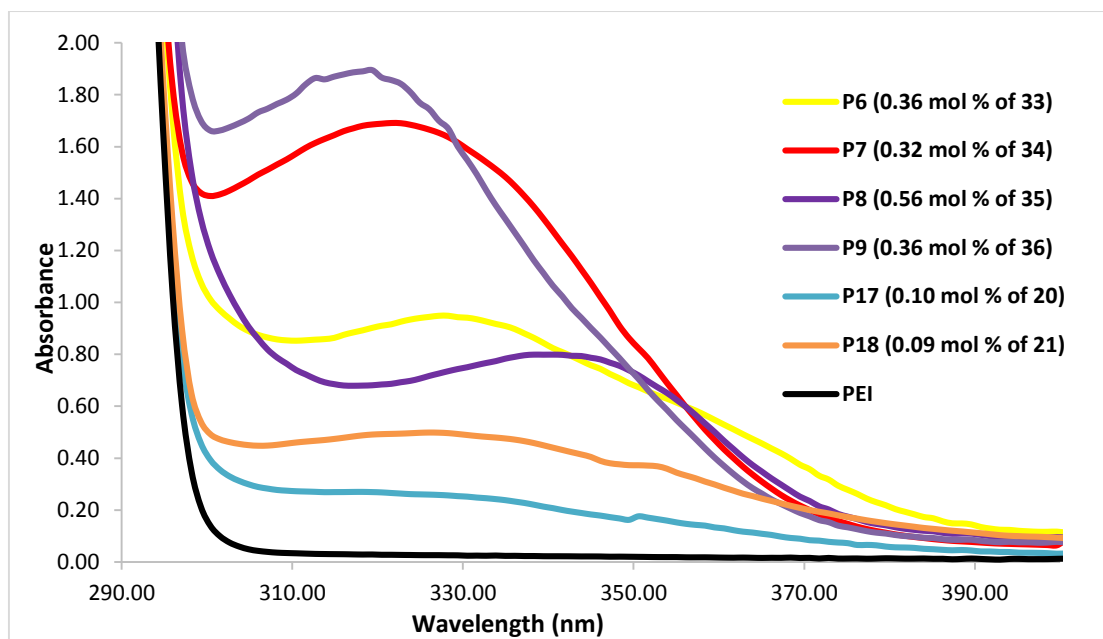


Fig. 4.29 - UV Spectra of P6, P7, P8, P9, P17, P18 and PEI in CHCl_3 (10 mg/mL)

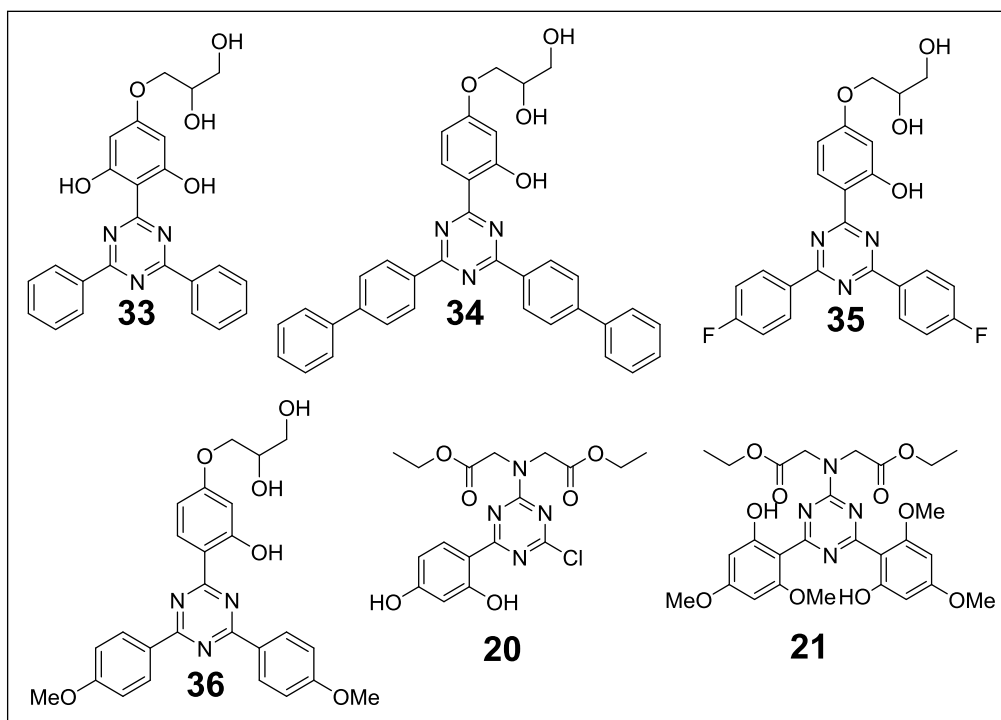


Fig. 4.30 – Chemical structures of UVAMs 20, 21, 33, 34, 35 and 36

The UV spectra of **P10** and **P11** showed the difference in the strength of absorbance when employing 1 wt % and 2 wt % of UVAM **37** in the feed (Figure 4.31). At 1 wt % loadings of UVAM **37** and **38** (Figure 4.32), the former showed a considerably stronger molar absorptivity after copolymerisation and a 10 nm blue-shift of the λ_{max}

was observed upon copolymerisation of UVAM **38**. UVAM **39** had a stronger molar absorptivity in comparison to the less conjugated **37** and **38**, which resulted in copolymer **P13** exhibiting a higher molar extinction coefficient in comparison to **P10** and **P12**. Taking into consideration all the PEI copolymers in this study, **P6**, **P10**, **P11**, **P12** and **P13** showed the strongest coverage at wavelengths above 355 nm. The copolymers depicted in Figure 4.31 contained UVAMs with two IMHBs which enhanced coverage at longer UV wavelengths, and **37** in particular was identified as the UVAM which provided the highest molar absorptivity at longer wavelengths. Therefore **33**, **37**, **38** and **39** would be the most efficient UVAMs for preventing the formation of fluorescent materials during photodegradation.

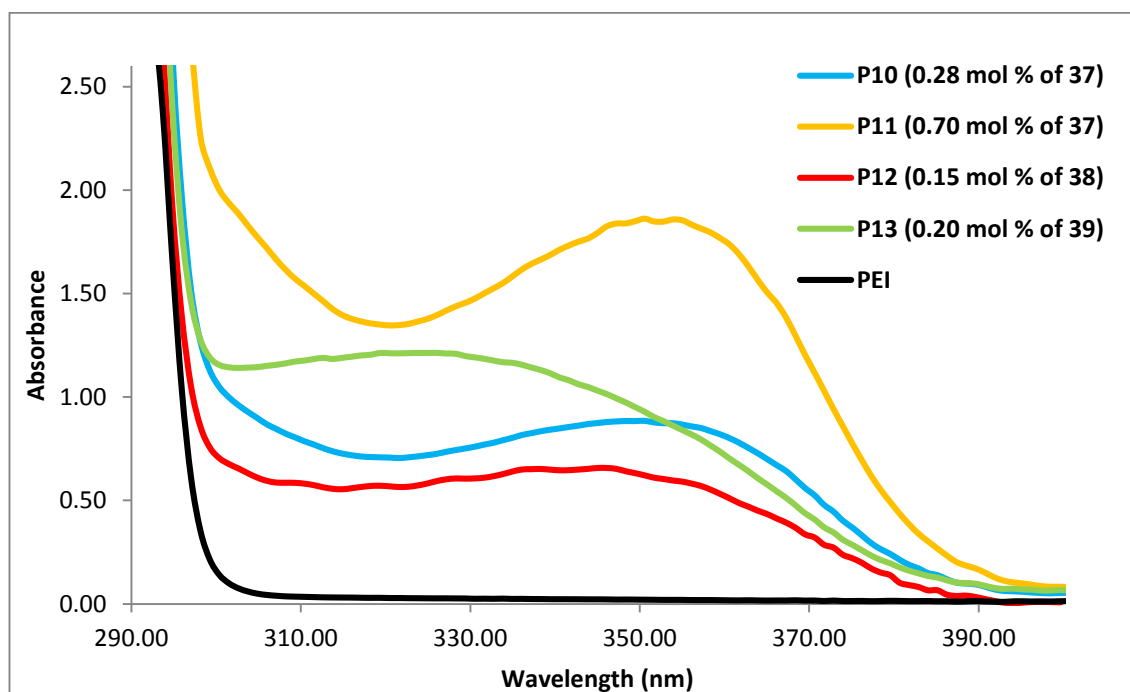


Fig. 4.31 - UV Spectra of P10, P11, P12, P13 and PEI in CHCl_3 (10 mg/mL)

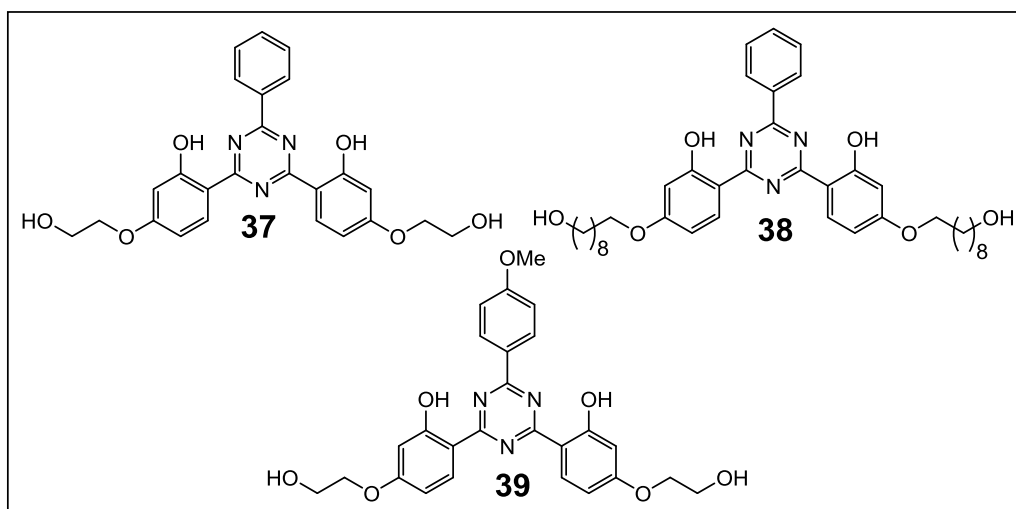


Fig. 4.32 – Chemical structures of UVAMs 37, 38 and 39

The UV spectra of copolymers containing bifunctional UVAMs displayed higher molar extinction coefficients compared to copolymers containing the monofunctional counterparts (Figure 4.33 and Figure 4.34). Only **P8** showed a significantly higher molar absorptivity and incorporation of the bifunctional **35** in comparison to **P15** which contained the monofunctional derivative **41**. The bifunctional **33** showed increased UV absorbance compared to the monofunctional **40**, but the level of incorporation of both monomers was similar. It seems that using chain stopper UVAM does not always have significant effect on the level of incorporation. Although a bifunctional UVAM is more likely to react than a monofunctional UVAM, the probability of one polymerisable functional group reacting is high enough so that the level of incorporation is not greatly affected by an increase in polymerisable functionality. When comparing **P6** and **P16**, there was very little difference in the intensity of the UV curves and the level of incorporation as judged from the ^1H NMR spectra. One thing to consider is that the reactivity of the polymerisable hydroxyl groups of the propanediol moiety are different, with one being a primary alcohol and the other a secondary alcohol. Higher levels of incorporation and higher molar absorptivity could be gained from using bifunctional UVAMs bearing two primary alcohol functional groups.

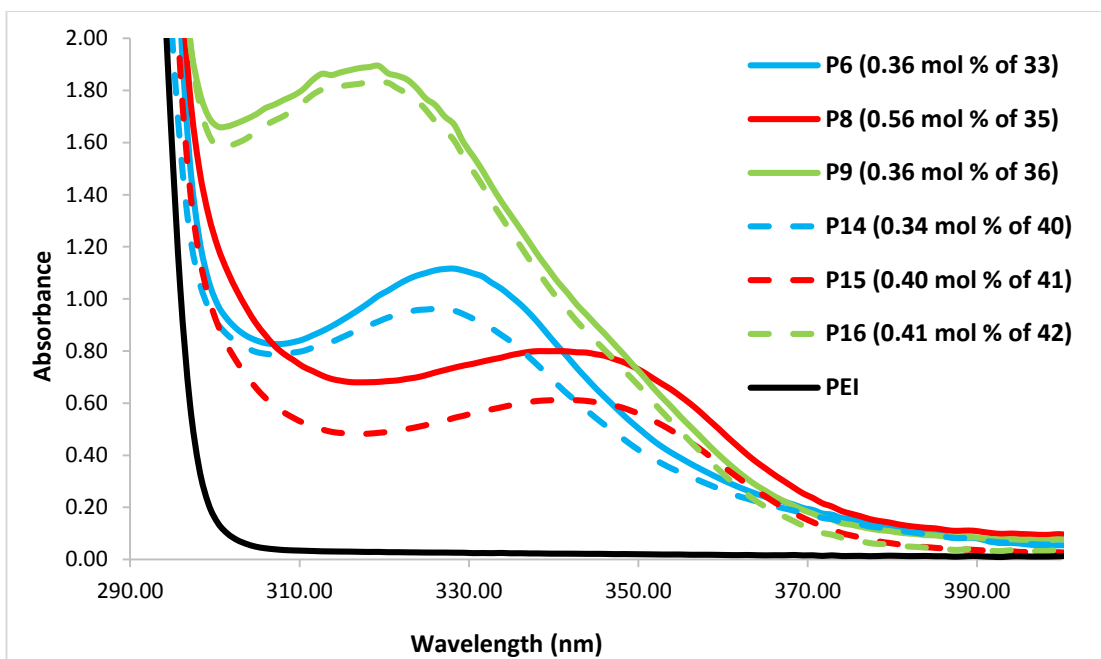


Fig. 4.33 - UV Spectra of P6, P8, P9, P14, P15, P16 and PEI in CHCl_3 (10 mg/mL)

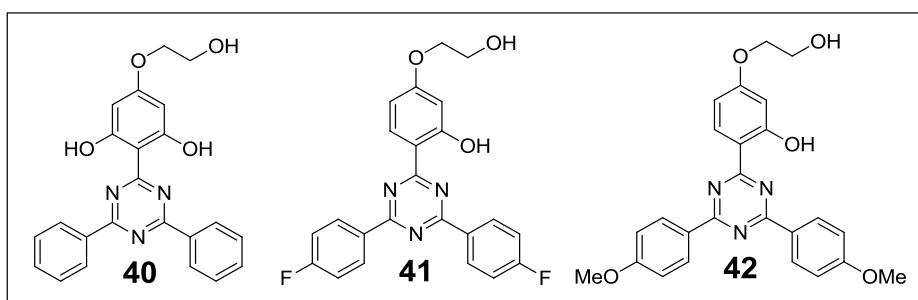


Fig. 4.34 – Chemical structures of UVAM 40, 41 and 42

The copolymers containing two UVAMs in the same polymer chain showed interesting UV spectra with strong UV coverage across the entire 290-400 nm range, particularly for copolymers **P19**, **P20**, **P21**, **P23**, **P25** and **P26** (Figure 4.35). Since **37** and **39** possessed the highest molar extinction coefficients at longer wavelengths, these two UVAMs were employed to offer good coverage at wavelengths above 350 nm, which can be observed in the UV spectra of **P19**, **P20**, **P21**, **P23**, **P25** and **P26**.

Using monofunctional UVAMs in combination with bifunctional UVAMs is a method in which to incorporate UVAMs in the middle and on the end of polymer chains. This approach could ultimately provide a more even distribution throughout the polymer

matrix so it was encouraging to observe that the monofunctional UVAMs, **40** and **42**, did not have a detrimental effect on the UV absorbance of **P25** and **P26**.

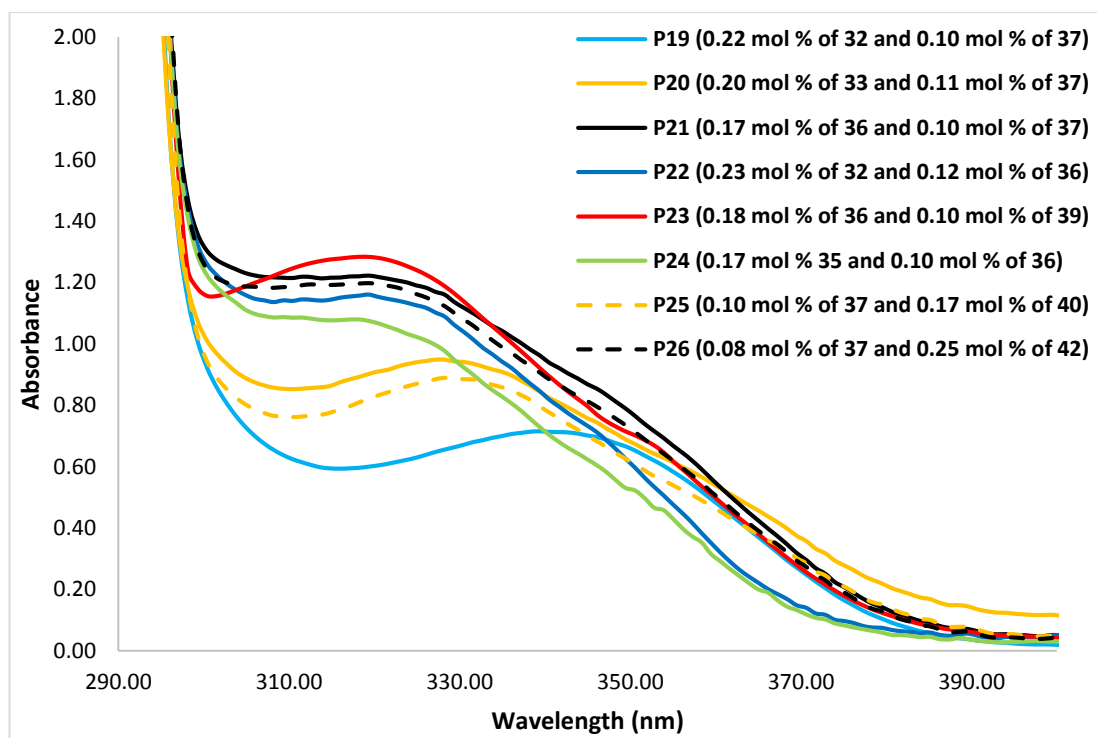


Fig. 4.35 - UV Spectra of P19, P20, P21, P22, P23, P24, P25, P26 and PEI in CHCl_3 (10 mg/mL)

The UV profiles of **32** and **37** complemented each other well since **37** had λ_{max} at 295 and 349 nm whilst **32** had λ_{max} at 342 nm. The UV spectra of **P5** (Figure 4.36) displayed weak molar absorptivity at wavelengths above 370 nm which potentially leaves the polymer chains susceptible to photodegradation at deeply penetrating low energy UV light. However, employing **32** together with **37** in the copolymerisation of **P19** enhanced coverage at wavelengths above 370 nm. Taking into consideration the λ_{max} of the UVAMs and how well one complemented the other was crucial in achieving broad range of coverage in the UV spectra of the copolymers.

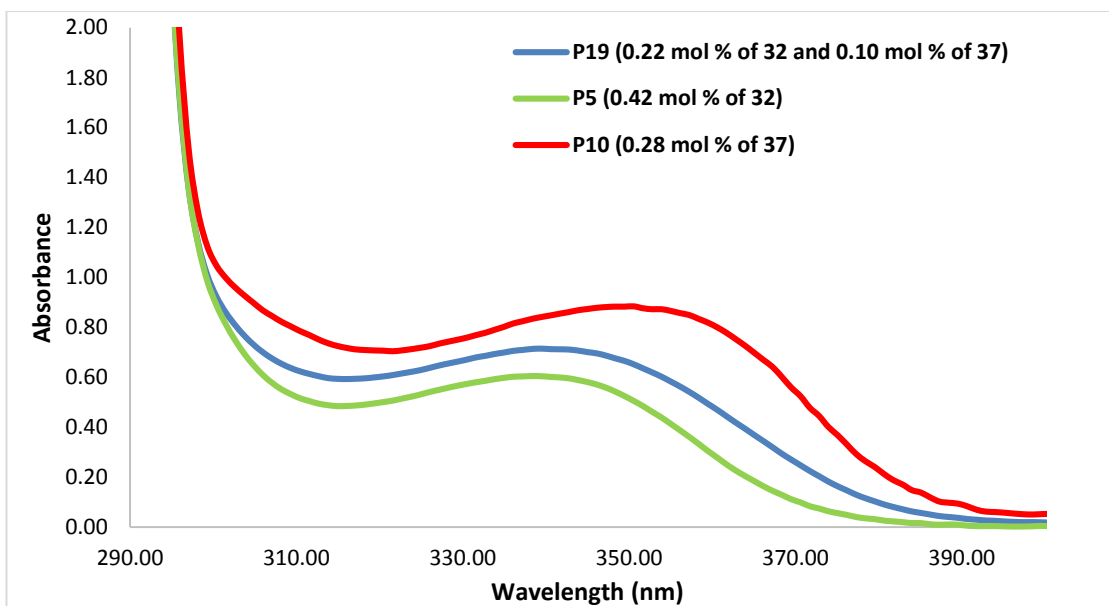


Fig. 4.36 - UV Spectra of P5, P10 and P19 in CHCl_3 (10 mg/mL)

Wavelengths between 310-315 nm comprise a crucial region to protect against photodegradation of PET.^{29,42,43} **P21**, **P22**, **P23** and **P24** had the highest extinction coefficients at 320 nm due to the presence of the powerful UVAM **36**. When **36** was copolymerised together with **37** or **39**, to obtain **P21** and **P23**, respectively, a strong absorbance between 310-330 nm was observed and coupled with increased molar absorptivity above 350 nm (Figure 4.37).

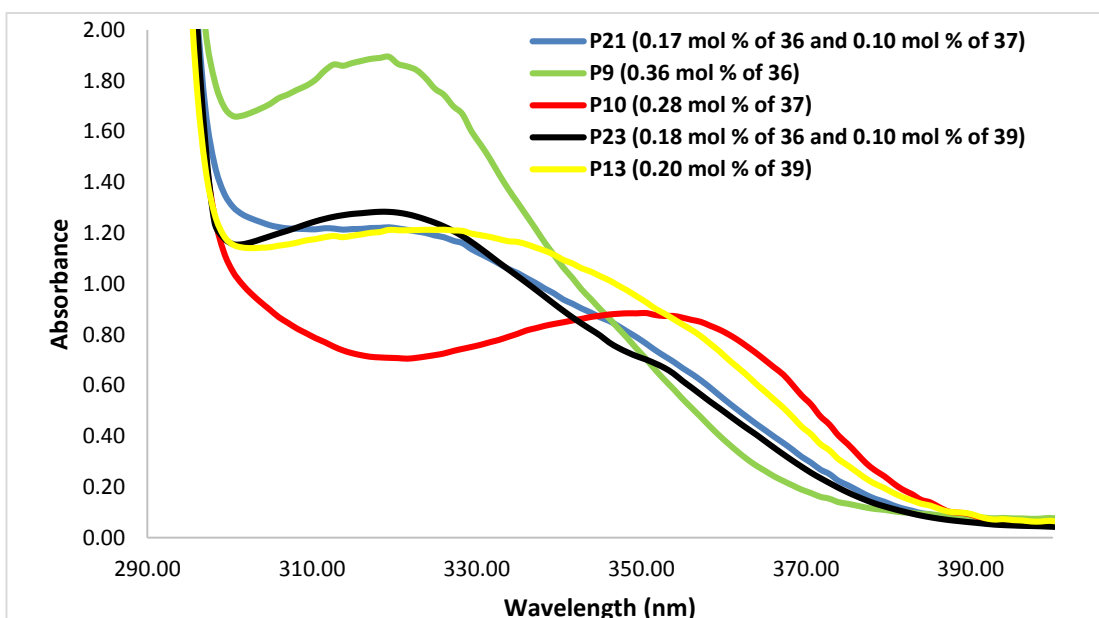


Fig. 4.37 - UV Spectra of P9, P10, P13, P21 and P23 in CHCl_3 (10 mg/mL)

4.2.2 DSC and GPC Analysis of PEI Copolymers

Differential scanning calorimetry (DSC) analysis of the copolymers showed lower glass transition temperatures (T_g) compared to that of PEI, with the exception of a slight increase for **P13** (Table 4.36). The lower T_g was caused by the polymerisable moieties decreasing the rigidity of the polymer chains which was indicative of successful copolymerisation. In addition to lowering the rigidity of the polymer chains, the inclusion of the bulky UVAMs interferes with the packing of the polymer chains which in turn marginally lowers the T_g . The fall in T_g observed from the monofunctional UVAMs is thought to be caused from the bulky end group UVAMs reducing intermolecular interactions and obstructing packing. Further evidence of successful polymerisation was presented in the DSC thermogram of **P12**, where the long aliphatic polymerisable moieties of UVAM **38** greatly decreased the rigidity of the polymer chains. This resulted in a fall in the glass transition temperature of 11.3 °C with respect to the PEI control. A melting transition was not observed for the copolymers since PEI is an amorphous polymer which does not crystallise during the cooling process.

The weight average molecular weights (M_w) and the number average molecular weights (M_n) of most of the PEI copolymers far exceeded that of the PET copolymers synthesised in this study. This was attributed to the BHEI **4.1** being more reactive and to the longer processing times of PEI. During the production of PET, the viscosity increased rapidly in the final stages of polymerisation and had to be cast before the polymer became too viscous for extrusion. In addition to this, the polymer chains become more restricted at higher viscosities which can reduce the rate of reaction at the crucial final stages of polymerisation. The viscosity did not increase as rapidly during the synthesis of PEI, therefore the polymerisation was maintained at high temperature and vacuum for a longer period of time which facilitated the formation of higher molecular weight products.

The copolymers exhibiting the lowest weight average molecular weights were **P14** and **P15** which contained monofunctional monomers that acted as chain stoppers.

P2 also displayed similarly low Mw and this was attributed to the impurities present in the crude mixture of **27** from the transesterification reaction. The copolymerisation of the monofunctional **42** did yield a copolymer with a high Mw of 44,900, however the bifunctional derivative of **42**, UVAM **36**, was copolymerised at similar levels and generated a copolymer with a higher Mw of 55,000. Employing less chain-stopper UVAMs together with bifunctional UVAMs yielded copolymers with higher Mw and Mn compared to copolymers using monofunctional UVAMs alone. For example, monofunctional UVAMs **40** and **42** were copolymerised together with the bifunctional **37** to yield copolymers **P25** and **P26** with Mw values of 39,700 and 36,200, respectively.

PEI copolymers with particularly high Mw, **P10** and **P11**, were copolymerised on consecutive days using 1 wt % and 2 wt % of UVAM **37**, respectively. This raised initial concerns regarding the behaviour of UVAM **37** and whether the UVAM was causing branching *via* the phenolic moieties. However, high molecular weights were not reproduced when **37** was employed in other PEI and PET copolymers. No significant discrepancies were identified in the process batch sheets of **P10** and **P11** compared to other copolymers. Despite there being a number of other copolymers that were processed below 1 mbar, a possible explanation is that a particularly excellent vacuum was achieved for **P10** and **P11**.

<i>Copolymer</i>	<i>UVAM(s)</i>	<i>T_g (°C)</i>	<i>M_w</i>	<i>M_w/M_n</i>	
P1	25	67.0	40,900	2.5	
P2	27	63.7	24,100	3.5	
P3	28	66.0	35,500	2.6	
P4	29	66.3	43,100	2.5	
P5	32	67.1	38,500	2.7	
P6	33	67.5	54,200	3.4	
P7	34	66.8	33,300	2.7	
P8	35	66.6	51,000	4.3	
P9	36	65.8	55,000	3.9	
P10	37	68.3	107,000	3.8	
P11	37	67.5	85,700	3.6	
P12	38	57.6	45,700	2.9	
P13	39	69.2	67,000	3.7	
P14	40	65.1	23,700	3.0	
P15	41	66.1	21,000	2.6	
P16	42	66.1	44,900	3.5	
P17	20	68.8	59,400	3.5	
P18	21	66.0	64,900	3.5	
P19	32	37	64.6	36,700	2.7
P20	33	37	66.8	35,700	2.7
P21	36	37	68.5	42,000	3.1
P22	32	36	68.4	52,000	2.9
P23	36	39	65.6	62,600	3.7
P24	35	36	66.4	46,600	3
P25	37	40	65.8	39,700	3.3
P26	37	42	68.1	36,200	3.2
PEI	-	68.9	55,200	2.5	

Table 4.36 – Table showing glass transition temperatures, number average molecular weights and polydispersities of copolymers and PEI

4.3 Conclusions

UVAMs were incorporated successfully into the polymeric chains of PEI. Additionally, a variety of UVAMs were selected carefully and combinations of two different UVAMs were successfully copolymerised into the same polymer chain. ¹H NMR and UV spectroscopy analysis of the copolymers showed clear evidence of the presence of polymerised UVAMs, even after rigorous purification.

The majority of copolymerised UVAMs displayed no blue- or red-shifts which indicated that the UV profile of most of the monomers were unaffected by chemical incorporation into the polymer chain. An exception to this was UVAM **38** which displayed a 10 nm blue-shift upon copolymerisation. UV spectroscopy of the purified copolymers **P1-P5** showed that polymerisable derivatives of Tinuvin 1577 **1.10** provided good coverage between 290-370 nm but a weak molar absorptivity above wavelengths of 370 nm. Employing UVAMs with higher extinction coefficients resulted in superior molar extinction coefficients in the UV spectra of the copolymers. The highest extinction coefficients were located in the 320 nm region for copolymers **P6** and **P7**, both of which contained highly conjugated UVAMs **34** and **36**, respectively. Since wavelengths between 310-315 nm were determined to be critical for photodegradation of PET,^{29,42,43} this highlighted the potential of **34** and **36** which both displayed high molar extinction coefficients at these shorter wavelengths. UVAMs **33**, **37**, **38** and **39** possessed two IMHBs and provided a broader range of coverage especially at wavelengths between 370-400 nm, which is an important region of low energy and highly penetrating UV light responsible for the formation of fluorescent material during photodegradation.

Carefully selecting two different UVAMs and chemically incorporating them into the same polymeric chains led to coverage at both long and short wavelengths. The superior long wavelength absorber **37** was copolymerised into PEI with UVAMs which had lower λ_{max} . The UV spectra of the cocktail copolymers showed that the correct combinations provided a wider range of protection against short wavelength chain

scissions and long wavelength fluorescent mono-/di-hydroxyterephthalate production.

Mono-functional UVAMs generally showed similar levels of incorporation in the copolymers compared to the bifunctional derivatives. A significantly higher level of incorporation and molar absorptivity was achieved for the bifunctional **35** in comparison to the monofunctional **41**. Bifunctional UVAMs yielded higher molecular weight copolymers in comparison to the monofunctional chain-stopper UVAMs.

The copolymers containing UVAMs with short polymerisable aliphatic chains had marginally lower glass transition temperatures than a PEI control. The long polymerisable chain moieties of UVAM **38** resulted in a drastic increase of rotational freedom in the polymer chains, which significantly lowered the glass transition temperature of **P12**.

The weight average molecular weights (M_w) of all the copolymers were high and exhibited a wide variation above and below that of the PEI control. The polydispersities of the copolymers were all higher than the control PEI by 0.1-1.7. Copolymers with considerably lower M_w and M_n were produced when using the chain-stopper UVAMs.

**Chapter 5 - Poly(ethylene terephthalate)
Copolymers and Accelerated Weathering Study**

5.1 Experimental

After successful incorporation of UVAMs into poly(ethylene isophthalate) (PEI) the focus was diverted to copolymerising UVAMs into poly(ethylene terephthalate) (PET). The PET polymers were processed into films by thermal pressing and biaxial stretching in order to study the extent of UV degradation in a QUV weatherometer.

5.1.1 Reagents

Reagent	Purity	Supplier
Antimony trioxide	>99.65 %	SICA
<i>Bis</i> (2-Hydroxyethyl)terephthalate (BHET)	-	Synthesised at DTF
Chloroform	99.0-99.4%	Aldrich
Methanol	99.7%	Aldrich

Table 5.1 - List of solvents and reagents used

5.1.2 Equipment and Methods

The polymers were synthesised in a polycondensation (PC) rig at DuPont Teijin Films, Wilton, UK. The equipment included a polycondensation head, stirrer guide, air stirrer, delivery side-arm, distillate tube inside an ice-filled Dewar flask, thermocouples and optical revolution counter. The system was connected to a gas and vacuum manifold.

The polymers synthesised in the PC rig were moulded into cast films (width 6 cm, length 6 cm, thickness 0.1 cm) using a thermal press at Strathclyde University (Appendix, Figure 7.2). A combination of; a steel mould, steel plates, aluminium sheets and poly(tetrafluoroethylene) (PTFE) baking paper were used to sandwich the polymer. The polymers were compressed (35 kg/cm²) at a temperature of 275 °C. The cast films were stretched biaxially on a Long stretcher at DTF in Wilton. The polymer was held at 105 °C for 15 seconds before stretching biaxially at a rate of 1 in/sec to give approximately 14 x 14 cm film. The thickness of the films was measured using a Sylvac D100S digital unit.

UV-Visible absorption spectra of the polymer films were recorded using a Shimadzu UV-1800 UV spectrophotometer. Solution state UV-Visible absorption spectra were acquired using a Photonics CCD array UV-VIS spectrophotometer with a 1 mm

pathlength quartz cell. DMSO and CHCl_3 were used as solvents and the scan range was 290-500 nm.

Soxhlet extraction was carried out using CHCl_3 (200 mL) and 0.5 g of polymer, subjecting the polymer to reflux temperatures for 24 hours. The extraction solvent was transferred to a 250 mL volumetric flask, made up to the volumetric mark and analysed using UV-Vis spectroscopy.

ATR FT-IR measurements were carried out on a Thermo Scientific Nicolet iS50 FT-IR Spectrometer at a spectral resolution of 4 cm^{-1} , averaged over 32 scans. A piece of filter paper was placed on top of all thin film samples to ensure an even and complete contact was made between the film and the diamond. An 'Advanced ATR Correction' algorithm, provided within the software supplied was used to correct the data (as recommended by Thermo Fischer Scientific, Hemel Hempstead) before analysis was carried out. A ratio of the peak heights at 3290 cm^{-1} (O-H stretch of COOH) and 2960 cm^{-1} (C-H stretch reference peak) with a baseline from 4000 cm^{-1} and 400 cm^{-1} was used.

The PET films were subjected to UV degradation using a QUV accelerated weathering machine under UV-A radiation in accordance with the ISO 4893-3 standard. The weathering cycle consisted of 8 hours of continuous UV luminescence at 0.76 Wm^{-2} (340 nm) at $60\text{ }^\circ\text{C}$ followed by 4 hours of dark condensation at $50\text{ }^\circ\text{C}$.

TGA of UVA monomers was performed using a Perkin Elmer TGA 7. Approximately 10 mg of sample was heated under air at a rate of $10\text{ }^\circ\text{C}/\text{min}$ from $40\text{ }^\circ\text{C}$ to $500\text{ }^\circ\text{C}$.

Thermal analyses of polymer samples were carried out using a 6000 Enhanced Single-Furnace Differential Scanning Calorimeter (DSC). The samples were heated from $-20\text{ }^\circ\text{C}$ to 310 ° at a rate of $20\text{ }^\circ\text{C}/\text{min}$, cooled back to $-20\text{ }^\circ\text{C}$ at a rate of $50\text{ }^\circ\text{C}/\text{min}$ and reheated to $310\text{ }^\circ\text{C}$ at a rate of $20\text{ }^\circ\text{C}/\text{min}$.

The molar masses of the polymers were determined using Gel Permeation Chromatography (GPC) which was carried out at Smithers Rapra Limited on a

Malvern/Viscotek TDA 301 instrument with a refractive index detector. The samples were dissolved (2 mg/mL) in hexafluoroisopropanol (HFIP), filtered through 0.45 µm membrane and passed through an Agilent PL HFIP Gel Column at a flow rate of 0.8 mL/min at 40 °C.

5.1.3 Synthesis of Poly(ethylene terephthalate) (PET) Films

A stirred slurry of BHET **1.4**, UVAM/Tinuvin **1577 1.10** and Sb₂O₃ (0.15 g, 0.52 mmol) was added into a PC rig tube. The PC rig tube was scored lightly on the stem, using a Stanley blade, to ensure safe extrusion and clamped inside a heating block (Appendix, Figure 7.1). The PC rig tube was fitted with a polycondensation head, stirrer guide, air stirrer, delivery side-arm, distillate tube inside an ice-filled Dewar flask, thermocouples, optical revolution counter and connected to a gas manifold. The temperature was raised using a control box to 230 °C over 60 mins under a nitrogen purge. The air stirrer was then started with a pressure of 9.5 psi, with the stirrer speed reaching 175 rpm. After stirring under a nitrogen purge at 230 °C for 30 mins, the system was put under vacuum. The pressure was reduced gradually to less than 3 mbar as the temperature was increased to 290 °C at a rate of 1 °C/min. Once the stirrer speed dropped by 30-40 rpm, the polymerisation was judged to be complete and the vacuum was slowly replaced with a nitrogen purge. A hammer and chisel was used to break the stem of the PC rig tube, and the synthesised copolymer was extruded and quenched into an ice-water bath. The copolymer lace formed was left to dry in air.

The polymer fibres were moulded into a cast film using a thermal press (Appendix, Figure 7.2). The polymer fibres were cut into small pieces using scissors and 7 grams of polymer cuttings were placed between two layers of PTFE baking paper (9 cm x 9 cm) which was positioned in the middle of a steel mould (width 6 cm, length 6 cm, height 0.1 cm). This was sandwiched between two 0.1 mm thick aluminium sheets which, in turn, were sandwiched by two 1 mm thick steel plates. This was then placed in a thermal press at 275 °C and allowed to melt for 30 seconds. 35 kg/cm² of pressure was applied and released, repeating this 50 times to ensure all the air

bubbles were released. The sandwich was removed from the press and quickly dropped into a bucket of ice water. The aluminium sheets and baking paper were peeled off to give a 1 mm thick cast polymer, 6 cm in length and 6 cm in width.

The cast film was stretched biaxially on a Long stretcher at DTF in Wilton. The cast polymer was clipped onto draw arms (6 x 6 cm) inside an oven set at 105 °C. The polymer was held at this temperature for 15 seconds before stretching biaxially at a rate of 1 in/sec to give 14 x 14 cm film.

PET Control (P27)

Polymer	UVAM or Tinuvin 1577 1.10 mass (g)	BHET 1.4 mass (g)
P27	0	100.00

Table 5.2 – BHET 1.4 loading for polymerisation of P27

Yield = 78 %

DSC of biaxially stretched film: Tg = 77.2 °C; Tm = 256.3 °C; Crystallinity = 15.3 %

GPC after thermal pressing: Mw = 11,750; Mn = 3,605; Mz = 19,900; Mw/Mn = 3.3

Average film thickness: 48.1 µm

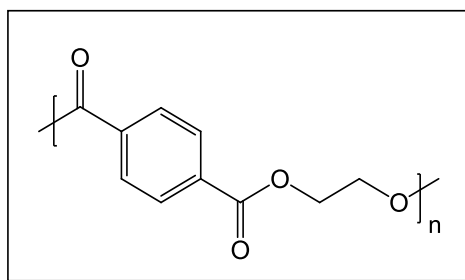


Fig. 5.1 – Chemical structure of PET control (P27)

PET + Tinuvin 1577 1.10 (P28)

Polymer	Tinuvin 1577 1.10 mass (g)	BHET 1.4 mass (g)	Tinuvin 1577 1.10 in the feed	
			Wt %	Mol %
P28	1.00	99.00	1.00	0.60

Table 5.3 – Theoretical Tinuvin 1577 1.10 loading in copolymerisation of P28

Yield = 80 %

DSC of biaxially stretched film: Tg = 77.8 °C; Tm = 257.3 °C; Crystallinity = 17.5 %

GPC after thermal pressing: Mw = 14,350; Mn = 4,255; Mz = 24,450; Mw/Mn = 3.4

Average film thickness: 60.1 μm

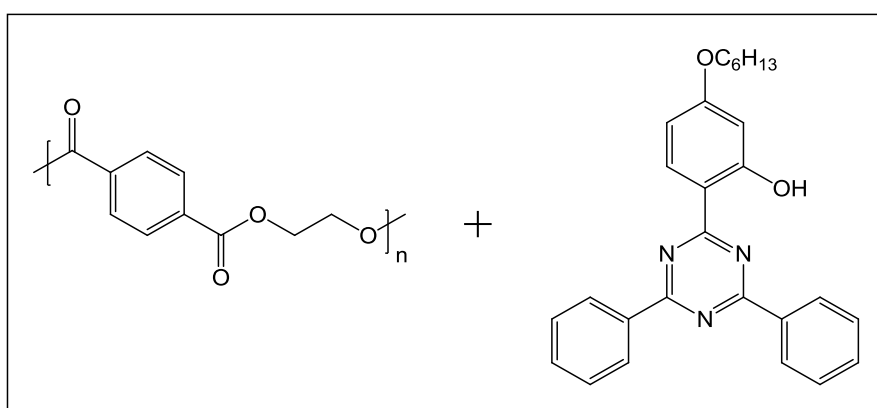


Fig. 5.2 – Chemical structure of P28

Poly(ET-co-32) (P29)

Copolymer	UVAM 32	BHET 1.4	UVAM 32 in the feed	
	mass (g)	mass (g)	Wt %	Mol %
P29	0.97	99.00	0.97	0.60

Table 5.4 – Theoretical UVAM 32 loading in copolymerisation of P29

Yield = 74 %

DSC of biaxially stretched film: T_g = 76.2 °C; T_m = 256.2 °C; Crystallinity = 17.3 %

GPC after thermal pressing: M_w = 11,750; M_n = 3,480; M_z = 20,300; M_w/M_n = 3.4

Average film thickness: 38.2 μm

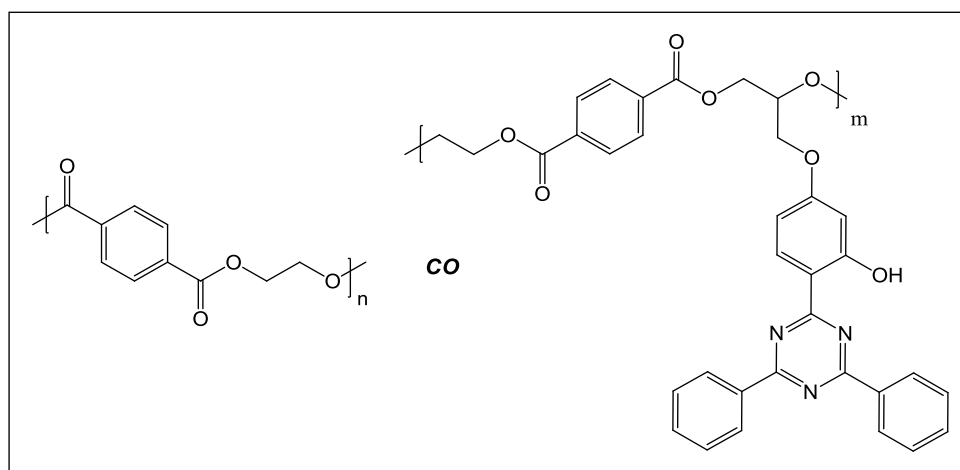


Fig. 5.3 – Chemical structure of P29

Poly(ET-co-37) (P30)

<i>Copolymer</i>	<i>UVAM 37</i>	<i>BHET 1.4</i>	<i>UVAM 37 in the feed</i>	
	<i>mass (g)</i>	<i>mass (g)</i>	<i>Wt %</i>	<i>Mol %</i>
P30	1.08	99.00	1.08	0.60

Table 5.5 - Theoretical UVAM 37 loading in copolymerisation of P30

Yield = 80 %

DSC of biaxially stretched film: T_g = 75.1 °C; T_m = 253.3 °C; Crystallinity = 13.3 %

GPC after thermal pressing: M_w = 11,550; M_n = 3,370; M_z = 20,350, M_w/M_n = 3.4

Average film thickness: 53.6 μm

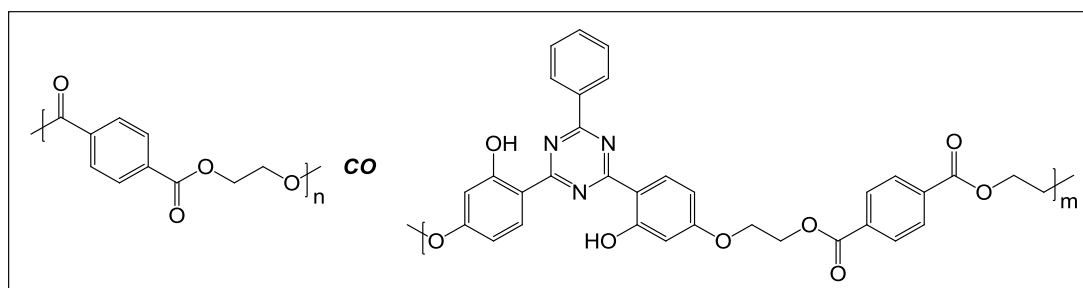


Fig. 5.4 – Chemical structure of P30

Poly(ET-co-32-co-37) (P31)

Copolymer	UVAM 32	BHET 1.4	UVAM 32 in the feed	
	mass (g)	mass (g)	Wt %	Mol %
P31	0.49	99.00	0.49	0.30

Table 5.6 - Theoretical UVAM 32 loading in copolymerisation of P31

Copolymer	UVAM 37	BHET 1.4	UVAM 37 in the feed	
	mass (g)	mass (g)	Wt %	Mol %
P31	0.54	99.00	0.54	0.30

Table 5.7 - Theoretical UVAM 37 loading in copolymerisation of P31

Yield = 80 %

DSC of biaxially stretched film: Tg = 76.6 °C; Tm = 252.9 °C; Crystallinity = 21.9 %

GPC after thermal pressing: Mw = 12,450; Mn = 3,705; Mz = 21,700 Mw/Mn = 3.4

Average film thickness: 41.1 μm

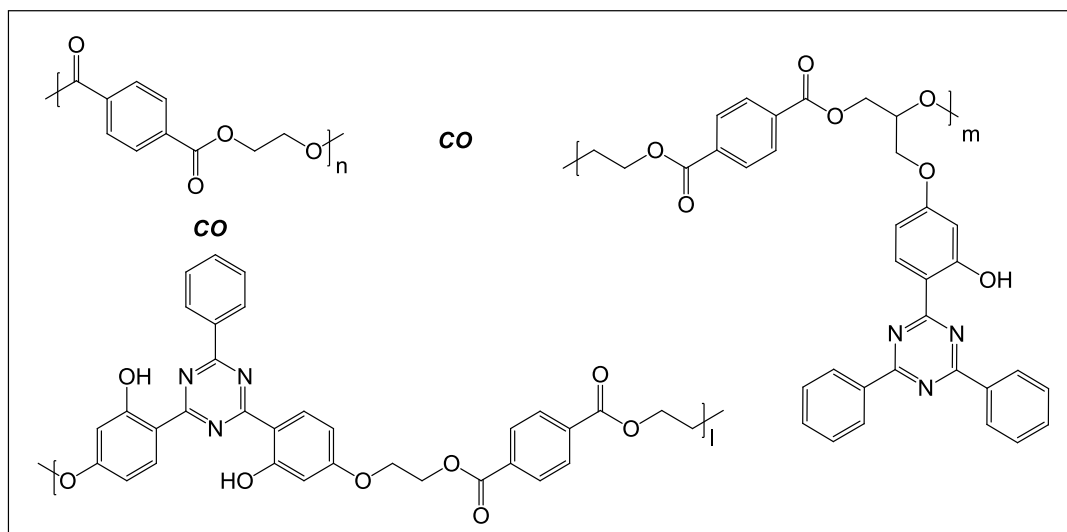


Fig. 5.5 – Chemical structure of P31

5.2 Results and Discussion

The PET polymers were processed into films in order to study the extent of UV degradation in a QUV weatherometer. The degree of UV degradation was monitored periodically using attenuated total reflection (ATR) Fourier-transform infrared spectroscopy (FT-IR) and gel permeation chromatography (GPC).

5.2.1 Synthesis and Processing of PET Films

After considering a number of factors such as UV profiles, thermal stability and industrial scalability, UVAM **32** and **37** (Figure 5.6) were identified as suitable polymerisable UV absorbers for this degradation study. UVAM **32** mimicked the UV profile and thermal stability of Tinuvin 1577 **1.10**, meaning **32** served as a direct comparison with the commercial additive to determine whether polymerisable UV absorbers were more effective than UV absorber additives (Figures 5.7 and 5.8). DuPont Teijin Films had freedom to operate with UVAM **37**, which exhibited a broad UV absorption within the wavelength range of 290-400 nm and was more thermally robust than Tinuvin 1577 **1.10**. 0.6 mol % of Tinuvin 1577 **1.10**, **32** and **37** were employed in the feed of **P28**, **P29** and **P30**, respectively. To investigate the photostabilising effect of a cocktail copolymer, 0.3 mol % of **32** and 0.3 mol % of **37** were copolymerised in the synthesis of **P31**.

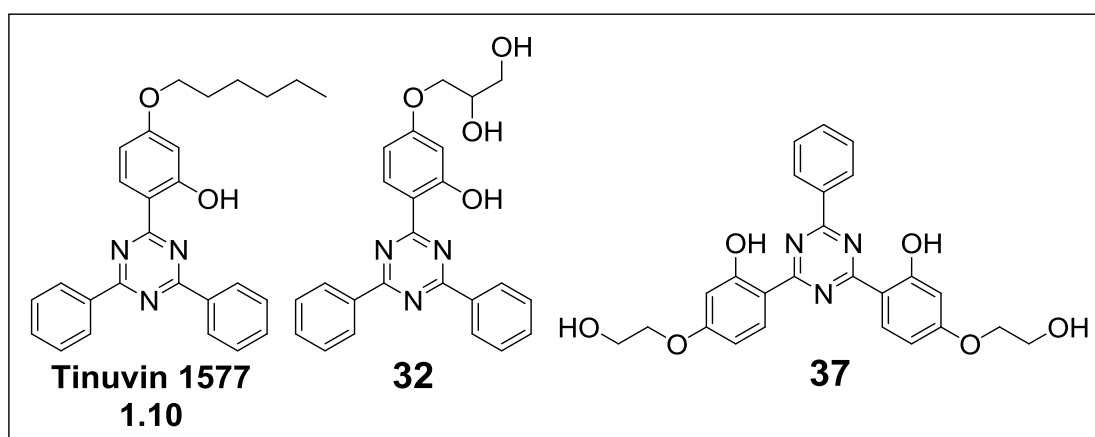


Fig. 5.6 – Chemical structures of Tinuvin 1577 1.10, 32 and 37

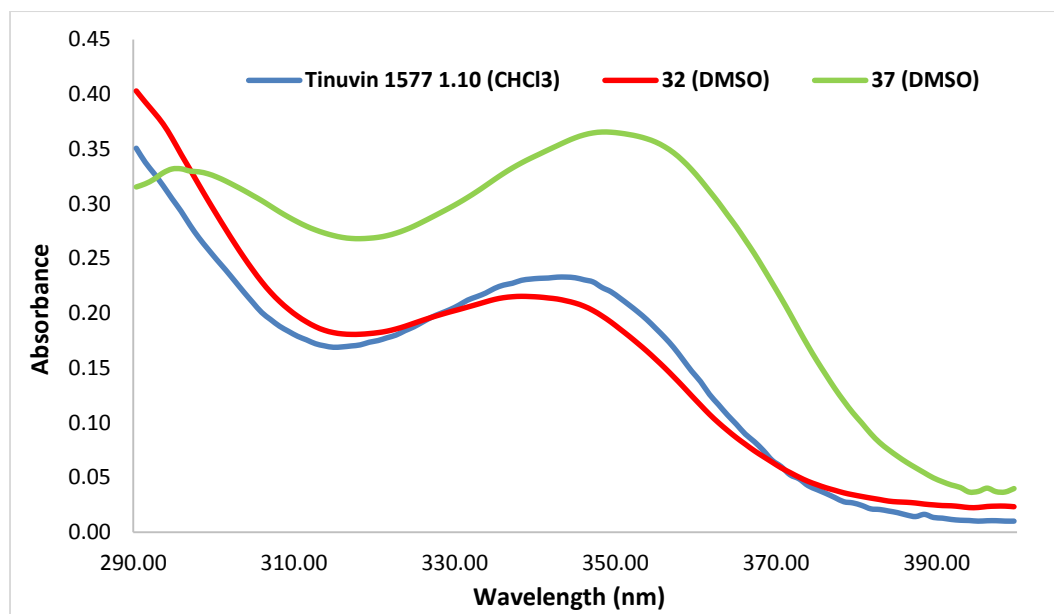


Fig. 5.7 – UV spectra of 0.1 mM solutions of UVAMs 32, 37 and Tinuvin 1577 1.10

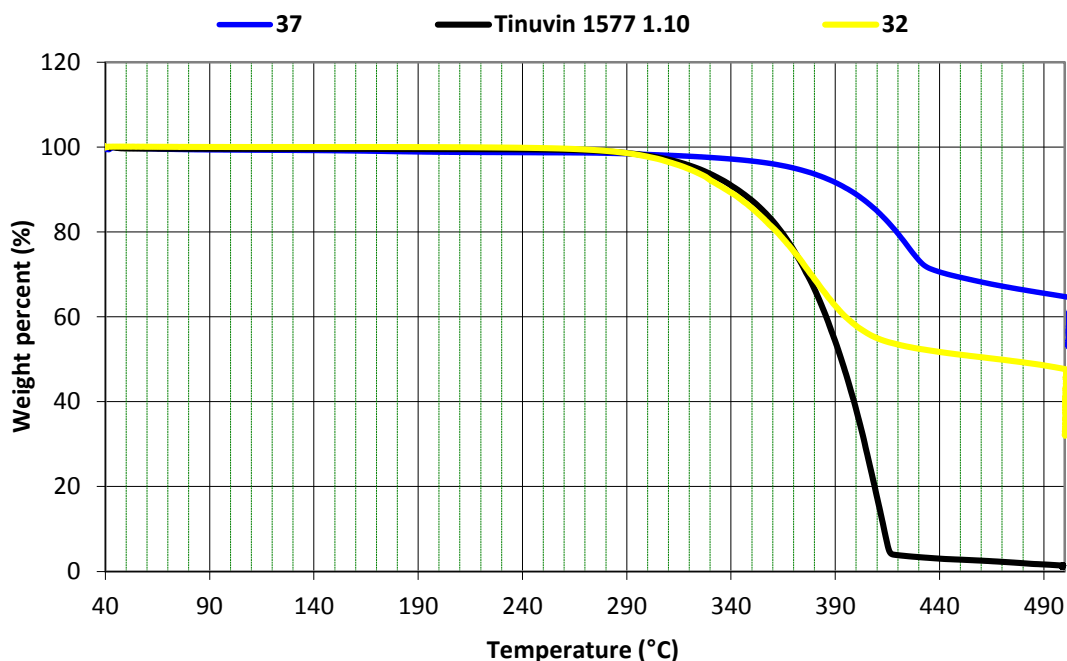


Fig. 5.8 – Thermogravimetric (TGA) analysis graph of 32, 37 and Tinuvin 1577 1.10

The initial strategy was to carry out polymerisations in a 5 gallon reactor, however after careful consideration of the cost of scaling up the synthesis of **32** and **37** it was decided to synthesise the PET copolymers on 100 gram scale in the PC rig (Appendix, Figure 7.1). The polymer fibres were processed into film using a thermal press which required only 7 grams of polymer per cycle. If the results from this small scale

approach impressed, then this would justify the funds required for 5 gallon scale copolymerisations.

When first using the thermal press, a major difficulty was encountered when attempting to remove the PET from the steel mould. The polymer would strongly adhere to the steel and crack when applying gentle force to remove the cast film from the mould. A number of release agents were employed without success, however PTFE baking paper was successful. Sandwiching the polymer between two layers of PTFE paper to prevent the polymer from coming in contact with the steel mould allowed easy removal of the polymer without cracking. An additional problem was the formation of air bubbles in the cast film which caused large cavities upon stretching. As a precaution against air bubbles, 40 % excess of polymer with respect to the volume of the mould cavity was used and the polymer fibres were cut into small pieces. Remaining air bubbles were forced out by a series of compressions and decompressions in the thermal press. Preventing crystallisation was important to facilitate stretching of the cast film in the subsequent step, thus the molten polymer was cooled quickly by dropping into iced water.

These films were then stretched biaxially on a Long stretcher at Wilton to give films with average thicknesses in the range 38.2-60.1 μm . The polymers were held above their glass transition temperature (105 °C) for 15 seconds and stretched biaxially (Appendix, Figure 7.3). Biaxial stretching aligned the polymer chains in a more ordered arrangement to improve mechanical strength in both the transverse and longitudinal directions. Differential scanning calorimetry (DSC) analysis showed that the films had relatively comparable crystallinities. Cast films which were held longer than 15 seconds at 105 °C tended to crack due to crystallisation beginning to take place before stretching.

GPC analysis showed a slight decrease in the molar mass of the films due to thermal degradation taking place during thermal pressing at 275 °C. Reducing the thermal degradation was possible by simply compressing the films at lower temperatures, such as 260-265 °C, but this had a detrimental effect on the quality of the films which

failed to stretch due to the presence of air pockets. Branching occurred when copolymerising **37** into PEI, however GPC analysis showed no evidence of **37** causing chain branching when copolymerising into PET.

DSC analysis showed marginally lower glass transition and melting temperatures for the copolymers in comparison to the PET control (**P27**) and Tinuvin 1577 **1.10** treated PET (**P28**), which was expected after observing a slight reduction in the glass transition temperatures of the PEI copolymers.

The UV spectra of the copolymer films (Figure 5.9) showed **P28** and **P29** having similar UV profiles, whereas **P30** and **P31** exhibited stronger molar absorptivity within the 320-400 nm region. The higher molar extinction coefficient of **P30** and **P31** was attributed to the presence of UVAM **37**. **P29**, **P30** and **P31** films had a light yellow colour in comparison to **P27** and **P28**, however there was no sign of protrusion into the visible region in the UV spectra.

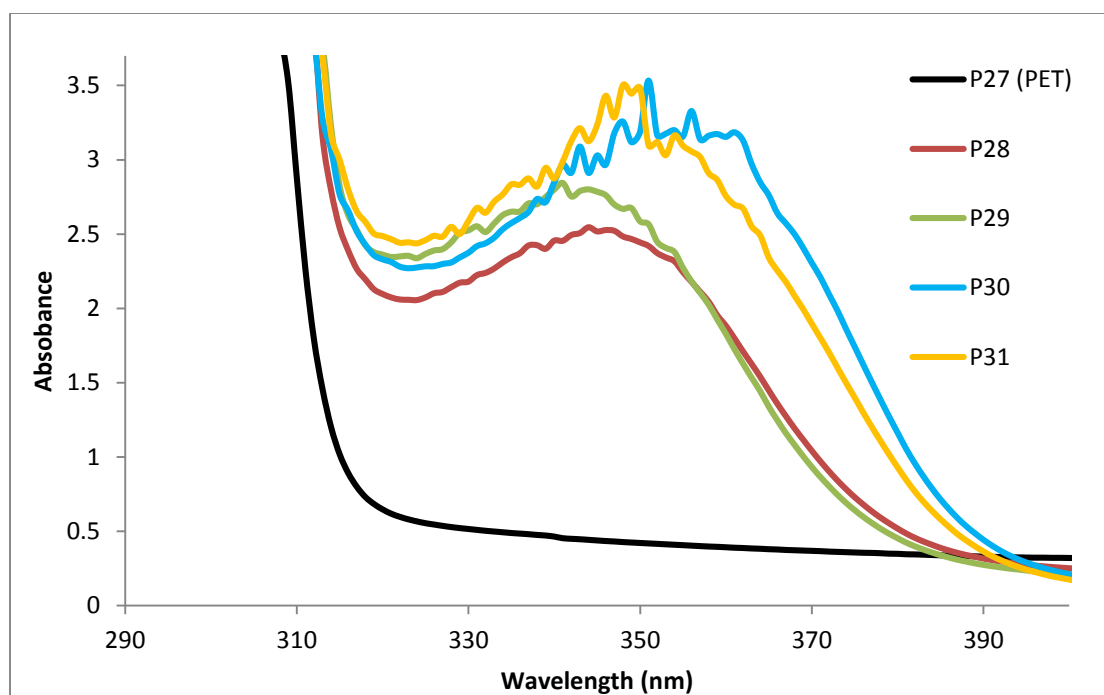


Fig. 5.9 – UV spectra of P27, P28, P29, P30 and P31

5.2.2 Solvent Extraction

Solvent extraction tests were carried out to investigate the potential leaching of stabiliser from the polymer matrices. CHCl_3 was used as an extraction solvent and the chloroform solubles analysed using UV-Vis spectroscopy.

The UV spectra of the extraction solvent showed that Tinuvin 1577 **1.10** was highly vulnerable to washing out of the polymer (Figure 5.10). The results displayed clear evidence that UVAMs **32** and **37** had successfully polymerised into the polymer backbone, making them much less susceptible to leaching. Using the molar extinction coefficient of Tinuvin 1577 **1.10** ($\epsilon = 23,000 \text{ Lmol}^{-1}\text{cm}^{-1}$), 84 % of the additive was calculated to have migrated into the solvent. The extent of leaching of Tinuvin 1577 **1.10** in the solvent extraction study is not comparable to the levels of leaching that occur in a weatherometer, whereby Tinuvin 1577 **1.10** would migrate at a much slower rate during the weathering process.

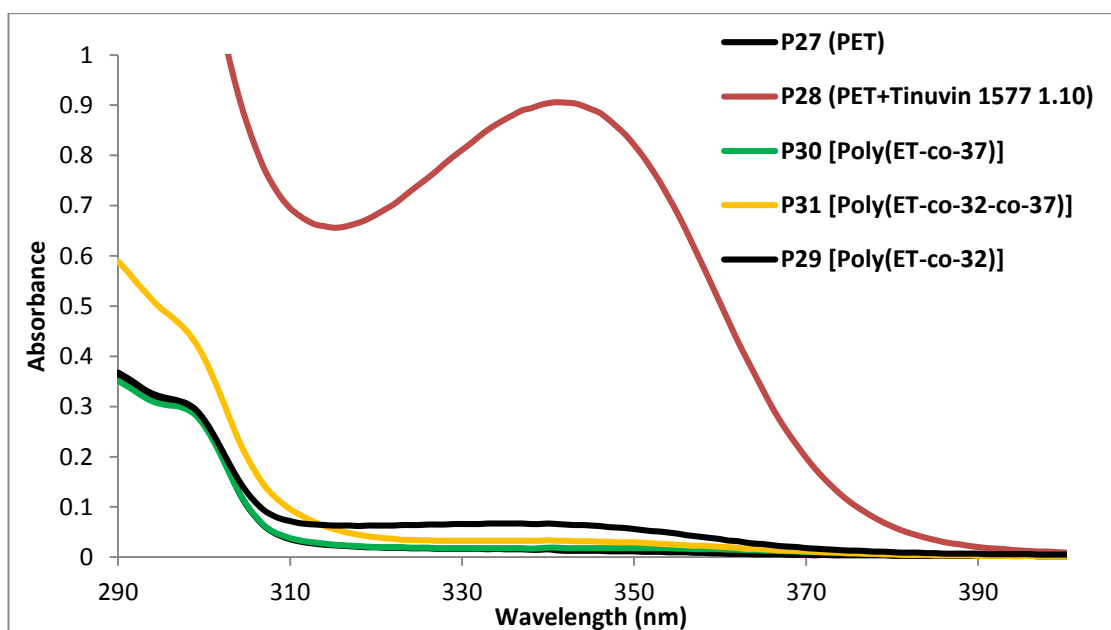


Fig. 5.10 – UV spectra of solvent after solvent extraction for P27, P28, P29, P30 and P31

5.2.3 Weathering of PET Films

The films were weathered in a QUV weatherometer and analysed periodically by ATR FT-IR spectroscopy and GPC. **P28**, **P29**, **P30** and **P31** were exposed for a total of 1082

hours (45 days), whereas the PET control **P27** was removed after becoming extremely brittle at 859 hours. The stabilised films exhibited wrinkles and became noticeably more brittle after 653 hours. None of the films displayed distinct yellowing to the eye after weathering (Appendix, Figure 7.4).

5.2.3.1 ATR FT-IR Measurements

ATR FT-IR spectroscopy measurements were carried out on the front surface of each film at regular intervals between 0 and 1082 hours of exposure. This technique analysed the first 2-3 microns of the films surface and emphasises the oxidative degradation more than the anaerobic degradation. Day and Wiles²⁸ monitored surface degradation of PET by using a ratio of the bands at 3290 and 2970 cm^{-1} , assigned to the carboxylic O-H stretch and the aliphatic C-H stretch, respectively. The C-H vibration for these films appeared at 2960 cm^{-1} , so the ratios were calculated using this wavenumber instead of 2970 cm^{-1} (Figure 5.11). The values plateaued for each sample once the penetration depth of the ATR became saturated with COOH functional groups. In a fashion similar to results reported by Day and Wiles, a rapid increase in COOH formation preceded a plateau for the PET control (**P27**). The films containing Tinuvin 1577 **1.10 (P28)** and **32 (P29)** displayed similar behaviour to the control, although at a slower rate. **P30** and **P31** had slower rates of COOH formation, which can be credited to the presence of UVAM **37**. The cocktail polymer **P31** containing both **32** and **37** had the slowest rate of chain scissions at the surface which highlighted the prospect of employing UVAMs as cocktails. The error bars correspond to standard deviations based on three repeat measurements calculated for each sample at 169 and 448 hours of exposure.

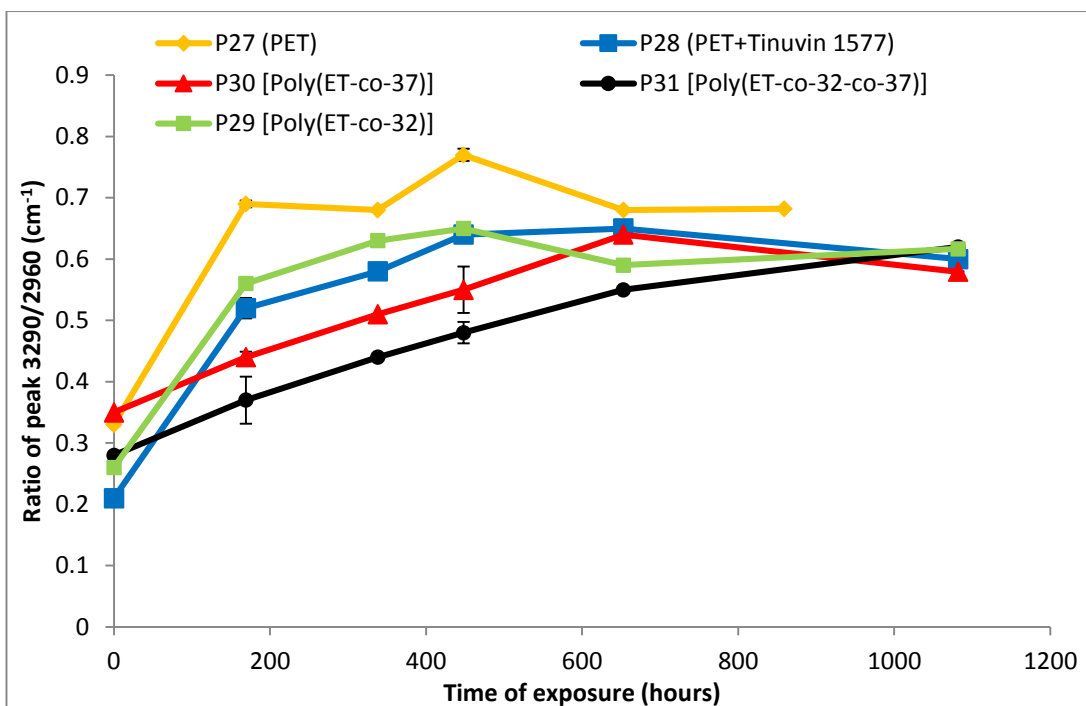


Fig. 5.11 – ATR FT-IR ratios of 3290/2960 cm⁻¹ for P27, P28, P29, P30 and P31

5.2.3.2 GPC Measurements

To a certain extent, GPC analysis supports the FT-IR measurements, with the control **P27** showing the most rapid increase in degradation whilst UVAM **37** was the most effective UV absorber to prevent chain scissions in the bulk and at the surface of the polymer (Tables 5.8-5.12). The GPC data of **P31** showed that a mixture of **32** and **37** was not as adept at preventing chain scissions within the bulk of the polymer compared to inhibiting the chain scissions at the surface, which was evident in the FT-IR technique.

Wang^{44,45} postulated that the average degree of degradation ($\bar{\alpha}$) was related to the number average molecular weight at 0 hours (\overline{M}_{n0}) and at time t hours of exposure (\overline{M}_{nt}) (Equation 5.1). This equation could be rearranged to obtain the number of chain scissions per molecule (S) (Equation 5.2).

$$\text{Eq. 5.1} \quad \bar{\alpha} = \frac{S}{\overline{M}_{n0}} = \frac{1}{\overline{M}_{nt}} - \frac{1}{\overline{M}_{n0}}$$

$$\text{Eq. 5.2} \quad S = \frac{\overline{M}_{n0}}{\overline{M}_{nt}} - 1$$

Plotting S against exposure time further reinforced that the UVAMs were more effective than Tinuvin 1577 **1.10** in preventing chain scissions during UV degradation (Figure 5.18). Similarly to Wang and Lawrence, the films showed a two-step degradation process with a rapid rise in chain scissions of ‘weak links’ between 0 and 338 hours followed by a slower rise in chain scissions of the remaining ‘normal links’ proceeding 338 hours. The polymerised UVAMs resulted in a slower rise in chain scissions for both the initial and later phases of UV degradation compared to the commercial additive. UVAM **37** was the most effective stabiliser at preventing ‘weak link’ and ‘normal link’ chain scissions, so much so that after 653 hours crosslinking begins to take a more prominent role than chain scissions in **P30**.

P27 (PET Control)	Time of exposure (hours)			
	0	338	653	859
<i>Mw</i>	11,750	13,300	13,400	27,050
<i>Mn</i>	3,605	2,445	2,830	1,835
<i>Mz</i>	19,900	45,350	43,550	277,500
<i>Polydispersity</i>	3.3	5.4	4.7	14.7
<i>Number of chain scissions per molecule</i>	0	0.47	0.27	0.97

Table 5.8 – Table showing Mw, Mn, Mz, polydispersities and average chain scissions per molecule of P27 after 0, 338, 653 and 859 hours in the QUV weatherometer

P28 (PET + Tinuvin 1577 1.10)	Time of exposure (hours)			
	0	338	653	1082
<i>Mw</i>	14,350	12,700	12,200	11,800
<i>Mn</i>	4,255	3,470	3,150	2,935
<i>Mz</i>	24,450	22,550	22,500	23,650
<i>Polydispersity</i>	3.4	3.7	3.9	4.0
<i>Number of chain scissions per molecule</i>	0	0.23	0.35	0.45

Table 5.9 - Table showing Mw, Mn, Mz, polydispersities and average chain scissions per molecule of P28 after 0, 338, 653 and 859 hours in the QUV weatherometer

P29 (P[ET-co-32])	Time of exposure (hours)			
	0	338	653	1082
<i>Mw</i>	11,750	10,800	10,800	10,800
<i>Mn</i>	3,480	3,090	3,055	2,885
<i>Mz</i>	20,300	19,500	19,750	20,100
<i>Polydispersity</i>	3.4	3.5	3.5	3.8
<i>Number of chain scissions per molecule</i>	0	0.13	0.14	0.21

Table 5.10 - Table showing Mw, Mn, Mz, polydispersities and average chain scissions per molecule of P29 after 0, 338, 653 and 859 hours in the QUV weatherometer

P30 (P[ET-co-37])	Time of exposure (hours)			
	0	338	653	1082
<i>Mw</i>	11,550	11,100	10,550	10,700
<i>Mn</i>	3,370	3,235	2,885	2,930
<i>Mz</i>	20,350	19,650	19,900	19,800
<i>Polydispersity</i>	3.4	3.4	3.7	3.7
<i>Number of chain scissions per molecule</i>	0	0.04	0.17	0.15

Table 5.11 - Table showing Mw, Mn, Mz, polydispersities and average chain scissions per molecule of P30 after 0, 338, 653 and 859 hours in the QUV weatherometer

P31 (P[ET-co-32-co-37])	Time of exposure (hours)			
	0	338	653	1082
<i>Mw</i>	12450	11250	11100	11400
<i>Mn</i>	3705	3245	3005	2990
<i>Mz</i>	21,700	19,900	20,400	21,250
<i>Polydispersity</i>	3.4	3.5	3.7	3.8
<i>Number of chain scissions per molecule</i>	0	0.14	0.23	0.24

Table 5.12 - Table showing Mw, Mn, Mz, polydispersities and average chain scissions per molecule of P31 after 0, 338, 653 and 859 hours in the QUV weatherometer

Similar to the work carried out by Sankey and Raine,⁴⁶ the weight average molecular weight (Mw) of unprotected PET was found to increase rapidly which was a clear sign of crosslinking (Figure 5.12 and 5.15). The formation of crosslinked chains explained the extremely brittle state of **P27** after 859 hours. The presence of Tinuvin 1577 **1.10**, **32** and **37** resulted in a decrease in both the Mw and Mn which showed that the UV absorbing stabilisers were effective in combating crosslinking. A graph of the Mz values emphasised the extent of crosslinking that took place in the untreated PET and the impact of the stabilisers to slow down the rate of crosslinking (Figure 5.13)

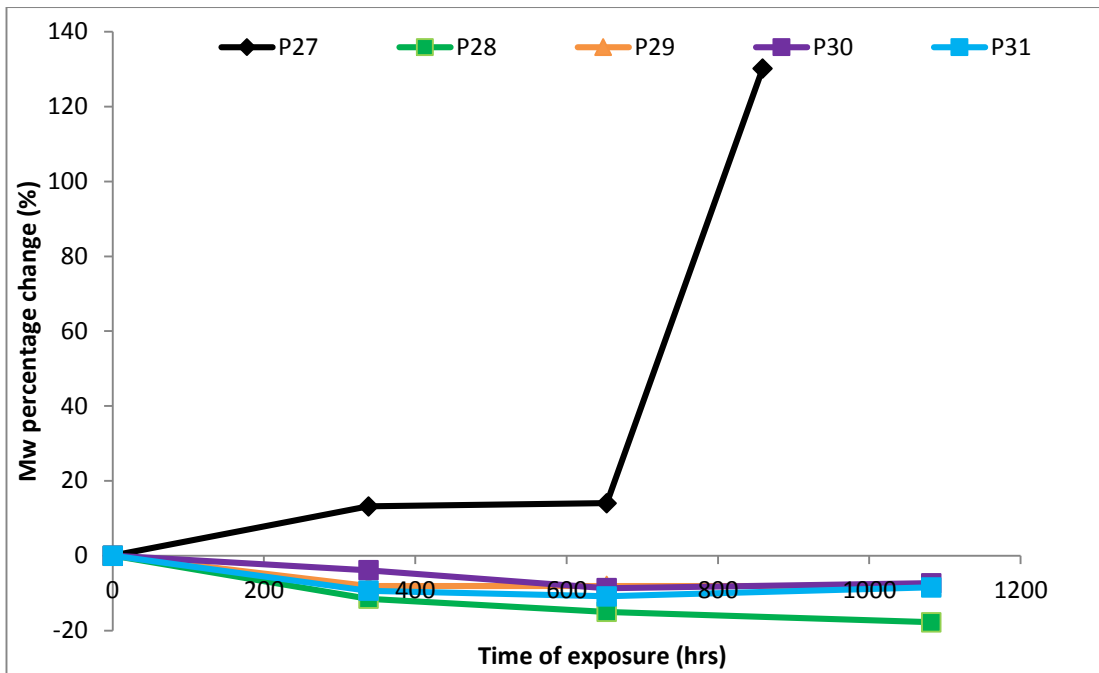


Fig. 5.12 – Plot of percentage change in the Mw against hours of exposure for P27, P28, P29, P30 and P31

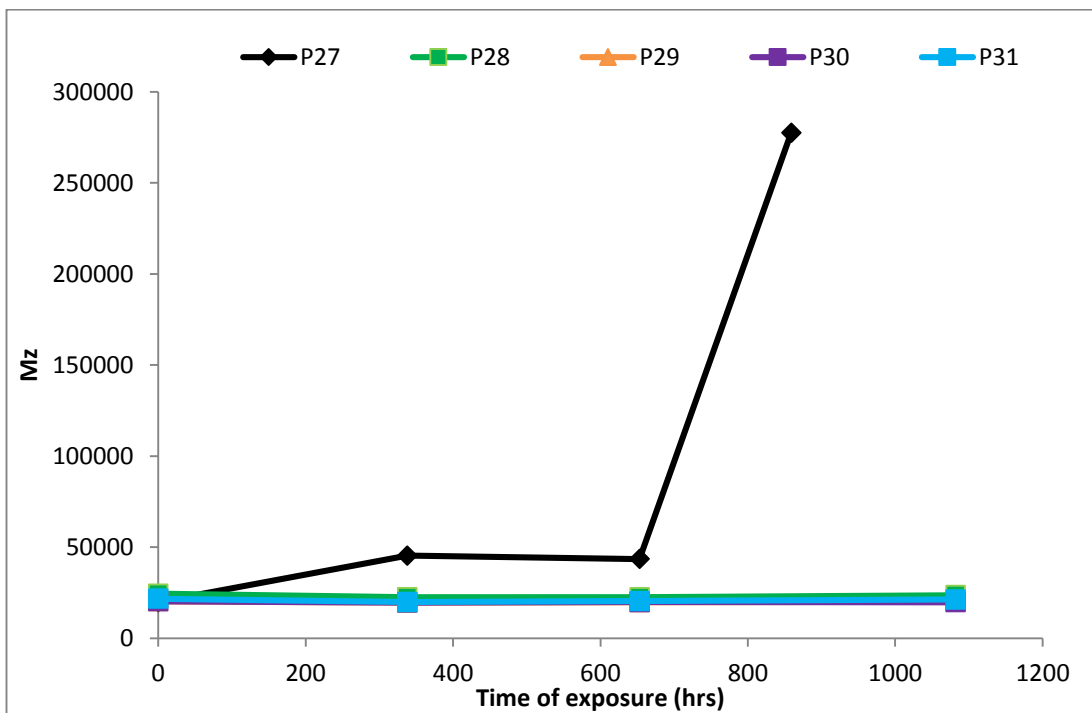


Fig. 5.13 – Plot of Mz against hours of exposure for P27, P28, P29, P30 and P31

The percentage change in Mw and Mn as a function of time of exposure show that the UVAMs offered greater photostability than Tinuvin 1577 **1.10** (Figure 5.14 and 5.15). **P28** - containing Tinuvin 1577 **1.10** showed the most rapid decrease in Mw and

Mn for the treated films which continued to fall after 338 hours. The Mw of the UVAM protected PET films seemed to reach a plateau at 859 hours after a loss of 8-11 %. **P30** and **P31** showed a slight increase in Mw at 1082 hours with respect to the Mw at 859 hours due to crosslinking beginning to make more of an impact than chain scissions. **P30** - containing UVAM **37** exhibited the slowest decrease in Mw and Mn which strongly supported the FT-IR surface analysis. In this study UVAM **37** was the most adept stabiliser at preventing chain scissions in both the bulk and the surface of the polymer. The GPC analysis of the cocktail PET (**P31**), containing both **32** and **37**, was outperformed by polymers containing only one UVAM, **P29** and **P30**. This contrasts with the FT-IR measurements which showed a slower increase in chain scissions at the surface for **P31** compared to **P29** and **P30**.

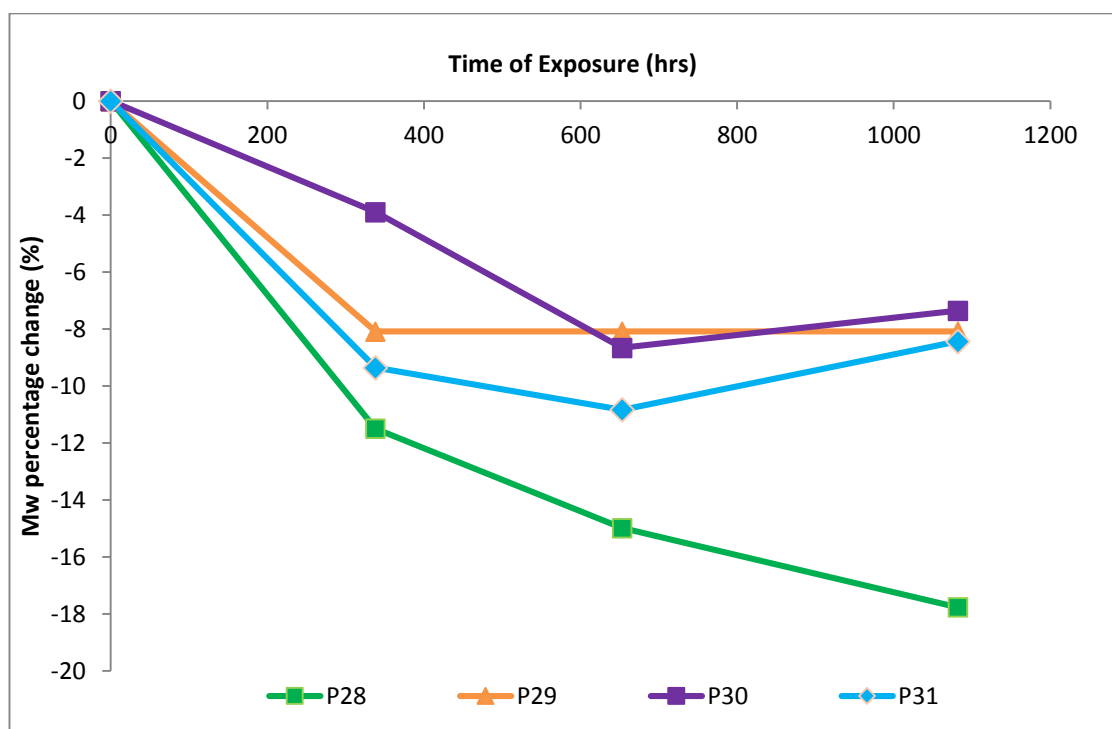


Fig. 5.14 – Plot of percentage change in the Mw against hours of exposure for P28, P29, P30 and P31

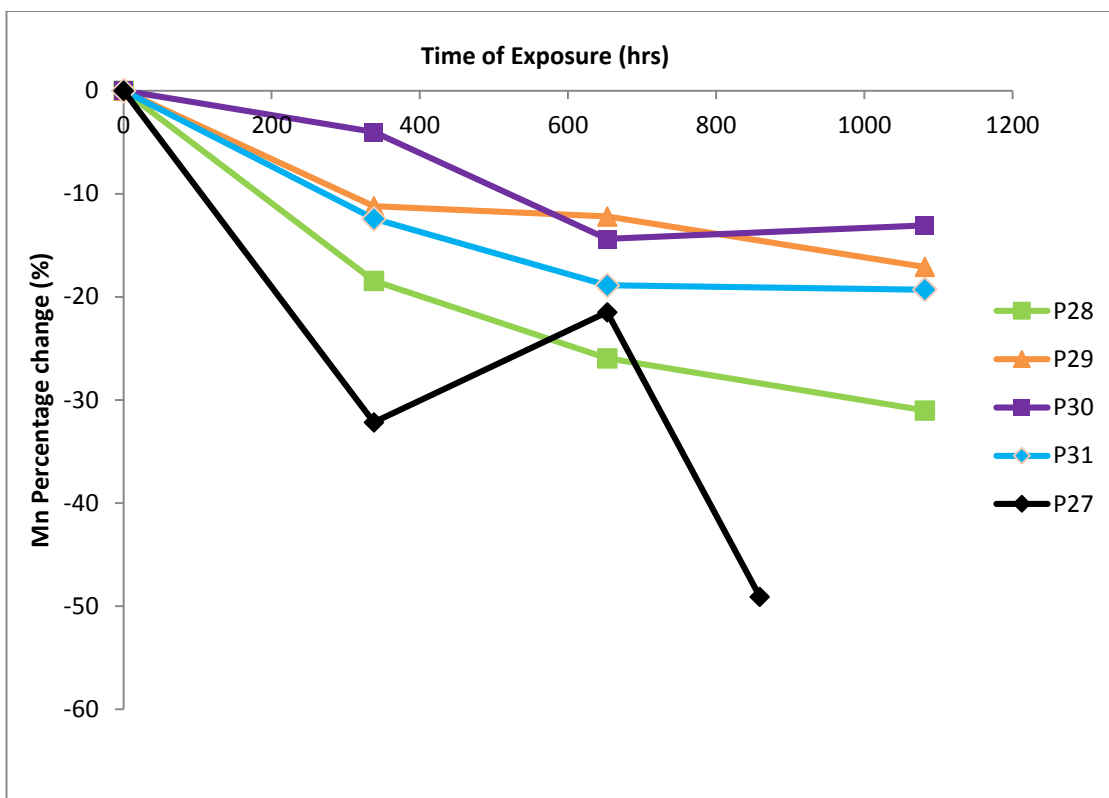


Fig. 5.15 – Plot of percentage change in the Mn against hours of exposure for P27, P28, P29, P30 and P31

The PET control displayed a rapid rise in polydispersity as crosslinking increased the Mw and the chain scissions decreased the Mn (Figure 5.16). The FT-IR analysis of the control showed high levels of chain scissions at the surface which also played a large role in reducing the Mn.

The polydispersities increased at a much slower rate for the stabilised PET films due to the UV absorbers effectively slowing the rate of crosslinking. A decrease in both Mw and Mn showed that the main outcome of degradation for the stabilised films was chain scissions and that crosslinking was playing a smaller role compared to the PET control. The UVAMs limited the chain scissions more effectively than Tinuvin 1577 1.10, which led to a slower increase in the polydispersities of P29, P30 and P31 compared to P29 (Figure 5.17).

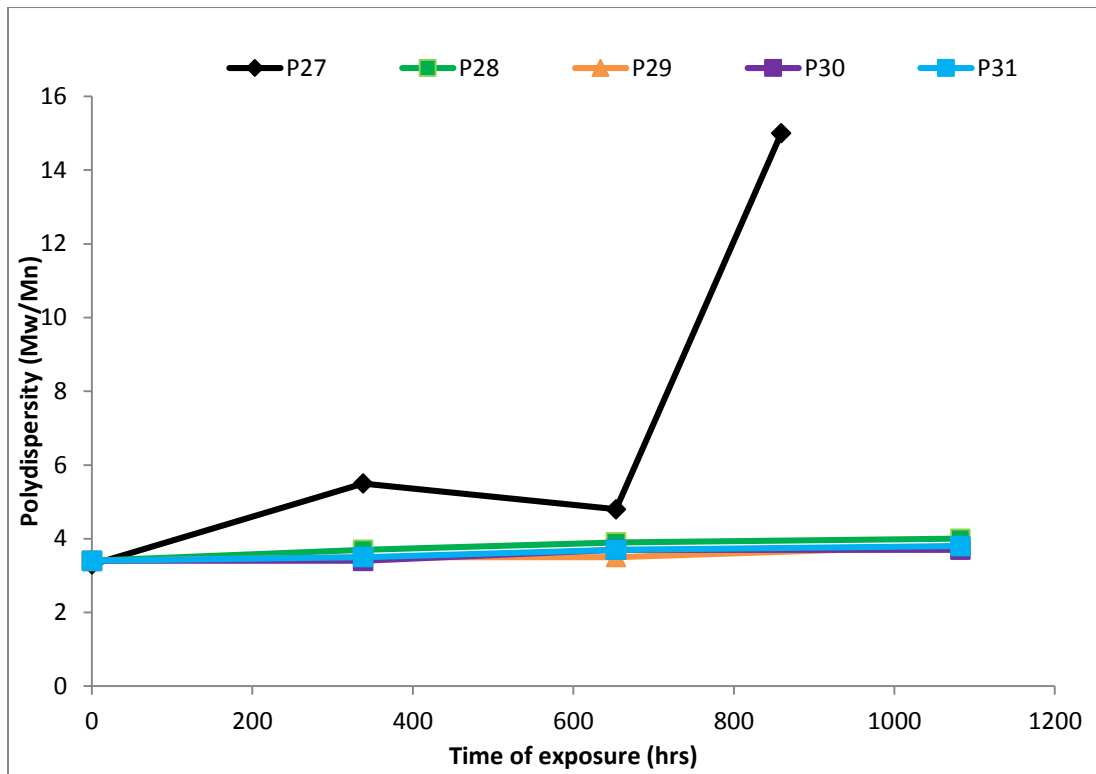


Fig. 5.16 - Plot of polydispersities against the hours of exposure for P27, P28, P29, P30 and P31

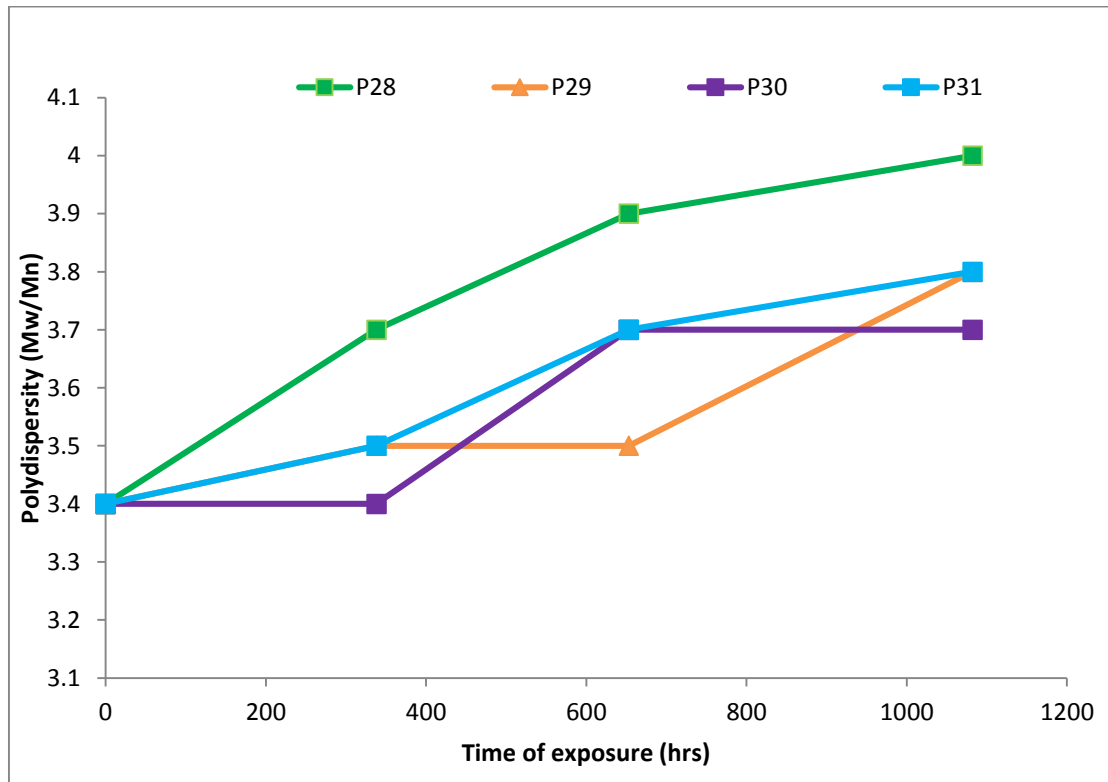


Fig. 5.17 - Plot of polydispersities against the hours of exposure for P28, P29, P30 and P31

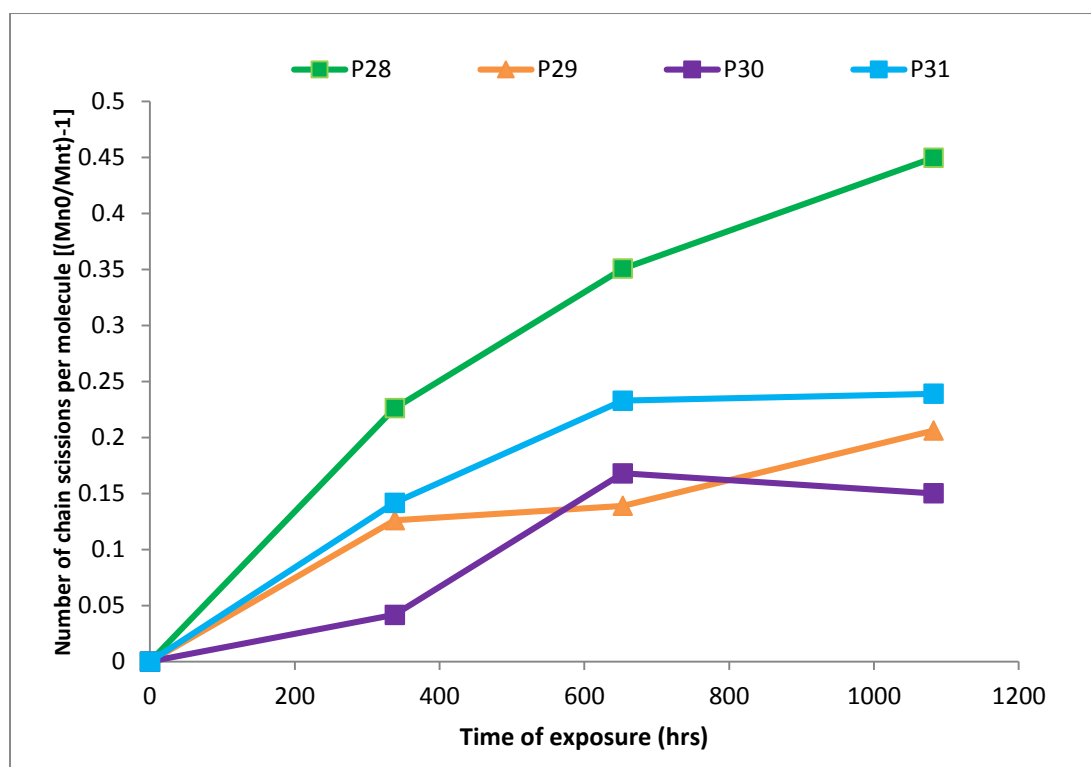


Fig. 5.18 – Plot of number of chain scissions per molecule against hours of exposure for P28, P29, P30 and P31

UVAM **32** mimicked both the UV profile (Figure 5.7) and the thermal stability (Figure 5.8) of Tinuvin 1577 **1.10**. Comparing the photostabilising effect of UVAM **32** with that of Tinuvin 1577 **1.10** shows that polymerising UV absorbers into the polymer chain offers a greater protection against UV degradation. It was extremely promising to observe the UVAMs outperforming the commercial additive in both the early and later stages of UV degradation. Since leaching from the polymer matrix takes time, one would expect **32** to offer greater stabilisation than the commercial additive primarily in the latter stages of degradation. The superiority of the UVAMs over Tinuvin 1577 **1.10** in the early stages of weathering suggested that the UVAMs possess other useful advantages in addition to higher leaching resistance, such as increased thermal resistance and lower volatility.

As mentioned previously, one other major imperfection of using Tinuvin 1577 **1.10** is that the volatile commercial additive fumes during processing which creates difficulties when handling industrial scale polymerisations and leads to a loss of stabiliser. The dominance of the UVAMs over Tinuvin 1577 **1.10** in the initial phase of degradation may indicate that there are higher levels of UVAMs in the polymer

despite employing equal loadings in the feed. Covalent tethering of the UV stabiliser to the polymer backbone can circumvent the loss of UVAM from fuming. This would result in higher levels of the UVAMs in the films compared to Tinuvin 1577 **1.10** and therefore lead to slower rates of degradation for **P29**, **P30** and **P31** with respect to **P28**. Employing the less volatile UVAMs would reduce waste and cost, as well as increase the ease of handling for large scale processes.

The UVAMs become increasingly impressive in the 2nd phase of degradation, with **P29**, **P30** and **P31** reaching a plateau whereas the number of chain scissions continued to rise for the Tinuvin 1577 **1.10** protected **P28**. The effect of leaching is expected to become even more prominent in the latter stages of degradation which ultimately leaves **P28** increasingly vulnerable to photodegradation. The covalently tethered UVAMs remain locked in the polymer matrix and offer **P29**, **P30** and **P31** greater protection over time.

Taking into account the FT-IR and GPC analysis, UVAM **37** was the most effective stabiliser in this degradation study. One obvious reason for this was the higher molar extinction coefficient throughout the 290-400 nm region for **37** in comparison to **32** and Tinuvin 1577 **1.10**. Dobashi⁵⁶ postulated that ultraviolet absorbers with higher λ_{\max} were the superior photostabilisers. Dobashi claimed that the strength of absorbance only comes into play for UVAs with the same λ_{\max} and, in this case, the UVA with the higher ϵ was the superior stabiliser. This offers an explanation for the excellent performance of UVAM **37** which has a higher λ_{\max} and a higher molar absorptivity compared to Tinuvin 1577 **1.10** and **32**.

The GPC analysis showed that using both **32** and **37** together in the same polymer was not as effective at preventing chain scissions as using only **32** or **37**. Further degradation work using different UVAM combinations must be carried out to attain a true understanding of the interaction of different UVAMs. As well as attaining a broad coverage across the 290-400 nm region, a particularly important prospect would be using monofunctional UVAMs together with bifunctional UVAMs to accomplish a more even distribution across the polymer matrix.

5.3 Conclusions

UVAMs were successfully polymerised into PET at 0.6 mol % loadings without significantly affecting the glass transition temperature, melting temperature and molar mass of the polymers. Solvent extraction tests on the films showed the tendency for Tinuvin 1577 **1.10** to leach out of the polymer matrix. The covalently anchored UVAMs did not show any sign of migration which emphasised the main advantage of using UVAMs over UV absorbing additives.

ATR FT-IR analysis showed that the films containing UVAM **37 (P30 and P31)** were the most effective at slowing the increase in carboxylic acid group formation at the surface of the film. The copolymer incorporating both **32** and **37** showed the slowest increase in the rate of chain scissions at the surface. The PET control showed the most rapid increase in chain scissions followed by a plateau once the depth of ATR penetration became saturated with COOH groups. Films containing Tinuvin 1577 **1.10** and UVAM **32** showed similar behaviour to the PET control, albeit at a slower rate of COOH production.

GPC analysis supports the FT-IR study in a number of ways, with the PET control showing the most rapid rate of degradation. Crosslinking was the major photodegradation product of the PET control whilst chain scissions were the primary photodegradation product of the stabilised films. The stabilised films displayed a decrease in the Mw and Mn, with the UVAMs significantly outperforming Tinuvin 1577 **1.10** in both the initial and latter stages of degradation.

UVAM **32** was used as direct comparison to Tinuvin 1577 **1.10** since they had essentially identical UV profiles and thermal stabilities. The supremacy of UVAM **32** categorically proved that polymerisable UV absorbers were more effective stabilisers than the commercial additive. It was thought that there were higher levels of UVAMs than Tinuvin 1577 **1.10** in the films due to retarded loss of the polymerisable stabiliser from fuming with respect to the volatile commercial additive. UVAM **37** was the most effective stabiliser in this study, combating chain scissions more effectively in both the surface and the interior of the polymer. In contrast to the FT-

IR study, GPC analysis showed that employing **37** and **32** on their own was more effective than copolymerising them into the same polymer.

6.0 General Conclusions and Future Work

Novel UVAMs were synthesised successfully from cyanuric chloride **1.90** using a wide range of synthetic reactions. UVAMs that were based on the chromophore of Tinuvin 1577 **1.10** mimicked the UV profile of the commercial additive. Alternative chromophoric structures were designed and synthesised to deliver polymerisable stabilisers with superior UV absorption properties in comparison to Tinuvin 1577 **1.10**. Tri-aryl triazine UVAMs exhibited impressive UV coverage and thermal stability, in comparison to the mono- and di-aryl triazine UVAMs.

A wide range of bifunctional and mono-functional UVAMs were incorporated successfully into PEI. Mono-functional UVAMs generally showed similar levels of incorporation and resulted in lower molecular weight copolymers compared to the bifunctional derivatives. UVAMs which possessed two IMHBs exhibited higher molar absorptivity and a broader range of coverage. UVAM **37** yielded extremely high molecular weight products for linear step-growth polymerisation which suggested crosslinking from one or more of the phenolic moieties.

With the aim of attaining the broadest range of coverage possible, combinations of two different UVAMs were chemically incorporated into the same polymeric chains. The UV spectra of the cocktail copolymers showed that the correct combinations provided a wider range of protection.

UVAMs **32** and **37** were successfully polymerised into PET without significantly affecting the glass transition temperature, melting temperature and molar mass of the polymers. Solvent extraction tests on the films showed that the UVAMs were unsusceptible to leaching out of the polymer matrix unlike Tinuvin 1577 **1.10**. FT-IR analysis showed that the films containing UVAM **37** (**P30** and **P31**) were the most effective at slowing the increase in carboxylic acid group formation at the surface of the film. GPC analysis showed that the UVAMs significantly outperformed Tinuvin 1577 **1.10** in both the initial and latter stages of degradation. The superior performance of UVAM **32** compared to Tinuvin 1577 **1.10** proved that polymerisable UV absorbers were more effective stabilisers than the commercial additive due to the

resistance of migration from the polymer matrix. In addition to this it was thought that employing polymerisable stabilisers retarded the loss of the stabiliser from fuming. UVAM **37** was the most effective stabiliser in the degradation study, combating chain scissions more effectively in both the surface and the interior of the polymer.

Future work will involve weathering films **P28**, **P29**, **P30** and **P31** for up to 4000 hours (167 days) to further understand the photostabilising capabilities of **32** and **37** over much longer exposure times. The following phase would be to synthesise PET films containing UVAMs such as **33**, **34**, **35**, **36** and **39** and implementing an identical weathering study to screen for the finest polymerisable UV stabilisers with the aim of selecting the most effective UVAMs for larger scale polymerisations (Figure 6.1). The synergistic effect of incorporating a mixture of UVAMs must be scrutinised further by attempting different combinations of polymerisable UV absorbers to gain further insight into the interaction of UVAMs which are copolymerised into the same polymer.

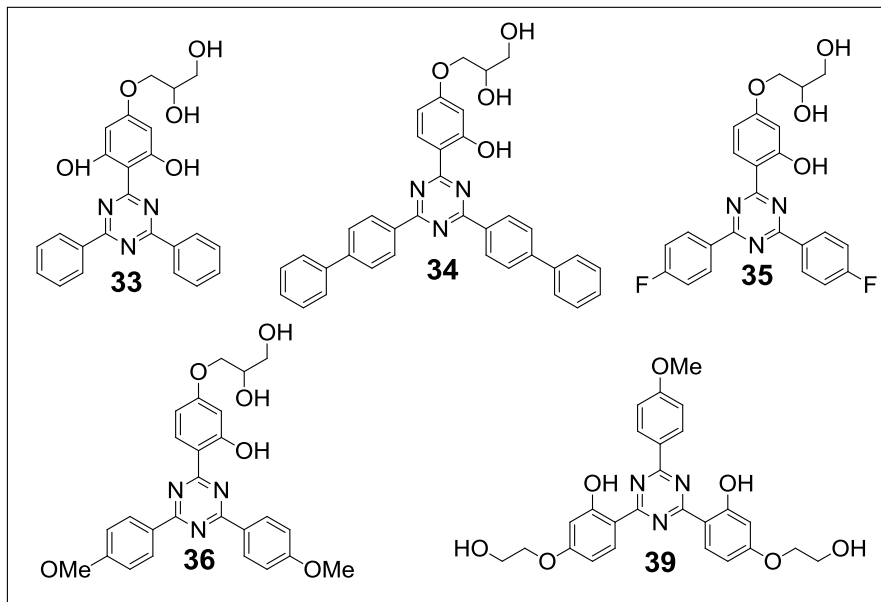


Fig. 6.1 – Chemical structures of UVAMs **33**, **34**, **35**, **36** and **39**

Having solely focused on polymerising UV absorbers into the polymer bulk, a future aim would be to polymerise UVAMs in coatings on the surfaces of PET film. The

coating could be applied to commercial PET film which would provide an ideal platform for monitoring the degree of degradation by mechanical testing as well as conventional methods such as GPC and FT-IR spectroscopy.

7.0 Appendix

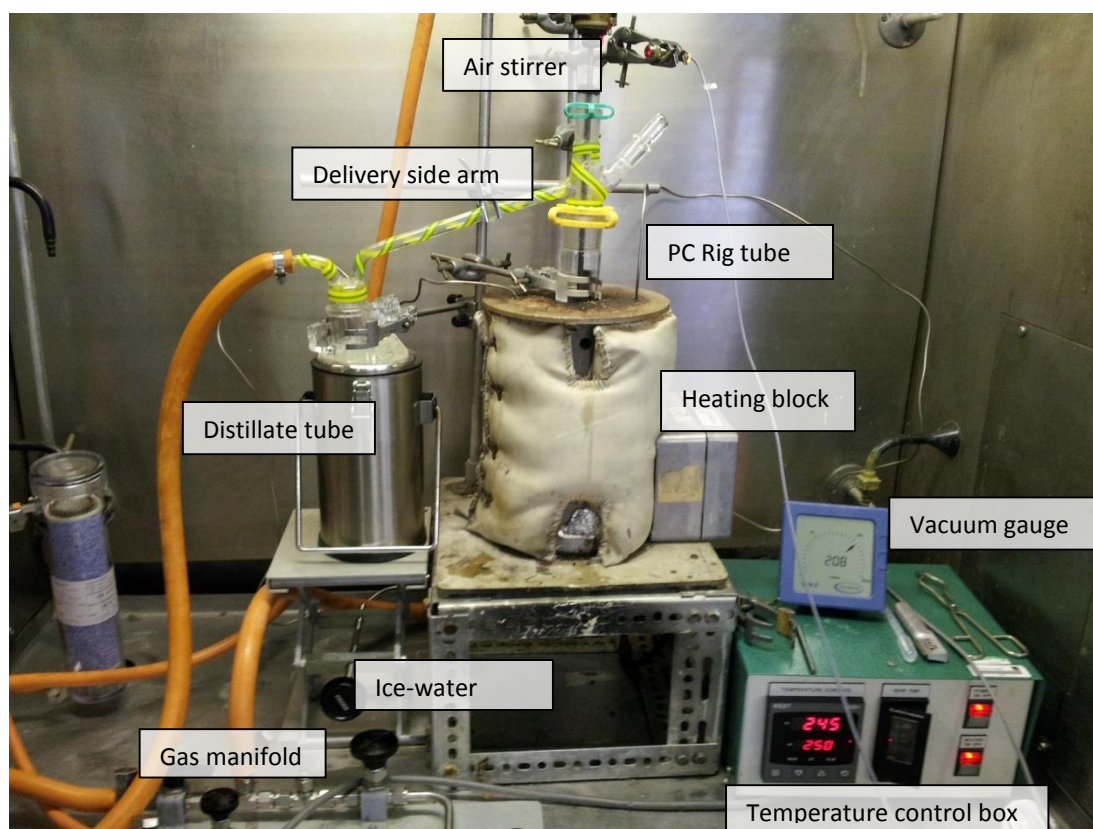


Fig. 7.1– Picture of the polycondensation rig used for copolymerisations at DTF

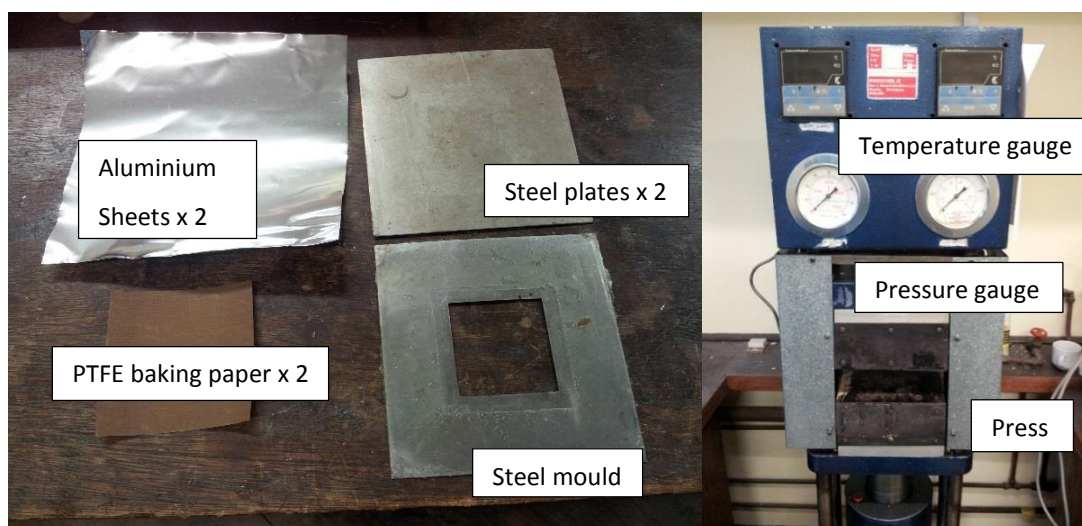


Fig. 7.2 – Components used to prepare cast film (left) and the thermal press (right)

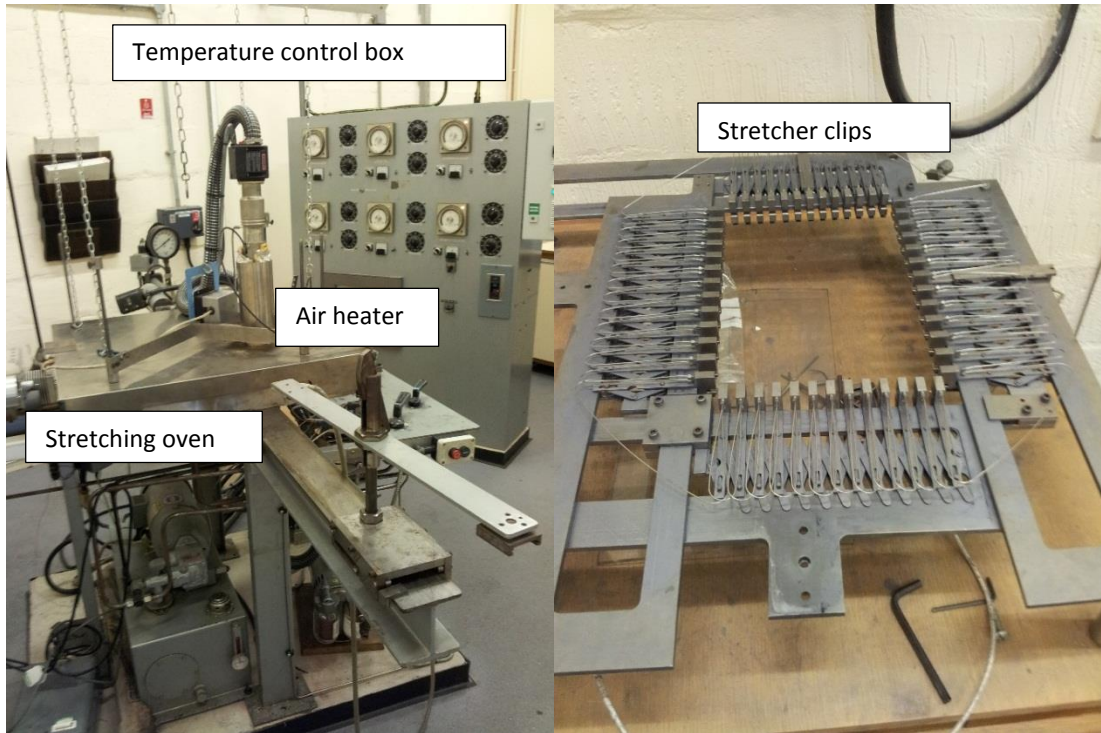


Fig. 7.3 – Picture of the stretching oven (left) and stretching clips inside the oven (right)



Fig. 7.4 – Picture of weathered films. From left to right: P27 (859 hours), P28 (1082 hours), P29 (1082 hours), P30 (1082 hours) and P31 (1082 hours)

8.0 References

- 1 A. Ahmed, H. Y. Moustafa, A. M. El-Masry and S. Hassan, *J. Appl. Polym. Sci.*, 2014, **131**, 40458–40468.
- 2 J. Cowie and V. Arrighi, *Polymers: Chemistry and Physics of Modern Materials*, Taylor and Francis Group, USA, 3rd edn., 2007.
- 3 M. P. Stevens, *Polymer Chemistry: An Introduction*, OUP USA, 3rd edn., 1999.
- 4 J. Zhao, H. Schlaad, S. Weidner and M. Antonietti, *Polym. Chem.*, 2012, **3**, 1763–1768.
- 5 P. J. Flory, *Chem. Rev.*, 1946, **39**, 137–197.
- 6 R. Spindler and J. M. J. Fréchet, *Macromolecules*, 1993, **26**, 4809–4813.
- 7 W. H. Carothers, *Trans. Faraday Soc.*, 1935, **32**, 39–49.
- 8 J. Stille, *J. Chem. Educ.*, 1981, **58**, 862–866.
- 9 F. W. Harris, *J. Chem. Educ.*, 1981, **58**, 837–843.
- 10 D. Cava, E. Gimenez, R. Gavara and J. M. Lagaron, *J. Plast. Film Sheeting*, 2006, **22**, 265–274.
- 11 M. R. Lilliedal, A. J. Medford, M. V. Madsen, K. Norrman and F. C. Krebs, *Sol. Energy Mater. Sol. Cells*, 2010, **94**, 2018–2031.
- 12 L. W. Mckeen, *Film Properties of Plastics and Elastomers*, William Andrew, USA, 3rd edn., 2012.
- 13 C. H. Park, M. Hara and M. Akazaki, *Trans. Electr. Insul.*, 1984, **E1-19**, 273–280.
- 14 D. J. Sekelik, E. V Stepanov, S. Nazarenko, D. Schiraldi, A. Hiltner and E. Baer, *J. Polym. Sci.*, 1998, **37**, 847–857.
- 15 E. Dixon and J. Jackson, *J. Mater. Sci.*, 1968, **3**, 464–470.
- 16 S. Jabarin, *J. Appl. Polym. Sci.*, 1987, **34**, 97–102.
- 17 C. J. Heffelfinger and P. G. Schmidt, *J. Appl. Polym. Sci.*, 1965, **9**, 2661–2680.
- 18 W. H. Carothers and G. L. Dorough, *J. Am. Chem. Soc.*, 1930, **52**, 711–721.
- 19 W. H. Carothers, G. L. Dorough and A. Arvin, *J. Am. Chem. Soc.*, 1930, **52**, 3292–3300.

- 20 W. H. Carothers, *US2071250*, 1937, DuPont.
- 21 J. R. Whinfield, *Text. Res. J.*, 1953, **23**, 289–293.
- 22 A. Brown and K. Reinhart, *Science*, 1971, **173**, 287–293.
- 23 W. Romão, M. A. S. Spinacé and M. De Paoli, *Polym. Degrad. Stab.*, 2009, **19**, 121–132.
- 24 W. MacDonald, *Polym. Int.*, 2002, **51**, 923–930.
- 25 S. Habaue, Y. Takahashi, Y. Hosogoe, H. Yamashita and M. Kajiwara, *Nat. Sci.*, 2010, **2**, 557–562.
- 26 M. Lee, J. Son and M. Oh, *J. Sci. Food Agric.*, 2014, **94**, 197–204.
- 27 S. Jones and S.W. Sankey, *MChem Thesis (University of Durham)*, 2012, Confidential Property of DuPont Teijin Film Ltd.
- 28 M. Day and D. Wiles, *J. Appl. Polym. Sci.*, 1972, **16**, 175–189.
- 29 M. Day and D. Wiles, *J. Appl. Polym. Sci.*, 1972, **16**, 191–202.
- 30 D. Wiles and M. Day, *J. Appl. Polym. Sci.*, 1972, **16**, 203–215.
- 31 P. Blais, M. Day and D. M. Wiles, *J. Appl. Polym. Sci.*, 1973, **17**, 1895–1907.
- 32 J. Gardette, A. Colin, S. Trivis, S. German and S. Therias, *Polym. Degrad. Stab.*, 2014, **103**, 35–41.
- 33 G. Fechine, M. Rabello, R. Souto Maior and L. Catalani, *Polym. J.*, 2004, **45**, 2303–2308.
- 34 G. Fechine, M. Rabello and R. Souto-Maior, *Polym. Degrad. Stab.*, 2002, **75**, 153–159.
- 35 A. Rivaton, J. Gardette, C. Hoyle, M. Ziemer, D. Fagerburg and T. Grossetête, *Polym. J.*, 2000, **41**, 3541–3554.
- 36 C. R. Hurley and G. J. Leggett, *ACS Appl. Mater. Interfaces*, 2009, **1**, 1688–97.
- 37 G. Fechine, P. Christensen, T. Egerton and J. White, *Polym. Degrad. Stab.*, 2009, **94**, 234–239.
- 38 S. S. Fernando, P. A. Christensen, T. A. Egerton, R. Eveson, S. M. Martins-Franchetti, D. Voisin and J. R. White, *Mater. Sci. Technol.*, 2009, **25**, 549–555.
- 39 G. Fechine and M. Rabello, *J. Mater. Sci.*, 2002, **7**, 4979–4984.

- 40 F. Zoepfl, V. Markovic and J. Silverman, *J. Polym. Sci.*, 1984, **22**, 2033–2045.
- 41 Z. Kac, S. Galovic and D. Milic, *Polym. Degrad. Stab.*, 2005, **87**, 279–286.
- 42 A. Shultz and S. Leahy, *J. Appl. Polym. Sci.*, 1961, **5**, 64–66.
- 43 G. Wypych, *Handbook of Material Weathering*, ChemTec Publishing, Canada, 4th edn., 2008.
- 44 W. E. Wang, A. Taniguchi, M. Fukuhara and T. Okada, *J. Appl. Polym. Sci.*, 1998, **67**, 705–714.
- 45 W. E. I. Wang, A. Taniguchi, M. Fukuhara and T. Okada, *J. Appl. Polym. Sci.*, 1998, **74**, 306–310.
- 46 T. Raine and S.W. Sankey, *MChem Thesis (University of Durham)*, 2013, Confidential Property of DuPont Teijin Film Ltd.
- 47 L. Ávár and K. Bechtold, *Prog. Org. Coatings*, 1999, **35**, 11–17.
- 48 S. Al-Malaika, A. Q. Ibrahim, M. J. Rao and G. Scott, *J. Appl. Polym. Sci.*, 1992, **44**, 1287–1296.
- 49 S. K. Chittimalla, T. Chang, T. Liu, H. Hsieh and C. Liao, *Tetrahedron*, 2008, **64**, 2586–2595.
- 50 L. Lu and L. He, *J. Mol. Struct.*, 2012, **1010**, 79–84.
- 51 J. Crawford, *Prog. Polym. Sci.*, 1999, **24**, 7–43.
- 52 J. Keck, M. Roessler, C. Schroeder, G. J. Stueber, F. Waiblinger, M. Stein, D. Legourrie, H. E. A. Kramer, H. Hoier, O. S. Henkel, P. Fischer, H. Port, T. Hirsch, G. Rytz and P. Hayoz, *J. Phys. Chem. B*, 1998, **5647**, 6975–6985.
- 53 F. Waiblinger, J. Keck, A. P. Fluegge, H. E. Kramer, D. Leppard and G. Rytz, *J. Photochem. Photobiol. A Chem.*, 1999, **126**, 43–49.
- 54 R. Di Capua, F. Offi and F. Fontana, *Eur. J. Phys.*, 2014, **35**.
- 55 Y. Dobashi, J. Kondou and Y. Ohkatsu, *Polym. Degrad. Stab.*, 2005, **89**, 140–144.
- 56 Y. Dobashi and Y. Ohkatsu, *Polym. Degrad. Stab.*, 2008, **93**, 436–447.
- 57 H. Shizuka, M. Masanori and H. Yasunori, *J. Phys. Chem. A*, 1985, **89**, 320–326.
- 58 J. Otterstedt, *J. Chem. Phys.*, 1973, **58**, 5716–5725.

- 59 H. Shizuka and K. Matsul, *J. Phys. Chem. A*, 1977, **81**, 2243–2246.
- 60 M. Moriyama, M. Kosuge, S. Tobita and H. Shizuka, *Chem. Phys.*, 2000, **253**, 91–103.
- 61 S. Tobita, M. Yamamoto, N. Kurahayashi, R. Tsukagoshi, Y. Nakamura and H. Shizuka, *J. Phys. Chem. A*, 1998, **5639**, 5206–5214.
- 62 G. J. Stueber, M. Kieninger, H. Schettler, W. Busch, B. Goeller, J. Franke, H. E. A. Kramer, H. Sonja, P. Fischer, H. Port, T. Hirsch, G. Rytz and J. Birbauml, *J. Phys. Chem.*, 1995, **99**, 10097–10109.
- 63 P. F. McGarry, S. Jockusch, Y. Fujiwara, N. A. Kaprinidis and N. J. Turro, *J. Phys. Chem. A*, 1997, **5639**, 764–767.
- 64 J. Keck, H. Kramer and H. Port, *J. Phys. Chem.*, 1996, **100**, 14468–14475.
- 65 V. Rajan, R. Wäber and J. Wieser, *J. Appl. Polym. Sci.*, 2012, **124**, 3988–3995.
- 66 V. Rajan, R. Wäber and J. Wieser, *J. Appl. Polym. Sci.*, 2012, **124**, 4007–4015.
- 67 M. J. Paterson, M. A. Robb, L. Blancafort and A. D. De Bellis, *J. Phys. Chem. A*, 2005, **109**, 7527–37.
- 68 C. Schaller and D. Rogez, *J. Coatings Technol. Res.*, 2007, **5**, 25–31.
- 69 F. A. Bottino, G. D. I. Pasquale, A. Pollicino and A. Recca, *J. Appl. Polym. Sci.*, 1996, **69**, 1251–1256.
- 70 S. Fu, S. Li and O. Vogl, *Chem. Mon.*, 1988, **119**, 1299–1309.
- 71 D. Bailey and O. Vogl, *Polym. Sci. Eng.*, 1976, **14**, 267–293.
- 72 D. Bailey, D. Tirrell and C. Pinazzi, *Polym. Sci. Eng.*, 1978, **11**, 312–320.
- 73 A. Al-Mobasher, S. Attari and H. Pasch, *Polym. Bull.*, 1991, **26**, 39–46.
- 74 H. Pasch, K. Shuhaibar and S. Attari, *J. Appl. Polym. Sci.*, 1991, **42**, 263–271.
- 75 O. Vogl, A. C. Albertsson and Z. Janovic, *Polym. J.*, 1985, **26**, 1289–1296.
- 76 Y. Mizutani and K. Kusumoto, *J. Appl. Polym. Sci.*, 1975, **19**, 713–717.
- 77 M. Duennenberger, H. Rudoif and C. Luethi, *US3244708*, 1966, Ciba Ltd.
- 78 M. Duenneberger, H. Huber, P. Schaefer and C. Luethi, *US3423360*, 1969, Ciba Ltd.

- 79 M. Stein, J. Keck, F. Waiblinger, A. P. Fluegge, H. E. Kramer, A. Hartschuh, H. Port, D. Leppard and G. Rytz, *J. Phys. Chem. A*, 2002, **106**, 2055–2066.
- 80 J. Birbauml, J. Rody, M. Slongo and A. Valet, *US5189084*, 1993, Ciba–Geigy Corp.
- 81 V. B. Bojinov, N. I. Georgiev and N. V. Marinova, *Sensors Actuators B Chem.*, 2010, **148**, 6–16.
- 82 V. B. Bojinov and D. B. Simeonov, *Polym. Degrad. Stab.*, 2010, **95**, 43–52.
- 83 V. B. Bojinov, I. P. Panova and D. B. Simeonov, *Dye. Pigment.*, 2009, **83**, 135–143.
- 84 V. B. Bojinov, I. P. Panova and D. B. Simeonov, *Dye. Pigment.*, 2008, **78**, 101–110.
- 85 V. B. Bojinov and I. P. Panova, *Polym. Degrad. Stab.*, 2008, **93**, 1142–1150.
- 86 V. B. Bojinov and D. B. Simeonov, *J. Photochem. Photobiol. A Chem.*, 2006, **180**, 205–212.
- 87 V. B. Bojinov, *Polym. Degrad. Stab.*, 2006, **91**, 128–135.
- 88 D. Kuila, G. Kvakovszky, M. Murphy, R. Vicari, M. Rood, K. Fritch, J. Fritch, S. Wellinghoff and S. Timmons, *Chem. Mater.*, 1999, **11**, 109–116.
- 89 C. Migdal, J. Hines and E. Kluger, *US4826978A*, 1989, Milliken Research Corporation.
- 90 T. Bolle, V. Valet, G. Leppar, M. Andrews, R. Ravichandran, M. Grob and S. D., *US2005075465*, 2005.
- 91 T. Bolle, A. Valet, D. Leppard, S. Andrews, R. Ravichandran, M. Grob and D. Simon, *WO3046068A1*, 2003, Ciba Ltd.
- 92 A. Valet and G. Berner, *US5322868A*, 1994, Ciba–Geigy Corp.
- 93 T. Carofiglio and A. Varotto, *J. Org. Chem.*, 2004, **69**, 8121–8124.
- 94 P. Gamez and J. Reedijk, *Eur. J. Inorg. Chem.*, 2006, 29–42.
- 95 H. R. Bhat, P. K. Pandey, S. K. Ghosh and U. P. Singh, *Med. Chem. Res.*, 2013, **22**, 5056–5065.
- 96 J. Pinson, Z. Zheng, M. S. Miller, D. K. Chalmers, I. G. Jennings and P. E. Thompson, *ACS Med. Chem. Lett.*, 2013, **4**, 206–210.

- 97 A. Rolfe, D. Probst, K. Volp, I. Omar, D. L. Flynn and P. R. Hanson, *J. Org. Chem.*, 2008, **73**, 8785–90.
- 98 R. Bhushan and M. Lal, *Chromatographia*, 2013, **76**, 1087–1096.
- 99 X. Li, J. Zhang, Y. Geng and Z. Jin, *J. Org. Chem.*, 2013, **78**, 5078–84.
- 100 M. Hayashi, T. Yamasaki, Y. Kobayashi, Y. Imai and Y. Watanabe, *Eur. J. Org. Chem.*, 2009, **2009**, 4956–4962.
- 101 G. Blotny, *Tetrahedron*, 2006, **62**, 9507–9522.
- 102 S. V. Vasylyuk, V. I. Lubenets, Y. I. Bychko and V. P. Novikov, *Chem. Heterocycl. Compd.*, 2008, **44**, 111–112.
- 103 C. Tao, Q. Wang, L. Nallan, T. Polat, L. Koroniak and N. Desal, *WO2010144338*, 2010, Abraxis Bioscience.
- 104 W. J. Pitts, J. Guo, Z. Shen, H. Gu, S. Watterson and M. Bednarz, *Bioorg. Med. Chem. Lett.*, 2002, **12**, 2137–2140.
- 105 Z. An, R. Chen, J. Yin, G. Xie, H. Shi, T. Tsuboi and W. Huang, *Chem. - A Eur. J.*, 2011, **17**, 10871–8.
- 106 R. Menicagli, S. Samaritani and V. Zucchelli, *Tetrahedron*, 2000, **56**, 9705–9711.
- 107 L. Hintermann, L. Xiao and A. Labonne, *Angew. Chem.*, 2008, **47**, 8246–50.
- 108 L. Hintermann, T. T. Dang, A. Labonne, T. Kribber, L. Xiao and P. Naumov, *Chem. - A Eur. J.*, 2009, **15**, 7167–79.
- 109 N. S. Kim, M. S. Kang, S. H. Jung, D. M. Kang and N. H. Lee, *US2011156013*, 2011.
- 110 T. Sekiguchi, N. Yamada, H. Iwawaki and T. Yamaguchi, *WO2010067894*, 2010, Canon Kabushiki Kaisha.
- 111 S. Abe, M. Hashimoto, C. Nishiura and H. Nitta, *WO2011070991*, 2011, Canon Kabushiki Kaisha.
- 112 H. Zhong, E. Xu, D. Zeng, J. Du, J. Sun, S. Ren, B. Jiang and Q. Fang, *Org. Lett.*, 2008, **10**, 709–12.
- 113 A. Naka, R. Fukuda, R. Kishimoto, Y. Yamashita, Y. Ooyama, J. Ohshita and M. Ishikawa, *J. Organomet. Chem.*, 2012, **702**, 67–72.
- 114 W.-F. Jiang, H.-L. Wang and Z.-Q. Li, *J. Chem. Res.*, 2008, **2008**, 664–665.

- 115 R. Gupta, J. D. S. Venimadhavan, R. Capadona and V. Pai, *WO0029392*, 2000, Cytect Technology Corp.
- 116 G. Conn and S. Eisler, *Org. Lett.*, 2011, **13**, 2669–2672.
- 117 E. Bosch and C. L. Barnes, *Inorg. Chem.*, 2002, **41**, 2543–2547.
- 118 C. Trullas, C. Pelejero, D. Panyella, J. Corbera and J. Holenz, *WO2006128920*, 2006, ISDIN.
- 119 S. Achelle, Y. Ramondenc, F. Marsais and N. Plé, *Eur. J. Org. Chem.*, 2008, **2008**, 3129–3140.
- 120 P. M. Lahti, Y. Liao, M. Julier and F. Palacio, *Synth. Met.*, 2001, **122**, 485–493.
- 121 C. Lee, H. Lim, J. Lee, Y. Lee, J. Ko, H. Nakamura and S. Ook Kang, *Appl. Organomet. Chem.*, 2003, **17**, 539–548.
- 122 C. Zhang, C.-L. Zou, Y. Yan, R. Hao, F.-W. Sun, Z.-F. Han, Y. S. Zhao and J. Yao, *J. Am. Chem. Soc.*, 2011, **133**, 7276–9.
- 123 R. Hao, M. Li, Y. Wang, J. Zhang, Y. Ma, L. Fu, X. Wen, Y. Wu, X. Ai, S. Zhang and Y. Wei, *Adv. Funct. Mater.*, 2007, **17**, 3663–3669.
- 124 R. Anemian, S. Heun, T. Eberle and P. Stoessel, *WO2011032686*, 2011, Merck.
- 125 C. Di Nicola, F. Garau, F. Marchetti, M. Monari, L. Pandolfo, C. Pettinari and a Venzo, *Dalton Trans.*, 2011, **40**, 4941–53.
- 126 H. Schmelzer, E. Degener and H. Holtschmidt, *Angew. Chem.*, 1966, **5**, 4–5.
- 127 J. Harris, *Aust. J. Chem.*, 1981, **34**, 623–626.
- 128 M. Duennenberger, H. Biland and C. Luethi, *US3394134*, 1968, Ciba Ltd.
- 129 T. Shafer, F. Wenderborn, M. Gerster, P. Hayoz, B. Schmidhalter and J. Budry, *WO2004106311*, 2004, Ciba Specialty Chemicals.
- 130 S. Yanagida, H. Hayama, M. Yokoe and S. Komori, *J. Org. Chem.*, 1969, **34**, 4125–4127.
- 131 J. P. Milionis and F. G. Pinto, *US3118887*, 1964, American Cyanamid Company.
- 132 J. Bribaum, J. Kaschig, D. Reinehr, M. Rembold, A. Schmitter, H. Luther, B. Herzog and D. Huglin, *US5591850*, 1997, Ciba–Geigy Corporation.
- 133 C. Luethi, M. Duennenberger and H. Biland, *US3244708A*, 1966, Ciba Ltd.

- 134 T. Bolle, A. Valet, D. Leppard, S. Andrews, R. Ravichandran, M. Grob and D. Simon, *WO03046068*, 2003, Ciba Specialty Chemicals.
- 135 G. Knobloch, P. Rota-Graziosi, S. Evans, P. Dubs and M. Gerster, *WO02081432*, 2002, Ciba Specialty Chemicals.
- 136 I. Fletcher, J. Kaschig, G. Metzger, D. Reinehr and P. Hayoz, *US6255483*, 2001, Ciba Specialty Chemicals.
- 137 V. B. Bojinov, N. I. Georgiev and P. Bosch, *J. Fluoresc.*, 2009, **19**, 127–39.
- 138 D. Atamanyuk, A. Denis, V. Gerusz, B. Ledoussal and Y. Bonvin, *WO2012172043*, 2012, Laboratoire Biodim.
- 139 R. A. Abramovitch, *Can. J. Chem.*, 1958, **36**, 151–158.
- 140 R. D. Chai, S. J. Chen and J. Zhang, *J. Thermoplast. Compos. Mater.*, 2011, **25**, 879–894.
- 141 Y. Dobashi, T. Yuyama and Y. Ohkatsu, *Polym. Degrad. Stab.*, 2007, **92**, 1227–1233.